

Braiding Knots with Topological Strings

Dissertation
zur
Erlangung des Doktorgrades (Dr. rer. nat.)
der
Mathematisch-Naturwissenschaftlichen Fakultät
der
Rheinischen Friedrich-Wilhelms-Universität Bonn

von
Jie Gu
aus
Ningbo, China

Bonn, March 2015

Dieser Forschungsbericht wurde als Dissertation von der
Mathematisch-Naturwissenschaftlichen Fakultät der Universität Bonn angenommen und ist
auf dem Hochschulschriftenserver der ULB Bonn
http://hss.ulb.uni-bonn.de/diss_online elektronisch publiziert.

1. Gutachter: Prof. Dr. Albrecht Klemm
2. Gutachter: Priv. Doz. Stefan Förste

Tag der Promotion: 12.08.2015
Erscheinungsjahr: 2015

Abstract

For an arbitrary knot in a three–sphere, the Ooguri–Vafa conjecture associates to it a unique stack of branes in type A topological string on the resolved conifold, and relates the colored HOMFLY invariants of the knot to the free energies on the branes. For torus knots, we use a modified version of the topological recursion developed by Eynard and Orantin to compute the free energies on the branes from the Aganagic–Vafa spectral curves of the branes, and find they are consistent with the known colored HOMFLY knot invariants à la the Ooguri–Vafa conjecture. In addition our modified topological recursion can reproduce the correct closed string free energies, which encode the information of the background geometry. We conjecture the modified topological recursion is applicable for branes associated to hyperbolic knots as well, encouraged by the observation that the modified topological recursion yields the correct planar closed string free energy from the Aganagic–Vafa spectral curves of hyperbolic knots. This has implications for the knot theory concerning distinguishing mutant knots with colored HOMFLY invariants. Furthermore, for hyperbolic knots, we present methods to compute colored HOMFLY invariants in nonsymmetric representations of $U(N)$. The key step in this computation is computing quantum $6j$ –symbols in the quantum group $\mathcal{U}_q(\mathfrak{sl}_N)$.

Acknowledgements

I will always be in debt to my direct supervisor Dr. Hans Jockers, without whose continuous support and encouragement I could not have made the transition from an astroparticle physicist to a string theoretician, gone through the PhD studies, and in the end finished this dissertation. I am grateful for his seemingly inexhaustible patience to bear with my numerous and sometimes stupid questions. I also thank him for proofreading my thesis. I would like to thank my supervisor Prof. Dr. Albrecht Klemm, who not only provided financial support for my PhD studies and various academic trips, but also inspired me through his impressive passions for researches and his insights. I would like to thank Prof. Manuel Dress. He kindly agreed to write the third reference letter for my post-doctoral application, and also gave me many good advices concerning the BCGS (Bonn-Cologne Graduate School) program. I would like to thank Priv. Doz. Stefan Förste to be my second thesis referee, as well as Prof. Dr. Ian Brock, Prof. Dr. Daniel Huybrechts for taking time to be on my thesis committee.

I would like to thank Dr. Masoud Soroush for the collaboration on my first string paper. In addition I am grateful for him inviting me to give a talk at Brandeis and his hospitality during my visit to Boston. I thank Jonas Reuter as well as Prof. Dr. Marcos Mariño in Geneva for an interesting collaboration. I would also like to thank many other fellows in the BCTP (Bethe Center for Theoretical Physics) for many warm memories we shared together: for instance, the Wednesday seminars, the company of Thorsten Schimannek and Pwl Oilmann in the dead of many nights in the institute, and many a nonacademic discussion including some very cunning plans with Raghuvveer Garani.

During my PhD studies, I was supported by the Honors Branches of the BCGS program, and the successive secretaries of the BCGS program were all very helpful, especially Frau Doris Thrun, who has now retired. I was also very lucky to have the service of the amazing group of the BCTP secretaries, and all of their names deserve to be spelled out: Christa Börsch, Dagmar Fassbender, Petra Weiß, and Patricia Zündorf. I also should not forget the IT magician in the institute, Dr. Andreas Wisskirchen.

I leave my last thanks to my parents, to whom I owe everything.

Contents

| | | |
|----------|---|----------|
| 1 | Introduction | 1 |
| 1.1 | String Theory as a Logical Next Step | 1 |
| 1.2 | A Useful Exercise of Topological String | 4 |
| 2 | Topological String and Field Theories | 7 |
| 2.1 | 2d Topological Sigma Models | 7 |
| 2.1.1 | 2d $\mathcal{N} = (2, 2)$ Nonlinear Sigma Model | 7 |
| 2.1.2 | Topological Twists and Topological QFT of the Witten Type | 10 |
| 2.1.3 | Topological A–Twist | 13 |
| 2.1.4 | Topological B–Twist | 16 |
| 2.1.5 | A Diversion: Complex Structure Moduli Space of Calabi–Yau Threefold | 18 |
| 2.2 | Topological String Theory | 21 |
| 2.2.1 | General Ideas | 21 |
| 2.2.2 | Type A Closed String | 23 |
| 2.2.3 | Type A Open String | 26 |
| 2.2.4 | Type B Closed String | 30 |
| 2.2.5 | Type B Open String | 33 |
| 2.2.6 | Mirror Symmetry | 33 |
| 2.3 | Chern–Simons Theory | 37 |
| 2.3.1 | Basic Definitions | 37 |
| 2.3.2 | HOMFLY Knot Invariants | 39 |
| 2.3.3 | Surgery and Nonperturbative Solutions | 40 |
| 2.3.4 | Symmetry Properties | 44 |
| 2.3.5 | Free Energies $1/N$ Expansion | 45 |
| 2.3.6 | Relation to Topological String Theory | 46 |
| 2.4 | Matrix Models | 47 |
| 2.4.1 | Basic Definitions | 47 |
| 2.4.2 | Saddle Point Approximation | 50 |
| 2.4.3 | Relation to Chern–Simons Theory | 53 |
| 2.4.4 | Relation to Topological String Theory | 55 |
| 2.4.5 | Large N Duality | 56 |
| 2.5 | Topological Recursion | 58 |
| 2.5.1 | Loop Equations and Their Solutions | 58 |
| 2.5.2 | Topological Recursion and Symplectic Invariants | 60 |
| 2.5.3 | Properties of Symplectic Invariants | 63 |
| 2.5.4 | Resolvents, Unknot, and Special Lagrangian Branes | 66 |
| 2.5.5 | The BKMP Theorem | 68 |
| 2.5.6 | Ooguri–Vafa Conjecture and Open Problems | 70 |

| | | |
|----------|---|------------|
| 3 | Topological String and Knot Invariants | 71 |
| 3.1 | Spectral Curves | 71 |
| 3.1.1 | Brini–Eynard–Mariño Spectral Curve | 71 |
| 3.1.2 | Aganagic–Vafa Spectral Curve | 73 |
| 3.2 | Annulus Kernel | 80 |
| 3.2.1 | Problems with Bergman Kernel | 80 |
| 3.2.2 | Constructing the Annulus Kernel | 84 |
| 3.2.3 | Calibration and Poles | 86 |
| 3.2.4 | Stretched Annulus Instantons | 89 |
| 3.3 | Modified Topological Recursion | 91 |
| 3.3.1 | Normalization and Free Energies | 91 |
| 3.3.2 | Computing Correlation Differentials | 93 |
| 3.3.3 | Computing Free Energies | 95 |
| 3.4 | Implications for and from Knot Theory | 96 |
| 4 | Knot Invariants and RCFT | 99 |
| 4.1 | Braiding Method | 100 |
| 4.1.1 | Basic Ideas | 100 |
| 4.1.2 | Eigenstates of Braiding Operators | 101 |
| 4.1.3 | Summary | 107 |
| 4.2 | Quantum Group and Quantum $6j$ -Symbols | 109 |
| 4.3 | Computing $6j$ -Symbols | 115 |
| 4.3.1 | Phase Convention | 117 |
| 4.3.2 | Eigenvector Method | 118 |
| 4.3.3 | Bootstrap: Reduction to Cores | 119 |
| 4.3.4 | Bootstrap: Crushing the Cores | 121 |
| 4.4 | Results | 124 |
| 4.4.1 | Quantum $6j$ -Symbols of the Two Kinds | 124 |
| 4.4.2 | HOMFLY Invariants Colored in $(2,1)$ Representation | 128 |
| 5 | Conclusions and Prospect | 135 |
| A | Composite Representations of $U(N)$ | 137 |
| B | Calibrated Annulus Kernel | 141 |
| | Bibliography | 145 |
| | List of Figures | 159 |
| | List of Tables | 161 |

1.1 String Theory as a Logical Next Step

The Standard Model of fundamental particles is one of the most successful theory of physics. On the one hand, it is a very comprehensive theory, covering length scales from down to the size of quarks up to the macroscopic world. On the other hand, it is also extremely accurate. For almost every experiment particle physicists could think of, the Standard Model can produce results consistent with the measurements, often with stunningly high precisions. With the discovery of the Higgs-like particle at the LHC in 2012, the last piece of the Standard Model fell into place. However, the Standard Model is short of being a *complete* fundamental theory of physics. As a relativistic quantum field theory, the Standard Model incorporates only three out of the four fundamental interactions, leaving out the gravitational interaction. When the energy scale of the theory is pushed toward the Planck scale, the quantum fluctuation of matter fields would become so violent that the spacetime structure, due to the laws of general relativity, would be induced into a state of wild quantum fluctuation as well. It is therefore logically necessary¹ to develop a quantum theory for the gravitational field at high energy scale as part of a complete fundamental theory, of which the Standard Model is only the low energy approximation. However the marriage between quantum field theory and general relativity faces great problems, as the Hilbert–Einstein action of the gravitational field in general relativity is non–renormalizable, and as a consequence a naive quantum field theory of gravity would lose predicative power.

Therefore to quantize general relativity, one has to generalize the Standard Model, or rather quantum field theories in general, by relaxing some of the fundamental assumptions. One way to generalize the Standard Model is to enhance its symmetry. The Lie algebra of symmetry the S–matrices respect in a relativistic quantum field theory has to be the direct product of the Poincaré algebra and some Lie algebra describing the internal symmetry, whose generators are Lorentzian scalars [1]. One possible way of enhancing the symmetry is to allow graded Lie algebra, and the only consistent graded Lie algebra extension is the supersymmetry algebra [2]. The supersymmetry generators Q_α^A convert a bosonic field to a fermionic field and vice versa. Therefore supersymmetry organizes all the fields in a theory into supermultiplets, each of which consists of fields that can be changed into each other via supersymmetry transformations. Here α is the Weyl spinor index and the index A goes from 1 through \mathcal{N} , which is the number of supersymmetries. Since the supersymmetry generators are intimately convoluted with the

¹ Recall that the general relativity itself was born out of the logical inconsistency between special relativity and Newtonian gravitational theory.

Poincaré algebra, as seen in the anti-commutation relation

$$\{Q_\alpha^A, \bar{Q}_{\dot{\beta}B}\} = 2\sigma_{\alpha\dot{\beta}}^m P_m \delta_B^A, \quad (1.1)$$

where P_m is the energy-momentum operator and m the Lorentz index, in a gravity theory where the Poincaré symmetry becomes a local symmetry, the supersymmetry algebra should also be gauged, giving rise to a supergravity theory². In a supergravity theory, the bosonic particles of gravitons, which are the force carriers of the gravitational interaction, have fermionic counterparts called gravitini (plural of gravitino). Their loop contributions have opposite signs. Therefore there is some cancellation of the infinite loop corrections to the scattering amplitudes, although the cancellation is not perfect. So the problem of ultraviolet divergence is mitigated but not eliminated in supergravity theories.

A second way to generalize the Standard Model is concerned with the basic assumption that before quantization a fundamental particle can be understood as a point propagating in the spacetime manifold. The trajectory of the propagation is called the worldline of the particle. A natural generalization of this picture is the propagation of a string, be it open or closed, and it sweeps out a worldsheet in the spacetime manifold. Various fundamental particles with different masses then can be regarded as distinct vibrational modes of the string. The string has a fundamental *string scale*, and the string can not probe spacetime scale smaller than this string scale³, just like the resolution of an optical picture is limited by the wavelength of the probing photons. Effectively the string scale acts as a cutoff of the energy scale of the quantum gravity theory, therefore bypassing the problem of non-renormalizability. This so-called *bosonic string theory*⁴, however suffers from several serious problems. It cannot describe fermions, for one things, and it has nasty tachyonic states with negative square masses, which make the ground state of the theory unstable.

The combination of these two ideas, supersymmetry and propagating string, gives rise to superstring theory⁵. In superstring theory the worldsheet of string carries a superconformal field theory, in other words, a 2d conformal field theory with supersymmetry, which includes both bosonic and fermionic vibrational modes. Together they give rise to both bosonic particles and fermionic particles at low energy physics. Not all the vibrational modes are allowed though, and one needs a selection rule, called the GSO projection [10], which eliminates tachyonic modes and which makes superstring a supersymmetric field theory in low energy.

Up to now superstring theory remains the most fruitful among all proposals of quantum gravity theories. It is a unified framework, which describes not only gravitons, but also matter particles and the interaction between gravitons and matter particles. In fact, there has been promising progress towards embedding the minimal supersymmetric extension of the Standard Model (MSSM) in superstring theory⁶. This is not surprising given that superstring theory is a generalization of quantum field theory of particles. Rather it is surprising that this generalization contains graviton fields at all.

Furthermore, superstring theory has connections to many branches of theoretical physics and mathematics, providing sometimes surprising and paradigm shifting insights into the latter

² Interested readers can read [3] as an excellent textbook on this subject.

³ In fact, the backreaction of the string would warp the spacetime such that it is meaningless to talk about scales below the string scale in a full string theory.

⁴ For a comprehensive discussion of the bosonic string theory one can read [4].

⁵ Up to now there are many excellent textbooks on superstring theory, including [5–9].

⁶ A very incomplete list [11–15] taken from the talk of Prof. Eran Palti [16] at the String Phenomenology 2014.

fields. This is due to two facts about superstring theory. The first fact is that a consistent superstring theory demands the spacetime has in total ten dimensions. Since we only observe a four dimensional spacetime, the other six spatial dimensions must form a compact manifold, whose size is so tiny that it is much below the probing limit of our experiments/observations; in other words, these six dimensions must be *compactified*. The geometry of the compact space X is restricted by the properties of the superstring theory. If we require that in 4d $\mathcal{N} = 1$ supersymmetry is preserved from a $\mathcal{N} = 1$ 10 dimensional superstring theory, the compact X must be a Calabi–Yau threefold, which is a 6 dimensional simply connected Kähler manifold whose Ricci tensor vanishes. The second fact is that there is not one but five different versions of perturbative superstring theories, called type IIA, type IIB, type I, $E_8 \times E_8$ heterotic string, and $SO(32)$ heterotic string respectively. At low energy, they reduce to five different 10d supergravity theories. In addition, there is a unique 11d $\mathcal{N} = 1$ supergravity and its conjectured high energy completion called M–theory.

These six different theories are revealed to be dual to each other. In other words, two theories with different couplings or different compactification spaces describe completely the same physics. These dualities provide much of the richness of superstring theory. From mathematical point of view, some dualities relating superstring theories compactified on two different Calabi–Yau threefolds are rather surprising. For instance, the mirror symmetry claims that for each Calabi–Yau threefold X there exists a mirror partner Y with the properties⁷

$$h^{1,1}(X) = h^{2,1}(Y), \quad h^{2,1}(X) = h^{1,1}(Y), \quad (1.2)$$

such that type IIA superstring compactified on X is dual to type IIB superstring compactified on Y . Mathematically speaking there is a priori no reason to relate these two manifolds, since they have different topologies and different moduli spaces. However, in the 90s string physicists surprised mathematicians by using the mirror symmetry to make striking predictions, like the counting of holomorphic spheres in (some) Calabi–Yau threefolds, which eventually were proved to be correct with rigorous mathematics.

Another type of superstring duality involves a new kind of objects called Dirichlet branes, or D–branes in short. They were initially conceived as the loci in spacetime where the endpoints of open string are restricted to. Later it was argued that they should also be treated as dynamical objects, themselves having associated energy and momentum. Therefore a stack of many branes wrapping a cycle in the compact manifold M with the number N of branes sent to infinity can induce a sizeable change of the background geometry, according to the general relativity. On the other hand, the vibrational modes of open string give rise to a gauge theory on the worldvolume of the branes. This line of reasoning lead to the famous AdS/CFT correspondence [17], which relates a $d + 1$ dimensional quantum gravity theory on an AdS space X to a d dimensional gauge theory (which is also conformal) on the boundary of X . For obvious reasons, this correspondence is also known as the large N duality or the gauge/gravity duality. It was a beautiful realization of the holographic principle proposed by 't Hooft [18], and has since provided insights into both quantum gravity and gauge theory.

Despite its many applications, there are some significant difficulties in superstring theory. Since it is a quantum gravity theory, most of its effects are only seen in extreme conditions, like energy scales far beyond the current technology. Therefore it is difficult to conceive of any

⁷ There are rare exceptions. A Calabi–Yau threefold X with $h^{2,1}(X) = 0$ does not have a mirror manifold. To be precise, the type II superstring theory on X still has a mirror theory, but the latter does not allow a geometric interpretation.

experiment to verify superstring theory at this stage. Furthermore, many crucial aspects of superstring theory are still poorly understood. Computations in superstring theory are usually simplified by the supersymmetry condition. On the other hand, to compute for instance the free energy in superstring theory one needs to perturbatively sum over contributions from the worldsheets on Riemann surfaces of different genera weighted by powers of the string coupling g_s

$$\mathcal{F} = \sum_g g_s^{2g-2} \mathcal{F}_g . \quad (1.3)$$

But on a worldsheet of genus greater than one, the supersymmetry can only be preserved on local coordinate patches but not on the worldsheet as a whole, which makes the computations very difficult (see more discussions in section 2.1.2). Furthermore, the sum over genera is an asymptotic series, which only has meanings in the limit of infinitesimal string coupling. Interpreting this asymptotic series with finite string coupling is difficult, especially since it is not known what kinds of nonperturbative effects would arise.

To help solving the last two problems, it may be beneficial to first study a simplified version of superstring theory.

1.2 A Useful Exercise of Topological String

Type A/type B topological string theory is a simplification of the $\mathcal{N} = 2$ type IIA/IIB superstring theory compactified on a Calabi–Yau threefold. This is achieved through a “topological twisting” in the worldsheet theory, so that the supersymmetry is always preserved on the whole worldsheet regardless of the genus of the Riemann surface the worldsheet is on. It is called topological string because after the twisting the theory no longer depends on the metric of the worldsheet. In some sense, this removes the difference between Riemann surfaces of different genera, which is the reason the supersymmetry can always be preserved globally. The price to pay is that (nearly) half of the fields in the theory are projected out. The massless fields in a 4d $\mathcal{N} = 2$ superstring theory are organized into vector multiplets, hypermultiplets, and one gravity multiplet. Topological string theories lose track of the hypermultiplets. Besides, among the numerous terms involving the vector multiplets and the gravity multiplet in the action of a 4d $\mathcal{N} = 2$ supergravity, one can only compute the kinetic terms of the fields in the vector multiplets and the couplings of the scalars in the vector multiplets to the gravity multiplet in topological string theories. The former are encoded in the planar free energy \mathcal{F}_0 , while the latter are given by higher genera free energies \mathcal{F}_g with $g \geq 1$ [19].

However, whatever little one can compute with topological strings, one can compute them well. Because of the supersymmetry on worldsheets, powerful methods have been developed to compute the free energies \mathcal{F}_g in both type A and type B topological string theories order by order (see section 2.2 and references therein). Furthermore, various dualities, like mirror symmetry and larger N duality, are either inherited or have their own manifestations in topological string theories, and they often conspire to form a chain or a web of dualities. Given the computational powers and better understandings in topological string theories, these dualities can be verified explicitly or sometimes even be proved rigorously, in contrast to cases in superstring theories.

The large N duality in topological string (also called the Gopakumar–Vafa duality) claims that the type A topological string compactified on the resolved conifold, i.e. the double line bundle over $\mathbb{P}^1 : \mathcal{O}(-1) \oplus \mathcal{O}(-1) \rightarrow \mathbb{P}^1$, is dual to 3d $U(N)$ Chern–Simons theory on three sphere in the large N limit. The Chern–Simons theory is a topological pure gauge theory, and

the boundary of the double line bundle over \mathbb{P}^1 at infinity is indeed a three sphere. Therefore this large N duality exactly parallels the AdS/CFT correspondence in superstring theories. There are well-established methods to compute the free energies in the Chern–Simons theory. For instance one can use the surgery method of Witten [20] to compute the partition function with relative ease, and then deduce the free energies from the partition function. The large N duality has been verified by directly matching the free energies from the Chern–Simons theory and the type A topological string theory [21].

The large N duality can be further extended to a chain of dualities. Given the relation between topological strings and type II superstrings, the mirror symmetry is directly inherited by topological string theories, mapping type A topological string on a Calabi–Yau threefold X to type B topological string on the mirror Calabi–Yau Y satisfying eq. (1.2). In particular, the mirror manifold of the resolved conifold is a three complex dimensional hypersurface Y in $\mathbb{C}^2 \times (\mathbb{C}^*)^2$. Furthermore, type B topological string on Y is dual to a matrix model. All put together, we have the following chain of dualities

$$\text{Chern–Simons theory} \xleftarrow[\text{duality}]{\text{large } N} \text{type A on resolved conifold} \longleftrightarrow \text{type B on } Y \longleftrightarrow \text{matrix model}$$

A matrix model is a zero dimensional $U(N)$ pure gauge theory. It is associated with a function of a Hermitian matrix M , and the function is invariant under an adjoint $U(N)$ transformation

$$M \mapsto U M U^\dagger, \quad U \in U(N) \tag{1.4}$$

on the matrix (here we focus on Hermitian 1–matrix models). The partition function of the matrix model is then a path integral of the invariant function over all possible configurations of the Hermitian matrix modulo $U(N)$ transformations. The study of matrix models has a long history. Recently, Eynard and Orantin have developed the powerful method of topological recursion which can solve matrix models at all orders in the large N limit [22–24].

We are interested in the Ooguri–Vafa conjecture [25], which is a generalization of the large N duality by the insertion of branes in the type A topological string. This corresponds to the insertion of Wilson loops in the Chern–Simons theory on three sphere. The path of a Wilson loop in three sphere is a knot. Witten showed [20] that the vev of a Wilson loop evaluated in the fundamental representation of $U(N)$ in the Chern–Simons theory can be identified with the HOMFLY invariant of the knot. In the knot theory, the HOMFLY invariant [26] is a unique bivariate algebraic expression for each knot, and for two different knots, the associated two algebraic expressions are usually also different⁸. Therefore the HOMFLY knot invariants can be used to distinguish or identify knots. The HOMFLY invariants can be computed from a single simple linear relation called the skein relation, which is described in section 2.3.2. On the other hand, given the identification of the HOMFLY knot invariants and the vevs of the Wilson loops in the fundamental representation, the vevs of the Wilson loops in more complicated representations of $U(N)$ in the Chern–Simons theory are called the colored HOMFLY invariants. They can also be defined in the knot theory, but the computations there are significantly more complicated.

Using this terminology of the knot theory, the Ooguri–Vafa conjecture relates colored HOMFLY knot invariants to free energies of branes in type A topological string theory. Our goal is to verify the Ooguri–Vafa conjecture by directly comparing the colored HOMFLY invariants

⁸ The exceptional cases when the HOMFLY invariants of two different knots are identical are discussed in section 3.4.

with the brane free energies. For a type of relatively simple knots called torus knots, all of their colored HOMFLY invariants can be computed. On the other hand, the right half of the duality chain in the diagram above indicates the brane free energies can be computed via techniques in matrix models, in particular the topological recursion. We use a modified version of the topological recursion to compute the brane free energies and find they match the results of the colored HOMFLY invariants à la the Ooguri–Vafa conjecture. In addition, our modified topological recursion can reproduce the correct free energies of the topological closed string theory. This is in accord with the fact that these branes probe the background geometry, since the closed string free energies encode the information of the background geometry. Furthermore, emboldened by our observation that the modified topological recursion can reproduce the correct planar closed string free energy even from the data of more complicated knots (hyperbolic knots), we conjecture that the modified topological recursion can be applied on these knots as well. If proved correct, our conjecture will have interesting implications also for the knot theory. On the other hand, it would be difficult to verify our conjecture or the Ooguri–Vafa conjecture for these knots, because even the colored HOMFLY invariants for these knots are poorly understood. There has been much work on the HOMFLY invariants in symmetric representations of $U(N)$. We build on these results and present computations of the HOMFLY invariants for these knots in nonsymmetric representations of $U(N)$ in the framework of the Chern–Simons theory.

Finally, due to its relative simplicity, it is easier to first try to understand nonperturbative completion of free energies \mathcal{F}_g in topological string theory and then see what it can teach us about superstring theory. This is especially the case if the topological string theory in question has a dual matrix model, and if the partition function of the matrix model is convergent, because the partition function of a matrix model is defined nonperturbatively and is understood rather well. Interesting progress has been made along this line, including for instance refs. [27–29] as well as our work in progress [30]. Unfortunately this topic will not be covered in this thesis.

The outline of the thesis is as follows. We prepare the theoretical background in chapter 2. We explain what topological strings actually compute by the free energies \mathcal{F}_g , and gloss over the methods to compute them. We describe various dualities in topological string theories, including the dualities to the Chern–Simons theory and matrix models, as well as the Ooguri–Vafa conjecture. We also explain the basic computational methods in the Chern–Simons theory and matrix models that will be used in our work. In chapter 3 we verify the Ooguri–Vafa conjecture for torus knots by computing the free energies of the branes via the modified topological recursion and comparing with the known data of the colored HOMFLY invariants. In chapter 4 we describe a method to compute colored HOMFLY invariants for non–torus knots colored in nonsymmetric representations. We conclude in chapter 5 and propose future directions.

Topological String and Field Theories

In this chapter we summarize the theoretical background of the thesis. In the first two sections, we explain the origin of topological string theories. For this purpose, we first discuss in section 2.1 how to twist the 2d $\mathcal{N} = (2, 2)$ nonlinear sigma model on a superstring worldsheet to get 2d topological field theories. Then we briefly explain in section 2.2 how to couple these topological field theories to 2d gravity to get topological string theories. We cover some other salient points in topological strings in this section as well, like what are the computables, and the major computational methods. In some scenarios topological string theories can be reduced to 3d Chern–Simons theories or Hermitian matrix models, which will be discussed in section 2.3 and section 2.4 respectively. Section 2.5 is dedicated to the topological recursion, an extremely powerful method for solving matrix models, and we emphasize its relevance to topological string theories in section 2.5.5. Along the way at various places we discuss mirror symmetry (section 2.2.6) and large N duality (section 2.4.5), which together form a beautiful circle of dualities that connects all these topological theories to each other. We also describe the generalization of this circle dualities via the insertion of branes in topological strings (section 2.5.4, section 2.5.6). Emphasis is placed on the Ooguri–Vafa conjecture, which is a key link in this generalized circle of dualities.

2.1 2d Topological Sigma Models

2.1.1 2d $\mathcal{N} = (2, 2)$ Nonlinear Sigma Model

When type II superstring theory is compactified on a Calabi–Yau threefold X , the worldsheet of string carries a $\mathcal{N} = 2$ supersymmetric nonlinear sigma model, which maps the worldsheet into the target space X . We give a short description of this nonlinear sigma model and follow closely the discussions in ref. [31]. The nonlinear sigma model is a 2d $\mathcal{N} = (2, 2)$ supersymmetric field theory. It has two $U(1)$ R–symmetries in the left and right channels respectively, and their Noether charges are denoted by F_L and F_R . It is also customary to combine them into vector or axial R–symmetries with Noether charges

$$F_V = F_L + F_R, \quad F_A = F_L - F_R . \tag{2.1}$$

There are four supercharges in the $\mathcal{N} = (2, 2)$ supersymmetric field theory denoted by

$$Q_+, \quad Q_-, \quad \bar{Q}_+, \quad \bar{Q}_- \tag{2.2}$$

where the subscript $+$ or $-$ means propagation in the left or right channel, while with or without bar overhead means having R–symmetry charge $+1$ or -1 in the respective channel.

The 2d $\mathcal{N} = (2, 2)$ supersymmetry algebra is generated by Hamiltonian, momentum, angular momentum in the Poincaré algebra

$$H, P, M,$$

the supercharges, and the R-symmetries charges. They satisfy the (anti-) commutation relations

$$Q_+^2 = Q_-^2 = \bar{Q}_+^2 = \bar{Q}_-^2 = 0 \quad (2.3)$$

$$\{Q_\pm, \bar{Q}_\pm\} = H \pm P, \quad (2.4)$$

$$\{\bar{Q}_+, \bar{Q}_-\} = \{Q_+, Q_-\} = 0, \quad (2.5)$$

$$\{Q_-, \bar{Q}_+\} = \{Q_+, \bar{Q}_-\} = 0, \quad (2.6)$$

$$[iM, Q_\pm] = \mp Q_\pm, [iM, \bar{Q}_\pm] = \mp \bar{Q}_\pm, \quad (2.7)$$

$$[iF_V, Q_\pm] = -iQ_\pm, [iF_V, \bar{Q}_\pm] = i\bar{Q}_\pm, \quad (2.8)$$

$$[iF_A, Q_\pm] = \mp iQ_\pm, [iF_A, \bar{Q}_\pm] = \pm i\bar{Q}_\pm. \quad (2.9)$$

In principle there can also be central charges arising on the right hand side of eqs. (2.5), (2.6).

$$\{\bar{Q}_+, \bar{Q}_-\} = Z, \{Q_+, Q_-\} = Z^*,$$

$$\{Q_-, \bar{Q}_+\} = \tilde{Z}, \{Q_+, \bar{Q}_-\} = \tilde{Z}^*,$$

provided that they commute with all the generators in the algebra. But they are necessarily zero in the presence of the F_V and F_A R-charges. For instance the super-Jacobi identity dictates

$$0 = [iF_V, \{\bar{Q}_+, \bar{Q}_-\}] - \{\bar{Q}_-, [iF_V, \bar{Q}_+]\} + \{\bar{Q}_+, [\bar{Q}_-, iF_V]\} = -2Z.$$

The supersymmetric field theory is most conveniently described in terms of the 2d $\mathcal{N} = (2, 2)$ superspace, which is discussed in detail in chapter 12 of ref. [31]. The superspace has in addition to the spacetime coordinates x_0, x_1 ¹ four fermionic coordinates

$$\theta^+, \theta^-, \bar{\theta}^+, \bar{\theta}^-. \quad (2.10)$$

There are also four covariant differential operators D_\pm, \bar{D}_\pm , which anticommute with the representation of the supercharges in the superspace

$$\{D_\pm, Q_\pm\} = 0. \quad (2.11)$$

Besides, they satisfy the anti-commutation relation

$$\{D_\pm, \bar{D}_\pm\} = 2i\partial_\pm. \quad (2.12)$$

In the superspace the bosonic and fermionic fields in the same supermultiplet are packaged into a single superfield. We are interested in chiral superfields, which are defined by

$$\bar{D}_\pm \Phi = 0. \quad (2.13)$$

¹ Here we take the flat Minkowski metric $\eta = \text{diag}(-1, 1)$.

A chiral superfield Φ

$$\Phi = \phi + \theta^\alpha \psi_\alpha + \theta^+ \theta^- F \quad (2.14)$$

has one scalar component field ϕ , two Weyl component fields ψ_\pm with opposite chiralities, and an auxiliary field F . The last component field is not dynamical and gets integrated out in an on-shell theory. These fields constitute a chiral supermultiplet. One can assign the following R-charges to the component fields by performing proper vector or axial R rotations on the fermionic coordinates θ inside the chiral superfield Φ ,

| | | | | |
|-------|--------|----------|----------|-----|
| | ϕ | ψ_+ | ψ_- | F |
| F_V | 0 | -1 | -1 | -2 |
| F_A | 0 | -1 | +1 | 0 |

Furthermore one can find the supersymmetric transformation laws for the fields in a chiral supermultiplet by applying the representation of supercharges in the superspace on the chiral superfield Φ ,

$$\begin{aligned} \delta\phi &= \epsilon_+ \psi_- - \epsilon_- \psi_+ , \\ \delta\psi_\pm &= \pm 2i\bar{\epsilon}_\mp \partial_\pm \phi + \epsilon_\pm F , \\ \delta F &= -2i\bar{\epsilon}_+ \partial_- \psi_+ - 2i\bar{\epsilon}_- \partial_+ \psi_- . \end{aligned} \quad (2.15)$$

Let us now construct a 2d $\mathcal{N} = (2, 2)$ nonlinear sigma model that maps the worldsheet of string into an n complex dimensional Kähler manifold X . The theory has n copies of chiral superfields Φ^i . The n scalar fields ϕ^i are the holomorphic coordinates on the target space X (the conjugate fields $\bar{\phi}^{\bar{i}}$ serve as the anti-holomorphic coordinates). The Lagrangian of the 2d supersymmetric nonlinear sigma model is built from the D-term only²,

$$\mathcal{L}_{\text{sigma}} = \int d^4\theta K(\Phi^i, \bar{\Phi}^{\bar{i}}) , \quad (2.16)$$

where $K(\cdot, \cdot)$ is the Kähler potential of the target space X . Due to its very construction, the Lagrangian is supersymmetrically invariant.

When the 2d $\mathcal{N} = (2, 2)$ nonlinear sigma model is quantized, both the algebra generators and the fields are promoted to operators. If the supersymmetry is still preserved, the supersymmetric transformation laws in eqs. (2.15) can be translated into (anti-)commutation relations via the correspondence,

$$\delta\mathcal{O} = [\hat{\delta}, \mathcal{O}] , \quad (2.17)$$

with

$$\hat{\delta} := i\epsilon_+ Q_- - i\epsilon_- Q_+ - i\bar{\epsilon}_+ \bar{Q}_- + i\bar{\epsilon}_- \bar{Q}_+ . \quad (2.18)$$

For instance, the lowest component field ϕ of a chiral multiplet then satisfies

$$[\bar{Q}_\pm, \phi] = 0 . \quad (2.19)$$

On the other hand, in the quantum theory axial $U(1)$ R-symmetry may be anomalously broken; for the axial R-symmetry to be anomaly free, the target space X must obey

$$c_1(X) = 0 , \quad (2.20)$$

² The explicit form of the Lagrangian can be found for instance in chapter 13 of [31].

where c_1 is the first Chern class of the tangent vector bundle on X . This condition is satisfied if the Kähler manifold X is a Calabi–Yau manifold.

2.1.2 Topological Twists and Topological QFT of the Witten Type

To be precise, when placed on a generic curved Riemann surface Σ , globally speaking the 2d $\mathcal{N} = (2, 2)$ nonlinear sigma model with the Lagrangian eq. (2.16) is not necessarily supersymmetrically invariant. The Lagrangian constructed from D–term yields under supersymmetry transformation a term of total differential, which may not integrate to zero on a Riemann surface Σ with non–trivial curvature. Another way to look at the problem is to consider the variation of the action of the sigma model under a supersymmetric transformation (2.18),

$$\delta S = \int_{\Sigma} (\nabla_{\mu} \epsilon_{+} G_{-}^{\mu} - \nabla_{\mu} \epsilon_{-} G_{+}^{\mu} - \nabla_{\mu} \bar{\epsilon}_{+} \bar{G}_{-}^{\mu} + \nabla_{\mu} \bar{\epsilon}_{-} \bar{G}_{+}^{\mu}) \sqrt{h} d^2 x . \quad (2.21)$$

Here h is the metric on the Riemann surface and $G_{\pm}^{\mu}, \bar{G}_{\pm}^{\mu}$ are the would–be supercurrents if the supersymmetry is preserved. On a generic Riemann surface Σ the supersymmetry variation δS only vanishes if the fermionic variation parameters $\epsilon_{\pm}, \bar{\epsilon}_{\pm}$ are covariantly constant spinors on Σ . However on a curved Riemann surface of higher genus covariantly constant spinors are not available. As a consequence, we can still formulate a 2d field theory with equal amount of bosonic and fermionic degrees of freedom on a curved Riemann surface (worldsheet supersymmetry), but the supersymmetry invariance of the action of the nonlinear sigma model has to break down. This is the source of complication of many perturbative computations in superstring theory, where one has to sum over worldsheets with different genera.

It would be desirable to have some fermionic symmetry globally preserved on the Riemann surface Σ , so that the *localization principle* can be applied to simplify the partition function computation. In general the computation of a partition function in a quantum field theory involves integrating over all possible field configurations, which are infinitely many. In the semiclassical limit it is known that the partition function is dominated by configurations around instanton solutions which solve the equations of motion of the theory. On the other hand if there is a fermionic symmetry Q in the theory like supersymmetry, the partition function would *only* pick up instanton configurations, which are usually finitely many, and one–loop fluctuations around them. Since instanton configurations solve equations of motion, which are usually proportional to the variations of fermionic fields associated to the fermionic symmetry Q ³, the above statement can also be rephrased as that the partition function is localized to the vicinity of the fixed loci of the transformations of the fermionic symmetry Q . This statement was first proposed in [32] with the following supporting argument. If a symmetry exists in the theory, one can cut out small neighborhoods of the fixed loci of the symmetry transformations and treat the rest of the field configuration space as a fiber bundle \mathcal{F} , with the field configurations in each fiber being closed under the symmetry transformations. The computation of the partition function on \mathcal{F} then can be performed in two steps. In the first step one integrates over field configurations on each fiber, and in the second step one proceeds to integrate over the base of the fiber bundle. The integral along a fiber is proportional to the volume of the symmetry group,

³ This is observed in many supersymmetric field theories. A rough argument goes as follows. We assume the lowest component of the supermultiplet is a bosonic field ϕ and its Q –variation is proportional to the fermionic field ψ . The Q –variation of ψ when divided out the variation parameter ϵ is a dimension two expression, and it consists of only bosonic fields. Let us denote it by $P(\phi)$. But the nilpotency of Q demands that $P(\phi) \propto \delta_Q \psi = \delta_Q^2 \phi = 0$ and it is only possible if $P(\phi)$ is proportional to the bosonic equation of motion.

| | $U(1)_V$ | $U(1)_A$ | $U(1)_E$ | $U(1)_E^A$ | $U(1)_E^B$ |
|------------------|----------|----------|----------|------------|------------|
| Q_+ | -1 | -1 | -1 | -2 | -2 |
| Q_- | -1 | 1 | 1 | 0 | 2 |
| \overline{Q}_+ | 1 | 1 | -1 | 0 | 0 |
| \overline{Q}_- | 1 | -1 | 1 | 2 | 0 |

Table 2.1: $U(1)$ R-charges as well as the chiralities (twice of spin) of the supercharges before and after the topological twistings.

which is zero in the case of a fermionic symmetry. So nonzero contributions of the partition function can only come from the small neighborhoods of the fixed loci of the fermionic symmetry transformations⁴.

In the case of the 2d $\mathcal{N} = (2, 2)$ supersymmetric field theory, a fermionic symmetry can be obtained by *twisting* the rotation generator of the 2d Lorentz group via $U(1)$ R-charge, so that some combination Q of supercharges becomes a scalar, albeit still Grassmannian, which can be trivially placed globally on a curved Riemann surface [32–35]. Put it in another way, the variation parameter ϵ associated to the charge Q is now also a scalar and can always be made covariantly constant. It can be shown that in fact the “fermionic” symmetry charge Q has the additional benefit of making the sigma model a topological field theory, which is independent of the metric of the worldsheet, simplifying the theory even further.

Let us be more specific. From now on we work with the Euclidean version of the 2d $\mathcal{N} = (2, 2)$ sigma model obtained by performing the Wick rotation $x^0 = -ix^2$. We also denote $z = x^1 + ix^2$. Then the 2d Lorentz group becomes the Euclidean rotation group $SO(2)_E = U(1)_E$ with the generator

$$M_E = iM . \quad (2.22)$$

Correspondingly the commutation relations eqs. (2.7), (2.8), and (2.9) in the supersymmetry algebra become

$$[M_E, Q_\pm] = \mp Q_\pm, \quad [M_E, \overline{Q}_\pm] = \mp \overline{Q}_\pm , \quad (2.23)$$

$$[F_V, Q_\pm] = -Q_\pm, \quad [F_V, \overline{Q}_\pm] = \overline{Q}_\pm , \quad (2.24)$$

$$[F_A, Q_\pm] = \mp Q_\pm, \quad [F_A, \overline{Q}_\pm] = \pm \overline{Q}_\pm . \quad (2.25)$$

For the sake of clarity and later convenience, let us now summarize the $U(1)$ R-charges as well as the chiralities of the supercharges in the second block (columns 2 to 4) of Tab. 2.1. All of them can be read off from the commutation relations eqs. (2.23), (2.24), (2.25). Keep in mind that chirality is twice the value of spin. We also list the R-charges and chiralities of the fields in the chiral supermultiplet in the second block of Tab. 2.2.

Now we define two new Euclidean rotation generators $M_E^{A/B}$,

$$\text{A-twist:} \quad M_E^A = M_E + F_V , \quad (2.26)$$

$$\text{B-twist:} \quad M_E^B = M_E + F_A . \quad (2.27)$$

⁴ In practice when one does a localization computation, if the action of the theory is not Q -exact, one needs to add a Q -exact term to the action by hand to localize to semiclassical configurations. See for instance [31] for more details.

| | $U(1)_V$ | $U(1)_A$ | $U(1)_E$ | $U(1)_E^A$ | $U(1)_E^B$ |
|----------------|----------|----------|----------|------------|------------|
| ϕ | 0 | 0 | 0 | 0 | 0 |
| ψ_+ | -1 | -1 | -1 | -2 | -2 |
| ψ_- | -1 | 1 | 1 | 0 | 2 |
| $\bar{\psi}_+$ | 1 | 1 | -1 | 0 | 0 |
| $\bar{\psi}_-$ | 1 | -1 | 1 | 2 | 0 |

Table 2.2: $U(1)$ R-charges and the chiralities (twice of spin) of the chiral fields before and after the topological twistings.

They are obtained through *twisting* the old rotation generator by either the vector or the axial R-charge. In either case, the chiralities, or the spins, of the chiral fields and supercharges will be changed, as listed in the last two columns of Tabs. 2.2 and 2.1.

More concretely the change of chiralities or spins of fields can be understood as the modification of the action by coupling either the vector or the axial R-symmetry current to the spin connection, as explained in detail in chapter 3 of ref. [36]. For instance one can show that before twisting one of the kinetic terms in the Lagrangian is

$$ig_{i\bar{j}}\bar{\psi}_-^{\bar{j}}D_{\bar{z}}\psi_-^i$$

where the covariant derivative is

$$D_{\bar{z}}\psi_-^i = \partial_{\bar{z}}\psi_-^i + \frac{i}{2}\omega_{\bar{z}}\psi_-^i + \Gamma_{jk}^i\partial_{\bar{z}}\phi^j\psi_-^k .$$

On the right hand side, $\omega_{\bar{z}}$ is the spin connection, and Γ_{jk}^i is the Christopher symbol. The coefficient $1/2$ in front of the spin connection (dropping the imaginary unit) is the spin of the fermionic field ψ_-^i . Let the vector and axial R-charge currents be j_V^μ and j_A^μ respectively. Then the A-twist can be realized by adding $-\frac{1}{2}\omega_{\mu}j_V^\mu$ to the Lagrangian so that the covariant derivative of ψ_-^i becomes

$$D_{\bar{z}}\psi_-^i \mapsto \partial_{\bar{z}}\psi_-^i + \Gamma_{jk}^i\partial_{\bar{z}}\phi^j\psi_-^k .$$

On the other hand if we perform the B-twist by adding $\frac{1}{2}\omega_{\mu}j_A^\mu$ to the Lagrangian the covariant derivative of ψ_-^i is changed to

$$D_{\bar{z}}\psi_-^i \mapsto \partial_{\bar{z}}\psi_-^i + i\omega_{\bar{z}}\psi_-^i + \Gamma_{jk}^i\partial_{\bar{z}}\phi^j\psi_-^k .$$

Notice how the spin of ψ_-^i gets shifted in accordance with Tab. 2.2.

After the twisting the most important thing is that the supercharges Q_- and \bar{Q}_+ become scalars in the case of A-twist, while the supercharges \bar{Q}_+ and \bar{Q}_- become scalars in the case of B-twist. So we can define the following combinations

$$\text{A-twist: } Q_A = \bar{Q}_+ + Q_-, \quad (2.28)$$

$$\text{B-twist: } Q_B = \bar{Q}_+ + \bar{Q}_-, \quad (2.29)$$

which are the scalar fermionic (Grassmannian) symmetry charges we have been looking for!

Now let us denote $Q = Q_A$ or Q_B and explore the topological nature of the new theory. We

define in the new theory *physical* operators \mathcal{O}_i to be those which commute with Q , and call them Q -closed. Since the action of the theory is Q invariant, we can show that all the operators which are Q -exact, i.e., the operators which can be written as commutators of Q , decouple from physical observables. For instance, if

$$\mathcal{O}' = [Q, G] ,$$

then

$$\langle \mathcal{O}' \mathcal{O}_1 \dots \mathcal{O}_s \rangle = \langle [Q, G] \mathcal{O}_1 \dots \mathcal{O}_s \rangle = -\langle G [Q, \mathcal{O}_1 \dots \mathcal{O}_s] \rangle = 0 .$$

Since the symmetry charge Q is nilpotent,

$$Q^2 = 0 , \tag{2.30}$$

Q -exact operators are necessarily Q -closed. Therefore physical operators are actually one-to-one correspondent with the elements of the Q -cohomology group

$$H_Q = \frac{\{Q\text{-closed operators}\}}{\{Q\text{-exact operators}\}} . \tag{2.31}$$

If in addition the energy-momentum tensor⁵ $T_{\mu\nu}^{\text{twisted}}$ is Q -exact

$$T_{\mu\nu}^{\text{twisted}} = \{Q, G_{\mu\nu}\} , \tag{2.32}$$

correlation functions of physical operators are independent of the metric h of the 2d Euclidean spacetime, because

$$\delta_h \langle \mathcal{O}_1 \dots \mathcal{O}_s \rangle = \frac{1}{4\pi} \int \sqrt{h} d^x \delta h^{\mu\nu} \langle T_{\mu\nu} \mathcal{O}_1 \dots \mathcal{O}_s \rangle ,$$

while as a Q -exact operator $T_{\mu\nu}$ decouples from all the physical operators. A topological quantum field theory defined in this way, i.e., through a fermionic symmetry operator, is called topological quantum field theory of the Witten type. Note that since the action of the theory manifestly contains the metric, it is topological only at the quantum level but not at the classical level. It has been shown in ref. [32] for the on-shell case and in ref. [35] for the off-shell case that the energy momentum tensor $T_{\mu\nu}^{\text{twisted}}$ in the supersymmetric nonlinear sigma model with either A-twist or B-twist is Q -exact. Let us discuss the two types of topological twists in a little more detail. We will follow closely the discussions in refs. [31, 36].

2.1.3 Topological A-Twist

After the topological A-twist, by looking at Tab. 2.2 we know that the fermionic fields ψ_- and $\bar{\psi}_+$ become scalars, while ψ_+ and $\bar{\psi}_-$ with spins -1 and $+1$ are now antiholomorphic and

⁵ Note earlier in this subsection we have pointed out the Lagrangian of the sigma model is changed after the twist, and therefore so is the energy-momentum tensor.

holomorphic 1-forms⁶. We rename the fields to make the new spins manifest,

$$\begin{aligned}\chi^i &:= \psi_-^i, & \chi^{\bar{i}} &:= \overline{\psi}_+^{\bar{i}}, \\ \rho_z^{\bar{i}} &:= \overline{\rho}_-^{\bar{i}}, & \rho_{\bar{z}}^i &:= \psi_+^i.\end{aligned}\tag{2.33}$$

Then the action can be obtained, as discussed in the previous subsection, by modifying eq. (2.16) with a coupling term between the vector R-symmetry current and the spin connection after Wick rotation and integrating out fields F^i to make the action on shell,

$$S_A = \int d^2z \left(g_{i\bar{j}} \left(\frac{1}{2} \partial_z \phi^i \partial_{\bar{z}} \overline{\phi}^{\bar{j}} + \frac{1}{2} \partial_{\bar{z}} \phi^i \partial_z \overline{\phi}^{\bar{j}} - i \rho_z^{\bar{j}} D_{\bar{z}} \chi^i + i \rho_{\bar{z}}^i D_z \chi^{\bar{j}} \right) - \frac{1}{2} R_{i\bar{k}j\bar{l}} \rho_z^i \chi^j \rho_{\bar{z}}^{\bar{k}} \chi^{\bar{l}} \right).\tag{2.34}$$

Since we are now only concerned with the supersymmetry transformation induced by

$$Q_A = \overline{Q}_+ + Q_- ,$$

accordingly to the correspondence in eq. (2.17) the supersymmetry transformation laws can be deduced from the generic transformation laws eqs. (2.15) with the restriction $\epsilon_- = \bar{\epsilon}_+ = 0$ and $\epsilon_+ = \bar{\epsilon}_- =: \epsilon$,

$$\begin{aligned}\delta \phi^i &= \epsilon \chi^i, & \delta \overline{\phi}^{\bar{i}} &= \epsilon \chi^{\bar{i}}, \\ \delta \rho_z^i &= 2i\epsilon \partial_{\bar{z}} \phi^i + \epsilon \Gamma_{j\bar{k}}^i \rho_z^j \chi^{\bar{k}}, & \delta \chi^{\bar{i}} &= 0, \\ \delta \chi^i &= 0, & \delta \rho_z^{\bar{i}} &= -2i\epsilon \partial_z \overline{\phi}^{\bar{i}} + \epsilon \Gamma_{j\bar{k}}^{\bar{i}} \rho_z^{\bar{k}} \chi^{\bar{j}}.\end{aligned}\tag{2.35}$$

When this theory is quantized, as argued at the end of the last subsection, it is a topological quantum field theory of the Witten type, independent of the metric of the worldsheet. Furthermore it was argued in ref. [32] that correlation functions computed in this theory are independent of the complex structure moduli of the target space X as well, and they only depend on the complexified Kähler moduli of X . This will become clear later in the discussion of these correlation functions.

The physical operators in this theory are the combinations of the fields which commute with Q_A . Using the Q_A -symmetry transformation laws (2.35) one can convince himself/herself that the following combination

$$\omega_{i_1 \dots i_p \bar{j}_1 \dots \bar{j}_q}(\phi) \chi^{i_1} \dots \chi^{i_p} \chi^{\bar{j}_1} \dots \chi^{\bar{j}_q},\tag{2.36}$$

is a physical operator as long as

$$\omega_{i_1 \dots i_p \bar{j}_1 \dots \bar{j}_q}(\phi) dz^{i_1} \dots dz^{i_p} d\bar{z}^{\bar{j}_1} \dots d\bar{z}^{\bar{j}_q}$$

is a d -closed form of degree (p, q) . The correspondence between physical operators and d -closed forms is no coincidence, since if we identify χ^i with dz^i and recall that ϕ^i are holomorphic coordinates on X , the Q_A -symmetry variations in (2.35) look exactly like the action of the exterior differential operator d . In other words the operator Q_A can be identified with the differential operator d , and therefore the Q_A cohomology group, which is equivalent with the set of all physical operators, is isomorphic to the de Rham cohomology group of the target

⁶ Similarly in a gauge field theory the gauge fields with spin 1 are interpreted as 1-forms.

space X ,

$$\{\text{physical operators}\} \cong H_{Q_A} \cong H_{DR}^*(X) . \quad (2.37)$$

A correlation function of physical operators \mathcal{O}_i is given by

$$\langle \mathcal{O}_1 \cdots \mathcal{O}_s \rangle = \int \mathcal{D}\phi \mathcal{D}\chi \mathcal{D}\rho e^{-S_A} \mathcal{O}_1 \cdots \mathcal{O}_s . \quad (2.38)$$

As pointed out in the beginning of section 2.1.2, because of the presence of the fermionic symmetry Q_A , the computation of the partition function localizes to the vicinities of the fixed loci of the symmetry transformations of Q_A . By looking at the right hand side of eqs. (2.35), it is clear the fixed loci are given by

$$\partial_z \phi^i = \partial_z \bar{\phi}^{\bar{i}} = 0 ; \quad (2.39)$$

in other words, the map $\phi : \Sigma \rightarrow X$ has to be holomorphic. They are called *worldsheet instantons*. Denote the homology class of the image $\phi(\Sigma)$ in X by $\beta \in H_2(X, \mathbb{Z})$. At these loci, the bosonic part of the action becomes,

$$\begin{aligned} S_{A, \text{bosonic}} &= \int_{\Sigma} \frac{1}{2} g_{i\bar{j}} (\partial_z \phi^i \partial_z \bar{\phi}^{\bar{j}} + \partial_{\bar{z}} \phi^i \partial_{\bar{z}} \bar{\phi}^{\bar{j}}) d^2 z \\ &= \int_{\Sigma} g_{i\bar{j}} \partial_z \phi^i \partial_z \bar{\phi}^{\bar{j}} d^2 z + \int_{\Sigma} \phi^* \omega = \int_{\Sigma} \phi^* \omega = \omega \cdot \beta , \end{aligned}$$

where ω is the Kähler form, and $\phi^* \omega$ its pullback to the worldsheet. So the bosonic part of the action simply measures the size of the holomorphic image of the worldsheet. We can decompose the homology class β in terms of a basis $\{S_i\}$ of the homology group $H_2(X, \mathbb{Z})$

$$\beta = \sum_{i=1}^{b_2(X)} n_i S_i , \quad (2.40)$$

and write the bosonic action as $\sum_i n_i t_i$, with

$$t_i = \int_{S_i} \omega , i = 1, \dots, b_2(X) , \quad (2.41)$$

the Kähler moduli of the target space X .

Furthermore one can use the two $U(1)$ R-symmetries to derive selection rules for the correlation functions, which read, that the correlation function (2.38) vanishes unless

$$\sum_{i=1}^s p_i = \sum_{i=1}^s q_i = \dim X(1 - g) + c_1(X) \cdot \beta , \quad (2.42)$$

where p_i and q_i are the holomorphic and antiholomorphic degrees of the operator \mathcal{O}_i , and g is the genus of the worldsheet. In the case that X is a Calabi–Yau manifold, the right hand side of the selection rule is reduced to $\dim X(1 - g)$, and it is only positive if $g = 0$. Therefore the correlation function (2.38) only receives contributions from holomorphic maps from genus 0 worldsheet into the target space X .

Let us suppose for the moment that the target space X is a Calabi–Yau manifold of complex

dimension three, and a physical operator \mathcal{O}_i has degrees $(1, 1)$. Then the operator \mathcal{O}_i corresponds to a d -closed $(1, 1)$ form ω_i , whose Poincaré dual is a divisor D_i in X . With a bit of careful analysis one can show that

$$\langle \mathcal{O}_1 \mathcal{O}_2 \mathcal{O}_3 \rangle = (D_1 \cap D_2 \cap D_3) + \sum_{\beta} I_{0,3,\beta}(\omega_1, \omega_2, \omega_3) Q^{\beta} , \quad (2.43)$$

where the first term is the classical intersection number of the three divisors, while in the second term Q^{β} denotes $\prod_i Q_i^{n_i} = e^{-\sum_i n_i t_i}$. The coefficient $I_{0,3,\beta}(\omega_1, \omega_2, \omega_3)$ counts the number of holomorphic maps of genus 0 worldsheet Σ into a two cycle of homology class β such that the three points x_1, x_2, x_3 on the worldsheet where the local operators $\mathcal{O}_1, \mathcal{O}_2, \mathcal{O}_3$ are inserted are mapped into the divisors D_1, D_2, D_3 respectively. Furthermore one can show that

$$I_{0,3,\beta}(\omega_1, \omega_2, \omega_3) = N_{0,\beta} \int_{\beta} \omega_1 \int_{\beta} \omega_2 \int_{\beta} \omega_3 , \quad (2.44)$$

where $N_{0,\beta}$ simply counts the number of holomorphic maps from genus 0 worldsheet into the homology class β in X , and they are called the genus 0 *Gromov–Witten* invariants. They can be collected in the A–model *prepotential*

$$\mathcal{F}_0(t) = \sum_{0,\beta} N_{0,\beta} Q^{\beta} . \quad (2.45)$$

Note that if we choose \mathcal{O}_i so that the associated divisors D_i are the basis elements S_i in the homology group $H_2(X, \mathbb{Z})$, the dual Poincaré cohomology classes ω_i satisfy

$$\int_{S_i} \omega_j = \delta_{ij} ,$$

and as a consequence

$$\int_{\beta} \omega_i = \sum_j n_j \int_{S_j} \omega_i = n_i .$$

It is easy to see then the three–point correlation function and the prepotential are related by

$$\langle \mathcal{O}_1 \mathcal{O}_2 \mathcal{O}_3 \rangle = (D_1 \cap D_2 \cap D_3) - \frac{\partial^3 \mathcal{F}_0}{\partial t_1 \partial t_2 \partial t_3} . \quad (2.46)$$

Finally we comment that from eqs. (2.43), (2.44) the correlation functions only depend on the Kähler moduli of the target space.

2.1.4 Topological B–Twist

After the B–twist, as seen in Tab. 2.2, the fermionic fields $\bar{\psi}_+$ and $\bar{\psi}_-$ become scalars, while ψ_+ and ψ_- with spins -1 and $+1$ are now antiholomorphic and holomorphic 1-forms respectively. It is more convenient to redefine the fields as

$$\begin{aligned} \bar{\psi}_- + \bar{\psi}_+ &= -\eta^{\bar{i}}, & \bar{\psi}_- - \bar{\psi}_+ &= g^{\bar{i}j} \theta_j \\ \rho_z^i &= \psi_-^i, & \rho_{\bar{z}}^i &= \psi_+^i . \end{aligned} \quad (2.47)$$

Then given the symmetry charge

$$Q_B = \bar{Q}_+ + \bar{Q}_- ,$$

the Q_B symmetry transformation laws are derived from the generic supersymmetry transformation laws eqs. (2.15) by demanding $\epsilon_+ = \epsilon_- = 0$ and $\bar{\epsilon}_+ = \bar{\epsilon}_- =: \bar{\epsilon}$,

$$\begin{aligned} \delta\phi^i &= 0, \quad \delta\theta_i = 0 , \\ \delta\bar{\phi}^{\bar{i}} &= \bar{\epsilon}\eta^{\bar{i}}, \quad \delta\eta^{\bar{i}} = 0 , \\ \delta\rho_\mu^i &= \pm 2i\bar{\epsilon}\partial_\mu\phi^i . \end{aligned} \tag{2.48}$$

Since the axial R-symmetry has quantum anomaly proportional to $c_1(X)$ and the B-twist is performed by using the axial R-charge F_A , the quantum nonlinear sigma model of B-twist is only well-defined if the target space X is a Calabi-Yau manifold. It was seen at the end of subsection 2.1.2 that after quantization this nonlinear sigma model is a topological quantum field theory of the Witten type, and it was further argued in [32], as opposed to the case of A-twist, the theory only depends on the complex structure moduli of the target space X but not the Kähler moduli. This will also become clear later in the discussion of correlation functions.

The physical operators in this case are those which commute with Q_B . It can be shown that the combination

$$\omega_{\bar{i}_1 \dots \bar{i}_p}^{j_1 \dots j_q}(\phi) \eta^{\bar{i}_1} \dots \eta^{\bar{i}_p} \theta_{j_1} \dots \theta_{j_q} \tag{2.49}$$

is a physical operator if the associated antiholomorphic p -form with values in $\wedge^q TX$

$$\omega_{\bar{i}_1 \dots \bar{i}_p}^{j_1 \dots j_q}(\phi) d\bar{z}^{\bar{i}_1} \dots d\bar{z}^{\bar{i}_p} \frac{\partial}{\partial z^{j_1}} \dots \frac{\partial}{\partial z^{j_q}} \tag{2.50}$$

is closed under the action of $\bar{\partial}$. Again the connection of physical operators to $\bar{\partial}$ -closed forms is no coincidence. With $\eta^{\bar{i}}$ identified with $d\bar{z}^{\bar{i}}$ and $\bar{\phi}^{\bar{i}}$ recognized as the antiholomorphic coordinates on X , the equivalence between Q_B and $\bar{\partial}$ is obvious. Therefore the Q_B cohomology group, which is the collection of all physical operators, is isomorphic to the Dolbeault cohomology group

$$\bigoplus_{p,q=0}^n H^{0,p}(X, \wedge^q TX) , \tag{2.51}$$

where $n = \dim X$.

A correlation function of the physical operators \mathcal{O}_i is given by

$$\langle \mathcal{O}_1 \dots \mathcal{O}_s \rangle = \int \mathcal{D}\phi \mathcal{D}\eta \mathcal{D}\theta e^{-S_B} \mathcal{O}_1 \dots \mathcal{O}_s . \tag{2.52}$$

One can again use the vector and axial R-symmetries to derive selection rules, which read, that the correlation functions vanish unless

$$\sum_{i=1}^s p_i = \sum_{i=1}^s q_i = \dim X(1-g) . \tag{2.53}$$

The selection rules are only non-trivially satisfied if the genus g of worldsheet is 0. Furthermore the correlation function localizes to the small neighborhoods of fixed loci of Q_B transformation.

The fixed loci according to eqs. (2.48) satisfy

$$\partial_\mu \phi^i = 0, \quad (2.54)$$

in other words, they correspond to constant maps $\phi : \Sigma \rightarrow X$ which map the worldsheet to a point in X . As a consequence the path integral in the correlation function is reduced to an integral over the Calabi–Yau manifold X .

Let us choose physical operators \mathcal{O}_i which correspond to elements μ_i in $H^{0,1}(X, TX)$

$$\mu_i = (\mu_i)_{\bar{j}}^k d\bar{z}^{\bar{j}} \frac{\partial}{\partial z^k}. \quad (2.55)$$

Such a differential form is called a *Beltrami differential*, and it can be used to infinitesimally deform the complex structure of X^7 ; in other words, it is a tangent vector on the complex structure moduli space of X . Then the integral over X can be obtained by

$$\langle \mathcal{O}_1 \cdots \mathcal{O}_s \rangle = \int_X \langle \mu_1 \wedge \cdots \wedge \mu_s, \Omega \rangle \wedge \Omega = \int_X (\mu_1)_{\bar{j}_1}^{k_1} \cdots (\mu_s)_{\bar{j}_s}^{k_s} \Omega_{k_1 \cdots k_s} d\bar{z}^{\bar{j}_1} \wedge \cdots \wedge d\bar{z}^{\bar{j}_s} \wedge \Omega, \quad (2.56)$$

where $\Omega = \Omega_{k_1 \cdots k_s} dz^{k_1} \cdots dz^{k_s}$ is the nowhere–vanishing holomorphic $(n, 0)$ form on the Calabi–Yau manifold X . This formula clearly demonstrates that the correlation functions only depend on the complex structure moduli of the target space.

2.1.5 A Diversion: Complex Structure Moduli Space of Calabi–Yau Threefold

From the discussion in the previous subsection, we already saw that the correlation functions $\langle \mathcal{O}_1 \cdots \mathcal{O}_s \rangle$ in the B–twisted supersymmetric nonlinear sigma model only depends on the complex structure moduli of the Calabi–Yau manifold X . Here we suppose the target space X has complex dimension three, and discuss the special geometry property of the complex structure moduli space of the Calabi–Yau threefold X [37, 38], after which we can make it more explicit the relation between the B–twisted supersymmetric nonlinear sigma model and the complex structure moduli space of X .

The homology group $H_3(X, \mathbb{Z})$ of X is an integral lattice with integral intersection numbers between its elements. We choose a symplectic basis $\mathcal{A}^I, \mathcal{B}_J, I, J = 0, \dots, h^{2,1}$ of $H_3(X, \mathbb{Z})$ such that the (oriented) intersection numbers are

$$\mathcal{A}^I \cap \mathcal{B}_J = -\mathcal{B}_J \cap \mathcal{A}^I = \delta_J^I, \quad \mathcal{A}^I \cap \mathcal{A}^J = \mathcal{B}_I \cap \mathcal{B}_J = 0. \quad (2.57)$$

Here $h^{2,1} = \dim H^{2,1}(X)$. A different symplectic basis $\mathcal{A}'^I, \mathcal{B}'_J$ of $H_3(X, \mathbb{Z})$ can be obtained by a symplectic transformation,

$$\begin{pmatrix} \mathcal{B}'_J \\ \mathcal{A}'^I \end{pmatrix} = \begin{pmatrix} A & B \\ C & D \end{pmatrix} \begin{pmatrix} \mathcal{B}_J \\ \mathcal{A}^I \end{pmatrix}, \quad M = \begin{pmatrix} A & B \\ C & D \end{pmatrix} \in Sp(2h^{2,1} + 2, \mathbb{Z}). \quad (2.58)$$

The Poincaré dual cohomology classes of the three cycles $\mathcal{A}^I, \mathcal{B}_J$ are denoted by α_I, β^J , and

⁷ In fact even for an arbitrary smooth complex geometry, which may not be a Calabi–Yau manifold, one can use its Beltrami differentials to infinitesimally deform its complex structure. We will later use them to deform the complex structure of a Riemann surface in section 2.2.1.

they satisfy

$$\int_{\mathcal{A}^J} \alpha_I = \int_X \alpha_I \wedge \beta^J = \delta_I^J, \quad \int_{\mathcal{B}_J} \beta^I = \int_X \beta^I \wedge \alpha_J = -\delta_J^I. \quad (2.59)$$

We also define the *A-periods* and *B-periods* of the holomorphic $(3, 0)$ form Ω by

$$X^I = \int_{\mathcal{A}^I} \Omega, \quad F_I = \int_{\mathcal{B}_I} \Omega. \quad (2.60)$$

Then the *period matrix*

$$\underline{\tau} := \tau_{IJ} = \frac{\partial}{\partial X^J} F_I \quad (2.61)$$

can be used to characterize the complex structure of the Calabi–Yau threefold X . It is the direct analog of the elliptic modulus τ of a torus, which itself is a complex one dimensional Calabi–Yau manifold,

$$\tau = \omega_1 / \omega_2.$$

Here ω_1 and ω_2 are two periods of the torus. Note a symplectic transformation $M \in Sp(2h^{2,1} + 2, \mathbb{Z})$ transforms the period matrix τ_{IJ} by

$$\underline{\tau}' = (A\underline{\tau} + B)(C\underline{\tau} + D)^{-1}. \quad (2.62)$$

The old and new period matrices describe the same complex structure.

On the other hand, the A-periods X^I can serve as projective coordinates on the complex structure moduli space \mathcal{M}_X [39]. Since the multiplication of Ω by a nonvanishing complex number is still a holomorphic $(3, 0)$ form on X , X^I are actually homogeneous coordinates on \mathcal{M}_X , and the latter has complex dimension $h^{2,1}$. We define the following affine coordinates (normalized A-periods)

$$t^i = \frac{X^i}{X^0}, \quad i = 1, \dots, h^{2,1}. \quad (2.63)$$

It is consistent with the fact that an infinitesimal deformation⁸ of the complex structure is induced by a Beltrami differential. The number of Beltrami differentials is $\dim H^{0,1}(X, TX)$, which is equal to $h^{2,1}$ due to the following one-to-one map

$$\mu_i = (\mu_i)_j^k d\bar{z}^j \frac{\partial}{\partial k} \mapsto \chi_i = (\mu_i)_j^k \Omega_{kmn} d\bar{z}^j \wedge dz^m \wedge dz^n. \quad (2.64)$$

In fact after an infinitesimal deformation of the complex structure of X along the direction of t^i , the holomorphic form Ω changes by

$$\frac{\partial}{\partial t^i} \Omega = K_i \Omega + \chi_i \in H^{3,0}(X) + H^{2,1}(X), \quad (2.65)$$

where K_i only depends on the coordinates t_i , while χ_i is precisely the $(2, 1)$ form in eq. (2.64).

Since the A-periods X^I alone already suffice to parametrize the complex structure moduli space \mathcal{M}_X , the B-periods F_J have to be functions of X^I , and so are the components of the

⁸ One may worry about whether there is any obstruction from an infinitesimal deformation to a finite one of the complex structure of X so that the dimension of \mathcal{M}_X is smaller than $h^{2,1}$. However it was shown for instance in [40, 41] that a unique finite deformation can always be found from an infinitesimal one for a Calabi–Yau threefold.

period matrix τ_{IJ} . τ_{IJ} is in fact a collection of multivalued functions. They are singular on the moduli space \mathcal{M}_X along divisors where a period vanishes, indicating that the underlying three cycle ν has shrunk to zero. When parallel transported around the singular divisor back to the original point on \mathcal{M}_X , the three cycles undergo the linear transformation according to the Picard–Lefschetz formula (see for example [42, 43])

$$M_\nu : \gamma \rightarrow \gamma - (\gamma \cap \nu)\nu , \quad (2.66)$$

where $\gamma \cap \nu$ is the intersection number of the two 3–cycles γ and ν . The corresponding periods undergo the same linear transformation, and it is called the monodromy of the periods around the singular divisor. Furthermore the moduli space \mathcal{M}_X can have orbifold singularities. The periods when parallel transported around a divisor of orbifold singularity also undergo a monodromy. Since the complex structure of X is uniquely defined at the each point on the moduli space, the monodromies must be symplectic transformations. As a consequence the monodromies around all the singular divisors of \mathcal{M}_X generate a subgroup Γ of the symplectic group $Sp(2h^{2,1} + 2, \mathbb{Z})$ and it is called the modular group of the model.

Using the definition of the periods in eqs. (2.60) one can decompose the holomorphic 3–form Ω as

$$\Omega = X^I \alpha_I - F_J (X^J) \beta^J . \quad (2.67)$$

On the other hand the deformation formula eq. (2.65) implies

$$\int_X \Omega \wedge \partial_I \Omega = 0 . \quad (2.68)$$

Combining these two facts one finds

$$F_I (X^J) = \frac{1}{2} \frac{\partial}{\partial X^I} (X^J F_J) . \quad (2.69)$$

In other words all the B–periods can be written as the derivatives of a single holomorphic function

$$F = \frac{1}{2} X^J F_J \quad (2.70)$$

which is called the *prepotential* of the complex structure moduli space. Besides since

$$2F = X^I \frac{\partial F}{\partial X^I} \quad (2.71)$$

it is a homogeneous function of degree 2. So we can define

$$\mathcal{F}_0(t) = \frac{1}{(X^0)^2} F(X) \quad (2.72)$$

which only depends on the affine coordinates $t^i, i = 1, \dots, h^{2,1}$.

Now we can state the relation between the correlation functions in the B–twisted supersymmetric nonlinear sigma model and the prepotential of the complex structure moduli space of the Calabi–Yau threefold X . According to the selection rule eq. (2.53), only three–point correlation functions do not vanish. With a bit of work one can show they are related to the prepotential

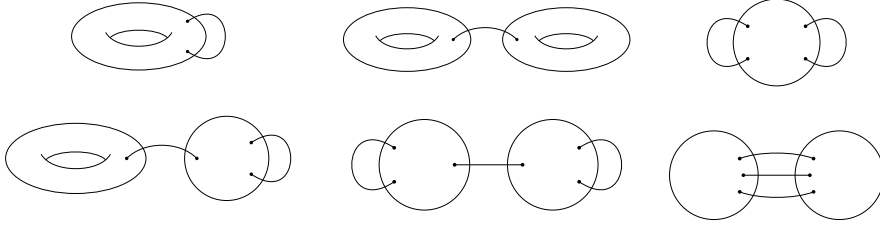


Figure 2.1: All possible stable degenerations of a genus two Riemann surface. Here we represent a double point by two marked points connected through a line.

by

$$\langle \mathcal{O}_1 \mathcal{O}_2 \mathcal{O}_3 \rangle = \frac{\partial^3 \mathcal{F}_0(t)}{\partial t_1 \partial t_2 \partial t_3}. \quad (2.73)$$

2.2 Topological String Theory

2.2.1 General Ideas

In the discussion in the last section of the topologically twisted supersymmetric nonlinear sigma models, we always fix the metric on the worldsheet. Furthermore the two topological sigma models appear to be a bit boring as the correlation functions, according to the selection rules (2.42) and (2.53), can only have nonvanishing values if the genus of the worldsheet is zero and only for certain types of operator insertions. It would be more interesting if this were not the case. Besides, computations in a full-fledged string theory would require summing over worldsheets of all genera, just like one has to sum over all loop diagrams in a quantum field theory, and for each genus g integrating over the moduli space \mathcal{M}_g of the corresponding Riemann surface. In other words we have to couple the 2d topological sigma model to 2d gravity where the metric of the worldsheet is allowed to vary.

This was achieved by exploiting the similarity between topological nonlinear sigma models and bosonic string theory noticed in refs. [44–46]. Let Σ_g be a Riemann surface of genus g . One defines the genus $g \geq 1$ *free energy* of topological string theory by [47]

$$F_g = \int_{\mathcal{M}_g} \langle \prod_{k=1}^{6g-6} (G, \mu_k) \rangle, \quad (2.74)$$

where

$$(G, \mu_k) = \int_{\Sigma_g} d^2z (G_{zz}(\mu_k)_{\bar{z}^z} + G_{\bar{z}\bar{z}}(\bar{\mu}_k)_z^{\bar{z}}), \quad (2.75)$$

while the genus 0 free energy is simply identified with the prepotentials defined in the A- and B-twisted nonlinear sigma models respectively.

This definition needs some explanation. Eq. (2.74) is manifestly an integration over the moduli space \mathcal{M}_g of Σ_g with the measure constructed from the Beltrami differential⁹ $\mu_k = (\mu_k)_{\bar{z}^z} d\bar{z} \partial_z$ on \mathcal{M}_g . Since the moduli space of Σ_g has real dimension $6g - 6$, one needs a product of $6g - 6$ copies of the Beltrami differentials to construct a volume form. The integration domain in eq. (2.74) is actually larger than the moduli space \mathcal{M}_g of smooth Riemann surface of genus g .

⁹ Note this is not the Beltrami differential of the target space used in the previous section.

The *compactified moduli space* $\overline{\mathcal{M}}_g$ includes all the stable degenerations of the Riemann surface Σ_g as well [48]. A *stable degeneration* of the Riemann surface Σ_g is a collection of Riemann surfaces of lower genera connected to each other through double points such that

- the total genus of the collection is g , and
- each component Riemann surface is stable¹⁰, namely it belongs to one of the following three cases: a Riemann sphere touching other components or itself at three or more points, a torus touching other components or itself at one or more points, a Riemann surface of genus greater than one.

As an example, all possible stable degenerations of a genus two Riemann surface are listed in Fig. 2.1. The stable degenerations will play a crucial role later in section 2.2.4 and section 2.5.3. Finally in eq. (2.75) G_{zz} is defined in eq. (2.32) the Q -exact condition of the twisted energy momentum tensor $T_{\mu\nu}^{\text{twisted}}$, and it depends on the concrete topological nonlinear sigma model in question. The topological string theory constructed from A-twisted and B-twisted topological nonlinear sigma models are called type A and type B topological string theories respectively. As their names suggest, they are related to type IIA and type IIB superstring theories respectively. The moduli space of type A (type B) topological string are identified with the vector multiplet moduli space of the type IIA (type IIB) superstring compactified on the Calabi–Yau threefold. The vector moduli space of type IIA superstring theory is the (complexified) Kähler moduli space of the target space corrected by \mathbb{P}^1 worldsheet instantons, whose contributions are suppressed in the large volume limit; the moduli space of type IIB superstring theory is the complex structure moduli space of the target space without quantum corrections (see for instance [49]). This is consistent with the moduli dependence of the two topological nonlinear sigma models from which the topological strings are constructed.

Similar to the case in genus 0, the correlation functions of an arbitrary genus can be computed through the free energy of the same genus via some covariant derivatives on the Kähler moduli space (complex structure moduli space) of the target space X in the type A (type B) topological string theory [47]

$$\langle \mathcal{O}_1 \cdots \mathcal{O}_s \rangle_g = D_1 \cdots D_s F_g . \quad (2.76)$$

One can also derive selection rules for the correlation functions. Different from eqs. (2.42) and (2.53), now they read¹¹ (see an explanation for instance in [31])

$$\sum_{i=1}^s p_i = \sum_{i=1}^s q_i = (\dim X - 3)(1 - g) + s + c_1(X) \cdot \beta . \quad (2.77)$$

They are now trivially satisfied as long as X is a Calabi–Yau threefold and each operator \mathcal{O}_i has degree $(1, 1)$, even if the genus is greater than zero or the number of insertions is different from three.

In the following we explain briefly what the free energies F_g actually compute and what major methods can be used to compute them in the two topological string theories. We will always assume the target space is a Calabi–Yau threefold. We follow various sources including [31, 36, 47, 50–52].

¹⁰ A Riemann surface which only has finite number of diffeomorphisms is called *stable*. As a counter-example a smooth and isolated Riemann sphere has diffeomorphism group $SL(2, \mathbb{C})$ and is therefore not stable.

¹¹ In the type B theory the last term disappears because the theory is only well-defined if X is a Calabi–Yau manifold.

2.2.2 Type A Closed String

Like the prepotential of the A-twisted topological nonlinear sigma model in eq. (2.45), the free energy \mathcal{F}_g in type A topological string theory localizes to the instanton sectors, which are holomorphic maps of the worldsheet of genus g into the target space X . It has the structure,

$$\mathcal{F}_g(t) = \sum_{\beta} N_{g,\beta} Q^\beta. \quad (2.78)$$

Here $N_{g,\beta}$ counts in an appropriate sense¹² the number of holomorphic maps of the worldsheet Σ_g of genus g into the homology class $\beta \in H_2(X, \mathbb{Z})$ in the target space X . These numbers $N_{g,\beta}$ are called the *Gromov–Witten* invariants, and they have been rigorously defined in mathematics. We can assemble all the \mathcal{F}_g in a formal series

$$\mathcal{F}(g_s, t) = \sum_{g=0}^{\infty} \mathcal{F}_g(t) g_s^{2g-2} \quad (2.79)$$

where the fugacity g_s is also called the string coupling.

Effective methods, such as equivariant localization, have been developed in algebraic geometry to compute the Gromov–Witten invariants [53–55]. $N_{g,\beta}$ can be understood as the result of the integration of some cohomology class ϕ over the moduli space $\overline{\mathcal{M}}_g(X, \beta)$ of (stable) holomorphic maps from Σ_g to the homology class β in X . If the Calabi–Yau threefold X is invariant under some $U(1)$ symmetry, the action of the $U(1)$ symmetry can be lifted to $\overline{\mathcal{M}}_g(X, \beta)$. According to the Atiyah–Bott localization formula, if the cohomology class ϕ is compatible (equivariant) with the $U(1)$ action¹³, the integration can be localized to the fixed loci of the $U(1)$ action on $\overline{\mathcal{M}}_g(X, \beta)$. Note the idea of equivariant localization is similar in spirit but still quite different from the localization of partition function in the presence of a fermionic symmetry in physics. Such $U(1)$ symmetries exist abundantly in a category of geometries called *toric geometries*, and when the target space is a toric geometry the equivariant localization techniques for computing the Gromov–Witten invariants become particularly powerful [57–59].

A toric geometry¹⁴ X of complex dimension three contains as a dense open set $(\mathbb{C}^*)^3$ which naturally enjoys $U(1)^3$ symmetry, and the $U(1)^3$ symmetry can be extended over the entirety of X . In other words X is a superset of $(\mathbb{C}^*)^3$, and each point in the complement, which necessarily has lower dimension, can be realized as the limit point of some one-parameter $U(1)$ subgroup of $U(1)^3$. Each toric geometry X is associated with $n - 3$ charge vectors \vec{Q}^a , $a = 1, \dots, n - 3$ of dimension $n > 3$. Then X is the submanifold of \mathbb{C}^n constrained by

$$\sum_{i=1}^n Q_i^a |x_i|^2 = r^a, \quad a = 1, \dots, n - 3 \quad (2.80)$$

¹² Precisely speaking they count the number of *stable* holomorphic maps, such that the worldsheet Σ_g can be degenerate, and only stable components of Σ can be mapped to a point in X . These maps are called stable because there are only finite number of diffeomorphisms of them.

¹³ We refer to, for example refs. [31, 56], for the precise meaning of the equivariant cohomology and the Atiyah–Bott formula.

¹⁴ The canonical reference on toric geometry is [60], while refs. [31, 56, 61, 62] provide excellent reviews on toric geometry for physicists.

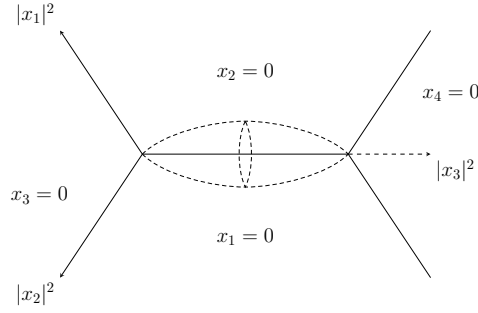


Figure 2.2: Toric diagram of $\mathcal{O}(-1) \oplus \mathcal{O}(-1) \rightarrow \mathbb{P}^1$. The base \mathbb{P}^1 as indicated by the dashed lines is an S^1 fibration over the bounded edge in the center.

modulo the $U(1)^{n-3}$ gauge symmetry with real gauge parameters ϵ_a

$$x_i \rightarrow e^{i\epsilon_a Q_i^a} x_i, \quad i = 1, \dots, n. \quad (2.81)$$

Without loss of generality we can assume $r^a \geq 0$ in eq. (2.80), and they characterize the sizes of two-dimensional submanifolds of X . Furthermore \mathbb{C}^n naturally has $U(1)^n$ symmetry. After gauging $U(1)^{n-3}$ the toric geometry X indeed has $U(1)^3$ symmetry left.

One can draw the *toric diagram* Υ_X of X by projecting X onto the base space $B \subset \mathbb{R}^3$ parametrized by $|x_1|^2$, $|x_2|^2$, and $|x_3|^2$ to help visualizing the fixed loci of the $U(1)$ actions. On the one hand X can be regarded as $T^3 = U(1)^3$ fibration over Υ_X whose fibers are the leftover $U(1)^3$ rotations on the phases of x_i . On the other hand, the conditions $|x_i|^2 \geq 0, i = 1, \dots, n$ determine that Υ_X is partially bounded with faces, edges, and vertices, which are various fixed loci of the $U(1)^3$ actions. A face is given by $|x_i|^2 = 0$ for some x_i . It is therefore the fixed loci of the linear combination of $U(1)$ s acting solely on the phase of x_i , and the fiber over the face degenerates to T^2 . Two faces intersect at an edge, over which the T^3 fiber degenerates to S^1 . Over a vertex the T^3 fiber degenerates completely.

Consider a toric geometry X which is also a Calabi–Yau threefold. The Calabi–Yau condition is equivalent to requiring $\sum_i Q_i^a = 0$ for each charge vector. It implies due to eq. (2.80) there are unbounded directions and X is therefore called a noncompact Calabi–Yau threefold. One simple example is the double line bundle $\mathcal{O}(-1) \oplus \mathcal{O}(-1) \rightarrow \mathbb{P}^1$ which has a single charge vector $\vec{Q} = (-1, -1, 1, 1)$, and therefore the defining equation

$$|x_3|^2 + |x_4|^2 - |x_1|^2 - |x_2|^2 = r, \quad r > 0. \quad (2.82)$$

The corresponding toric diagram is given in Fig. 2.2. The base space $\mathbb{P}^1 = S^2$ of the double line bundle is located at $x_1 = x_2 = 0$ where eq. (2.82) is reduced to the sphere equation $|x_3|^2 + |x_4|^2 = r$. Let z and $z' = 1/z$ be the local affine coordinates in the north and south coordinate patches of the \mathbb{P}^1 . We note here that the coordinates ϕ and ϕ' on the fiber of a generic line bundle $\mathcal{O}(n) \rightarrow \mathbb{P}^1$ in the two coordinate patches are related by the transition function

$$\phi' = z^{-n} \phi. \quad (2.83)$$

Since it will be important later in section 2.4.5, we point out here that the smooth Calabi–Yau threefold $\mathcal{O}(-1) \oplus \mathcal{O}(-1) \rightarrow \mathbb{P}^1$ is the *small resolution* of a singular Calabi–Yau threefold

called *conifold*. A conifold is a hypersurface in \mathbb{C}^4 defined by

$$uv - xy = 0 , \quad (2.84)$$

and it is clearly singular at the origin. One way of removing the singularity is to introduce the variable λ satisfying

$$x = \lambda v, \quad u = \lambda y , \quad (2.85)$$

which are compatible with eq. (2.84). The singular origin of the conifold is now replaced by, or *blown-up* to, a \mathbb{P}^1 for which λ is a local affine coordinate, and eqs. (2.85) describe two $\mathcal{O}(-1)$ bundles over \mathbb{P}^1 whose fibers are parametrized by (x, v) and (u, y) respectively. This is called a small resolution of the conifold singularity.

Let us delve a little bit into the application of the equivariant localization on a toric Calabi–Yau threefold X . The computation of the Gromov–Witten invariant $N_{g,\beta}$ is localized to summing over stable holomorphic maps $f : \Sigma_g \rightarrow X$ which are invariant under the $U(1)$ actions on X . The worldsheet Σ_g may be degenerate with component Riemann surfaces connected to each other through nodal points. A stable holomorphic map requires that genus zero components with ≥ 3 nodal points, genus one components with ≥ 1 nodal point, and higher genera components be mapped to points, while other components be mapped holomorphically to nontrivial 2-cycles in X . An invariant map means the images of the map should be in the fixed loci of the toric action, and therefore can only be either a vertex or the S^1 fibration over an edge in the toric diagram Υ_X . The latter is a \mathbb{P}^1 with two points removed. Each invariant stable holomorphic map can be represented by a graph G consisting of vertices connected through edges. Each vertex v represents a constant map, and it is labelled by (g_v, n_v, σ_v) , where g_v is the genus of a component Riemann surface, n_v is the number of edges connected to v in G , and σ_v is the vertex in Υ_X the component Riemann surface is mapped to. If $(g_v, n_v) = (0, 2)$ or $(0, 1)$ the preimage of the map is actually a nodal point or a smooth point on the Riemann sphere(s) represented by the edge(s) connected to v . Each edge e is labelled by (ϵ_e, d_e) representing a component Riemann sphere with either one or two nodal points mapped holomorphically to (S^1 bundle over) the edge ϵ_e in Υ_X , and the degree of the map is d_e . An example of graph G is given in Fig. 2.3. We denote $\mathcal{G}_{g,0}$ the set of graphs satisfying

$$\sum_v (2 - 2g_v - n_v) = 2 - 2g , \quad (2.86)$$

and in addition $\tilde{\mathcal{G}}_{g,0}$ the set of the same graphs but without degrees on the edges. Next we need to assign to each graph G in $\mathcal{G}_{g,0}$ a weight $w(G)$ which factorizes to the contribution H_{g_v, n_v, σ_v} from each vertex and the contribution F_{ϵ_e, d_e} from each edge [63, 64]. Then the free energy $\mathcal{F}_g(t)$ is computed by summing over the weights of the graphs in $\mathcal{G}_{g,0}$

$$\mathcal{F}_g(t) = \sum_{G \in \mathcal{G}_{g,0}} \frac{1}{\#\text{Aut}(G)} \prod_v H_{g_v, n_v, \sigma_v} \prod_e F_{\epsilon_e, d_e}(t) \quad (2.87)$$

where $\#\text{Aut}(G)$ is the order of the symmetry (automorphism) group of the graph G . The exact expressions of H_{g_v, n_v, σ_v} and $F_{\epsilon_e, d_e}(t)$ can be found in [63, 64] and will not be needed in this thesis. We just comment that the degrees of edges only affect $F_{\epsilon_e, d_e}(t)$ and therefore we can first sum over graphs which only differ by the degrees on the edges, and then sum over graphs \tilde{G} in $\tilde{\mathcal{G}}_{g,0}$. The weights of \tilde{G} still factorize. A similar picture of summing over weighted graphs

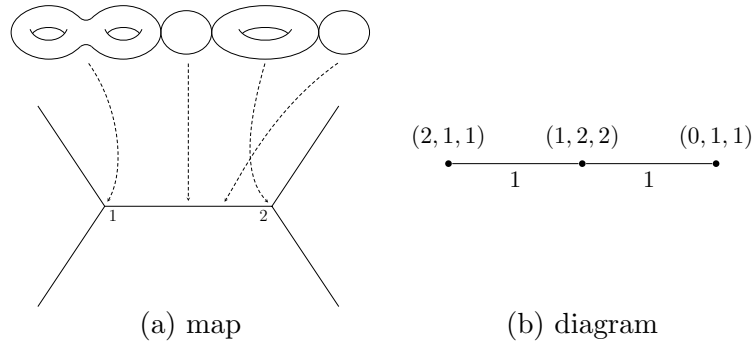


Figure 2.3: An invariant stable holomorphic map from a worldsheet on degenerate Σ_3 to the resolved conifold (represented by its toric digram), and the diagram $G \in \mathcal{G}_{3,0}$ that represents it. Here in G we suppress the ϵ_e symbols on the edges (see text).

in $\tilde{\mathcal{G}}_{g,0}$ will rise again in a completely different context.

The Gromov–Witten invariants computed for instance by equivariant localization are actually fractional numbers instead of integers, which is counter-intuitive since they are enumerative quantities. However two phenomena need to be taken into account. The first is *multicovering*. Given a holomorphic map $f : \mathbb{P}^1 \rightarrow X$ in genus 0 and homology class β , one can immediately construct a holomorphic map in genus 0 and homology class $d\beta$ by composing f with the covering map $\mathbb{P}^1 \rightarrow \mathbb{P}^1$ of degree d . The second phenomenon is *bubbling*. Given a holomorphic map $f : \Sigma \rightarrow X$ in genus g , a map f' in genus g' greater than g can be constructed by attaching to Σ a Riemann surface of genus $g' - g$ which is mapped to a point in X . To count the number of primitive maps one has to subtract in the Gromov–Witten invariants the contributions from multicovering and bubbling. Indeed it was shown in ref. [65] the free energy \mathcal{F}_g has the structure

$$\mathcal{F}(g_s, t) = \sum_{g,d,\beta} \frac{n_{g,\beta}}{d} \left(2 \sin \frac{dg_s}{2} \right)^{2g-2} Q^{d\beta}. \quad (2.88)$$

with *integer* coefficients $n_{g,\beta}$, which are called the *Gopakumar–Vafa* invariants¹⁵. By performing the genus expansion, one can find the Gromov–Witten invariants in terms of the integral Gopakumar–Vafa invariants. The examples of the lowest genera are¹⁶

$$\mathcal{F}_0(t) = \sum_{d=1,\beta} \frac{n_{0,\beta}}{d^3} e^{-d\beta \cdot t}, \quad \mathcal{F}_1(t) = \sum_{d=1,\beta} \frac{1}{d} \left(\frac{n_{0,\beta}}{12} + n_{1,\beta} \right) e^{-d\beta \cdot t}. \quad (2.89)$$

2.2.3 Type A Open String

In the previous subsection we have only considered the holomorphic maps from the worldsheet on Riemann surfaces Σ_g with no boundary to the target space X . We can also consider the theory which maps the worldsheet on Riemann surfaces $\Sigma_{g,h}$ with genus g and h boundary components to X . They correspond to the worldsheet instanton sector of a topological open string theory of type A. The additional question then is what boundary condition the image of the worldsheet has to satisfy. Witten showed in ref. [68] (see also [69, 70]) that the requirement

¹⁵ They are actually BPS indices which count the numbers of bosonic modes minus the numbers of fermionic modes arising from D -branes wrapping holomorphic Riemann surfaces in X . Therefore $n_{g,\beta}$ can be negative.

¹⁶ The genus 0 formula was first found in [66] and later proved in [67].

of Q_A invariance on the boundary demands that the boundary components of the worldsheet be mapped into a Lagrangian submanifold \mathcal{L} with Dirichlet boundary condition. A Lagrangian submanifold on a Calabi–Yau threefold X is a three cycle on which the (complexified) Kähler form ω of X vanishes

$$\omega|_{\mathcal{L}} = 0 . \quad (2.90)$$

The Dirichlet boundary condition simply means the images of the boundary components of the worldsheet cannot move in the transverse direction to the Lagrangian submanifold \mathcal{L} . Therefore, let the boundary components of $\Sigma_{g,h}$ be $C_i, i = 1, \dots, h$, the holomorphic map $\phi : \Sigma_{g,h} \rightarrow X$ should satisfy

$$\phi(C_i) \subset \mathcal{L} . \quad (2.91)$$

In addition, the Grassmannian fields χ and ρ at each boundary C_i should take values in $\phi^*(T_{\mathcal{L}})$, i.e. the pullback ϕ^* of the holomorphic tangent bundle $T_{\mathcal{L}}$ onto $\Sigma_{g,h}$.

As in superstring theory, We can regard the Lagrangian submanifold \mathcal{L} to be wrapped by a D -brane (D for Dirichlet. It is also called a Lagrangian brane) and the two endpoints of the open string have to lie on the D -brane. The perturbative open string propagating on the D -brane induces a $U(1)$ gauge vector field A on the brane. Suppose there are N coincident D -branes wrapping the Lagrangian submanifold \mathcal{L} together, since each endpoint of the open string can lie on any of the N D -branes, a total of $N \times N$ indices arise and the gauge vector field A is enhanced to that of the gauge group $U(N)$. When A is not zero, the path integral for computing free energies should be modified with the insertion of the Wilson loop operator

$$\prod_{i=1}^h \text{Tr P exp} \oint_{C_i} \phi^*(A) . \quad (2.92)$$

Here the trace Tr is always taken in the fundamental representation of $U(N)$.

Let us consider the problem of enumerating holomorphic maps from $\Sigma_{g,h}$ into X with the boundary of $\Sigma_{g,h}$ mapped to the Lagrangian brane \mathcal{L} in X . The holomorphic maps are classified according to two types of data: the first is the homology class $\beta \in H_2(X)$ in the target space the image of $\Sigma_{g,h}$ wraps (bulk data), and the second is the homology class $\gamma \in H_1(\mathcal{L})$ on the brane the image of each boundary component C_i belongs to (boundary data). For the simplest case where $b_1(\mathcal{L}) = 1$, which we will always assume in this thesis, the images of the boundary components C_i are integral multiples of the only generator γ of $H_1(\mathcal{L})$,

$$\phi(C_i) = \omega_i \gamma, \quad \omega_i \in \mathbb{Z}_+ . \quad (2.93)$$

In other words, the boundary component C_i winds around the γ cycle ω_i times.

Given the bulk data β and the boundary data $\omega = (\omega_1, \dots, \omega_h)$ we can analogously define the number $N_{g,\omega,\beta}$ of holomorphic maps of $\Sigma_{g,h}$ (in an appropriate sense) to be the *open Gromov–Witten invariant*. We assemble them into the free energies $\mathcal{F}_{g,\omega}$

$$\mathcal{F}_{g,\omega}(t) = \sum N_{g,\omega,\beta} Q^\beta . \quad (2.94)$$

via the Kähler parameters $Q_i = e^{-t_i}$ and further into a single open topological string free energy \mathcal{F}

$$\mathcal{F}(g_s, t, V) = \sum_{g=0}^{\infty} \sum_{h=1}^{\infty} \sum_{\omega_1, \dots, \omega_h} \frac{i^h}{h!} g_s^{2g-2+h} \mathcal{F}_{g,\omega}(t) \text{Tr } V^{\omega_1} \dots \text{Tr } V^{\omega_h} . \quad (2.95)$$

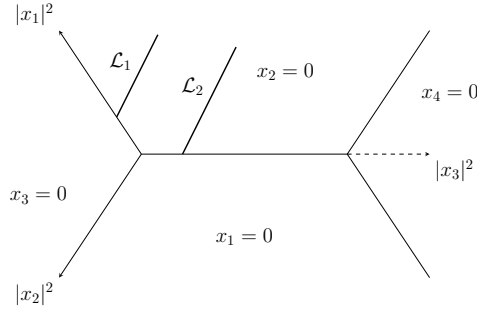


Figure 2.4: Two toric special Lagrangian branes $\mathcal{L}_1, \mathcal{L}_2$ in the resolved conifold X . In the toric diagram Υ_X they are represented by two rays touching the edges of Υ_X .

Here V defined by

$$V = \text{P exp} \oint_{\gamma} A \quad (2.96)$$

is the Wilson loop of the vector field A on the 1-cycle γ in \mathcal{L} . The product of traces is then identical with the operator insertion in eq. (2.92). Note that if the rank N of the gauge group is finite, not all the trace products are independent. In order to distinguish all the instanton sectors, we take the limit $N \rightarrow \infty$. Finally g_s is the string coupling. And we include the factor i^h as in ref. [36] for later convenience.

The open Gromov–Witten invariants have also been computed via the equivariant localization techniques for a special type of Lagrangian branes in toric Calabi–Yau threefolds [71–74]. Let us take a ray $R = \mathbb{R}_+$ in the base space B of the toric Calabi–Yau X touching an edge of its toric diagram Υ_X and construct a Lagrangian submanifold \mathcal{L} by restricting the generic T^3 fiber over R to T^2 via the Lagrangian condition

$$\omega = i \sum_i dx_i \wedge d\bar{x}_i = \sum_i d|x_i|^2 \wedge d\theta^i = 0 ,$$

where θ^i is the phase of x_i . Note the T^2 fiber further degenerates to S^1 at the boundary of R where it touches the edge so \mathcal{L} itself is without boundary. \mathcal{L} has the topology of $\mathbb{R}_+ \times T^2 \sim \mathbb{R}^2 \times S^1$. It has a single 1-cycle γ , which is homologous to the S^1 fiber that does not vanish at the boundary point of R and it is compatible with the $U(1)$ action along the edge of the toric diagram Υ_X that R touches. Examples of \mathcal{L} in $\mathcal{O}(-1) \oplus \mathcal{O}(-1) \rightarrow \mathbb{P}^1$ are given in Fig. 2.4.

The submanifold \mathcal{L} is actually not only Lagrangian but *special Lagrangian* [75] satisfying the extra phase condition $\text{Re}(\Omega)|_{\mathcal{L}} = 0$ [50]. It is a direct generalization of the construction in [75] to toric Calabi–Yau threefold backgrounds so that it is compatible with the toric action of the background [50]. \mathcal{L} is sometimes called “toric special Lagrangian” or “Harvey–Lawson” submanifold. Let us wrap M D -branes around \mathcal{L} and denote them by \mathcal{L} as well. Since \mathcal{L} is constructed on the toric diagram of X , the open Gromov–Witten invariants counting the worldsheet instantons ending on the branes \mathcal{L} can be computed by adapting the equivariant localization techniques discussed in the previous section. The computation of the open Gromov–Witten invariants is localized to counting those holomorphic maps whose preimages are (degenerate) Riemann surfaces $\Sigma_{g,0}$ without boundary and h disks connected to $\Sigma_{g,0}$ at nodal points. $\Sigma_{g,0}$ is mapped to X in the same way as discussed in the last subsection while a disk is mapped to the S^1 fibration over one of the two half-edges in Υ_X that intersect with R . Let us denote by x_i the size of the image of the i -th disk. The graph G representing the holomorphic map has

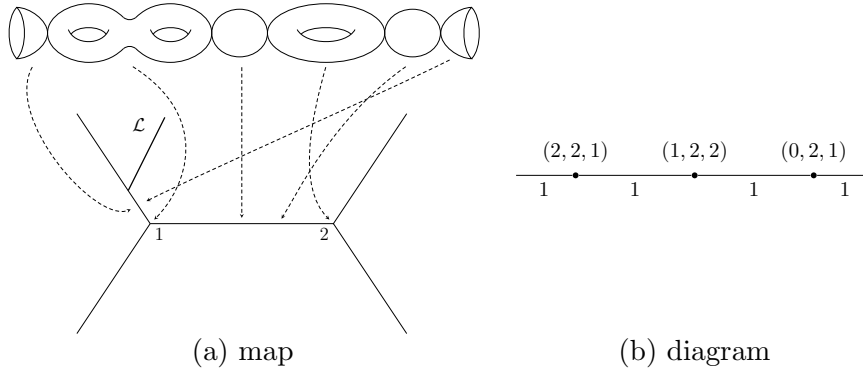


Figure 2.5: An invariant stable holomorphic map from a worldsheet on degenerate $\Sigma_{3,2}$ to the resolved conifold (represented by its toric digram) ending on the Lagrangian brane \mathcal{L} , as well as the diagram $G \in \mathcal{G}_{3,2}$ that represents it. Here in G we suppress the $\epsilon_c(\epsilon_c)$ symbols on the edges (half edges) (see text).

accordingly in addition h half edges with labels (ϵ_c, d_c) representing a disk mapped holomorphically to the half-edge ϵ_c and the degree of the map is d_c . An example of G is given in Fig. 2.5. We denote by $\mathcal{G}_{g,h}$ the set of graphs containing h half edges and satisfying

$$2 - 2g_v + n_v = 2 - 2g + h, \quad (2.97)$$

and by $\tilde{\mathcal{G}}_{g,h}$ the set of the same graphs but without degrees on edges and half-edges.

The weight $w(G)$ of a graph G factorizes as in the case of closed string and now in addition has contribution D_{ϵ_c, d_c} from each half-edge c . We refer to [52] for the explicit expression of D_{ϵ_c, d_c} , and only point out here that they are the only factors that contain the parameters x_i . We further define the open string amplitude

$$A_h^{(g)}(t, x_1, \dots, x_h) = \sum_{\omega} \mathcal{F}_{g, \omega}(t) e^{-\sum_i \omega_i x_i}. \quad (2.98)$$

which encodes the open Gromov–Witten invariants in $\mathcal{F}_{g, \omega}(t)$. Then the open string amplitude $A_h^{(g)}(t, x_1, \dots, x_h)$ is computed by

$$A_h^{(g)}(t, x_1, \dots, x_h) = \sum_{G \in \mathcal{G}_{g,h}} \frac{(-1)^h}{\#\text{Aut}(G)} \prod_v H_{g_v, n_v, \sigma_v} \prod_e F_{\epsilon_e, d_e}(t) \prod_c D_{\epsilon_c, d_c}(x). \quad (2.99)$$

As in the closed case we can first sum over graphs which only differ by the degrees on edges and half-edges and then sum over graphs \tilde{G} in $\tilde{\mathcal{G}}_{g,h}$. The weights of \tilde{G} still factorize.

The open Gromov–Witten invariants computed in this way are again only rational numbers due to the multicovering and bubbling phenomena. The integrality structure of the free energy $\mathcal{F}(g_s, t, V)$ was analyzed in refs. [25, 76]. It was shown the free energy can be written as

$$\mathcal{F}(g_s, t, V) = \sum_R \sum_{d=1}^{\infty} \frac{1}{d} f_R(q^d, e^{-d\beta-t}) \text{tr}_R V^d, \quad (2.100)$$

where R is a representation in $U(M)$, the gauge group on the coincident M Lagrangian branes,

and we take the limit $M \rightarrow \infty$. Furthermore $q = e^{ig_s}$ and

$$f_R(q, e^{-\beta \cdot t}) = \sum_{g=0} \sum_{\beta, R', R''} C_{RR'R''} S_{R'}(q) n_{g, R'', \beta} \left(2 \sin \frac{dg_s}{2} \right)^{2g-1} e^{-\beta \cdot t}. \quad (2.101)$$

In the formula above, $C_{RR'R''}$ is the Clebsch–Gordan coefficient of the symmetric group S_ℓ with ℓ being the number of boxes in the Young diagram associated to R . The function $S_R(q)$ is defined as

$$S_R(q) = \begin{cases} (-1)^m q^{-\frac{\ell-1}{2}+m}, & \text{if } R \text{ is a hook representation,} \\ 0, & \text{otherwise} \end{cases}, \quad (2.102)$$

where m is the height of the hook representation minus one. The integer coefficients $n_{g, R'', \beta}$ are called the Ooguri–Vafa coefficients.

Using the Frobenius formula the above result can be written in a form more in line with eq. (2.95). To each boundary condition labelled by $\omega = (\omega_1, \dots, \omega_h)$ there is associated a natural conjugate class $C(\omega)$ in the symmetric group S_ℓ with $\ell = \sum_i \omega_i$. The cycle type of the conjugacy class is obtained by writing down an ω_i cycle for each ω_i . Let $\chi_R(C(\omega))$ be the character of the conjugacy class $C(\omega)$ in the representation R of the symmetric group S_ℓ . We can define the combinations

$$n_{g, \omega, \beta} = \sum_R \chi_R(C(\omega)) n_{g, R, \beta}, \quad (2.103)$$

which are also integers. It can be shown the integrality condition of eqs. (2.100), (2.101) can be cast in the following form [76]

$$\sum_{g=0}^{\infty} g_s^{2g-2+h} \mathcal{F}_{g, \omega}(t) = \frac{(-1)^{h-1}}{\prod_j \omega_j} \sum_{g, \beta, d|\omega} n_{g, \omega/d, \beta} d^{h-1} \left(2 \sin \frac{dg_s}{2} \right)^{2g-2} \prod_{i=1}^h \left(2 \sin \frac{\omega_i g_s}{2} \right) e^{-d\beta \cdot t}. \quad (2.104)$$

We can perform genus expansion to find the open Gromov–Witten invariants in terms of the integral Ooguri–Vafa invariants. The first few results are [36, 77]

$$\mathcal{F}_{0, \omega}(t) = (-1)^{h-1} \sum_{d|\omega} d^{h-3} n_{0, \omega/d, \beta} e^{-d\beta \cdot t}. \quad (2.105)$$

2.2.4 Type B Closed String

As seen in the previous subsections, type A topological string theory is better understood from the mathematical point of view as an enumerative problem, but not so much as a quantum gravity theory. On the contrary, type B topological string theory is much better understood from the latter perspective. As discussed in subsections 2.1.4 and 2.1.5 the genus 0 free energy of type B topological string is closely related to the deformation theory of the complex structure of the target space. The latter theory can actually be formulated in terms of a field theory.

The deformation of the complex structure of the Calabi–Yau threefold X can also be described as the deformation of the $\bar{\partial}$ differential operator

$$\bar{\partial} \rightarrow \bar{\partial} + A. \quad (2.106)$$

Here

$$\bar{\partial} = \partial_i d\bar{z}^i, \quad (2.107)$$

and A is a Beltrami differential,

$$A = A_i^j d\bar{z}^i \partial_j =: A^j \partial_j. \quad (2.108)$$

Given an arbitrary holomorphic function f in the new complex structure defined by

$$(\bar{\partial} + A^i \partial_i)f = 0, \quad (2.109)$$

the consistency condition

$$0 = \bar{\partial}(\bar{\partial} + A^i \partial_i)f = \bar{\partial}(A^i) \partial_i f - A^i \partial_i \bar{\partial} f = (\bar{\partial} A^i + A^j \partial_j A^i) \partial_i f,$$

demands that

$$\bar{\partial} A + \frac{1}{2}[A, A] = 0. \quad (2.110)$$

This is called the Kodaira–Spencer equation [78–81] in the theory of complex structure deformation. It can also be understood as the equation of motion of the field A in a classical field theory. To quantize this field theory one can find the action whose equation of motion is eq. (2.110), and then apply the usual quantization procedure on the action. This was done in [47], and it was shown that the free energies F_g of the quantum field theory are precisely those in the type B topological string theory defined via eq. (2.74). Therefore the type B topological string is the quantum deformation theory of the complex structure of the Calabi–Yau manifold X ¹⁷.

Free energies $F_g(t, \bar{t})$ defined in the quantum deformation theory and also those via eq. (2.74) in type B topological string theory actually depend on in general not only the complex structure moduli t_i , but also their antiholomorphic counterparts \bar{t}_i , with the only exception of $F_0(t)$ which is holomorphic. This phenomenon, which is called *holomorphic anomaly*, in fact also arises in type A topological string theory, where the free energies $F_g(t, \bar{t})$ defined via eq. (2.74) depend on the antiholomorphic counterparts of the (complexified) Kähler moduli of the target space as well. The holomorphic free energies $\mathcal{F}_g(t)$ described in the enumerative problem in section 2.2.2 are $F_g(t, \bar{t})$ in the limit $\bar{t}_i \rightarrow 0$. The mild dependence of $F_g(t, \bar{t}), g \geq 1$ on \bar{t}_i was exploited in refs. [47, 82] to construct the *holomorphic anomaly equations*, a set of infinitely many differential equations, from which $F_g(t, \bar{t}), g \geq 1$ can be solved recursively¹⁸. We do not spell out the explicit form of the holomorphic anomaly equations since they will not be needed in the thesis. However the generic form of the solutions to the equations can be written down in a way familiar to those versed in quantum field theories.

Let us focus on type B topological string theory. We have discussed in section 2.1.5 that the complex structure moduli space of a Calabi–Yau threefold X can have singular divisors, and the periods $X^I, F_J(X^I)$ as well as the period matrix τ_{IJ} undergo monodromy when they are parallel transported around a singular divisor. All the monodromies generate the modular group $\Gamma \subset Sp(2h^{2,1} + 2, \mathbb{Z})$. It turns out that the free energies $F_g(t, \bar{t})$ are modular invariant (almost holomorphic modular forms of Γ of weight 0), in the sense that they do not change even

¹⁷ To be precise the quantum field theory alluded to here is the string field theory that describes the creation and annihilation of strings.

¹⁸ The holomorphic anomaly equations only determine $F_g(t, \bar{t})$ upto a modular invariant holomorphic term, which needs to be fixed via some boundary conditions. This issue will be clarified in a little detail below.

$$\begin{aligned}
 F_2(t, \bar{t}) = & \text{diagram 1} + \frac{\Delta}{2} \text{diagram 2} + \frac{\Delta}{2} \text{diagram 3} + \frac{\Delta^2}{8} \text{diagram 4} \\
 & + \frac{\Delta^2}{2} \text{diagram 5} + \frac{\Delta^3}{12} \text{diagram 6} + \frac{\Delta^3}{8} \text{diagram 7}
 \end{aligned}$$

Figure 2.6: Diagrammatic illustration of the expansion of $F_2(t, \bar{t})$ in eq. (2.113). Here each connecting line with endpoints (I, J) is a factor of Δ^{IJ} , and each Riemann surface of genus g with h marked points I_1, \dots, I_h is $\partial_{I_1} \dots \partial_{I_h} \mathcal{F}_g$.

if the periods, and therefore the complex structure moduli t_i , go through a monodromy¹⁹. On the other hand, the holomorphic limit $\mathcal{F}_g(t)$ of $F_g(t, \bar{t})$ lose the property of modular invariance (quasi-modular forms of Γ). It was shown in [51] that one can relate $F_g(t, \bar{t})$ to $\mathcal{F}_g(t)$ via

$$F_g(t, \bar{t}) = \mathcal{F}_g(t) + \Gamma_g(\Delta^{IJ}, \partial_{I_1} \dots \partial_{I_n} \mathcal{F}_{r < g}(t)) , \quad (2.111)$$

where Γ_g sums over all possible stable degenerations of the genus g Riemann surface Σ_g with each component Riemann surface $\Sigma_{r,n}$ having genus r (necessarily smaller than g) and n marked points represented by $\partial_{I_1} \dots \partial_{I_n} \mathcal{F}_{r < g}(t)$ and each connecting line replaced by

$$\Delta^{IJ} = ((\bar{\tau} - \tau)^{-1})^{IJ} . \quad (2.112)$$

For example the genus two free energy satisfies

$$\begin{aligned}
 F_2(t, \bar{t}) = & \mathcal{F}_2 + \frac{\Delta^{IJ}}{2} (\partial_I \partial_J \mathcal{F}_1 + \partial_I \mathcal{F}_1 \partial_J \mathcal{F}_1) + \frac{\Delta^{IJ} \Delta^{KL}}{8} (\partial_I \partial_J \partial_K \partial_L \mathcal{F}_0 + 4 \partial_I \mathcal{F}_1 \partial_J \partial_K \partial_L \mathcal{F}_0) \\
 & + \frac{\Delta^{IJ} \Delta^{KL} \Delta^{MN}}{48} (4 \partial_I \partial_K \partial_M \mathcal{F}_0 \partial_J \partial_L \partial_N \mathcal{F}_0 + 6 \partial_I \partial_J \partial_K \mathcal{F}_0 \partial_L \partial_M \partial_N \mathcal{F}_0)
 \end{aligned} \quad (2.113)$$

which is illustrated in Fig. 2.6. The denominators of the linear coefficients are symmetry factors, in other words the orders of the symmetry groups the corresponding diagrams enjoy. For example the last diagram has \mathbb{Z}_2 symmetry of swapping the curved line linked only to the left sphere, another \mathbb{Z}_2 symmetry of swapping the curved line linked only to the right sphere, and a third \mathbb{Z}_2 exchanging the two spheres. The total symmetry factor is $2 \times 2 \times 2 = 8$. On the other hand, each stably degenerate Riemann surface can be regarded as a Feynman diagram, where each component Riemann surface is understood as a subdiagram, each line a propagator, and the linear coefficient with the correct symmetry factor. $F_g(t, \bar{t})$ depends on antiholomorphic moduli \bar{t}_i only through $\bar{\tau}$ ²⁰, and it can be shown eq. (2.111) provides the general form of the solutions to the holomorphic anomaly equations.

When we try to solve $F_g(t, \bar{t})$ recursively, we assume the lower genera free energies $F_{r < g}(t, \bar{t})$ and hence their holomorphic limit in $\Gamma_g(\dots)$ in eq. (2.111) are already known. We only need to find a holomorphic function $\mathcal{F}_g(t)$ such that the sum is modular invariant. Obviously in this way $F(t, \bar{t})$ is only determined up to a holomorphic modular invariant term, which is called the *holomorphic ambiguity*. It can be fixed by demanding suitable behavior of $F_g(t, \bar{t})$ at the boundary as well as singular loci of the complex structure moduli space $\mathcal{M}(X)$ of X explored in ref. [84]. The holomorphic anomaly equations have been thus solved for various target space geometries [84–87] through the direct integration method developed in refs. [88–90], which

¹⁹ F_0 actually needs some modification to be modular invariant. For details see [83].

²⁰ The holomorphic limit $\bar{t}_i \rightarrow 0$ corresponds to sending $\bar{\tau}$ to $i\infty$.

exploits the structure of the ring of almost holomorphic modular forms of Γ .

2.2.5 Type B Open String

We can also consider the theory of constant maps from Riemann surface $\Sigma_{g,h}$ with genus g and h boundary components. It was shown [68] that the boundary components should be mapped into a holomorphic submanifold \mathcal{S} of the target space X with Dirichlet boundary condition in the transverse direction to the submanifold \mathcal{S} . The submanifold \mathcal{S} can be regarded as being wrapped by a D -brane (holomorphic brane), on which a $U(1)$ gauge field propagates. If the holomorphic submanifold \mathcal{S} is wrapped by a stack of N branes, the gauge group is enhanced to $U(N)$.

A nice review on type B topological open string theory is given by Aspinwall [91]. In the case of X being a noncompact Calabi–Yau threefold, the type B topological open string theory is most conveniently studied in connection with matrix models or topological recursion, which will be discussed in section 2.4 and section 2.5 respectively.

2.2.6 Mirror Symmetry

Here we discuss a remarkable duality called mirror symmetry in string theory. It was first suggested in [92, 93] that Calabi–Yau threefolds should exist in pairs (X, Y) satisfying²¹

$$h^{1,1}(X) = h^{2,1}(Y), \quad h^{2,1}(X) = h^{1,1}(Y), \quad (2.114)$$

such that the superconformal field theory on the worldsheet propagating in X in type IIA superstring theory is equivalent to the superconformal field theory on the worldsheet propagating in Y in type IIB superstring theory. X and Y are called *mirror manifolds*, and the two superstring theories *mirror dual* to each other. First examples of mirror manifolds were explicitly constructed in [94]. The authors also pointed out the equivalence of superconformal field theories on worldsheets lead to several striking implications, including the identification of Yukawa couplings, which behave very differently in the two mirror superstring theories. These predictions were verified in [66, 95] followed by [96–103] in a series of illuminating examples. Furthermore, if we extend the equivalence of worldsheet theories to open strings, it implies D -branes in type IIA superstring in X can be mapped to D -branes in type IIB superstring in Y , and the worldvolume theories on the D -branes in the two superstring theories are equivalent as well. This lead to the interesting Strominger–Yau–Zaslow conjecture [104]. Finally, numerous pairs of Calabi–Yau threefolds satisfying eq. (2.114) were constructed by Batyrev [105] using toric geometry.

Because of the connection between type IIA/B superstring and type A/B topological string alluded to in section 2.2.1, mirror symmetry is naturally inherited by topological string. And the statement of mirror symmetry in the latter case can be made rather precise, since quantities in topological string are much better under control. The mirror symmetry claims that the moduli spaces of type A topological string on X and type B topological string on Y ²² can be identified with a proper *mirror map* relating the moduli of the two theories, and the free energies in the two theories coincide. In the case of closed topological string, the mirror symmetry was proved by Givental as well as Yau [106–108] in genus zero for Calabi–Yau’s that were hypersurfaces or

²¹ Although note the caveat stated in the footnote 7 on page 3.

²² One can of course switch X and Y .

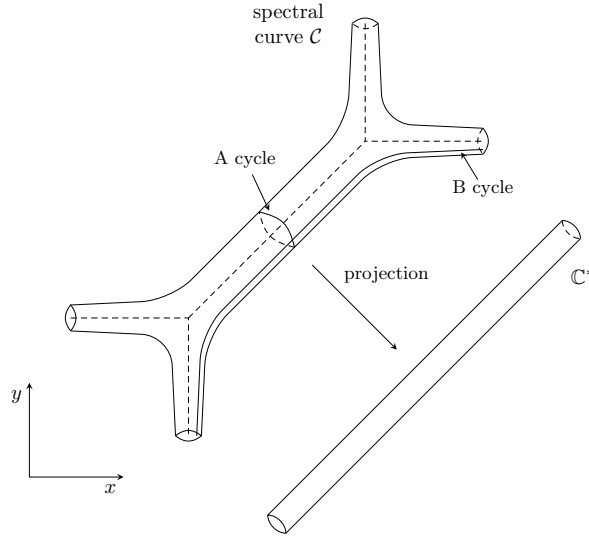


Figure 2.7: Spectral curve \mathcal{C} of the mirror of $\mathcal{O}(-1) \oplus \mathcal{O}(-1) \rightarrow \mathbb{P}^1$, the A and B cycles on \mathcal{C} , and its projection to \mathbb{C}^* .

complete intersections in compact toric geometry. Independently Hori and Vafa proved mirror symmetry for complete intersections in compact toric geometry as well as toric Calabi–Yau threefolds (which are necessarily noncompact) in a physicists’ way [109]²³. In this thesis we will be only concerned with topological string in toric Calabi–Yau threefolds.

The mirror dual of type A topological string on a toric Calabi–Yau threefold X is type B topological string on a noncompact complex manifold Y defined by

$$uv = H(x, y), \quad u, v, x, y \in \mathbb{C} \quad (2.115)$$

with some polynomial $H(x, y)$ in $\alpha := e^{-x}$ and $\beta := e^{-y}$. One has the freedom to reparametrize the function $H(x, y)$ as long as the symplectic form $dx \wedge dy$ is preserved. $H(x, y) = 0$ defines a noncompact Riemann surface \mathcal{C} with punctures at $x \rightarrow \pm\infty$ or $y \rightarrow \pm\infty$. The Riemann surface \mathcal{C} is called the spectral curve of the type B theory, and it can be visualized as the surface of the tubular neighborhood of the toric diagram Υ_X of X . For instance the mirror dual of type A topological string on $\mathcal{O}(-1) \oplus \mathcal{O}(-1) \rightarrow \mathbb{P}^1$ has the target space defined by

$$uv = H(x, y) = 1 - e^{-x} - e^{-y} + Qe^{-x-y}, \quad (2.116)$$

with parameter Q . The spectral curve given by $H(x, y) = 0$ is a Riemann sphere with four punctures illustrated in Fig. 2.7.

Next, to state the mirror map a coordinate patch on the moduli space has to be chosen. We choose in type A topological string the large volume limit where the Kähler moduli²⁴ t_i defined in eq. (2.41) are good coordinates due to the suppression of instanton corrections. They actually provide a set of flat coordinates²⁵ on the moduli space near the point of infinitely large

²³ We refer to [31, 56, 110] for reviews on mirror symmetry in topological string theory, and [111] for a nice review on the Greene–Plesser story of mirror symmetry in superstring theory.

²⁴ Their complexified version with the Kalb–Ramond field to be precise.

²⁵ Strictly speaking to talk about flat coordinates one has to specify the bundle and connection on the moduli space, which are naturally given by the special geometry structure of the moduli space. See for instance [47].

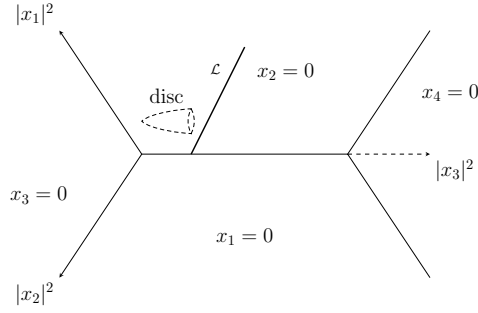


Figure 2.8: A toric special Lagrangian brane \mathcal{L} in the resolved conifold, and a disk instanton on \mathcal{L} .

volume. An additional advantage of using these coordinates is the exposition of the integrality structure of the free energies illustrated in eqs. (2.88) and (2.89). The flat coordinates in type B moduli space are provided by the normalized A-periods t_i defined by eq. (2.63), and the mirror map identifies them with the Kähler moduli t_i in type A topological string. In the case of noncompact Calabi–Yau there is always a constant A-period, and so by choosing it to be X^0 , t_i are given directly by integration of Ω over some 3-cycles. Furthermore if the local Calabi–Yau is of the type given by eq. (2.115), Ω can be reduced to ydx on the spectral curve \mathcal{C} and the three-cycles \mathcal{A}_i and \mathcal{B}_i of the Calabi–Yau project onto 1-cycles of \mathcal{C} (denoted also by \mathcal{A}_i and \mathcal{B}_i), so that the periods of the Calabi–Yau can be computed from \mathcal{C} alone

$$t_i = \frac{1}{4\pi i} \oint_{\mathcal{A}_i} ydx, \quad \frac{\partial \mathcal{F}_0}{\partial t_i} = \oint_{\mathcal{B}_i} ydx. \quad (2.117)$$

In the example of the mirror of the resolved conifold, the cycles on its spectral curve is illustrated in Fig. 2.7. Usually t_i can be expanded as $-\log z_i$ with z_i being some parameters of $H(x, y)$, plus a power series in z_i . However if \mathcal{C} is a Riemann sphere the power series corrections vanish. In particular for the Calabi–Yau in eq. (2.116) mirror to resolved conifold one has

$$t = -\log(Q). \quad (2.118)$$

We can also consider mirror symmetry in topological open string theory by for instance inserting Lagrangian branes in the type A theory. In particular we are interested in the toric special Lagrangian branes discussed in section 2.2.3. They are parametrized by two real moduli. The first is their position on the edges of the toric diagram, or equivalently the size r of the disk instanton stretched between the closest vertex in the toric diagram and the branes. This is illustrated for the example of resolved conifold in Fig. 2.8. The second is the gauge connection of the gauge bundle on the branes, which is characterized by the Wilson loop θ along the only 1-cycle on the branes. r and θ combine into one complex modulus $x = r + i\theta$.

These branes were discussed in [50, 112], and the authors found their mirror duals were the holomorphic branes that were either located at $u = 0$ and extended along the v direction or located at $v = 0$ and extended along the u direction. In either of the two cases, the holomorphic branes are represented by a point p on \mathcal{C} . Although the parametrization of \mathcal{C} has the freedom of symplectic transformations, there is a natural choice of the parametrization of the point p when it represents the mirror dual to branes in type A theory. Namely we choose x, y such that in the large volume limit $\text{Re}(x)$ is the size r of disk instanton, $\text{Im}(x)$ the Wilson loop θ , and $y \rightarrow 0$. With this parametrization, the authors of [50] showed that disk instanton amplitude

$A_1^{(0)}(t, x)$ is given by the Abel–Jacobi map on the spectral curve \mathcal{C}

$$A_1^{(0)}(t, x) = \int_{x^*}^x y(x') dx' . \quad (2.119)$$

Here the initial position x^* is irrelevant and can be dropped after the computation. It is natural then in the large volume limit, $\partial A_1^{(0)}(t, x)/\partial x = y(x) \rightarrow 0$, since the disk instanton corrections should be suppressed. Note that the picture in type A theory indicates there are various phases of the branes corresponding to them located on different edges of the toric diagram. On the one hand, when the branes pass through a vertex and move onto a neighboring edge, the disk instantons change, and accordingly the natural parametrization is changed. The new and old parametrizations are related through a symplectic transformation on the coordinates x, y [113]. On the other hand the apparent singularity in the brane moduli space corresponding to the branes located at a vertex due to the vanishing of both r and θ is an artifact of the large volume limit. The singularity is removed when disk instanton corrections to the brane moduli space are taken into account. This is clear from the picture in type B theory, where the brane moduli space can be identified with the spectral curve \mathcal{C} (there is no quantum correction to the moduli space in type B theory) which is smooth at these places.

We would like to have flat coordinates on the brane moduli space as well. It was derived in [112] and the result is as follows. As seen for instance from the spectral curve of the mirror of resolved conifold, $y(x)$ is a multivalued function on \mathcal{C} . For any point p on \mathcal{C} there exists a closed loop passing through p along which y enjoys the monodromy

$$C_p : y \rightarrow y + 2\pi i . \quad (2.120)$$

Then the flat coordinate at the point p is defined to be

$$\hat{x}(p) = \oint_{C_p} y(x) dx . \quad (2.121)$$

This definition parallels the definition of flat coordinates in the closed string sector. It was further shown in [112] that only expanded in terms of \hat{x} does the disk amplitude $A_1^{(0)}(t, x)$ have integrality coefficients as in eq. (2.105) (together with eq. (2.98)). In general the flat coordinate \hat{x} can be approximated by x plus power series in e^{-t} representing closed string instanton corrections. These instanton corrections vanish if \mathcal{C} is a Riemann sphere.

We point out that the natural choice of parametrizing \mathcal{C} corresponding to branes still has a \mathbb{Z} ambiguity: $x \rightarrow x + ny, n \in \mathbb{Z}$, since y vanishes in the large volume limit. One nevertheless has to fix this ambiguity in the quantum theory as y in general is not zero, and we call it the framing²⁶ of the branes. Note that here the coefficient n is restricted to integers because the algebraic coordinate $\alpha = e^{-x}$ should be invariant after one circles along the loop C_p that shifts y by $2\pi i$.

Finally since it will be of later use we discuss the mirror dual of type A topological string on T^*S^3 the cotangent bundle of a three–sphere. T^*S^3 is a smooth Calabi–Yau threefold because the curvature of S^3 is cancelled by the curvature of the cotangent bundle. Although T^*S^3 itself is not toric, it can be understood as the deformation of the singular conifold which is toric; in

²⁶ The purpose of choosing this name will become clear at the end of section 2.5.4.

other words T^*S^3 is given by the hypersurface equation

$$uv - xy = \epsilon , \quad (2.122)$$

with $u, v, x, y \in \mathbb{C}$ and the deformation parameter ϵ which, without loss of generality, is assumed to be real. To see that this indeed represents T^*S^3 , one only has to do the change of variables

$$\begin{aligned} u &= \eta_1 + i\eta_2, & y &= i(\eta_3 - i\eta_4) , \\ x &= i(\eta_3 + i\eta_4), & v &= \eta_1 - i\eta_2 , \end{aligned} \quad (2.123)$$

and then separate the real and imaginary parts $\eta_\mu = x_\mu + iv_\mu$. Eq. (2.122) becomes

$$\sum_{\mu=1}^4 (x_\mu^2 - v_\mu^2) = \epsilon , \quad \sum_{\mu=1}^4 x_\mu v_\mu = 0 . \quad (2.124)$$

The first equation indicates that the locus $v_\mu = 0$ is a three–sphere, while the second equation describes the cotangent space at the point x_μ . It was found out in [114] based on [115] that the mirror dual of T^*S^3 can be found via the deformation of the mirror construction of toric geometry alluded to earlier in this subsection and it was found to be the hypersurface

$$uv = (1 - e^{-x})(1 - e^{-y}) \quad (2.125)$$

with the conifold singularity at $u = v = x = y = 0$ blown up to \mathbb{P}^1 .

2.3 Chern–Simons Theory

2.3.1 Basic Definitions

In this section we follow closely [36]. Chern–Simons theory is a $2 + 1$ dimensional pure gauge theory on a generic three manifold M with gauge group G , which we assume to be a compact semi-simple Lie group. The action of Chern–Simons theory contains only the Chern–Simons term,

$$S = \frac{k}{4\pi} \int_M \text{Tr}(A \wedge dA + \frac{2}{3} A \wedge A \wedge A) . \quad (2.126)$$

Here the level k is a positive real number, and A the gauge connection. The representation in which the trace Tr is taken depends on the group G . If $G = U(N)$, it is the N -dimensional fundamental representation. Since the action does not contain metric, the theory is topological at least at the classical level, and there is no difference between the temporal and the spatial directions. We assume M to be compact.

When the theory is quantized, the gauge coupling $2\pi/k$ receives corrections and is shifted to

$$g_s = \frac{2\pi}{k + g} \quad (2.127)$$

where g is the dual coxeter number of the gauge group. It is N for $G = U(N)$. Furthermore as demonstrated in [20] the quantum theory indeed is still a topological field theory, with the

caveat that the partition function

$$Z(M) = \int \mathcal{D}A e^{iS} \quad (2.128)$$

depends on the *framing* of the three manifold M , defined as the homotopy class of the trivialization of the tangent bundle TM . The framing can be understood as a choice of three linearly independent sections s_i of the tangent bundle TM , where $\{s_i\}$ restricts to a basis of tangent vectors at each point on M . The framing is characterized by an integer. When the framing is shifted by Δf the partition function changes by

$$Z(M) \rightarrow e^{2\pi i \Delta f \cdot c/24} Z(M) , \quad (2.129)$$

where

$$c = \frac{k \dim G}{k + g} \quad (2.130)$$

is the central charge of the \hat{g} WZW model with level k . The appearance of elements from the rational conformal field theory is no coincidence, and we will see the deep connection between Chern–Simons theory and WZW models in section 2.3.3. Finally a large gauge transformation which cannot be continuously deformed to identity can shift the action by

$$S \rightarrow S + \text{const} \cdot m k$$

with some integer m . This puts constraint on k in a quantum theory since the partition function is only gauge invariant if the shift $\text{const} \cdot m k$ is an integral multiple of 2π . If $G = U(N)$ and Tr taken in the fundamental representation, k has to be an integer.

To construct physical observables, we embed a knot²⁷ \mathcal{K} in the three manifold M and compute the trace of the holonomy of the gauge field A along the knot \mathcal{K} in an irreducible representation R of G . In other words, we have

$$W_R^{\mathcal{K}}(A) = \text{Tr}_R U_{\mathcal{K}} , \quad (2.131)$$

where $U_{\mathcal{K}}$ is the holonomy

$$U_{\mathcal{K}} = \text{P exp} \oint_{\mathcal{K}} A . \quad (2.132)$$

Since the definition of this nonlocal operator does not involve metric, its (normalized) vev is necessarily a quantum topological invariant of the knot

$$\mathcal{W}_R(\mathcal{K}) = \langle W_R^{\mathcal{K}}(A) \rangle = \frac{1}{Z(M)} \int \mathcal{D}A W_R^{\mathcal{K}}(A) e^{iS} , \quad (2.133)$$

with the same caveat of framing dependence. We call it the quantum knot invariant of the knot \mathcal{K} . The framing of M induces a framing on the knot \mathcal{K} , which can be intuitively understood as the following. We choose a section of the normal bundle to the knot \mathcal{K} inside M and deform \mathcal{K} infinitesimally along the direction of the section at every point on the knot to get a new knot \mathcal{K}' . The framing of \mathcal{K} is then the linking number between the two knots old and new. The framing of \mathcal{K} is also characterized by an integer. When the framing is shifted by Δf , the

²⁷ We can equally embed a link which has several knot components. The discussion is similar.

quantum knot invariant changes by a phase,

$$\mathcal{W}_R(\mathcal{K}) \rightarrow e^{2\pi i h_R \Delta f} \mathcal{W}_R(\mathcal{K}) , \quad (2.134)$$

where

$$h_R = \sum_a \frac{(T^a)^2}{2(k+g)} = \frac{C_R}{k+g} , \quad (2.135)$$

is the conformal weight of the WZW primary in the integrable representation R . If $G = U(N)$, the quadratic Casimir C_R is

$$C_R = N\ell + \kappa_R , \quad (2.136)$$

where

$$\kappa_R = \ell + \sum_i (\ell_i^2 - 2i\ell_i) , \quad (2.137)$$

while ℓ_i and ℓ denote the number of boxes in the i -th row, and the total number of boxes in the Young diagram of R . Then the framing transformation is

$$\mathcal{W}_R(\mathcal{K}) \rightarrow \lambda^{\frac{1}{2}\ell\Delta f} q^{\frac{1}{2}\kappa_R\Delta f} \mathcal{W}_R(\mathcal{K}) . \quad (2.138)$$

Here we have defined

$$q = \exp\left(\frac{2\pi i}{k+N}\right), \quad \lambda = q^N . \quad (2.139)$$

Furthermore in the case of $M = S^3$, there is a canonical choice of zero framing.

Let us assume $M = S^3$ and $G = U(N)$ from now on. The quantum knot invariants are functions of q and λ , regardless of the framing f . One of the remarkable discoveries in [20] was that the quantum knot invariants $\mathcal{W}_\square(\mathcal{K})(q, \lambda)$ in the fundamental representation \square coincide with the HOMFLY knot invariants $H(\mathcal{K})(q, \lambda)$ defined by mathematicians [26]

$$\mathcal{W}_\square(\mathcal{K})(q, \lambda) = H(\mathcal{K})(q, \lambda) . \quad (2.140)$$

Therefore analogously we can define colored HOMFLY invariants $H_R(\mathcal{K})$ in an arbitrary irreducible representation R

$$H_R(\mathcal{K})(q, \lambda) = \mathcal{W}_R(\mathcal{K})(q, \lambda) . \quad (2.141)$$

It is also customary to normalize the knot invariants by that of unknot, the simplest knot \bigcirc

$$\overline{H}_R(\mathcal{K}) = \frac{H_R(\mathcal{K})}{H_R(\bigcirc)} . \quad (2.142)$$

The normalized HOMFLY invariants are *polynomials* in $q^{\pm 1}$ and $\lambda^{\pm 1}$. We briefly discuss HOMFLY knot invariants in the context of knot theory in the next subsection. We refer interested readers to refs. [116, 117].

2.3.2 HOMFLY Knot Invariants

In the mathematical branch of knot theory, the goal is to construct a topological invariant $P(\cdot)$ of knots so that if two knots \mathcal{K}_1 and \mathcal{K}_2 are different then $P(\mathcal{K}_1) \neq P(\mathcal{K}_2)$, effectively converting distinguishing knots from a topological problem to an algebraic problem. Knots

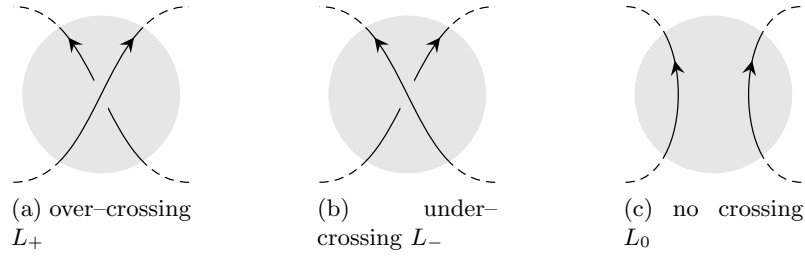


Figure 2.9: Overcrossing, undercrossing, and no crossing.

are usually represented by their projection graphs onto a plane with crossings classified into overcrossings and undercrossings (Fig. 2.9a and Fig. 2.9b). The crossing number of a knot, defined to be the minimal number of crossings one can find in any planar projection graph of a knot, characterizes the complexity of the knot. Some examples of two dimensional graphs of knots are given in Fig. 2.10a, Fig. 3.3, and Figs. B.1. A topological knot invariant should provide people a prescription to write down a unique algebraic expression for a knot from any of its planar projection graphs.

The normalized HOMFLY polynomial $\overline{H}(\mathcal{K})$ (uncolored) is defined by two conditions. The first is the *skein relation*

$$\lambda^{1/2}\overline{H}(L_+) - \lambda^{-1/2}\overline{H}(L_-) = (q^{1/2} - q^{-1/2})\overline{H}(L_0) . \quad (2.143)$$

Here L_+ , L_- , and L_0 are three knots which only differ at a small region containing either an overcrossing, an undercrossing, or no crossing, as shown in Fig. 2.9. The second is the normalization condition

$$\overline{H}(\bigcirc) = 1 . \quad (2.144)$$

To see that these conditions are already enough to compute the normalized HOMFLY polynomials from any projection graph, notice the fact that if overcrossings and undercrossings are freely exchangeable, any knot is equivalent to an unknot, while the obstruction is characterized by the term on the right hand side of the skein relation. Therefore, for a given knot \mathcal{K} , one can reduce its crossing number by using the skein relation to judiciously replace an overcrossing (undercrossing) by an undercrossing (overcrossing), at the cost of introducing an additional knot whose crossing number is smaller than that of \mathcal{K} by one. Perform this step recursively, one will end up with unknots only.

One can also find skein relations for colored HOMFLY invariants, but they are not powerful enough to enable people to compute these invariants. Very cumbersome techniques have to be employed to compute the colored HOMFLY polynomials with limited effects (See for example [118]). Furthermore from the mathematical definition of the HOMFLY polynomial it is not obvious why it should be a topological invariant. This is the reason the elegant method of computing HOMFLY polynomials via Chern–Simons theory, which will be explained in the next subsection, is very appealing.

2.3.3 Surgery and Nonperturbative Solutions

The quantum knot invariants $\mathcal{W}_R(\mathcal{K})$ can be solved exactly in Chern–Simons theory via the idea of surgery proposed by Witten [20]. We assume the three manifold is a three–sphere and the

gauge group is $U(N)$, and consequently the quantum knot invariants are identified with colored HOMFLY invariants. As was shown in [119], the $U(N)$ Chern–Simons action can be split into $U(1)$ Chern–Simons action and $SU(N)$ Chern–Simons action. The Abelian Chern–Simons theory is trivial, leaving us to focus on the $SU(N)$ Chern–Simons theory.

The action of $U(N)$ Chern–Simons theory can be split in the following way

$$S = \frac{k_1}{4\pi} \int_{S^3} B \wedge dB + \frac{k}{4\pi} \int_{S^3} \text{Tr}(A \wedge dA + \frac{2}{3} A \wedge A \wedge A) . \quad (2.145)$$

The first part of the action describes the $U(1)$ Chern–Simons theory with Abelian gauge field B , while the second part is the action of the $SU(N)$ Chern–Simons theory with A being the gauge connection. The level k_1 of the $U(1)$ theory is related to the level k of the $SU(N)$ theory by [119]

$$k_1 = N(k + N) . \quad (2.146)$$

Besides due to the factorization of the Wilson loop operator

$$W_R^{\mathcal{K}}(A) \text{Tr}_R U_{\mathcal{K}} = \text{Tr}_n U_{\mathcal{K}}(B) \text{Tr}_R U_{\mathcal{K}}(A) , \quad (2.147)$$

the quantum knot invariant also factorizes

$$\mathcal{W}_{(n,R)}^{U(1) \times SU(N)}(\mathcal{K}) = \mathcal{W}_n^{U(1)}(\mathcal{K}) \mathcal{W}_R^{SU(N)}(\mathcal{K}) . \quad (2.148)$$

Here the integer n for the representation of $U(1)$ should be identified with the number of boxes in the Young diagram of the irreducible representation R of $SU(N)$. The $U(1)$ quantum knot invariant only contains the framing dependence

$$\mathcal{W}_n^{U(1)}(\mathcal{K}) = \exp(2\pi i h_n^{U(1)} \cdot f) \cdot 1 = \exp\left(2\pi i \frac{n^2}{2k_1} f\right) , \quad (2.149)$$

because it is known that the Abelian quantum knot invariant in zero framing is always one. So the Abelian quantum knot invariant does not distinguish knots and only serves to provide a framing dependent phase, which is one in the zero framing. In the following we always assume zero framing unless otherwise specified.

To compute $SU(N)$ quantum knot invariants, Witten [20] proposed to cut the three–sphere to two three–manifolds M_1 and M_2 with shared boundary Σ . If one has to apply a homeomorphism $f : \Sigma \rightarrow \Sigma$ to glue M_1 and M_2 back to S^3 , we write $S^3 = M_1 \cup_f M_2$ ²⁸. Let us see some examples. The three–sphere can be split to two three dimensional discs D^3 glued at the boundary S^2 via an identity map. Using our notation we write $S^3 = D^3 \cup_{id} D^3$. We can also obtain S^3 by gluing two solid tori \mathbf{T}^2 together. Indeed if we embed a solid torus \mathbf{T}^2 in S^3 , the complement of the solid torus also has one contractible 1–cycle and one noncontractible 1–cycle and therefore is itself a solid torus. On the other hand, the contractible (noncontractible) 1–cycle of the embedded \mathbf{T}^2 is homologous²⁹ to the noncontractible (contractible) 1–cycle of the complement \mathbf{T}^2 , so the two solid tori \mathbf{T}^2 are glued together via an S transformation on the boundary torus T^2 . In other words, we have $S^3 = \mathbf{T}^2 \cup_S \mathbf{T}^2$. Recall the mapping class group of T^2 , i.e. the discrete group of homeomorphisms which cannot be continuously deformed to each other, is $SL(2, \mathbb{Z})$, and it is generated by T and S transformations. These are two linear transformations

²⁸ This operation is called *Heegaard splitting* in mathematics.

²⁹ Intuitively it means the two 1–cycles can be continuously deformed to each other.

acting on the two fundamental 1–cycles of a torus via,

$$T = \begin{pmatrix} 1 & 1 \\ 0 & 1 \end{pmatrix}, \quad S = \begin{pmatrix} 0 & -1 \\ 1 & 0 \end{pmatrix}. \quad (2.150)$$

The path integral for computing $\mathcal{W}_R(\mathcal{K})$ evaluated in M_1 depends on the gauge field configuration on the boundary Σ , and can be effectively regarded as the wave function of a quantum state $|\Psi_1\rangle$ in the Hilbert space $\mathcal{H}(\Sigma)$ on the boundary Σ . The quantum state depends on whether (part of) a knot is embedded in M_1 . Similarly the path integral in M_2 produces a quantum state $\langle\Psi_2|$ in the conjugate Hilbert space $\mathcal{H}^*(\Sigma)$ because of the opposite orientation. The homeomorphism f induces an operator on $\mathcal{H}(\Sigma)$

$$U_f : \mathcal{H}(\Sigma) \rightarrow \mathcal{H}(\Sigma). \quad (2.151)$$

Then the path integral in S^3 is identified with the inner product

$$\langle\Psi_2|U_f|\Psi_1\rangle. \quad (2.152)$$

Through canonical quantization of Chern–Simons theory on $\Sigma \times \mathbb{R}_+$ in the vicinity of the boundary Σ , Witten made the following crucial observation on the Hilbert space $\mathcal{H}(\Sigma)$ [20]. Suppose the boundary is a Riemann surface $\Sigma_{g,n}$ of genus g with n punctures where the strands of the embedded knot pass through the boundary. Let us color each puncture by R_i , which is either R or its conjugate \bar{R} , depending on whether the strand enters or exits M_1 . Then the Hilbert space $\mathcal{H}(\Sigma)$ is isomorphic to the vector space of n –point conformal blocks in the $\widehat{su}(N)_k$ WZW model with level k on the Riemann surface Σ_g , where the n points are WZW primaries in the representations R_i ³⁰. For instance, if the boundary Σ is a Riemann sphere with no puncture, the Hilbert space has only vacuum and is therefore one dimensional. If the boundary Σ is a torus with no puncture, the corresponding conformal block is a circle traversed by a WZW primary in an integrable highest weight representation of the affine Lie algebra $\widehat{su}(N)_k$. At a given level k the number of integrable highest weight representations of $\widehat{su}(N)_k$ is finite. The dimension of the Hilbert space $\mathcal{H}(T^2)$ is equal to the number of dominant weights, and we can choose a basis of $\mathcal{H}(T^2)$ such that, other than the vacuum $|0\rangle$, each quantum state $|\Psi_{T^2, R_\lambda}\rangle$ corresponds to an integrable representation R_λ with dominant affine weight $\hat{\lambda}$. Concretely, the vacuum state $|0\rangle$ corresponds to M_1 being an empty solid torus, while the quantum state R_λ is obtained via the insertion of the operator $\mathcal{O}_R = \text{Tr}_R U$, which is given by the Wilson loop along the noncontractible 1–cycle of \mathbf{T}^2 evaluated in the irreducible $SU(N)$ representation R_λ . We use λ to denote the finite part of the affine weight $\hat{\lambda}$. Furthermore, the T and S transformations in the mapping class group $SL(2, \mathbb{Z})$ of torus T^2 are promoted to quantum operators acting on $\mathcal{H}(T^2)$. They are identified with the matrix elements of the modular transformations T and S on the characters χ_λ in the $\widehat{su}(N)_k$ affine Lie algebra.

Now we are ready to compute the quantum knot invariants of unknot. First we compute the partition function $Z(S^3)$ of the Chern–Simons theory. According to the gluing scheme

³⁰ Note that R_i now represents an integrable representation of the affine Lie algebra $\widehat{su}(N)_k$. In general an irreducible $SU(N)$ representation cannot always be promoted to an affine integrable representation. However since we are only concerned with the functional forms of the quantum knot invariants which do not depend on the values of the level k and rank N , we can make convenient assumptions, say, $k \rightarrow \infty$, so that this is always possible. We also refer to [120] for a comprehensive review on WZW models and affine Lie algebras.

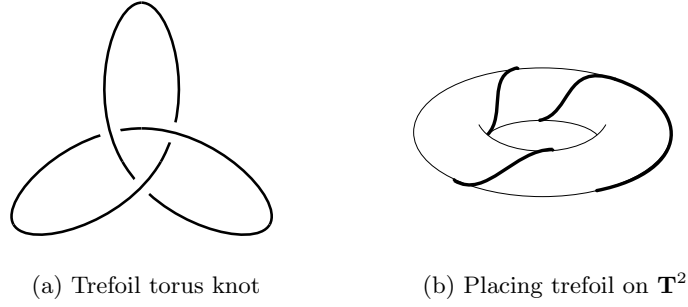


Figure 2.10: The torus knot $\mathcal{K}_{2,3} = \mathcal{K}_{3,2}$, also called the trefoil knot, and how to place it on the surface of a solid torus.

$S^3 = \mathbf{T}^2 \cup_S \mathbf{T}^2$, we can write the partition function as,

$$Z(S^3) = \langle 0|S|0 \rangle := S_{00} . \quad (2.153)$$

To compute the quantum knot invariant for unknot, we simply embed the unknot colored in representation R_λ along the noncontractible 1-cycle of the solid torus M_1 .

$$\mathcal{W}_{R_\lambda}(\bigcirc) = \frac{1}{Z(S^3)} \int \mathcal{D}A \operatorname{Tr}_{R_\lambda} U e^{iS} = \frac{\langle 0|S|R_\lambda \rangle}{\langle 0|S|0 \rangle} = \frac{S_{0R_\lambda}}{S_{00}} . \quad (2.154)$$

This is by definition the *quantum dimension*³¹ $\dim_q(R_\lambda)$ of the representation R_λ .

We can work a bit harder to compute the quantum knot invariants for a large category of nontrivial knots. A *torus knot* $\mathcal{K}_{r,s}$ labelled by two coprime integers (r, s) is defined to be a knot which can be placed on the surface of a solid torus \mathbf{T}^2 such that it is wound r times along the noncontractible cycle of \mathbf{T}^2 , and s times along the contractible cycle of \mathbf{T}^2 . It can be shown that the two torus knots $\mathcal{K}_{r,s}$ and $\mathcal{K}_{s,r}$ in fact are equivalent. The simplest torus knot $\mathcal{K}_{2,3} = \mathcal{K}_{3,2}$, also called the trefoil, is shown in Figs. 2.10. The quantum knot invariants of all torus knots colored in any irreducible representation can be computed by the *Rosso-Jones formula* [121]. The idea is as follows. Although the framing of a knot has to be an integer, it does not stop us from applying the framing transformation formula eq. (2.134) with a fractional framing shift. It turns out the quantum knot invariants of the torus knot $\mathcal{K}_{r,s}$ can be computed based on the understanding that $\mathcal{K}_{r,s}$ can be obtained by stacking r unknots with zero framing together, applying a fractional framing shift of s/r to each of them, and then gluing them to each other [122].

A crucial step in this computation is the application of the formula of the Adams' operation. Let ch_R be the character of the representation R of a Lie algebra \mathfrak{g} and U an algebra element. The relations

$$\operatorname{ch}_{R_1 \oplus R_2}(U) = \operatorname{ch}_{R_1}(U) + \operatorname{ch}_{R_2}(U), \quad \operatorname{ch}_{R_1 \otimes R_2}(U) = \operatorname{ch}_{R_1}(U) \cdot \operatorname{ch}_{R_2}(U) . \quad (2.155)$$

indicate there is a ring $R(\mathfrak{g})$ of functions $f : \mathfrak{g} \rightarrow \mathbb{C}$, which is generated by the characters of irreducible representations of \mathfrak{g} . The elements of the ring $R(\mathfrak{g})$ are called *virtual characters*.

³¹ Quantum dimension is defined both in the theory of quantum group and in WZW models. The former definition will be alluded to in section 4.2, while the latter definition is given precisely by the last part in eq. (2.154). It can be shown the two definitions are equivalent.

The virtual character $\text{ch}_R(U^r)$, being a function from \mathfrak{g} to \mathbb{C} , can therefore be written as a linear combination of the characters of the irreducible representations of \mathfrak{g} ; in other words

$$\text{ch}_R(U^r) = \sum_V c_{R,r}^V \text{ch}_V(U) . \quad (2.156)$$

This is called the Adams' operation. The right hand side of the formula is summed over a finite number of irreducible representations. In the case of $su(N)$, let $\ell(V)$ be the number of boxes in the Young diagram of V , V must satisfy $\ell(V) = r \cdot \ell(R)$. More details on the coefficients of the Adams' operation can be found for instance in the appendix A of [123]. Given the definition of the quantum knot invariants in eqs. (2.131), (2.133), we naturally have

$$\mathcal{W}_R(\mathcal{K}_{r,0}) = \sum_{\ell(V)=r \cdot \ell(R)} c_{R,r}^V \mathcal{W}_V(\mathcal{K}_{1,0}) = \sum_{\ell(V)=r \cdot \ell(R)} c_{R,r}^V \mathcal{W}_V(\bigcirc) . \quad (2.157)$$

Here $\mathcal{K}_{r,0}$ is a stack of r unknots. After shifting the framing by s/r on each unknot, we get the quantum knot invariant for the tours knot $\mathcal{K}_{r,s}$

$$\mathcal{W}_R(\mathcal{K}_{r,s}) = \sum_{\ell(V)=r \cdot \ell(R)} c_{R,r}^V e^{h_V \cdot 2\pi i s/r} \dim_q(V) . \quad (2.158)$$

It is necessary to point out that the quantum knot invariants obtained in this way are for the knot $\mathcal{K}_{r,s}$ with framing $r \cdot s$. One has to apply the framing transformation formula eq. (2.134) to convert them to framing zero if one so desires. Furthermore one can also use similar formula to compute the quantum knot invariants for the torus knot $\mathcal{K}_{s,r}$, and results would be the same.

2.3.4 Symmetry Properties

Here we list some symmetry properties of the quantum knot invariants/colored HOMFLY invariants, which will be useful later in section 4.4.

- The mirror \mathcal{K}^* of a knot \mathcal{K} is obtained from its planar projection by changing every undercrossing to overcrossing and vice versa. When we map a knot to its mirror, the quantum knot invariants transform by [36]

$$\mathcal{W}_R(\mathcal{K}^*)(q, \lambda) = \mathcal{W}_R(\mathcal{K})(q^{-1}, \lambda^{-1}) . \quad (2.159)$$

Amphicheiral knots are those knots which can be continuously deformed to their mirrors. If a knot is amphicheiral, its knot invariants satisfy the symmetry

$$\mathcal{W}_R(\mathcal{K})(q, \lambda) = \mathcal{W}_R(\mathcal{K})(q^{-1}, \lambda^{-1}) . \quad (2.160)$$

- When the representation R is replaced by its transpose R^T , the quantum knot invariants transform via [124, 125]

$$\mathcal{W}_{R^T}(\mathcal{K})(q, \lambda) = \mathcal{W}_R(\mathcal{K})(q^{-1}, \lambda) . \quad (2.161)$$

Therefore the quantum knot invariants in transpose-invariant representations enjoy the symmetry

$$\mathcal{W}_R(\mathcal{K})(q, \lambda) = \mathcal{W}_R(\mathcal{K})(q^{-1}, \lambda) . \quad (2.162)$$

2.3.5 Free Energies $1/N$ Expansion

Let us consider the large N expansion of the free energy in $U(N)$ Chern–Simons theory on S^3 defined by

$$\mathcal{F} = \log Z(S^3) . \quad (2.163)$$

In order to do the expansion, we first need to specify the ground state around which we expand the free energy. By studying the equation of motion of the Chern–Simons theory, it can be shown the ground states are given by flat connections on the three manifold, which are characterized by holonomies around nontrivial 1–cycles in the three manifold. Since S^3 is simply connected, the only flat connection is the trivial connection, which is the ground state we will be expanding around.

In the $U(N)$ Chern–Simons theory, the only propagating field is the gauge field A in the adjoint representation. As advocated by 't Hooft [126], in this case one can replace each propagator in a Feynman diagram in the perturbative expansion of \mathcal{F} by a double line with opposite directions. The Feynman diagram is then converted to a ribbon graph, which can be regarded as a Riemann surface with genus g and h boundary components. It can be shown that the contribution of this Feynman diagram to the free energy is proportional to $(ig_s)^{2g-2+h} N^h$, where the gauge coupling g_s is given by eq. (2.127). Collecting Feynman diagrams with the same topology, one can expand the free energy by

$$\mathcal{F}(g_s, N) = \sum_{g,h} \mathcal{F}_{g,h} (ig_s)^{2g-2+h} N^h . \quad (2.164)$$

The series in h with fixed g is convergent. So we can write

$$\mathcal{F}(g_s, t) = \sum_g \mathcal{F}_g(t) (ig_s)^{2g-2} , \quad (2.165)$$

where t is the 't Hooft coupling

$$t = ig_s N , \quad (2.166)$$

and we have performed the resummation

$$\mathcal{F}_g(t) = \sum_h \mathcal{F}_{g,h} t^h . \quad (2.167)$$

We can define a free energy which serves as the generating function of all the vevs of Wilson loops. For this purpose we introduce the Ooguri–Vafa operator [25]

$$Z(U, V) = \exp \left(\sum_{n=1}^{\infty} \frac{1}{n} \text{Tr} U^n \text{Tr} V^n \right) . \quad (2.168)$$

Here U is the $U(N)$ holonomy matrix for a knot \mathcal{K} , and V is some arbitrary $U(M)$ matrix (“source”). One can expand this operator with the help of the Frobenius formula and obtain

$$Z(U, V) = \sum_R \text{Tr}_R(U) \text{Tr}_R(V) . \quad (2.169)$$

After path integrated over field configurations of U we get,

$$Z(V) = \langle Z(U, V) \rangle = \sum_R \mathcal{W}_R(\mathcal{K}) \text{Tr}_R(V) , \quad (2.170)$$

i.e., we have the generating function of all the quantum knot invariants of \mathcal{K} . For the reason that will become clear in the next subsection, we call it the partition function of the deformed Chern–Simons theory. Likewise, we can define its logarithm to be the free energy,

$$\mathcal{F}(V) = \log Z(V) = \sum_{\vec{k}} \frac{1}{z_{\vec{k}}} \mathcal{W}_{\vec{k}}^{(c)} \Upsilon_{\vec{k}}(V) , \quad (2.171)$$

which is the generating function of the connected vevs $\mathcal{W}_{\vec{k}}^{(c)}(\mathcal{K})$ labelled by the vector $\vec{k} = (k_1, k_2, \dots)$

$$\mathcal{W}_{\vec{k}}^{(c)}(\mathcal{K}) = \langle \prod_{j=1}^{\infty} (\text{Tr } U^j)^{k_j} \rangle^{(c)} . \quad (2.172)$$

One can express the connected vevs in terms of quantum knot invariants. For instance

$$\mathcal{W}_{(2,0,\dots)}^{(c)} = \mathcal{W}_{\square} + \mathcal{W}_{\square} - (\mathcal{W}_{\square})^2 . \quad (2.173)$$

In the definition of $\mathcal{F}(V)$, the coefficient $z_{\vec{k}}$ is

$$z_{\vec{k}} = \prod_j k_j! j^{k_j} , \quad (2.174)$$

while

$$\Upsilon_{\vec{k}}(V) = \prod_{j=1}^{\infty} (\text{Tr } V^j)^{k_j} . \quad (2.175)$$

As in the definition of the free energy eq. (2.95) of type A topological open string theory, we need to assume $M \rightarrow \infty$ in order to distinguish all the source terms $\Upsilon_{\vec{k}}(V)$. Finally we can also consider the perturbative expansion of the connected vevs,

$$\mathcal{W}_{\vec{k}}^{(c)} = \sum_g \mathcal{W}_{\vec{k},g} (t) i^{|\vec{k}|} g_s^{2g-2+|\vec{k}|} . \quad (2.176)$$

2.3.6 Relation to Topological String Theory

It was shown by Witten [68] that with particular target spaces type A topological open string theory can be drastically simplified and in fact be reduced to Chern–Simons theory.

Take the smooth Calabi–Yau threefold T^*S^3 to be the target space. Let the local coordinates on S^3 be $q_i, i = 1, 2, 3$ and the local coordinates on the fibers of the cotangent bundle be $p_i, i = 1, 2, 3$. Then locally the Kähler form can be written as

$$\omega = \sum_{i=1}^3 dp_i \wedge dq_i . \quad (2.177)$$

It is easy to see S^3 is a Lagrangian submanifold in T^*S^3 because ω vanishes along the loci where p_i are constant. We can wrap N coincident D -branes around S^3 . Witten [68] showed that the type A topological open string theory on this stack of branes can be reduced to $U(N)$ Chern–Simons theory on S^3 , with the string coupling g_s identified with the gauge theory coupling $g_s = \exp(2\pi/(k + N))$. In other words, the open string free energy is the same as the Chern–Simons free energy after the identification of parameters mentioned above.

There is another type of Lagrangian submanifolds one can consider, which are associated to knots embedded in S^3 . Given a knot \mathcal{K} parametrized by $s \in [0, 2\pi)$, we can construct its conormal bundle $\tilde{\mathcal{L}}_{\mathcal{K}}$

$$\tilde{\mathcal{L}}_{\mathcal{K}} = \left\{ (q(s), p) \in T^*S^3 \mid \sum_i p_i \frac{dq_i}{ds} = 0, 0 \leq s < 2\pi \right\}. \quad (2.178)$$

This is obtained by considering at each point q on \mathcal{K} the two dimensional subspace of $T_q^*S^3$ orthogonal to the tangent vector to the knot and looping the subspace along the knot. The submanifold $\tilde{\mathcal{L}}_{\mathcal{K}}$ has the topology of $\mathbb{R}^2 \times S^1$ and it intersects with S^3 at the locus of the knot \mathcal{K} . It is easy to see the Kähler form when restricted to $\tilde{\mathcal{L}}_{\mathcal{K}}$ vanishes, so $\tilde{\mathcal{L}}_{\mathcal{K}}$ is also a Lagrangian submanifold. Let us wrap M coincident D -branes on it.

Now the open strings propagating on the N branes wrapping S^3 induce $U(N)$ Chern–Simons theory on S^3 with gauge field A and the open strings propagating on the M branes wrapping $\tilde{\mathcal{L}}_{\mathcal{K}}$ induce $U(M)$ Chern–Simons theory on $\tilde{\mathcal{L}}_{\mathcal{K}}$ with gauge field \tilde{A} . In addition there are open strings stretched between S^3 and $\tilde{\mathcal{L}}_{\mathcal{K}}$, which induce the scalar field ϕ in the bifundamental representation (N, \bar{M}) , as well as the scalar field $\bar{\phi}$ in the bifundamental representation (\bar{N}, M) . Since we focus on the Chern–Simons theory on S^3 , we regard \tilde{A} as a nondynamical source term. It can be shown that after the scalar fields are integrated out the action of the $U(N)$ Chern–Simons theory on S^3 is modified to

$$S_{CS}[A] - i \sum_{n=1}^{\infty} \frac{1}{n} \text{Tr} U^n \text{Tr} V^n, \quad (2.179)$$

where U and V^{-1} are the holonomies of A and \tilde{A} along the knot \mathcal{K} . The partition function of this deformed Chern–Simons theory is

$$Z_{\text{def}}(S^3) = \int \mathcal{D}A \exp \left(i S_{CS}[A] + \sum_{n=1}^{\infty} \frac{1}{n} \text{Tr} U^n \text{Tr} V^n \right) = \left\langle \exp \left(\sum_{n=1}^{\infty} \frac{1}{n} \text{Tr} U^n \text{Tr} V^n \right) \right\rangle. \quad (2.180)$$

We see that the Ooguri–Vafa operator appears, and the partition function here coincides with the one defined in eq. (2.170). The free energy of the deformed Chern–Simons theory is then given precisely by eq. (2.171).

2.4 Matrix Models

2.4.1 Basic Definitions

Here we review some basics of matrix models, focusing on the saddle point approximation in this section and loop equations in the next, the two aspects which are most relevant to topological

string theory. Comprehensive treatments on matrix models can be found in refs. [36, 127–129].

Matrix models are the simplest quantum gauge theories which are formulated on 0+0 dimensions. In fact since there is no propagation of gauge fields in spacetime manifold, they can also be understood as describing thermal fluctuations of a statistical ensemble which in addition enjoys a $U(N)$ gauge symmetry.

Let us suppose M is a Hermitian $N \times N$ matrix, and V is a function of M such that its trace is invariant under the gauge transformation

$$M \rightarrow U M U^\dagger, \quad U \in U(N). \quad (2.181)$$

A typical example of V is a polynomial

$$V(M) = \sum_{k \geq 1} \frac{g_k}{k} M^k. \quad (2.182)$$

Let us also define the Haar measure of the Hermitian matrices to be

$$dM = 2^{\frac{N(N-2)}{2}} \prod_{i=1}^N dM_{ii} \prod_{1 \leq i < j \leq N} d\text{Re } M_{ij} d\text{Im } M_{ij}, \quad (2.183)$$

and it is also invariant under the gauge transformation. Here M_{ij} is the (i, j) entry of the matrix M . The numerical factor in the front is for latter convenience. Then we can define the gauge invariant partition function that integrates over fluctuations of the matrix entries

$$Z = \frac{1}{\text{vol}(U(N))} \int dM e^{-\frac{1}{g_s} \text{Tr } V(M)}. \quad (2.184)$$

This is called the Hermitian 1–matrix model or matrix integral.

Since the only field in this theory is in the adjoint representation of $U(N)$, we can introduce the 't Hooft parameter

$$t = g_s N \quad (2.185)$$

and consider the 't Hooft limit

$$N \rightarrow \infty, \quad g_s \rightarrow 0, \quad t \text{ finite}. \quad (2.186)$$

Similar to the Chern–Simons theory, in this limit the free energy of the matrix model defined by

$$\mathcal{F} = \log Z, \quad (2.187)$$

enjoys the genus expansion

$$\mathcal{F} = \sum_{g=0}^{\infty} \mathcal{F}_g(t) g_s^{2g-2}, \quad \text{where} \quad \mathcal{F}_g(t) = \sum_{h=1}^{\infty} \mathcal{F}_{g,h} t^h. \quad (2.188)$$

We can also consider the one–trace correlation functions

$$\langle \text{Tr } M^k \rangle = \frac{1}{\text{vol}(U(N))} \int dM \text{Tr } M^k e^{-\frac{1}{g_s} \text{Tr } V(M)}. \quad (2.189)$$

and their generating function

$$W(p) = g_s \sum_{k=0}^{\infty} \frac{\langle \text{Tr } M^k \rangle}{p^{k+1}} = g_s \left\langle \text{Tr} \frac{1}{p - M} \right\rangle, \quad (2.190)$$

which is called the 1–point resolvent. It can be generalized to the s –point resolvent

$$W(p_1, \dots, p_s) = g_s^{2-s} \sum_{k_j=1}^{\infty} \frac{\langle \text{Tr } M^{k_1} \dots \text{Tr } M^{k_s} \rangle^{(c)}}{p_1^{k_1+1} \dots p_s^{k_s+1}} = g_s^{2-s} \left\langle \text{Tr} \frac{1}{p_1 - M} \dots \text{Tr} \frac{1}{p_s - M} \right\rangle^{(c)}, \quad (2.191)$$

which is the generating function of s –trace correlation functions. Here the superscript (c) means connected components. The resolvents also enjoy genus expansion

$$W(p_1, \dots, p_s) = \sum_{g=0}^{\infty} g_s^{2g} W_g(p_1, \dots, p_s), \quad s \geq 1. \quad (2.192)$$

Furthermore suppose the potential is a polynomial or has a power series expansion as in eq. (2.182), one can define the loop operator

$$\frac{\partial}{\partial V}(p) = - \sum_{k=1}^{\infty} \frac{k}{p^{k+1}} \frac{\partial}{\partial g_k}, \quad (2.193)$$

which relates all the resolvents to the free energy

$$W_g(p_1, \dots, p_s) = \frac{\partial}{\partial V}(p_1) \dots \frac{\partial}{\partial V}(p_s) \mathcal{F}_g = \frac{\partial}{\partial V}(p_2) \dots \frac{\partial}{\partial V}(p_s) W_g(p_1). \quad (2.194)$$

There is another way to formulate the matrix model in eq. (2.184) which is easier to manipulate. Since every Hermitian matrix can be converted via the gauge transformation eq. (2.181) to a diagonal matrix, we can use the Faddeev–Popov gauge fixing procedure to localize the matrix integral to only diagonal matrices. In other words we apply the Faddeev–Popov techniques and choose the gauge fixing condition

$$\delta(U M) := \prod_{i < j} \delta^{(2)}(U M_{ij}), \quad (2.195)$$

where $U M = U M U^\dagger$. The gauge fixing computation is explicitly carried out in [36]. The end result involves only the N eigenvalues $\lambda_i, i = 1, \dots, N$ of the Hermitian matrix M

$$\frac{1}{\text{vol}(U(N))} \int dM f(M) = \frac{1}{N!} \frac{1}{(2\pi)^N} \int \prod_{i=1}^N d\lambda_i \Delta^2(\lambda) f(\lambda). \quad (2.196)$$

Here $\Delta^2(\lambda)$ denotes

$$\Delta^2(\lambda) = \prod_{i < j} (\lambda_i - \lambda_j)^2, \quad (2.197)$$

which is the square of the Vandermonde determinant. It can be understood as the Jacobian that relates the Haar measure and new measure $\prod_{i=1}^N d\lambda_i$. Note the numerical factor $2^{\frac{N(N-2)}{2}}$ in the Haar measure has disappeared. $f(\lambda)$ is what one obtains after replacing M by $\text{diag}(\lambda_1, \dots, \lambda_N)$

in the function of matrix $f(M)$. Since the N eigenvalues are not ordered, we have to divide out the $N!$ symmetry factor. As a particular case of the generic result, the partition function can be written as

$$Z = \frac{1}{N!} \frac{1}{(2\pi)^N} \int \prod_{i=1}^N d\lambda_i \Delta^2(\lambda) e^{-\frac{1}{g_s} \sum_{i=1}^N V(\lambda_i)} . \quad (2.198)$$

2.4.2 Saddle Point Approximation

The planar contributions to the free energy and resolvents were solved in the classic paper [130], which showed that the matrix model in the planar limit is completely described by a Riemann surface.

In the 't Hooft limit, the path integral is dominated by semi-classical configurations, in other words, the ground states. To analyze these ground states, we write the partition function in the following form,

$$Z = \frac{1}{N!} \int \prod_{i=1}^N \frac{d\lambda_i}{2\pi} e^{\frac{1}{g_s^2} S_{\text{eff}}(\lambda)} . \quad (2.199)$$

where the effective action is

$$S_{\text{eff}}(\lambda) = -g_s \sum_{i=1}^{\infty} V(\lambda_i) + 2g_s^2 \sum_{i<j} \log |\lambda_i - \lambda_j| . \quad (2.200)$$

Then we can immediately derive the equation of motion by varying the eigenvalues in the effective action

$$V'(\lambda_i) = 2g_s \sum_{j \neq i} \frac{1}{\lambda_i - \lambda_j}, \quad i = 1, \dots, N . \quad (2.201)$$

and a solution of the equation of motion, i.e. a distribution of the eigenvalues $\{\lambda_i\}$, is a semi-classical configuration. We can formally encode the distribution in a single function

$$\rho(\lambda) = \frac{1}{N} \sum_{i=1}^N \delta(\lambda - \lambda_i) . \quad (2.202)$$

In the large N limit, ρ becomes a continuous function, and in all interesting cases it has a compact support. Let us assume for the sake of simplicity the compact support \mathcal{D} consists of s intervals, also called s cuts, on the real axis³²,

$$\mathcal{D} = [x_1, x_2] \cup \dots \cup [x_{2s-1}, x_{2s}] , \quad (2.203)$$

and the eigenvalue density ρ vanishes outside the s intervals. Naturally ρ satisfies

$$\int_{\mathcal{D}} \rho(\lambda) d\lambda = 1 . \quad (2.204)$$

To understand the shape of the compact support, we write down the effective potential from

³² In the path integral eq. (2.198) the eigenvalues are integrated over the real axis. However for a generic potential one may need to deform the path of integral away from the real axis for the integral to converge. Consequently the compact support \mathcal{D} is also lifted away from the real axis. These are called holomorphic matrix models.

the equation of motion

$$V_{\text{eff}}(\lambda_i) = V(\lambda_i) - 2g_s \sum_{j \neq i} \log |\lambda_i - \lambda_j|. \quad (2.205)$$

Suppose $V'(\lambda)$ has s zeroes. If the expansion parameter g_s is zero, all the eigenvalues condensate to the s extrema of $V(\lambda)$. When g_s increases, the repulsive potential $-2g_s \sum_{j \neq i} \log |\lambda_i - \lambda_j|$ pushes the eigenvalues away from each other, and the N_i eigenvalues at the i -th extremum spread out to form the interval $[x_{2i-1}, x_{2i}]$ centered around the extremum. We define the *filling fractions*

$$\epsilon_i = N_i/N = \int_{x_{2i-1}}^{x_{2i}} \rho(\lambda) d\lambda, \quad i = 1, \dots, s \quad (2.206)$$

to record the number of eigenvalues distributed in each interval. Among the s filling fractions only $s - 1$ of them are independent since all of them add up to 1. Note the choice of the filling fractions, in other words the eigenvalue distribution, is a choice of the ground state around which quantum (or thermal) fluctuations occur. Therefore it is a free choice. Once the filling fractions are chosen, they give us $s - 1$ constraining conditions³³. Note that similar to the filling fractions, we can also define the partial 't Hooft parameters

$$t_i = t\epsilon_i = g_s N_i, \quad i = 1, \dots, s. \quad (2.207)$$

But unlike filling fractions, all the s partial 't Hooft parameters are independent.

Using the substitution

$$\frac{1}{N} \sum_{i=1}^N f(\lambda_i) \rightarrow \int_{\mathcal{D}} f(\lambda) \rho(\lambda) d\lambda \quad (2.208)$$

we can express every planar quantity in terms of the eigenvalue density. For instance the planar free energy can be written as

$$\mathcal{F}_0 = S_{\text{eff}} = -t \int_{\mathcal{D}} d\lambda \rho(\lambda) V(\lambda) + t^2 \int_{\mathcal{D} \times \mathcal{D}} d\rho d\rho' \rho(\lambda) \rho(\lambda') \log |\lambda - \lambda'|, \quad (2.209)$$

and the planar 1-point resolvent has the form

$$W_0(p) = t \int_{\mathcal{D}} d\lambda \frac{\rho(\lambda)}{p - \lambda}. \quad (2.210)$$

So in order to solve the planar matrix model we only need to compute ρ .

The genus zero resolvent $W_0(p)$ has interesting properties. It has the following asymptotic behavior

$$W_0(p) = \frac{t}{p} + \mathcal{O}(p^{-2}), \quad p \rightarrow \infty, \quad (2.211)$$

because of the normalization of ρ in eq. (2.204). Besides, from its expression in eq. (2.210) it is easy to see $W_0(p)$ has branch cuts along \mathcal{D} the compact support of ρ (it is actually analytic everywhere else), and furthermore the discontinuity of $W_0(p)$ across \mathcal{D} is

$$\text{Disc } W_0(\lambda) = W_0(\lambda + i\epsilon) - W_0(\lambda - i\epsilon) = -2\pi i \cdot t \rho(\lambda). \quad (2.212)$$

³³ There is another choice of constraining conditions. It requires the effective potential, which is level inside each cut, be the same among all the cuts. It also yields $s - 1$ constraining conditions. The constraining conditions we choose is more relevant for topological string as we will see in section 2.4.4.

Therefore once we know the genus zero 1–point resolvent, the eigenvalue density immediately follows.

In order to compute $W_0(p)$ we multiply the equation of motion eq. (2.201) by $1/(\lambda_i - p)$ and sum over i . In the large N limit we find an algebraic equation for $W_0(p)$

$$W_0(p)^2 - V'(p)W_0(p) + R_{m-1}(p) = 0 , \quad (2.213)$$

where

$$R_{m-1}(p) = t \int_{\mathcal{D}} d\lambda \rho(\lambda) \frac{V'(p) - V'(\lambda)}{p - \lambda} = \oint_{C_\infty} \frac{d\lambda}{2\pi i} \frac{W_0(\lambda)V'(\lambda)}{p - \lambda} . \quad (2.214)$$

Here the second equality is derived by using eq. (2.212) to convert the line integral along the cuts to a contour integral around the cuts and then deforming the contour away from the cuts until it becomes a contour around the point p plus a contour around infinity. Let us assume the potential $V(p)$ is a polynomial of degree $m + 1$ with leading coefficient g_{m+1} . Then from the first equality in the formula above we find that $R_{m-1}(p)$ is a polynomial of degree at most $m - 1$, while the second equality, together with the asymptotic behavior of $W_0(p)$, fixes the leading coefficient of R_m to be tg_{m+1} .

We can solve the quadratic equation eq. (2.213) for the planar resolvent, and choose the solution

$$W_0(p) = \frac{1}{2} \left(V'(p) - \sqrt{V'(p)^2 - 4R_{m-1}(p)} \right) , \quad (2.215)$$

due to its asymptotic behavior. Let us define

$$y(p) := V'(p) - 2W_0(p) , \quad (2.216)$$

then the above solution implies

$$y(p)^2 = V'(p)^2 - 4R_{m-1}(p) , \quad (2.217)$$

which describes a Riemann surface (a hyperelliptic Riemann surface to be precise) parametrized by p and y . It is called the *spectral curve* of the matrix model, and it can be seen that it encodes all the planar information of the matrix model as well as the filling fractions.

The spectral curve \mathcal{C} described by eq. (2.217) can be highly singular. We factor out the smooth part

$$y(p)^2 = M(p)^2 \prod_{i=1}^{2s} (p - x_i) , \quad (2.218)$$

where $M(p)$ is a polynomial of degree $m - s$, and the branch points x_i are all distinct. The smooth *reduced spectral curve* $\tilde{\mathcal{C}}$

$$\tilde{y}(p)^2 = \prod_{i=1}^{2s} (p - x_i) , \quad (2.219)$$

has genus $s - 1$ and its branch points are precisely the end points of the compact support \mathcal{D} . We can choose the branch cuts of the reduced spectral curve so that they coincide with \mathcal{D} . Furthermore since $V'(p)$ is analytic along the cuts \mathcal{D} , the eigenvalue density — planar resolvent correspondence in eq. (2.212) can equally be written as

$$\rho(\lambda) = \frac{1}{4\pi i \cdot t} (y(\lambda + i\epsilon) - y(\lambda - i\epsilon)) , \quad (2.220)$$

in terms of $y(\lambda)$. Therefore we can use $y(\lambda)$ in place of $\rho(\lambda)$ to compute all the planar quantities. Besides, the definition of partial 't Hooft parameters in eq. (2.207) is translated to

$$t_i = \frac{1}{4\pi i} \oint_{A_i} y(\lambda) d\lambda, \quad (2.221)$$

where A_i is the clockwise contour around the cut $[x_{2i-1}, x_{2i}]$. One can also derive the following property of planar free energy by sending an eigenvalue λ_j to infinity and integrating the force acting upon it along the way

$$\frac{\partial \mathcal{F}_0}{\partial t_i} = \int_{B_i} y(\lambda) d\lambda. \quad (2.222)$$

Here B_i is the path going from the endpoint x_{2i} of the i -th cut to infinity. The integral actually diverges and has to be renormalized. This is done by regularizing the infinite distance with truncation Λ and throwing away after integration everything that contains Λ .

It remains to fix the spectral curve, which boils down to fixing the $m - 1$ coefficients in the polynomial $R_{m-1}(p)$ (recall the leading coefficient has already been determined). Suppose we are given the s partial 't Hooft parameters as the additional conditions. The genus of the reduced spectral curve is s , and we have $m - s$ nodal point conditions on the spectral curve equation eq. (2.217). The other $s - 1$ conditions are naturally provided by the partial 't Hooft parameters through eq. (2.221)³⁴.

Finally we comment that in section 2.5 we will see the spectral curve \mathcal{C} in fact contains not only the planar information of the matrix model, but the information in all genera in the large N expansion. Therefore the matrix model is (almost) completely described by its spectral curve³⁵. Besides we point out the solution of the planar resolvent eq. (2.215) can be packed into a compact form

$$W_0(p) = \frac{1}{2} \oint_{C_{\mathcal{D}}} \frac{d\lambda}{2\pi i} \frac{V'(\lambda) \tilde{y}(p)}{p - \lambda \tilde{y}(\lambda)}, \quad (2.223)$$

as explained in refs. [131, 132]. By unwinding the contour $C_{\mathcal{D}}$ around the cuts \mathcal{D} we get a contour around the point p and a contour around infinity. The first term on the right hand side of eq. (2.215) immediately emerges as the residue at p , while getting the second term requires slightly more work.

2.4.3 Relation to Chern–Simons Theory

It was shown in section 2.3.3 that the partition function of $U(N)$ Chern–Simons theory on S^3 can be computed via the surgery techniques and the result was eq. (2.153). This partition function can be cast in the following form [133]

$$Z_{CS}(S^3) = \frac{e^{-\frac{x}{i2}N(N^2-1)}}{N!} \int \prod_{i=1}^N \frac{d\beta_i}{2\pi} e^{-\sum_i \beta_i^2/2x} \prod_{i<j} \left(2 \sinh \frac{\beta_i - \beta_j}{2} \right)^2, \quad (2.224)$$

with

$$x = \frac{2\pi i}{k + N}, \quad (2.225)$$

³⁴ This is not the traditional way of fixing the spectral curve, which rather exploits the asymptotic behavior of the planar resolvent. This is explained for instance in ref. [36].

³⁵ There may be non-perturbative information not captured by the asymptotic series in the large N limit.

It looks very similar to the partition function of a Hermitian matrix model in eq. (2.198) with expansion parameter x and a quadratic potential

$$V(\beta) = \frac{1}{2}\beta^2, \quad (2.226)$$

although the integral measure

$$\prod_{i=1}^N \frac{d\beta_i}{2\pi} \prod_{i<j} \left(2 \sinh \frac{\beta_i - \beta_j}{2} \right)^2 \quad (2.227)$$

is different from that of a Hermitian matrix model. Eq. (2.224) is sometimes called the Chern–Simons matrix model. Note that since the potential has only one zero, the compact support of the eigenvalue density has only one interval. If the expansion parameter x is very small, all the eigenvalues β_i would be very close to each other. As a consequence,

$$\prod_{i<j} \left(2 \sinh \frac{\beta_i - \beta_j}{2} \right)^2 \sim \prod_{i<j} (\beta_i - \beta_j)^2, \quad (2.228)$$

meaning the integral measure can be approximated by that of a Hermitian matrix model.

Ideally we would like to write eq. (2.224) exactly in the form of a Hermitian matrix integral so that the techniques of the saddle point approximation can be applied. This can be done via a change of variables [134, 135], although the resulting Hermitian matrix integral has a nonconventional potential. Let us define new variables

$$\lambda_i = \exp(\beta_i + t), \quad (2.229)$$

where $t = xN$ is the 't Hooft parameter, then eq. (2.226) in terms of the new variables reads

$$Z_{CS}(S^3) = \frac{1}{N!} \prod_{i=1}^N \frac{d\lambda_i}{2\pi} \Delta^2(\lambda) \exp \left(- \sum_{i=1}^N (\log \lambda_i)^2 / 2x \right). \quad (2.230)$$

This is a Hermitian 1–matrix model with the potential

$$V(\lambda) = \frac{1}{2}(\log \lambda)^2. \quad (2.231)$$

Although the potential is not a polynomial, some results of the saddle point approximation as presented in the previous subsection can still be applied. For instance the formula for the planar 1–point resolvent in eq. (2.223) is still valid, and one can deform the contour of integral similar in spirit to the discussion following eq. (2.223) to simplify it, although now one has to take into account the branch cut of the logarithm. The result is

$$W_0(p) = -\frac{1}{p} \log \left(\frac{1 + e^{-t}p + \sqrt{(1 + e^{-t}p)^2 - 4p}}{2p} \right). \quad (2.232)$$

Let us define new variables

$$y(p) := t - pW_0(p) + \pi i, \quad x(p) := t - \log p. \quad (2.233)$$

The above result of the planar resolvent indicates

$$1 + e^y + e^x + e^{x-y+t} = 0 , \quad (2.234)$$

which we identify as the spectral curve of the Chern–Simons matrix model.

Finally recall that the Chern–Simons theory is only well–defined as a quantum topological field theory if a framing is specified, and the partition function eq. (2.224) was computed with framing zero. A framing shift by f in the Chern–Simons theory is reflected in the Chern–Simons matrix model by the change of variables

$$x = x' + fy', \quad y = y' \quad (2.235)$$

in the spectral curve.

2.4.4 Relation to Topological String Theory

In the remarkable paper [136] Dijkgraaf and Vafa showed that type B open topological string theory on a large variety of target spaces can be reduced to Hermitian matrix models. Let us consider the three complex dimensional hypersurface W in \mathbb{C}^4 defined by

$$uv = y^2 - V'(x)^2 , \quad (2.236)$$

where $V(x)$ is a degree $m + 1$ polynomial in x . This is a Calabi–Yau threefold, albeit it is singular at m points given by

$$u = v = y = 0, \quad x = x_i, \quad i = 1, \dots, m \quad (2.237)$$

where x_i are the m critical points of $V(x)$. Locally near a singular point of W , the hypersurface looks like a conifold singularity. This is evident after the change of variables $y \rightarrow (y + x)/2, V'(x) \rightarrow (y - x)/2$ and the defining equation for W becomes

$$uv - xy = 0 . \quad (2.238)$$

Therefore we can resolve the singularity by blowing up each singular point to a \mathbb{P}^1 as we did in section 2.2.2. The new smooth geometry remains a Calabi–Yau, and we denote it W_{res} . The m \mathbb{P}^1 's obtained from blow–ups are holomorphic submanifolds of W .

Let us consider type B open topological string theory with W_{res} being the target space and the i -th \mathbb{P}^1 being wrapped by N_i D–branes. It was shown in [136] that the partition function of the open topological string theory can be reduced to exactly the Hermitian matrix model in eq. (2.198) with the polynomial potential $V(\lambda)$. Furthermore the classical ground state of the matrix model is chosen such that N_i eigenvalues are located at the i -th critical point of $V(\lambda)$. We assume $N_i \neq 0$ for any i so that the number of cuts s is the same as m . Let $N = \sum_{i=1}^m N_i$, then the filling fractions are

$$\epsilon_i = \frac{N_i}{N} . \quad (2.239)$$

The large N expansion of the free energy $\mathcal{F} = \log Z$ of the matrix model has the form

$$\mathcal{F}(g_s, N_i) = \sum_{g, h_1, \dots, h_m} \mathcal{F}_{g, h_1, \dots, h_m} g_s^{2g-2+h} N_1^{h_1} \dots N_m^{h_m} , \quad (2.240)$$

where $h = \sum_{i=1}^m h_i$. We can identify $\mathcal{F}_{g,h_1,\dots,h_m}$ in the mirror type A theory as the contribution of the worldsheet with genus g and h_i boundary components mapped to the N_i mirror D-branes.

In addition to the Calabi–Yau threefold W_{res} we can also consider type B topological string theory on the resolution Y_{res} of the singular Calabi–Yau threefold

$$Y : uv = (1 - e^x)(1 - e^y) , \quad (2.241)$$

where $u, v, x, y \in \mathbb{C}$. The Calabi–Yau Y_{res} has already been discussed in section 2.2.2 and revealed to be the mirror dual of T^*S^3 . Since the type A open topological string theory of N D-branes wrapping S^3 in T^*S^3 is equivalent to $U(N)$ Chern–Simons theory on S^3 , as discussed in section 2.3.6, and the partition function of the Chern–Simons theory can be interpreted as a matrix model integral (section 2.4.3), it is natural to conjecture the existence of a matrix model interpretation of type B open topological string of N D-branes wrapping some appropriate holomorphic submanifold in Y_{res} . Such an interpretation was found in [114], and the holomorphic submanifold is the \mathbb{P}^1 arising from blowing up the conifold singularity in Y . Furthermore this matrix model turns out to be precisely the Chern–Simons matrix model.

2.4.5 Large N Duality

The idea that a $U(N)$ gauge theory in the limit $N \rightarrow \infty$ may have a closed string theory interpretation has a long history since 't Hooft [126] and was later for example concretely realized in the celebrated AdS/CFT correspondence [17]. The insight of 't Hooft was, if one replaces the propagator of a gauge field by a double line with opposite directions, a Feynman diagram with only gauge fields is converted to a ribbon graph which is basically a Riemann surface with boundary. All the ribbon graphs with genus g and h boundary components have contributions proportional to g_s^{2g-2+h} and N^h , and can be grouped together. Here g_s is the gauge coupling. Therefore the free energy has the decomposition

$$\mathcal{F}(g_s, N) = \sum_{g,h} \mathcal{F}_{g,h} g_s^{2g-2+h} N^h . \quad (2.242)$$

Furthermore one can define the 't Hooft parameter $t = g_s N$ and perform the summation in two steps

$$\mathcal{F}_g(t) = \sum_h \mathcal{F}_{g,h} t^h , \quad (2.243)$$

followed by

$$\mathcal{F}(g_s, t) = \sum_g \mathcal{F}_g(t) g_s^{2g-2} . \quad (2.244)$$

It can be shown³⁶ that in general the first sum can be explicitly carried out since the series (2.243) converges at $t = 0$ with finite radius of convergence, while the second sum is an asymptotic series. So in the 't Hooft limit

$$g_s \rightarrow 0, \quad t \text{ finite} \quad (\text{necessarily } N \rightarrow \infty) \quad (2.245)$$

eq. (2.244) is meaningful. On the other hand the form of this equation is typical of the free energy of a closed string theory.

³⁶ See for instance [137].

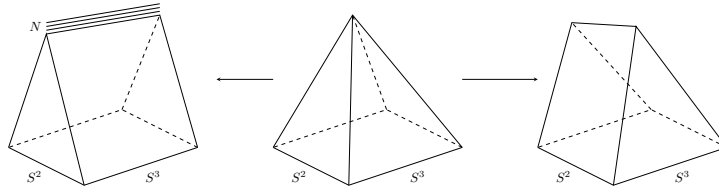


Figure 2.11: The conifold transition underlying the Gopakumar–Vafa conjecture. The three diagrams from left to right represent T^*S^3 , conifold singularity, and $\mathcal{O}(-1) \oplus \mathcal{O}(-1) \rightarrow \mathbb{P}^1$ respectively. In the first diagram, N stands for a stack of N branes wrapping S^3 .

We have seen that gauge theories like $U(N)$ Chern–Simons theory on S^3 and Hermitian 1–matrix models with polynomial potentials have open string interpretations, where N is the number of D –branes. It is conceivable that in the limit $N \rightarrow \infty$ the backreaction of the branes to the background geometry is sizeable, and therefore in the large N limit if the gauge theory has a dual closed string theory where the branes are removed, the background geometry of the latter should be different from that of the open string theory. In other words there will be a transition of the background geometry.

The $U(N)$ Chern–Simons theory on S^3 with level k was realized in section 2.3.6 as type A open topological string theory on N branes wrapping the three–sphere in the cotangent bundle T^*S^3 . We knew by eq. (2.122) the smooth Calabi–Yau T^*S^3 is the deformation of the conifold singularity. We also saw in section 2.2.2 another way to smooth the conifold singularity by blowing up the singular point to \mathbb{P}^1 . Taking this as a hint Gopakumar and Vafa conjectured [21] that in the large N limit the open topological string, and therefore the Chern–Simons theory, is equivalent to type A closed topological string theory on the resolved conifold $\mathcal{O}(-1) \oplus \mathcal{O}(-1) \rightarrow \mathbb{P}^1$ with the following dictionary

$$g_s = \frac{2\pi}{k + N}, \quad t = ig_s N, \quad (2.246)$$

where g_s is the closed string coupling and t the complexified Kähler modulus of the \mathbb{P}^1 . The change of the underlying background geometry is called the conifold transition, and it is illustrated in Fig. 2.11. The Gopakumar–Vafa conjecture was verified by directly matching the free energies of the Chern–Simons theory with those of the closed string theory at all genera [21].

One can also find the large N dual of the Hermitian matrix models along the same line of thought. As seen in section 2.4.4 the Hermitian 1–matrix model with polynomial potential $V(\lambda)$ of degree $m + 1$ can be interpreted as open type B topological string with N_i branes wrapping the i –th \mathbb{P}^1 in W_{res} obtained from blowing up the i –th singular point of W . Locally each singular point of W is of conifold type, and thus one can also smooth the singularity of W by deformation, resulting in the smooth hypersurface in \mathbb{C}^4

$$W_{\text{def}} : \quad uv = y^2 - (V'(x))^2 + 4R_{m-1}(x). \quad (2.247)$$

The extra polynomial $R_{m-1}(x)$ of degree $m - 1$ has m coefficients in accord with the freedom of deforming the m singular points of W . Dijkgraaf and Vafa [136] thus conjectured that in the large $N = \sum_i N_i$ limit, the matrix model is dual to close type B topological string in the target space W_{def} , where $R_{m-1}(x)$ depends on the distribution N_i of branes. Indeed the spectral curve

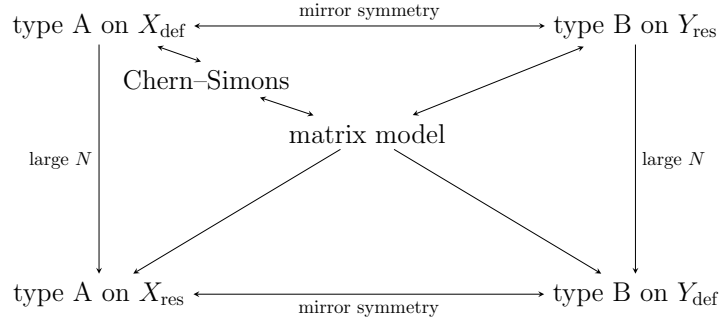


Figure 2.12: Mirror symmetry and large N duality form a circle of dualities. Here X is the conifold singularity and Y is the singular Calabi–Yau given by eq. (2.241).

of the closed string theory is

$$y^2 - (V'(x))^2 + 4R_{m-1}(x) = 0 , \quad (2.248)$$

where $R_{m-1}(x)$ can be chosen such that it is identical with the spectral curve of the matrix model in eq. (2.217). Note in type B closed string the complex structure moduli t_i and the (derivative of) genus zero free energy \mathcal{F}_0 are given by

$$t_i = \frac{1}{4\pi i} \oint_{\mathcal{A}_i} y dx, \quad \frac{\partial \mathcal{F}_0}{\partial t_i} = \oint_{\mathcal{B}_i} y dx , \quad (2.249)$$

while the same formulae give the partial 't Hooft parameters and the planar free energy F_0 in the matrix model. It is natural to identify the moduli in type B topological string with the partial 't Hooft parameters in the matrix model so that their genus 0 free energies coincide. In fact the identical spectral curve implies the matrix model and the type B topological string theory have the same free energies at all genera as a result of the BKMP theorem that will be discussed in section 2.5.5.

This also implies a new perspective to look at the large N duality between $U(N)$ Chern–Simons theory on S^3 and type A closed topological string on the resolved conifold. With the identification $Q = e^{-t}$, the spectral curve of the Chern–Simons matrix model in eq. (2.234) is same as the spectral curve eq. (2.116) of the mirror dual of the type A topological string theory, up to a reparametrization that preserves the symplectic form $dx \wedge dy$.

Finally we point out the large N duality together with mirror symmetry discussed in section 2.2.6 forms a beautiful circle of dualities that connects (closed) topological string theory, Chern–Simons theory, and Hermitian matrix models to each other. The example involving Chern–Simons theory on S^3 and the resolved conifold is illustrated in Fig. 2.12.

2.5 Topological Recursion

2.5.1 Loop Equations and Their Solutions

In this section we look beyond the planar limit of matrix models by solving the loop equations. In matrix models loop equations (also called the Schwinger–Dyson equations) are a chain of infinite integral equations which can be used to compute resolvents exactly to all genera. The k -th loop equation in Hermitian 1-matrix models can be derived from the invariance of the

matrix integral under the reparametrization [127, 138–141]

$$M \rightarrow M + \epsilon \frac{1}{x_1 - M} \prod_{j=2}^k \text{Tr} \frac{1}{x_j - M} . \quad (2.250)$$

For instance the first two loop equations read,

$$\widehat{K}(x)W(x) = W(x)^2 + g_s^2 W(x, x) , \quad (2.251)$$

$$\widehat{K}(x_1)W(x_1, x_2) = 2W(x_1)W(x_1, x_2) + g_s^2 W(x_1, x_1, x_2) + \frac{\partial}{\partial x_2} \frac{W(x_2) - W(x_1)}{x_2 - x_1} . \quad (2.252)$$

Here the integral operator $\widehat{K}(x)$ is defined to act on a function by

$$\widehat{K}(x)f(x, \dots) = \oint_{C_{\mathcal{D}}} \frac{d\lambda}{2\pi i} \frac{V'(\lambda)}{x - \lambda} f(\lambda, \dots) , \quad (2.253)$$

where the contour of integral $C_{\mathcal{D}}$ encircles all the branch cuts of $W(\lambda)$ ($W(p)$ and its planar limit have the same branch cuts) but leaves out the point p . Note that once we have the first loop equation, the second and higher loop equations can be obtained by applying the loop operator $\partial/\partial V$ on both sides of the equation.

To see that the loop equations can be used to recursively compute all the resolvents, one can do genus expansion on both sides of eqs. (2.251), (2.252) and obtain loop equations at different genera.

$$\left(\widehat{K}(x) - 2W_0(x) \right) W_g(x) = \sum_{g'=1}^{g-1} W_{g'}(x)W_{g-g'}(x) + W_{g-1}(x, x) , \quad (2.254)$$

$$\begin{aligned} \left(\widehat{K}(x_1) - 2W_0(x_1) \right) W_g(x_1, x_2) = & 2 \sum_{g'=1}^g W_{g'}(x_1)W_{g-g'}(x_1, x_2) + W_{g-1}(x_1, x_1, x_2) \\ & + \frac{\partial}{\partial x_2} \frac{W_g(x_2) - W_g(x_1)}{x_2 - x_1} . \end{aligned} \quad (2.255)$$

We assume that the planar resolvent $W_0(x)$ is already known. Notice that the k -th loop equation at genus g involves, other than $W_g(x_1, \dots, x_k)$, a) resolvents with lower genera but probably one more insertion point, like $W_{g-1}(x_1, x_1, \dots, x_k)$, $W_{g'}(x_1, \dots, x_k)$, and $W_{g'}(x_1, \dots, x_{k-1})$, $g' < g$; and b) resolvents with the same genus and fewer insertion points, like $W_g(x_1, \dots, x_{k-1})$. Therefore one can adopt the points–first–genus–second double recursion strategy: one computes recursively resolvents with increasingly more insertion points but with fixed genus, starting with genus zero, and then moves up to the next genus.

With this strategy Eynard solved beautifully the loop equations in [142]. Let us define

$$U(x_1; x_2, \dots, x_k) = g_s^{2-k} \left\langle \text{Tr} \frac{V'(x_1) - V'(M)}{x_1 - M} \text{Tr} \frac{1}{x_2 - M} \cdots \text{Tr} \frac{1}{x_k - M} \right\rangle . \quad (2.256)$$

and its genus expansion

$$U(x_1; x_2, \dots, x_k) = \sum_g g_s^{2g} U_g(x_1; x_2, \dots, x_k) . \quad (2.257)$$

It is easy to see $U(x_1; x_2, \dots, x_k)$ is a polynomial in x_1 with degree at most $m - 1$, m being the degree of $V'(\lambda)$. In fact if $k + g \geq 2$, $U_g(x_1; x_2, \dots, x_k)$ is at most a degree $m - 2$ polynomial in x_1 . Then instead of solving the integral equations, Eynard used the identity

$$\widehat{K}(x_1)W_g(x_1, x_2, \dots, x_k) = V'(x_1)W_g(x_1, x_2, \dots, x_k) - U_g(x_1; x_2, \dots, x_k), \quad (2.258)$$

to hide the troublesome $\widehat{K}(x_1)W_g(x_1, x_2, \dots, x_k)$ in the polynomial $U_g(x_1; x_2, \dots, x_k)$. Next by exploiting the analytic property of $U(x_1; x_2, \dots, x_k)$ and the loop equations he proved recursively that

$$\omega_k^{(g)} := W_g(x_1, \dots, x_k)dx_1 \cdots dx_k + \delta_{k,2}\delta_{g,0} \frac{dx_1 dx_2}{(x_1 - x_2)^2} \quad (2.259)$$

were meromorphic multidifferentials with poles only at the ramification points of the reduced spectral curve $\tilde{\mathcal{C}}$. Finally he reduced the polynomial $U_g(x_1; x_2, \dots, x_k)$ via the Euclidean division with respect to $M(x_1)$ (see eq. (2.218) for the definition of $M(x)$) to the quotient $P_g(x_1; \dots)$, a polynomial in x_1 with degree $m - 2 - (m - s) = s - 2$, and the remainder $R_g(x_1; \dots)$, a polynomial in x_1 with degree $< m - s$. Recall $s - 1$ is the genus of the reduced spectral curve. The polynomial $P(x_1; \dots)$ could be decomposed in terms of the fundamental polynomials³⁷ on $\tilde{\mathcal{C}}$ and further be fixed by exploiting the pole structures of $\omega_k^{(g)}$, while the polynomial $R_g(x_1; \dots)$ could be shown to be irrelevant.

A more direct way to solve the loop equations is to invert the integral operator $\widehat{K}(x) - 2W_0(x)$. It was later shown in [131, 132] that the inverse is the integral operator

$$\widehat{d\mathcal{G}}(f)(x) := \sum_{i=1}^{2s} \operatorname{Res}_{x' \rightarrow a_i} \frac{d\mathcal{G}(x, x')}{dx} \frac{dx'}{y(x')} f(x'), \quad (2.260)$$

provided that $f(x)$ only has poles at the ramification points on $\tilde{\mathcal{C}}$. Here a_i are the ramification points on the reduced spectral curve $\tilde{\mathcal{C}}$ and $d\mathcal{G}(x, x')$ is the indefinite integral with respect to x' of a symmetric bidifferential called the Bergman kernel $B(x, x')$ on $\tilde{\mathcal{C}}$. We relegate the definition of the Bergman kernel to the next subsection where the solutions of the loop equations by the name of the topological recursion will be explained in full detail.

It is worthy to point out that the kernel of the integral operator $\widehat{K}(x) - 2W_0(x)$ is in fact not trivial and is spanned by holomorphic differentials on $\tilde{\mathcal{C}}$. The inverse operator $\widehat{d\mathcal{G}}$ therefore only determines $\omega_k^{(g)}(x_1, \dots, x_k)$ up to a holomorphic multidifferential. The holomorphic ambiguity is fixed by demanding that the integral of $\omega_k^{(g)}(x_1, \dots, x_k)$ around each cut $A_i = [x_{2i-1}, x_{2i}]$, $i = 1, \dots, s$ vanish. This is called the *filling fraction conditions* and is justified in the framework of Hermitian matrix models as shown for instance in [142]. It can be shown with these conditions $\widehat{d\mathcal{G}}$ is the correct inverse operator. Solutions to the loop equations not constrained by the filling fraction conditions also exist. They may not correspond to matrix models but they still satisfy the symmetries underlying the loop equations which are in this sense more fundamental.

2.5.2 Topological Recursion and Symplectic Invariants

We saw at the end of section 2.4.2 that the spectral curve \mathcal{C} contains all the planar information of the associated matrix model as well as the filling fractions. We further saw in the last subsection

³⁷ These are $s - 1$ polynomials $H_i(x)$ appearing in the numerators of the $s - 1$ holomorphic 1-forms $H_i(x)dx/dy$ on the reduced spectral curve.

and especially in eq. (2.260) that the recursive procedures for solving the loop equations to get higher genera resolvents only depend on the Bergman kernel on the smooth reduced spectral curve $\tilde{\mathcal{C}}$, the function $y(x)$, and the ramification points a_i , which project onto the branch points on the x -plane. This motivated Eynard and Orantin [22, 23] to propose a paradigm shift treating the multidifferentials $\omega_k^{(g)}$ and free energies \mathcal{F}_g as geometric invariants associated to the curve $\tilde{\mathcal{C}}$ regardless of whether there is an underlying matrix model. They call the prescription to compute these invariants derived from solving the loop equations the *topological recursion*. Since then the topological recursion has seen applications in many branches of theoretical physics and mathematics³⁸ where either there is no underlying matrix model or the matrix model interpretation is not known, and it remains an open question how far we can extend the applicability of the topological recursion. The topological recursion has been nicely reviewed in [22–24]. Here we summarize the important points of the topological recursion which will be relevant for our work.

To apply the topological recursion, we need the following data:

- The spectral curve \mathcal{C} , which is a smooth but not necessarily compact Riemann surface of genus³⁹ g , as well as a choice of symplectic basis of 1-cycles $(\mathcal{A}_i, \mathcal{B}_j)$ on \mathcal{C} ;
- Two complex functions x, y on the curve \mathcal{C} such that dx, dy are meromorphic differentials;
- The Bergman kernel B on \mathcal{C} .

The symplectic basis of 1-cycles on \mathcal{C} satisfy the conditions

$$\mathcal{A}_i \cap \mathcal{B}_j = -\mathcal{B}_j \cap \mathcal{A}_i = \delta_{ij}, \quad \mathcal{A}_i \cap \mathcal{A}_j = \mathcal{B}_i \cap \mathcal{B}_j = 0. \quad (2.261)$$

\mathcal{A}_i and \mathcal{B}_j are called A - and B -cycles respectively. Once the A - and B -cycles are chosen one can find g holomorphic 1-forms on \mathcal{C} such that

$$\oint_{\mathcal{A}_i} du_i = \delta_{ij}. \quad (2.262)$$

The period matrix τ_{ij} given by

$$\oint_{\mathcal{B}_i} du_j = \tau_{ij} \quad (2.263)$$

characterizes the complex structure of the spectral curve. Choosing a different symplectic basis amounts to a modular transformation, and its effects on the invariants $\omega_n^{(g)}$ and \mathcal{F}_g will be discussed in the next subsection.

The complex function x can be used to project \mathcal{C} onto a complex plane with branch points. The zeros a_i of dx are the *ramification points* on the curve, and they project onto the branch points on the complex plane. We assume dx only has simple zeros⁴⁰ and that dy does not vanish at the ramification points.

The differential $\omega_1^{(0)}(p) = y(p)dx(p)$ will play an important role. It can be interpreted as the Seiberg–Witten differential⁴¹ [148, 149] on the curve \mathcal{C} .

³⁸ For a review of its current applications see [24].

³⁹ Do not confuse the genus of the spectral curve with the genera of the invariants $\omega_k^{(g)}$ or the free energies \mathcal{F}_g .

⁴⁰ The cases where dx has zeros of nontrivial multiplicity have been treated in [143–145].

⁴¹ For reviews on the Seiberg–Witten theory one can read [146, 147].

The spectral curve \mathcal{C} can be described by an equation of x and y

$$H(x, y) = 0 . \quad (2.264)$$

When the Riemann surface described by this equation is singular, as it may happen in Hermitian matrix models with

$$y^2 = M(x)^2 \prod_{i=1}^{2s} (x - x_i) ,$$

the spectral curve is actually chosen to be the reduced smooth curve

$$\tilde{y}^2 = \prod_{i=1}^{2s} (x - x_i) . \quad (2.265)$$

The differential $\omega_1^{(0)}(p) = y(p)dx(p)$ nevertheless is still constructed from $y(p)$ instead of $\tilde{y}(p)$.

In the vicinity of a ramification point a_i the spectral curve looks like two sheets glued together at the point a_i . Given a point p on one sheet we can define the conjugate point \bar{p} on the other sheet which projects onto the same point on the x -plane as p does

$$x(p) = x(\bar{p}) . \quad (2.266)$$

The Bergman kernel $B(p_1, p_2)$ is the unique symmetric bidifferential on \mathcal{C} whose only pole is the double pole at the diagonal loci $p_1 = p_2$ with the leading behavior

$$B(p_1, p_2) = \frac{dp_1 dp_2}{(p_1 - p_2)^2} + \text{regular terms} , \quad (2.267)$$

and whose integral along any A -cycle vanishes. Bidifferentials with the pole structure like eq. (2.267) differ from each other by a holomorphic bidifferential, and the normalization condition along A -cycles fixes the Bergman kernel completely. The Bergman kernel is to be identified with $\omega_2^{(0)}$, and therefore the A -cycle normalization conditions of $B(p_1, p_2)$ are consistent with the filling fraction conditions in Hermitian matrix models. Furthermore it can be shown the Bergman kernel satisfies

$$\oint_{q \in \mathcal{B}_i} B(p, q) = 2\pi i du_i(p) , \quad i = 1, \dots, g \quad (2.268)$$

where du_i are the g holomorphic differentials on the spectral curve. Note the Bergman kernel depends on the symplectic basis $(\mathcal{A}_i, \mathcal{B}_i)$.

Finally we define the recursion kernel

$$K(p, q) = -\frac{1}{2} \frac{\int_{q'=\bar{q}}^q B(p, q')}{\omega_1^{(0)}(q) - \omega_1^{(0)}(\bar{q})} . \quad (2.269)$$

Since the pair of conjugate points q, \bar{q} is only well-defined near a ramification point, it is understood that the second argument q of $K(p, q)$ is always given in the vicinity of a ramification point.

Now we can give a computational definition of the *correlation differentials* $\omega_k^{(g)}$ on the spectral

curve \mathcal{C} . We define recursively with decreasing $\chi = 2 - 2g - k$ the following meromorphic multidifferentials.

$$\omega_1^{(0)}(p) = y(p)dx(p) , \quad (2.270)$$

$$\omega_2^{(0)}(p_1, p_2) = B(p_1, p_2) . \quad (2.271)$$

Let J be the collective notation of a set of points $\{p_1, \dots, p_k\}$ on the curve. Then for $\chi < 0$ we have

$$\omega_{k+1}^{(g)}(p_0, J) = \sum_i \operatorname{Res}_{q \rightarrow a_i} K(p_0, q) \left(\omega_{k+2}^{(g-1)}(q, \bar{q}, J) + \sum_{h=0}^g \sum'_{I \subset J} \omega_{1+|I|}^{(h)}(q, I) \omega_{1+k-|I|}^{(g-h)}(\bar{q}, J \setminus I) \right) . \quad (2.272)$$

Here the notation \sum' means the terms with $(h, I) = (0, \emptyset)$ or (g, J) are not included in the sum.

We already know the pole structures of $\omega_1^{(0)}$ and $\omega_2^{(0)}$. The differentials $\omega_k^{(g)}$ with $2 - 2g - k < 0$ are called *stable*. They are invariant under a permutation of $\{p_i\}$ and only have poles at the ramification points with no residue for every variable

$$\operatorname{Res}_{p_1 \rightarrow a_i} \omega_k^{(g)}(p_1, \dots, p_k) = 0 . \quad (2.273)$$

This is again consistent with the filling fraction conditions in Hermitian matrix models.

We can also define free energies \mathcal{F}_g . For $g \geq 2$, the free energies are defined to be

$$\mathcal{F}_g = \frac{1}{2 - 2g} \sum_i \operatorname{Res}_{q \rightarrow a_i} \Phi(q) \omega_1^{(g)}(q) , \quad (2.274)$$

where $\Phi(q)$ is the indefinite integral of $\omega_1^{(0)}$. An integral constant in $\Phi(q)$ would drop out after taking residue because of eq. (2.273). The definitions of free energies \mathcal{F}_0 and \mathcal{F}_1 are much more complicated [22, 23]. It is more convenient to compute them via the variational formulae that we will discuss in the next subsection.

The recursive definitions of $\omega_k^{(g)}$ enjoy a particularly nice graphic representation, which is elaborated upon in refs. [22, 23].

2.5.3 Properties of Symplectic Invariants

Here we summarize some important properties of the invariants $\omega_k^{(g)}$, \mathcal{F}_g . We will see the connection to topological string toward the end of this subsection.

The first property is the symplectic invariance of the free energies \mathcal{F}_g , at least if \mathcal{C} is a compact Riemann surface and x, y themselves are meromorphic functions (recall in general we only require dx, dy to be meromorphic differentials) [22, 150, 151]. It means \mathcal{F}_g is invariant under a symplectic reparametrization of the spectral curve which preserves $dx \wedge dy$. In particular \mathcal{F}_g does not change under the transformation $(x, y) \rightarrow (y, -x)$. The differentials $\omega_k^{(g)}$ however can undergo a shift by a total differential. For instance with the transformation $(x, y) \rightarrow (y, -x)$

$$\omega_1^{(0)}(p) = y(p)dx(p) \rightarrow -x(p)dy(p) = y(p)dx(p) - d(x(p)y(p)) .$$

Because of this symmetry property, Eynard and Orantin call $\omega_k^{(g)}$ and \mathcal{F}_g the symplectic invariants of the spectral curve.

The second property is concerned with the variation of the symplectic invariants when one slightly changes the complex structure of the spectral curve. An infinitesimal change of the complex structure of \mathcal{C} is reflected in the variation of $\omega_1^{(0)}$

$$\delta_\Omega \omega_1^{(0)}(p) = \epsilon \Omega(p) , \quad (2.275)$$

where ϵ is the infinitesimal deformation parameter and Ω is a 1–differential. It can be shown that one can always find a path of integral $\partial\Omega$ (possibly closed) and a multiplier function $\Lambda(q)$ such that [23]

$$\Omega(p) = \int_{q \in \partial\Omega} B(p, q) \Lambda(q) . \quad (2.276)$$

Then the variations of correlation differentials satisfy the identity

$$\delta_\Omega \omega_k^{(g)}(p_1, \dots, p_k) = \int_{q \in \partial\Omega} \omega_{k+1}^{(g)}(p_1, \dots, p_k, q) \Lambda(q) . \quad (2.277)$$

This is called the *variational formula*. It can be generalized to free energies \mathcal{F}_g by regarding the latter as $\omega_0^{(g)}$

$$\delta_\Omega \mathcal{F}_g = \int_{q \in \partial\Omega} \omega_1^{(g)}(q) \Lambda(q) , \quad g \geq 1 , \quad (2.278)$$

$$\delta_{\Omega_1} \delta_{\Omega_2} \delta_{\Omega_3} \mathcal{F}_0 = \int_{q_1 \in \partial\Omega_1} \Lambda_1(q_1) \int_{q_2 \in \partial\Omega_2} \Lambda_2(q_2) \int_{q_3 \in \partial\Omega_3} \Lambda_3(q_3) \omega_3^{(0)}(q_1, q_2, q_3) . \quad (2.279)$$

If one varies the complex structure by deforming a parameter in the defining equation of the spectral curve, the left hand sides of the variational formulae become partial derivatives. This provides a convenient way to compute $\mathcal{F}_1, \mathcal{F}_0$ once we know $\omega_1^{(1)}$ and $\omega_3^{(0)}$.

Finally we are interested in the modular properties of the symplectic invariants, namely how they transform under the following change of the symplectic basis of 1–cycles on \mathcal{C}

$$\mathcal{B}_i = \sum_j A_{ij} \mathcal{B}'_j + B_{ij} \mathcal{A}'_j, \quad \mathcal{A}_i = \sum_j C_{ij} \mathcal{B}'_j + D_{ij} \mathcal{A}'_j . \quad (2.280)$$

Here A, B, C, D are $g \times g$ matrices, satisfying $AB^t = BA^t$, $CD^t = DC^t$, and $AD^t - BC^t = \mathbb{1}_g$. In other words

$$\begin{pmatrix} A & B \\ C & D \end{pmatrix} \quad (2.281)$$

is an element of $Sp(2g, \mathbb{Z})$. It turns out the free energies \mathcal{F}_g and the correlation differentials $\omega_k^{(g)}$ are not invariant under this transformation. The reason is that among the input data of the topological recursion, the Bergman kernel is not modular invariant and in fact transforms in the following nontrivial way [22, 23]

$$B(z_1, z_2) = B'(z_1, z_2) + 2\pi i \sum_{i,j=1}^g \kappa^{ij} du_i(z_1) du_j(z_2), \quad \kappa = (AC^{-1} - \tau)^{-1} . \quad (2.282)$$

We can nonetheless remedy it by introducing the generalized Bergman kernel (also called the Schiffer kernel)

$$B^\Delta(z_1, z_2) = B(z_1, z_2) + 2\pi i \sum_{i,j=1}^g \Delta_{ij} du_i(z_1) du_j(z_2) , \quad (2.283)$$

where we choose

$$\Delta = (\bar{\tau} - \tau)^{-1} , \quad (2.284)$$

and demonstrate easily this generalized Bergman kernel is modular invariant. The generalized Bergman kernel is normalized with respect to a different set of cycles

$$\mathcal{A}_i^\Delta = \mathcal{A}_i - \sum_j \Delta_{ij} (\mathcal{B}_j - \sum_l \tau_{jl} \mathcal{A}_l) , \mathcal{B}_i^\Delta = \mathcal{B}_i - \sum_j \Delta_{ij} \mathcal{A}_j , \quad (2.285)$$

satisfying

$$\mathcal{A}_i^\Delta \cap \mathcal{B}_j^\Delta = -\mathcal{B}_j^\Delta \cap \mathcal{A}_i^\Delta = \delta_{ij} , \quad \mathcal{A}_i^\Delta \cap \mathcal{A}_j^\Delta = \mathcal{B}_i^\Delta \cap \mathcal{B}_j^\Delta = 0 . \quad (2.286)$$

In other words,

$$\oint_{q \in \mathcal{A}_i^\Delta} B^\Delta(p, q) = 0 , \quad \oint_{q \in \mathcal{B}_i^\Delta} B^\Delta(p, q) = 2\pi i du_i(p) . \quad (2.287)$$

Now if we apply the topological recursion with the Bergman kernel replaced by $B^\Delta(z_1, z_2)$, the computed free energies F_g^Δ and correlation differentials $\omega_k^{(g), \Delta}$ will be modular invariant. The price to pay is introducing antiholomorphic dependence on the complex structure of the spectral curve \mathcal{C} because of $\bar{\tau}$ in Δ . Since $\bar{\tau}$ only appears in Δ , we can derive the dependence of the symplectic invariants on $\bar{\tau}$ via the usual Taylor expansion at $\Delta = 0$

$$\omega_k^{(g), \Delta} = \sum_{n=0}^{3g-3} \frac{1}{n!} \Delta^n \frac{\partial^n}{\partial \Delta^n} \omega_k^{(g), \Delta} \Big|_{\Delta=0} , \quad \text{including } F_g^\Delta \text{ when } k=0 , \quad (2.288)$$

together with the following formula [22, 23] (including F_g^Δ as the special case of $k=0$)

$$\begin{aligned} \frac{\partial}{\partial \Delta_{ij}} \omega_k^{(g), \Delta}(z_1, \dots, z_k) \Big|_{\Delta=0} &= \frac{1}{2} \frac{\partial}{\partial t_i} \frac{\partial}{\partial t_j} \omega_k^{(g-1)}(z_1, \dots, z_k) \\ &+ \frac{1}{2} \sum_{h=0}^g \sum_{I \subset J} \frac{\partial}{\partial t_i} \omega_{1+|I|}^{(h)}(I) \frac{\partial}{\partial t_j} \omega_{n-|I|}^{(g-h)}(J \setminus I) . \end{aligned} \quad (2.289)$$

Here the moduli t_i are the analog of partial 't Hooft parameters

$$t_i = \frac{1}{2\pi i} \oint_{\mathcal{A}_i} y dx . \quad (2.290)$$

For instance the dependence of $F_2^\Delta(\tau, \bar{\tau})$ on $\bar{\tau}$ can be seen in the following expansion

$$\begin{aligned} F_2^\Delta(\tau, \bar{\tau}) &= \mathcal{F}_2 + \frac{1}{2} \Delta_{ij} (\partial_i \partial_j \mathcal{F}_1 + \partial_i \mathcal{F}_1 \partial_j \mathcal{F}_1) + \frac{1}{8} \Delta_{ij} \Delta_{kl} (\partial_i \partial_j \partial_k \partial_l \mathcal{F}_0 + 4 \partial_i \mathcal{F}_1 \partial_j \partial_k \partial_l \mathcal{F}_0) \\ &+ \frac{1}{48} \Delta_{ij} \Delta_{kl} \Delta_{mn} (4 \partial_i \partial_k \partial_m \mathcal{F}_0 \partial_j \partial_l \partial_n \mathcal{F}_0 + 6 \partial_i \partial_j \partial_k \mathcal{F}_0 \partial_l \partial_m \partial_n \mathcal{F}_0) , \end{aligned} \quad (2.291)$$

$$\begin{aligned}
 F_2^\Delta(\tau, \bar{\tau}) = & \text{diagram 1} + \frac{\Delta}{2} \text{diagram 2} + \frac{\Delta}{2} \text{diagram 3} + \frac{\Delta^2}{8} \text{diagram 4} \\
 & + \frac{\Delta^2}{2} \text{diagram 5} + \frac{\Delta^3}{12} \text{diagram 6} + \frac{\Delta^3}{8} \text{diagram 7}
 \end{aligned}$$

Figure 2.13: Diagrammatic illustration of the expansion of $F_2^\Delta(\tau, \bar{\tau})$ in eq. (2.291). Here each connecting line with endpoints (i, j) is a factor of Δ_{ij} , and each Riemann surface of genus g with h marked points i_1, \dots, i_h is $\partial_{i_1} \dots \partial_{i_h} \mathcal{F}_g$.

where $\mathcal{F}_g = F^\Delta|_{\Delta=0}$ and $\partial_i = \frac{\partial}{\partial t_i}$. This is illustrated diagrammatically in Fig. 2.13.

The conflict between modular invariance and holomorphicity of the symplectic invariants is reminiscent of the free energies in type B topological string theory. By comparing Fig. 2.13 and Fig. 2.6 one finds out that the antiholomorphic dependence of the free energies computed by the topological recursion and that of the free energies in type B topological string as solutions to the holomorphic anomaly equations are strikingly similar. The connection actually runs deeper. If the target space of type B topological string is a noncompact Calabi–Yau X characterized by the spectral curve \mathcal{C} , the period matrix τ of X is the same as the period matrix of \mathcal{C} . Eynard and Marino showed in [152] that in this case if one identifies the partial ’t Hooft parameters with the complex structure moduli, the free energies F_g^Δ computed by the topological recursion using the spectral curve of X satisfy the holomorphic anomaly equations.

However one shall not conclude immediately that F_g^Δ computed via the topological recursion is *identical* with the free energies $F_g(t, \bar{t})$ in type B topological string theory. Both of them suffer from holomorphic ambiguity. The ambiguity of the former is fixed by the filling fraction conditions, while that of the latter is determined from certain conditions at the boundary/singular loci in the moduli space from physics considerations. It is a priori not clear why these two conditions should lead to the same results and therefore the two free energies could still differ by a holomorphic modular invariant term. This is further discussed in section 2.5.5.

2.5.4 Resolvents, Unknot, and Special Lagrangian Branes

We have seen in section 2.4.5 the beautiful circle of dualities relating $U(N)$ Chern–Simons theory on S^3 , the Chern–Simons matrix model, closed type A topological string on resolved conifold, and closed type B topological string with spectral curve eq. (2.116), where the free energies of all four theories are identical. It is natural to ask how the other quantities in these theories fit into the picture, including for instance the quantum knot invariants $\mathcal{W}_R(\mathcal{K})$ in the Chern–Simons theory and the resolvents $W_g(p_1, \dots, p_n)$ in the matrix model.

It was seen in section 2.3.6 that a knot \mathcal{K} in the Chern–Simons theory can be lifted to its conormal bundle $\tilde{\mathcal{L}}_{\mathcal{K}}$ in T^*S^3 in its type A open topological string interpretation. It is possible to find the unique Lagrangian brane $\mathcal{L}_{\mathcal{K}}$ as the counterpart of $\tilde{\mathcal{L}}_{\mathcal{K}}$ in the resolved conifold through the geometric transition in the $N \rightarrow \infty$ limit [25, 76, 153, 154], and therefore the large N dual of the Chern–Simons theory with the insertion of knot \mathcal{K} is the type A *open* topological string on $\mathcal{L}_{\mathcal{K}}$ in the resolved conifold. In the simplest case of unknot, $\mathcal{L}_{\mathcal{K}}$ is shown [25] to be the toric special Lagrangian branes touching the internal edge of the toric diagram of the resolved conifold, and their mirror dual in type B topological string theory has been discussed in section 2.2.6. It can be shown [25] the quantum knot invariants of unknot are related to

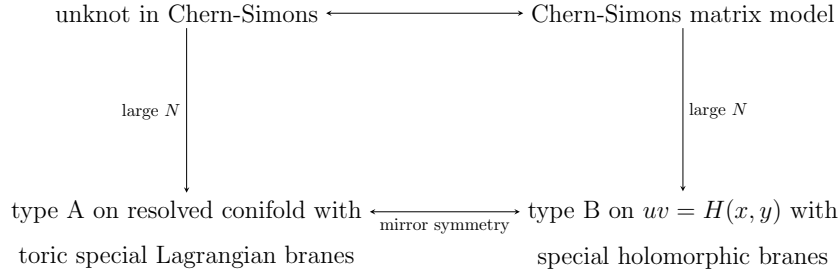


Figure 2.14: The same circle of dualities as in Fig.2.12, but with the insertion of the branes associated to unknot in the topological string theories.

open string free energies by the formula

$$\mathcal{F}_{\text{CS}}(V) = \mathcal{F}_{\text{top}}(V) . \quad (2.292)$$

$\mathcal{F}_{\text{CS}}(V)$ on the left hand side is the free energy of the deformed Chern–Simons theory given by eq. (2.171) which is the generating function of quantum knot invariants, while $\mathcal{F}_{\text{top}}(V)$ on the right hand side is the usual type A open topological string free energy defined in eq. (2.95) (it can of course also be understood as the open string free energy in the mirror dual type B theory). Here in addition to the large N dictionary eq. (2.246) we naturally identify the matrix V in the two theories. The above identity implies

$$\frac{1}{\prod_j j^{k_j}} \mathcal{W}_{\vec{k},g}^{(c)}(t) = \mathcal{F}_{g,\vec{k}}(t) . \quad (2.293)$$

Here the knot invariant $\mathcal{W}_{\vec{k},g}^{(c)}(t)$ was defined in eq. (2.176), and $\mathcal{F}_{g,\vec{k}}(t)$ is the same as $\mathcal{F}_{g,\omega}(t)$ in type A topological string. The label $\vec{k} = (k_1, k_2, \dots)$ is another way to record the boundary data $\omega = (\omega_1, \dots, \omega_h)$. It means that the winding number j appears k_j times in ω .

On the other hand, the resolvents, or equivalently the correlation differentials $\omega_h^{(g)}$, of the Chern–Simons matrix model are related to the open string free energies via

$$A_h^{(g)}(t, x_1, \dots, x_h) = \int^{x_1, \dots, x_h} \omega_h^{(g)}(x'_1, \dots, x'_h) - \delta_{g,0} \delta_{h,2} \frac{d\alpha_1 d\alpha_2}{(\alpha_1 - \alpha_2)^2} . \quad (2.294)$$

Here the open string amplitude $A_h^{(g)}$ was defined in eq. (2.98). On the right hand side the initial position of the integral is irrelevant, and $\alpha_i = e^{-x'_i}$ are the algebraic coordinates on the spectral curve. In summary, now we have a new version of the circle of dualities illustrated in Fig. 2.14.

An interesting aspect of this picture is that similar to the framing of knots in the Chern–Simons theory, there is also the integral choice of framing of branes as discussed at the end of section 2.2.6. It is not surprising that the identity eq. (2.292) remains valid under a simultaneous framing transformation in both Chern–Simons theory and topological string theory, where it corresponds to an integral shift of the brane coordinate x .

One can consider several ways to generalize this circle of dualities. Given an arbitrary toric Calabi–Yau threefold we can still talk about toric special Lagrangian branes in type A topological string and their mirror duals in type B topological string. On the one hand, for the type A topological strings on a large variety of but not all toric Calabi–Yau threefolds, it is still possible

to find a complicated construction of Chern–Simons theories with massive corrections, which are dual to them in the large N limit [114, 115, 155]. On the other hand, the link between matrix models and topological string theories is stronger. Although it may be difficult to find the dual matrix model in the large N limit (however, see recent progress in [29]), the computations of resolvents and free energies in the matrix model using the topological recursion require only the knowledge of its spectral curve, which can be identified with that of the type B topological string. Indeed as discussed in section 2.5.3 the topological recursion is deeply related to type B topological string theory. This connection is consolidated in the BKMP theorem.

2.5.5 The BKMP Theorem

It was conjectured by Bouchard, Klemm, Mariño, and Pasquetti [113, 156] that the topological recursion can be used in general to compute closed string free energies of type A topological string on a toric Calabi–Yau threefold M , as well as the open string free energies of toric special Lagrangian branes in M , using the spectral curve \mathcal{C} of the mirror dual type B string theory.

Given a toric Calabi–Yau threefold M and a stack of toric special Lagrangian branes \mathcal{L} in it, the spectral curve \mathcal{C} in the mirror type B topological string is given by a polynomial $H(x, y)$ in the algebraic coordinates $\alpha := e^x, \beta := e^y$. \mathcal{C} is parametrized according to the edge of the toric diagram of M the toric special Lagrangian branes \mathcal{L} are placed upon and the framing of the branes. \mathcal{C} can be highly singular, and as discussed in section 2.5.2 in this case the smooth reduced spectral curve $\tilde{\mathcal{C}}$ is used as the spectral curve for the topological recursion. Nevertheless x, y that parametrize \mathcal{C} still provide two complex functions on $\tilde{\mathcal{C}}$ and in particular ydx is used as the Seiberg–Witten differential $\omega_1^{(0)}$. Note that x, y are multivalued functions, as seen for example from the spectral curve of the resolved conifold in eq. (2.116), but dx, dy are globally defined meromorphic differentials on $\tilde{\mathcal{C}}$. Furthermore since the Bergman kernel is not modular invariant, one has to choose a symplectic basis of $H_1(\tilde{\mathcal{C}}, \mathbb{Z})$. The choice of the symplectic basis crucially depends on the coordinate patch on the closed string moduli space one works with [51]. When one is working with the coordinate patch mirror dual to the large volume limit in type A theory, one usually chooses the A cycles so that their periods (closed flat coordinates) are mirror dual to the Kähler moduli in type A theory⁴². Once the A and B cycles are separated, the Bergman kernel $B(p_1, p_2)$ of $\tilde{\mathcal{C}}$ can be written down.

Now one has all the ingredients $(\tilde{\mathcal{C}}, x, y, B)$ needed to run the topological recursion and to compute the symplectic invariants $\{\mathcal{F}_g, \omega_n^{(g)}\}$. The BKMP conjecture then claims that \mathcal{F}_g are identical with the free energies of the closed topological string theories in the holomorphic limit, and the open string free energies of the toric spectral Lagrangian branes \mathcal{L} in type A string, or equivalently of the special holomorphic branes in the mirror type B string, can be obtained from $\omega_n^{(g)}$ via eq. (2.294) (see Fig. 2.15). Furthermore, it is argued that a phase transition of the branes by moving them to a neighboring edge on the toric diagram or a framing transformation corresponds to a symplectic reparametrization of the spectral curve preserving $dx \wedge dy$. Given their interpretations in the BKMP conjecture, it is certainly satisfying to know from section 2.5.3 that among the quantities computed by the topological recursion, \mathcal{F}_g are invariant under this transformation, while $\omega_n^{(g)}$ are not.

In the special case when \mathcal{C} is a hyperelliptic curve, namely a double cover of \mathbb{C}^* which is

⁴² In this coordinate patch the closed flat coordinates should behave like $-\log(z_i) + \text{asymptotic series in } z_i$, with z_i being parameters of the spectral curve, as discussed in section 2.2.6.

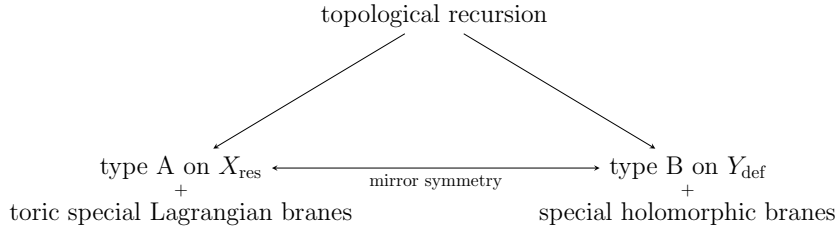


Figure 2.15: The BKMP conjecture. The topological recursion is applied on the spectral curve of the type B topological string.

glued together at a finite number of points (ramification points) described by

$$y^2 = M(x)^2 \prod_i (x - x_i), \quad i \neq j, \quad (2.295)$$

the computations are relatively simple and one can adapt the results in refs. [142, 157]. In particular a spectral curve of genus ≤ 2 is always hyperelliptic. If it has genus 0, the Bergman kernel is simply

$$B(p_1, p_2) = \frac{dy(p_1)dy(p_2)}{(y(p_1) - y(p_2))^2}; \quad (2.296)$$

if it has genus 1, the Bergman kernel can be written down using the Akemann's formula [158], which involves elliptic integrals and an ordering of the branch points (choice of A and B cycles). Note in these cases matrix model interpretations exist.

The BKMP conjecture was proved for $M = \mathbb{C}^3$ independently in [159] and [160]. The generic case with an arbitrary toric background in type A theory was proved in [52]. It was shown in [161] that the topological recursion has a direct enumerative interpretation of counting worldsheet instantons in line with type A topological string. Similar to the differential $\omega_1^{(0)}$, the Bergman kernel identified with $\omega_2^{(0)}$ can be regarded as the generating function of annulus worldsheet instantons, while the recursion kernel the generating function of pairs-of-pants worldsheet instantons. Since the recursive formula of the topological recursion eq. (2.272) can reduce any $\omega_n^{(g)}$ to a product of Bergman kernels and recursion kernels, it effectively serves to cut a worldsheet instanton with genus g and n boundary components to only tubes and pairs-of-pants. (This will be discussed again in section 3.2.1. Examples are given in Fig. 3.4) Given this enumerative interpretation, it may be possible to establish a link between the topological recursion and the equivariant localization in type A topological string, where uncertainties like holomorphic ambiguities in type B topological string are removed. On the one hand, the equivariant localization relies crucially on the toric diagram Υ_M . On the other hand, the spectral curve \mathcal{C} can be visualized as the surface of the tubular neighborhood of the skeleton of Υ_M , and it shrinks to this skeleton when the radius of the tubular neighborhood decreases to zero. Thus when \mathcal{C} is cut to tubes and pairs-of-pants, the former correspond one-to-one with the edges of Υ_M . Furthermore by projecting \mathcal{C} onto a single tube $= \mathbb{C}^*$, it is evident that the ramification points of \mathcal{C} correspond one-to-one with the vertices of Υ_M . The similarity actually runs deeper, as Eynard showed in [162] the symplectic invariants $\omega_n^{(g)}$ and \mathcal{F}_g (regarded as $\omega_0^{(g)}$) can be computed by summing over the weights of diagrams in $\tilde{\mathcal{G}}_{g,n}$ (recall its definition in section 2.2.2 and 2.2.3), and the weights factorize to contributions of vertices, edges, and half edges. Eynard and Orantin further demonstrated in [52] that the weight of a graph in the

topological recursion can be identified with the weight of a graph in the equivariant localization computation, thus completing the proof of the BKMP conjecture.

2.5.6 Ooguri–Vafa Conjecture and Open Problems

The BKMP theorem is one way of generalizing the circle of dualities discussed in section 2.5.4. We can also ask what the quantum knot invariants of a nontrivial knot in the $U(N)$ Chern–Simons theory on S^3 correspond to in the other theories. We have run out of observables in the matrix model, however we can still construct unique branes $\mathcal{L}_{\mathcal{K}}$ in the resolved conifold in type A topological string theories associated to an arbitrary knot \mathcal{K} in the Chern–Simons theory. The branes $\mathcal{L}_{\mathcal{K}}$ were constructed in [76] for torus knots, and generalized to arbitrary knots in [153]. It is then natural to conjecture that the quantum knot invariants for \mathcal{K} and the free energies of $\mathcal{L}_{\mathcal{K}}$ are still related by eq. (2.292), from now on also called the Ooguri–Vafa conjecture. Since the open string free energies of branes enjoy the integrality structure as shown in eqs. (2.100), (2.101), the Ooguri–Vafa conjecture immediately predicates similar integrality structures of quantum knot invariants [25, 76]. This integrality prediction⁴³ was confirmed and proved in [163–165] and it provides strong support for the Ooguri–Vafa conjecture.

What remains to be done is a direct comparison of free energies at the two sides of eq. (2.292). To compute $\mathcal{F}_{\text{CS}}(V)$ on the left hand side, one needs the knowledge of all the quantum knot invariants of \mathcal{K} . The quantum knot invariants have only been computed for torus knots via the Rosso–Jones formula [121] as explained in section 2.3.3, and only for a handful of non–torus knots (also called *hyperbolic knots* in the knot theory) colored in symmetric representations [118, 124, 125, 166–169]. Non–torus knots colored in nonsymmetric representations was explored in our work [119] and will be the focus of chapter 4. $\mathcal{F}_{\text{top}}(V)$ on the right hand side is the generating function of open Gromov–Witten invariants, which can be computed for low genera and low degrees of homology classes by adapting the equivariant localization techniques for branes associated to torus knots [154]. A more efficient way to compute the open free energies was attempted in our work [170] and it will be the focus of chapter 3.

⁴³ This is also called the Labastida–Mariño–Ooguri–Vafa conjecture in the literature.

Topological String and Knot Invariants

The Bouchard–Klemm–Mariño–Pasquetti theorem provides through the topological recursion a powerful tool for computing free energies of type A open topological string theory on toric special Lagrangian branes, which in the resolved conifold correspond to unknot in the Chern–Simons theory on a three–sphere. It is tempting to conjecture that the topological recursion can also be used to compute free energies for the Lagrangian branes associated to nontrivial knots. This is supported by ref. [171], which suggests for an arbitrary knot the existence of a matrix model integral which generates all the quantum knot invariants of this knot. In order to check this idea, one has first to find the spectral curve on which the topological recursion can be applied. This is not a problem for unknot, since the spectral curve for the associated branes coincides with that of the type B string theory on the mirror dual of resolved conifold. Since all the symplectic invariants computed from this spectral curve have found interpretations in topological string theory, it is necessary to find a different spectral curve $\mathcal{C}_{\mathcal{K}}$ for a nontrivial knot \mathcal{K} . Two different versions of the spectral curve $\mathcal{C}_{\mathcal{K}}$ have been proposed in the literature by Brini, Eynard, Mariño [172] and Aganagic, Vafa [173] respectively. We will argue in section 3.1 the Aganagic–Vafa curve is the better option of the two. We apply the topological recursion on the Aganagic–Vafa curve in section 3.2 and find out that necessary modifications of the topological recursion have to be adopted in order for it to work on the Aganagic–Vafa curve. The modified topological recursion is put to work and verified for some simple knots in section 3.3. Finally in section 3.4 we discuss the implications of our findings for the knot theory.

3.1 Spectral Curves

3.1.1 Brini–Eynard–Mariño Spectral Curve

We have discussed in section 2.2.6 that a phase transition (moving the branes onto a neighboring edge through a vertex in the toric diagram) or a framing transformation of toric special Lagrangian branes is given by a reparametrization of the spectral curve of the branes through a symplectic transformation of the pair of coordinates (x, y) . However these two types of transformations do not generate all possible symplectic transformations. Brini, Eynard, and Mariño [172] considered the generic symplectic transformation on the coordinates (x, y) of the spectral curve of unknot with framing zero

$$\begin{aligned} \tilde{x} &= rx - sy, \\ \tilde{y} &= -\delta x + \gamma y, \end{aligned} \quad \begin{pmatrix} r & -s \\ -\delta & \gamma \end{pmatrix} \in SL(2, \mathbb{Z}). \quad (3.1)$$

where r, s are different from one and they are coprime. Based on the observation the new \tilde{x} coordinate can be written as $\tilde{x} = r(x - s/ry)$, they claim that it represents r copies of unknot

with fractional framing s/r , which is precisely the interpretation of the Rosso–Jones formula. In other words, by performing the symplectic reparametrization given by eq. (3.1) on the spectral curve of unknot with framing zero, one could get the spectral curve of the torus knot $\mathcal{K}_{r,s}$ with framing $r s$, henceforth called the BEM spectral curve.

Before we write down the BEM spectral curve, we note that it is possible to simplify the BEM spectral curve by using the coordinate y instead of \tilde{y} in the curve *after* reparametrization; in other words, the new curve is parametrized by \tilde{x} and y , and it can be obtained by the single step of change of variables $x \rightarrow (\tilde{x} + sy)/r$. The reason is that we can write \tilde{y} as

$$\tilde{y} = -\frac{\delta}{r}\tilde{x} + \frac{1}{r}y . \quad (3.2)$$

The difference between y and \tilde{y} (up to the scaling r) is proportional to \tilde{x} , and in the disk amplitude $A_1^{(0)}$ this only gives rise to a classical term $\tilde{x}^2/2$ which does not contribute to the disk instanton counting (see eq. (2.98)). Furthermore since \tilde{y} enters the topological recursion formula only through $\omega_1^{(0)}(q) - \omega_1^{(0)}(\bar{q})$ in the denominator of the recursion kernel (see eq. (2.269)), replacing \tilde{y} by y would not change the results of the topological recursion as the difference \tilde{x} (up to the scaling r) cancels out in $\omega_1^{(0)}(q) - \omega_1^{(0)}(\bar{q})$.

Now let us start with the spectral curve of unknot with framing zero

$$(1 - Q\beta) - \alpha(1 - \beta) = 0 , \quad (3.3)$$

where $\alpha = e^{-x}, \beta = e^{-y}$ are the algebraic coordinates. Because the spectral curve is a Riemann sphere, x, y coincide with the open flat coordinates, and $t := -\log Q$ is the flat coordinate on the closed string moduli space. In order to write down the BEM spectral curve we replace α by $\tilde{\alpha}^{1/r}\beta^{s/r}$. For the ease of notation we will suppress the tilde in the new curve in the following, and it is always understood that α refers to an algebraic coordinate of the spectral curve in question and x the minus of its logarithm. This results is

$$(1 - Q\beta)^r - \alpha\beta^s(1 - \beta)^r = 0 . \quad (3.4)$$

It turns out the Seiberg–Witten differential $\omega_1^{(0)} = ydx = -\log \beta d\alpha/\alpha$ of this curve encodes the correct numbers of worldsheet disk instantons. The series expansion of the integral $-\int \log \beta d\alpha/\alpha$ near $\alpha = 0$ has terms proportional to $\alpha^{n/r}$, where n is a positive integer. If we interpret the coefficients (functions of Q) of the integral power terms with $n = m r$ as the open string free energies $\mathcal{F}_{0,\omega=(m)}$, which are the generating functions of the numbers of worldsheet disk instantons with winding number m around the only 1–cycle of the Lagrangian brane, they are consistent with what are expected from the colored HOMFLY invariants of the torus knot $\mathcal{K}_{r,s}$ through eq. (2.293) in the Ooguri–Vafa conjecture. Furthermore it can be demonstrated that other open string free energies could also be extracted from the correlation differentials computed by the topological recursion. For instance, since the spectral curve represented by eq. (3.4) has genus zero, the Bergman kernel can be easily written down

$$\omega_2^{(0)} = B_{r,s}^{\text{BEM}}(\beta_1, \beta_2) = \frac{d\beta_1 d\beta_2}{(\beta_1 - \beta_2)^2} , \quad (3.5)$$

where β_i is the coordinate of the i -th point on the curve. Near the point $\alpha_1 = \alpha_2 = 0$, the expansion of indefinite integral of the Bergman kernel has terms proportional to $\alpha_1^{n_1/r} \alpha_2^{n_2/r}$, where n_1, n_2 are positive integers. The coefficients of the integral power terms with $\alpha_1^{m_1} \alpha_2^{m_2}$ are the correct open string free energies $\mathcal{F}_{0,\omega=(m_1,m_2)}$, which encode the numbers of worldsheet

annulus instantons whose two boundary components wind around the 1-cycle of the brane m_1 and m_2 times respectively. These free energies $\mathcal{F}_{0,\omega=(m_1,m_2)}$ are again consistent with the expectation from the colored HOMFLY invariants. The same pattern is repeated for higher open string free energies. For the correlation differentials computed with the topological recursion, the expansion of their indefinite integrals near the origin contain both integral and fractional power terms, and the coefficients of the former can be identified with the correct open string free energies. Refs. [172, 174] argue that the success of the topological recursion on the BEM spectral curve is due to an underlying matrix model.

Remarkable as it is, the BEM spectral curve suffers from several problems and limitations. The correlation differentials $\omega_h^{(g)}$ including the Seiberg–Witten differential and the Bergman kernel are somehow not pure generating functions of worldsheet instantons in the sense that their series expansions also contain fractional power terms, whose meanings are very puzzling. What adds to the puzzle is that these fractional power terms are different for the BEM spectral curves of the torus knots $\mathcal{K}_{r,s}$ and $\mathcal{K}_{s,r}$. This is most clearly reflected in the fact that the BEM spectral curves themselves are different for these two knots. On the other hand the two torus knots $\mathcal{K}_{r,s}$ and $\mathcal{K}_{s,r}$ are topologically completely the same, and they only differ in the way they are placed on the surface of a solid torus. It seems the BEM spectral curve is therefore not a completely topologically invariant quantity. Finally the construction of the BEM spectral curve depends crucially on the special properties of the torus knots, and it is not likely it can be generalized to hyperbolic knots (nontorus knots), while the latter are far more numerous in number. It is therefore necessary to look for an alternative.

3.1.2 Aganagic–Vafa Spectral Curve

A second version of the spectral curve for knots can be obtained by addressing the first issue of the BEM spectral curve. We regard the spectral curve $F(x, y)$ as such that the natural Seiberg–Witten differential ydx would be the pure generating function of the worldsheet disk instanton numbers without any redundant terms. With this understanding in mind, the spectral curve for torus knot $\mathcal{K}_{r,s}$ can be derived in a brute force way. Namely one can make the ansatz $F(\alpha, \beta) = \sum_{i,j=0}^{d_\alpha d_\beta} c_{ij} \alpha^i \beta^j$ for the polynomial equation of the spectral curve with the algebraic coordinates α, β and proper upper bounds d_α, d_β of their powers, then solve for the coefficients c_{ij} such that the correct Seiberg–Witten differential is reproduced. This method was pursued in ref. [123]. However a more efficient algebraic algorithm can be developed to construct the same spectral curve by simply removing the fractional power terms in the BEM spectral curve.

Let us take a closer look at the BEM spectral curve. The appearance of fractional power terms $\alpha^{n/r}$ in the expansion of (integral of) the Seiberg–Witten differential near $\alpha = 0$ indicates that α is not a well-defined local affine coordinate. Instead we should use the coordinates $\zeta = \alpha^{1/r}, \rho = \beta^{1/r}$, in terms of which the BEM spectral curve reads

$$h_{r,s}(\zeta, \rho) = (1 - Q\rho^r) - \zeta\rho^s(1 - \rho^r) = 0. \quad (3.6)$$

When $\zeta = 0$, there are r different solutions of $\rho: e^{2\pi ik/r} Q^{-1/r}, k = 1, \dots, r$. So the coordinate patch near $\alpha = 0$ splits to r different ones centered at $(\zeta, \rho) = (0, e^{2\pi ik/r} Q^{-1/r})$, and in each coordinate patch ζ is a well-defined local affine coordinate. We denote the function ρ in the k -th coordinate patch by $\rho^{(k)}$ to distinguish the r different coordinate patches. Likewise the

disk instanton amplitude $W := A_1^{(0)}$ of the BEM spectral curve also splits

$$W_{r,s}^{(k)}(\zeta) = r^2 \int \frac{d\zeta}{\zeta} \log \rho^{(k)}(\zeta), k = 1, \dots, r. \quad (3.7)$$

Each disk instant amplitude can be expanded around $\zeta = 0$

$$W_{r,s}^{(k)}(\zeta) = r^2 \sum_{n=1}^{\infty} \tilde{P}_n^{(r,s)}(Q) \zeta^n + \text{classical terms}. \quad (3.8)$$

We learn from the discussion of the BEM spectral curve that the coefficients of the terms with the power n divisible by r encode the numbers of worldsheet disk instantons, and we would like to remove all the other terms. For this purpose we notice that the r different coordinate patches can be accessed cyclically through a phase shift¹ on ζ : $\zeta \rightarrow e^{2\pi i/r} \zeta$. Therefore we can cancel the terms with the power n not divisible by r by summing over all the r disk instanton amplitudes

$$W_{r,s} = \sum_{k=1}^r W_{r,s}^{(k)} = r^2 \int \frac{d\zeta}{\zeta} \log(\rho^{(1)} \dots \rho^{(r)}). \quad (3.9)$$

The form of this pure disk instanton amplitude also suggests the way to find the spectral curve of the torus knot $\mathcal{K}_{r,s}$, namely it is a curve parametrized by the coordinates²

$$\alpha = \zeta^r, \quad \beta = (-1)^{r+1} \rho^{(1)} \dots \rho^{(r)}. \quad (3.10)$$

and the defining equation for the spectral curve is given by the relation between these two coordinates. To find this defining equation, we consider r copies of the BEM spectral curves $h_{r,s}(\zeta, \rho^{(k)})$ with the coordinates $\zeta, \rho^{(k)}$, and construct the ideal

$$\tilde{\mathcal{I}}_{r,s} = \langle \alpha - \zeta^r, \beta + (-1)^r \rho^{(1)} \dots \rho^{(r)} \rangle \cup \left(\bigcup_{k=1}^r \langle h_{r,s}(\zeta, \rho^{(k)}) \rangle \right). \quad (3.11)$$

The defining equation can be found simply in the elimination ideal

$$\tilde{\mathcal{I}}_{r,s} \cap \mathbb{C}(Q)[\alpha, \beta]. \quad (3.12)$$

In other words we remove the the variables $\zeta, \rho^{(1)}, \dots, \rho^{(r)}$ from the ideal $\tilde{\mathcal{I}}_{r,s}$ by for instance using its Gröbner basis in the elimination monomial order³.

In fact we can improve this method further. The elimination ideal $\tilde{\mathcal{I}}_{r,s}$ also contains redundant elements including the original BEM spectral curve eq. (3.4) because $\rho^{(1)}, \dots, \rho^{(r)}$ in eq. (3.10) can all be identical. To obtain our spectral curve, as discussed above eq. (3.10) $\rho^{(1)}, \dots, \rho^{(r)}$ should all be distinct. To make sure of this, we enlarge the ideal $\tilde{\mathcal{I}}$ by including the polynomials

¹ Since r and s are coprime, we can always find integers p, q such that $rp - sq = 1$. It can be read off from eq. (3.6) that a phase shift $\zeta \rightarrow e^{2\pi i/r} \zeta$ is absorbed by simultaneously shifting $\rho \rightarrow e^{2\pi i q/r} \rho$, effectively sending one from the k -th coordinate patch to the $(k+q)$ -th.

² The sign $(-1)^{r+1}$ is chosen to match the conventions of ref. [123].

³ Given an ideal I in a polynomial ring R , the Gröbner basis $G(I)$ of the ideal I [175] is a minimal set of generators of I such that any polynomial in R has a unique remainder after division by the elements of $G(I)$ in an arbitrary order. For the application of the Gröbner basis in eliminating variables from an ideal, see for instance [176].

$h_{r,s}(\zeta, \rho^{(k_1)}, \dots, \rho^{(k_i)})$ with $1 \leq k_1 \leq \dots \leq k_i \leq r$ and $1 < i \leq r$, which are recursively defined by

$$h_{r,s}(\zeta, \rho^{(k_1)}, \dots, \rho^{(k_i)}) = \sum_{1 \leq n < m \leq i} \frac{h_{r,s}(\zeta, \rho^{(k_1)}, \dots, \widehat{\rho^{(k_n)}}, \dots, \rho^{(k_i)}) - h_{r,s}(\zeta, \rho^{(k_1)}, \dots, \widehat{\rho^{(k_m)}}, \dots, \rho^{(k_i)})}{\rho^{(k_n)} - \rho^{(k_m)}}. \quad (3.13)$$

Here $\widehat{\rho^{(k_n)}}$ means that the variable $\rho^{(k_n)}$ is omitted. By taking the difference of the two polynomials in the numerator and dividing out $\rho^{(k_n)} - \rho^{(k_m)}$, we make sure that $\rho^{(k_n)} \neq \rho^{(k_m)}$ for any two ρ 's. The enlarged ideal now reads

$$\widehat{\mathcal{I}}_{r,s} = \langle \alpha - \zeta^r, \beta + (-1)^r \rho^{(1)} \dots \rho^{(r)} \rangle \cup \left(\bigcup_{i=1}^r \bigcup_{1 \leq k_1 \leq \dots \leq k_i \leq r} \langle h_{r,s}(\zeta, \rho^{(k_1)}, \dots, \rho^{(k_i)}) \rangle \right). \quad (3.14)$$

The elimination ideal

$$\mathcal{I}_{r,s} = \widehat{\mathcal{I}}_{r,s} \cap \mathbb{C}(Q)[\alpha, \beta] \quad (3.15)$$

should have a single generator, which is the defining equation of the spectral curve we are after. For instance, the spectral curve for the trefoil torus knot $\mathcal{K}_{2,3}$ computed in this way is

$$F_{2,3}(\alpha, \beta) = 1 - Q\beta + \alpha\beta^3(1 - \beta + 2\beta^2 - 2Q\beta^2 - Q\beta^3 + Q^2\beta^4) - \alpha^2\beta^9(1 - \beta). \quad (3.16)$$

It has framing $2 \cdot 3 = 6$ just like the BEM spectra curve from which it is derived. One can convert it to framing 0 by the framing transformation $\alpha \rightarrow \alpha\beta^{-6}$. One can likewise compute the spectral curve for the torus knot $\mathcal{K}_{3,2}$ and it turns out to be the same as that of the knot torus $\mathcal{K}_{2,3}$. It is satisfactory since a topological invariant of knots should be the same for the two torus knots. On the other hand this is not surprising since the fractional power terms in the BEM spectral curve which cause the inequivalence between the two torus knots have now been removed. We also note that by its very construction, the Seiberg–Witten differential of the spectral curve is eq. (3.9), and when expanded about the point $(\alpha, \beta) = (0, Q^{-1})$ in terms of α it generates the correct numbers of worldsheet disk instantons.

Before we move on, we comment that since its construction is symmetric in $\rho^{(k)}$, the ideal $\widehat{\mathcal{I}}_{r,s}$ should also contain relations between the elementary symmetric functions $S^{(j)}$ ($j = 1, \dots, r$) of $\rho^{(k)}$. To see this more explicitly, we generate the ideal $\widehat{\mathcal{I}}_{r,s}$ not directly from $h_{r,s}(\zeta, \rho^{(k_1)}, \dots, \rho^{(k_i)})$ but from the symmetric sums of them (together with $\alpha - \zeta^r$ and $\beta + (-1)^r \rho^{(k_1)} \dots \rho^{(k_r)}$), and express these symmetric sums in terms of $S^{(j)}$. The Gröbner basis of this construction of $\widehat{\mathcal{I}}_{r,s}$ consists of polynomials in $S^{(j)}$ and α, β

$$R_{r,s}^{(k)}(\alpha, \beta, S^{(1)}, \dots, S^{(r)}) = 0, \quad k = 1, \dots, r. \quad (3.17)$$

They are the relations of $S^{(j)}$ we are after, and they can be used to eliminate $S^{(j)}$ in favor of α, β . This will be useful for constructing the so-called annulus kernel in section 3.2.

The spectral curves constructed this way actually have already been found by Aganagic and Vafa [173], and therefore we call them the AV spectral curve. The idea of their construction is as follows.

Suppose there is only one brane wrapping the Lagrangian submanifold in the resolved conifold corresponding to the knot \mathcal{K} in $U(N)$ Chern–Simons theory on a three–sphere. The source matrix V in the free energy of the brane in eq. (2.95) only has one entry, and let us denote it by e^{-x} . Then x serves as the modulus of the brane. The partition function of the brane

$$Z_{\text{top}}(x; g_s, t) = \exp(\mathcal{F}(g_s, t, V)). \quad (3.18)$$

can be expressed in terms of quantum knot invariants of the knot \mathcal{K} through the Ooguri–Vafa conjecture. The eq. (2.292) identifies $Z_{\text{top}}(x; g_s, t)$ with the partition function of the deformed Chern–Simons theory. The latter is computed from the Ooguri–Vafa operator, which can be expanded from its definition in eq. (2.168) as

$$Z(U, V) = 1 + \sum_{\vec{k}} \frac{1}{z_{\vec{k}}} \Upsilon_{\vec{k}}(U) \Upsilon_{\vec{k}}(V), \quad (3.19)$$

where the coefficient $z_{\vec{k}}$ and the factors $\Upsilon_{\vec{k}}$ have been defined in eq. (2.174) and eq. (2.175) respectively. When $V = e^{-x}$, the factor $\Upsilon_{\vec{k}}(V)$ is reduced to $\exp(-\ell(\vec{k})x)$ with $\ell(\vec{k}) = \sum_j j k_j$. When one sums over \vec{k} with fixed $\ell(\vec{k})$, $\Upsilon_{\vec{k}}(V)$ can be factored out, and the rest can be reduced by the Frobenius formula to

$$\sum_{\vec{k}, \ell(\vec{k})=n} \frac{1}{z_{\vec{k}}} \Upsilon_{\vec{k}}(U) = \text{Tr}_n(U). \quad (3.20)$$

Here the trace Tr_n is taken with the n -th symmetric representation, whose associated Young diagram has one row of n boxes. After taking the vev of U the partition function of the deformed Chern–Simons theory and therefore the partition function of the brane is expressed in terms of the quantum knot invariants of \mathcal{K} colored only in symmetric representations

$$Z_{\text{top}}(x; g_s, t) = Z_{\text{CS}}(x; U) = \sum_{n=0}^{\infty} \mathcal{W}_n(\mathcal{K}) e^{-nx}. \quad (3.21)$$

A crucial observation in ref. [177] is that the topological string partition function of brane can be regarded as a wavefunction on the moduli space, or in other words the on–shell phase space, of the brane. In the current context, it means that the partition function eq. (3.21) is a wavefunction on the moduli space of the brane associated to the knot \mathcal{K} , and the latter is understood to be the spectral curve of the brane we are after, characterized by an equation relating x and y

$$F_{\mathcal{K}}(x, y) = 0. \quad (3.22)$$

Here x is the brane modulus, while $p := y$ is regarded as the momentum. Furthermore we can quantize the spectral curve by promoting the variables x, p to operators \hat{x}, \hat{p} . When the wavefunction $Z_{\text{top}}(x; g_s, t)$ is in the coordinate representation, which it is, the effect of \hat{x} is multiplication by x , while \hat{p} is the differential operator $\hat{p} = g_s \partial_x$. They satisfy the commutation relation

$$[\hat{p}, \hat{x}] = g_s, \quad (3.23)$$

where g_s is now treated as the Planck constant in this quantum system. Then the quantum

spectral curve should annihilate the wave function of the brane⁴

$$\hat{F}_{\mathcal{K}}(\hat{x}, \hat{p})Z_{\text{top}}(x; g_s, t) = 0 . \quad (3.24)$$

Furthermore due to eq. (3.21) the quantum knot invariants are Fourier transforms of the partition function; in other words, they are the wave function in the momentum representation. So they are also annihilated by the quantum spectral curve

$$\hat{F}_{\mathcal{K}}(\hat{x}, \hat{p})\mathcal{W}_n(\mathcal{K}) = 0 , \quad (3.25)$$

where now the operators \hat{x} and \hat{p} act differently

$$e^{\hat{p}}\mathcal{W}_n(\mathcal{K}) = q^n\mathcal{W}_n(\mathcal{K}), \quad e^{\hat{x}}\mathcal{W}_n(\mathcal{K}) = \mathcal{W}_{n+1}(\mathcal{K}) . \quad (3.26)$$

In the representation above $q = e^{ig_s}$. Therefore eq. (3.25) effectively gives a recursive relation between quantum knot invariants in symmetric representations. Conversely if we know all the quantum knot invariants in symmetric representations of a knot we can try to find the quantum spectral curve by deducing the recursive relation, and the geometric spectral curve is obtained in the classical limit. In this way the spectral curves for torus knots can be computed, and they are the same as the spectral curves we derived by removing fractional power terms of the BEM spectral curves.

Yet another way to compute the AV spectral curve was found by mathematicians [178–183], and it is intimately related to the construction of the Lagrangian branes associated to knots. In T^*S^3 before the geometric transition the Lagrangian brane of knot \mathcal{K} is constructed to be wrapping the conormal bundle $\tilde{\mathcal{L}}_{\mathcal{K}}$ (we use the same symbol for both the brane and the submanifold) of the knot in eq. (2.178). The cotangent bundle T^*S^3 asymptotes at infinity to $(S^3 \times S^2) \times \mathbb{R}_+$, where in particular $S^2 \times \mathbb{R}_+ = \mathbb{R}^3$ (represented by the shaded face in the left diagram of Fig. 3.1) is the cotangent vector space over each point of S^3 . The conormal bundle $\tilde{\mathcal{L}}_{\mathcal{K}}$ imprints the S^3 at infinity in the shape of the knot. On the other hand since the conormal bundle over each point of the knot is simply $\mathbb{R}^2 \subset \mathbb{R}^3$, it imprints the S^2 at infinity in the shape of a simple S^1 (unknot). In order to find the Lagrangian brane after the geometric transition in the resolved conifold, it is most convenient to first lift the brane $\tilde{\mathcal{L}}_{\mathcal{K}}$ slightly off the three–sphere before deforming the three–sphere to a point and blowing it up. The brane $\tilde{\mathcal{L}}_{\mathcal{K}}$ naturally survives the geometric transition and we can then land it on the $S^2 = \mathbb{P}^1$ in the resolved conifold. The brane intersects \mathbb{P}^1 at the locus of a simple S^1 just like its imprint on the S^2 in the infinity, and in the \mathbb{C}^2 fiber over each point of \mathbb{P}^1 it imprints the S^3 at infinity in the shape of the knot. This approach of constructing the brane in the resolved conifold was advocated in refs. [77, 154], and it has the additional advantage that one can naturally deduce the framing of the brane from that of the knot in the process.

Ng took the idea a step further and argued that the information of the brane is encoded completely in its imprint on $S^2 \times S^3$ in the infinity, which is not changed over the course of the geometric transition, and this is the reason the partition functions of the brane are identical before and after the geometric transition. In particular the boundary $S^2 \times S^3$ at infinity is a contact geometry, and the two dimensional imprint of the brane on the boundary is a

⁴ The equation describing the on–shell phase space is the equation of motion of the system, and the quantum operator derived from it necessarily annihilates the wavefunction of the system.

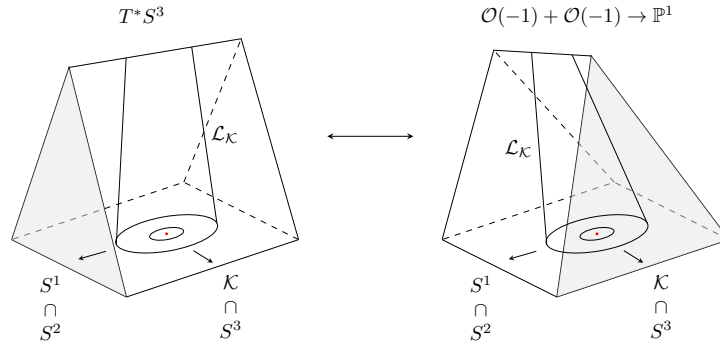


Figure 3.1: The Lagrangian branes in the transition of geometries underlying the Ooguri–Vafa conjecture.

Legendre submanifold. Using techniques in the theory of contact geometry, Ng devised a series of invariants of the Legendre submanifold, which are essentially defined by certain holomorphic disks in $(S^2 \times S^3) \times \mathbb{R}_+$ ending on the Legendre submanifold. The simplest invariant is the so-called augmentation variety, which is a complex curve in $(\mathbb{C}^*)^2$ defined by a polynomial equation⁵

$$\text{Aug}_{\mathcal{K}}(\alpha, \beta; Q) = 0 . \quad (3.27)$$

For the details of Ng’s invariants we refer readers to the review [182]. We only point out that it has been conjectured that Ng’s augmentation variety is the same as the AV spectral curve for an arbitrary knot [182, 184], and it has been verified for all the AV spectral curves that have been computed. This is not surprising since the Ng’s invariants are defined from the holomorphic disks ending on the brane. Furthermore Ng provides an algorithm to derive the augmentation variety for an arbitrary knot from its planar projection graph. In fact the augmentation varieties for many knots, many of which are hyperbolic, have been derived by Ng and can be found on Ng’s website.

Let us now summarize the reasons to regard the AV spectral curves as the real spectral curves for branes associated to knots. First, they are the moduli spaces of the branes associated to the knots in question according to the construction of Aganagic and Vafa. Second, their Seiberg–Witten differentials do not contain redundant and mysterious fractional power terms and are pure generating functions of the holomorphic disks ending on the branes. As a consequence they seem to be true topological invariants as opposed to the BEM spectral curves, in the sense that they are identical for the two torus knots $\mathcal{K}_{r,s}$ and $\mathcal{K}_{s,r}$ with swapped labels. And finally the most important of all mathematicians have devised an algorithm to derive the AV spectral curves for arbitrary knots, if the conjecture that augmentation varieties equal AV spectral curves is correct. In the following we will assume this is the case and use the name AV spectral curve and augmentation variety interchangeably.

Finally in this section we point out some properties of the AV spectral curves. The augmentation varieties and hence the AV spectral curves enjoy the an involution symmetry. The

⁵ Precisely speaking Ng treats the parameter Q also as a \mathbb{C}^* coordinate, and therefore the augmentation variety is a complex surface in $(\mathbb{C}^*)^3$.

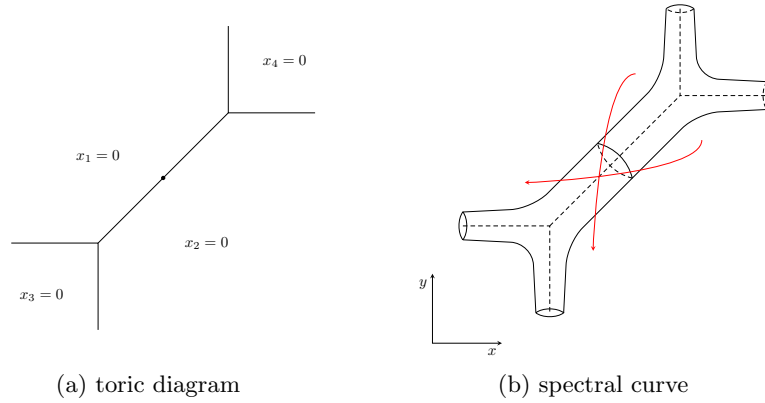


Figure 3.2: The toric diagram of the resolved conifold, and the spectral curve of its mirror. The former is invariant under the involution of eq. (3.30), and the latter is invariant under the involution of eq. (3.29).

augmentation variety of any knot is invariant under the map⁶

$$\iota : \alpha \mapsto \frac{Q^{f-1}}{\alpha}, \quad \beta \mapsto \frac{1}{Q\beta}, \quad (3.28)$$

where f is the framing of the knot. This actually reflects the involution symmetry of the background geometry the resolved conifold itself. The spectral curve eq. (2.116) of the mirror dual of the resolved conifold is invariant under the involution transformation

$$x \mapsto \log Q - x, \quad y \mapsto \log Q - y, \quad (3.29)$$

which is illustrated in Fig. 3.2b. This transformation is precisely the involution eq. (3.28) with framing zero (recall that $\alpha = e^{-x}, \beta = e^{-y}$). Accordingly the resolved conifold itself enjoys a symmetry under involution ,

$$(x_1, x_2, x_3, x_4) \rightarrow (\bar{x}_2, -\bar{x}_1, \bar{x}_4, -\bar{x}_3). \quad (3.30)$$

This is schematically described in its toric diagram by the 180° rotation about the central thick point in Fig. 3.2a. When a brane (not necessarily toric) in the resolved conifold is mapped by the involution, its spectral curve, in other words its moduli space, undergoes the transformation described by eq. (3.28). Since the background geometry is the same after the involution, the numbers of holomorphic disks ending on the brane are the same, which is the reason the spectral curve of the brane is invariant under the involution.

A second property of the AV spectral curves is that they are usually singular and of high genera. For instance, the AV spectral curve of the trefoil torus knot (see Fig. 2.10a), is a genus one curve with two nodal points⁷. This topology is not affected by a framing transformation of the spectral curve. The AV spectral curve of the figure eight knot with framing zero (denoted

⁶ Note the augmentation variety is only defined up to multiplications of α or β .

⁷ The genus of the spectral curve can be determined by the number of the integral lattice points inside the Newton polytope of the spectral curve, minus the contribution from the singular points.

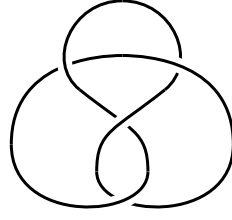


Figure 3.3: The figure eight knot, also denoted by $\mathbf{4}_1$ in the knot theory.

by $\mathbf{4}_1$ in knot theory), the simplest hyperbolic knot (see Fig. 3.3), is

$$F_{\mathbf{4}_1}(\alpha, \beta) = \beta^2 - Q\beta^3 + \alpha(-1 + 2\beta - 2Q^2\beta^4 + Q^2\beta^5) + \alpha^2(1 - 2Q\beta + 2Q^2\beta^4 - Q^3\beta^5) + \alpha^3(-Q^2\beta^2 + Q^2\beta^3). \quad (3.31)$$

It is a genus two curve with two degree three singular points. This topology is also not changed by a farming transformation of the spectral curve.

3.2 Annulus Kernel

3.2.1 Problems with Bergman Kernel

We have established in the previous section that the AV spectral curves are the real spectral curves for branes associated to knots. However when proceeding to apply the topological recursion we immediately face problems from the next input of the topological recursion, namely the Bergman kernel. As we mentioned in the previous section the AV spectral curves for branes associated to nontrivial knots have genera greater than zero. This implies that the Bergman kernel is a transcendental function of the parameter Q of the spectral curve. For instance the AV spectral curve for trefoil is an elliptic curve, and the Bergman kernel of an elliptic curve is given by the Akemann formula [158], which reads

$$B(\alpha_1, \alpha_2) = \frac{E(k^2)}{K(k^2)} \frac{(\lambda_1 - \lambda_3)(\lambda_4 - \lambda_2)}{4\sqrt{\prod_{i=1}^4 (\alpha_1 \lambda_i - 1)(\alpha_2 \lambda_i - 1)}} d\alpha_1 d\alpha_2 + \frac{1}{4(\alpha_1 - \alpha_2)^2} \left(\sqrt{\frac{(\alpha_1 \lambda_1 - 1)(\alpha_1 \lambda_2 - 1)(\alpha_2 \lambda_3 - 1)(\alpha_2 \lambda_4 - 1)}{(\alpha_1 \lambda_3 - 1)(\alpha_1 \lambda_4 - 1)(\alpha_2 \lambda_1 - 1)(\alpha_2 \lambda_2 - 1)}} + \sqrt{\frac{(\alpha_2 \lambda_1 - 1)(\alpha_2 \lambda_2 - 1)(\alpha_1 \lambda_3 - 1)(\alpha_1 \lambda_4 - 1)}{(\alpha_2 \lambda_3 - 1)(\alpha_2 \lambda_4 - 1)(\alpha_1 \lambda_1 - 1)(\alpha_1 \lambda_2 - 1)}} + 2 \right) d\alpha_1 d\alpha_2. \quad (3.32)$$

Here $\lambda_i, i = 1, \dots, 4$ are the four branch points of the elliptic curve, and $K(k^2), E(k^2)$ are the complete elliptic integrals of the first and second kinds respectively, with the elliptic modulus k defined by

$$k^2 = \frac{(\lambda_1 - \lambda_2)(\lambda_3 - \lambda_4)}{(\lambda_1 - \lambda_3)(\lambda_2 - \lambda_4)}. \quad (3.33)$$

The Akemann kernel clearly depends on the ordering of the four branch points, and hence the choice of A- and B-cycles. More importantly since the argument k^2 of the elliptic integrals is

a rational function of the parameter Q , the Akemann kernel is a transcendental function of Q . This is also true at each individual order when the Akemann kernel is expanded in terms of α_1 and α_2 near $\alpha_1 = \alpha_2 = 0$, since the ratio $E(k^2)/K(k^2)$ will appear in the series coefficients. However this contradicts squarely with the Ooguri–Vafa conjecture. Since the Bergman kernel is the generating function of worldsheet annulus instantons, the Ooguri–Vafa conjecture predicts that its expansion coefficients in the neighborhood of $\alpha_1 = \alpha_2 = 0$ are polynomials of $Q^{\pm 1}$. To see this, let us suppose the Bergman kernel is expanded as follows

$$B(p_1, p_2) = \frac{d\alpha_1 d\alpha_2}{(\alpha_1 - \alpha_2)^2} + d\alpha_1 d\alpha_2 (p_{(2)} + p_{(1,1)}(\alpha_1 + \alpha_2) + p_{(0,2)}\alpha_1\alpha_2 + p_{(1,0,1)}(\alpha_1^2 + \alpha_2^2) + \dots) . \quad (3.34)$$

The subscripts of the coefficients $p_{(*)}$ are vectors $\vec{k} = (k_1, k_2, \dots)$, which record the winding numbers of the boundary components of the worldsheet (annulus) instantons following the convention in eq. (2.293). According to eq. (2.294) and eq. (2.98) the coefficients $p_{(\vec{k})}$ of the Bergman kernel are identified with open string free energies $\mathcal{F}_{0, \vec{k}}(Q)$ with genus zero and $|\vec{k}| = \sum_j k_j = 2$ up to certain factors arising from the integration

$$p_{\vec{k}} = \prod_j j^{k_j} \mathcal{F}_{0, \vec{k}}(Q) \quad \text{for } |\vec{k}| = 2 . \quad (3.35)$$

On the other hand eq. (2.293) of the Ooguri–Vafa conjecture predicts that

$$\mathcal{F}_{0, \vec{k}} = \frac{1}{\prod_j j^{k_j}} \mathcal{W}_{\vec{k}, 0}^{(c)}(Q) = \frac{1}{\prod_j j^{k_j}} \mathcal{W}_{\vec{k}}^{(c)}(q = 1, Q) , \quad (3.36)$$

where in the last step we have used eq. (2.176) the genus expansion formula for the connected vev of Wilson loop along the knot. Therefore we have the simple identification

$$p_{\vec{k}} = \mathcal{W}_{\vec{k}}^{(c)}(q = 1, Q) . \quad (3.37)$$

The variable Q can be related to λ in the Chern–Simons theory by combining the mirror map of the resolved conifold eq. (2.118), the large N dictionary eq. (2.246), and the definition of λ eq. (2.139) in Chern–Simons theory

$$Q = \lambda^{-1} . \quad (3.38)$$

Finally by comparing eq. (2.171) and eq. (2.170) one can easily compute the connected vevs $\mathcal{W}_{\vec{k}}^{(c)}$ and find them to be polynomials in quantum knot invariants (a simple example is given in eq. (2.173)), and therefore polynomials in $Q^{\pm 1}$. As a consequence, the coefficients $p_{\vec{k}}$ of the Bergman kernel expansion are polynomials in $Q^{\pm 1}$. The coefficients of different monomials in these polynomials are the numbers of annulus instantons in different relative homology classes in the bulk data, which translate to how many times they wrap around the \mathbb{P}^1 in the background resolved conifold.

But does the polynomial nature of the Bergman kernel indicate the true spectral curve should actually be of genus zero, therefore is not the AV spectral curve? Let us assume this is the case, but insist that α is a good local coordinate⁸ near the origin. Being of genus zero, we can

⁸ We have seen that the BEM spectral curve fails this requirement and so the following argument does not apply.

always find a semi-global coordinate y on the spectral curve according to the uniformization theorem (see for instance [185]) such that its coordinate chart covers almost the whole spectral curve except for a single point⁹, and that it vanishes at $\alpha = 0$. In terms of this semi-global coordinate, the Bergman kernel has the simple form

$$B(y_1, y_2) = \frac{dy_1 dy_2}{(y_1 - y_2)^2} . \quad (3.39)$$

On the other hand, we can treat α as a function of y and expand it

$$\alpha(y) = y + c_1 y^2 + c_2 y^3 + \mathcal{O}(y^4) . \quad (3.40)$$

In the series expansion above, the linear term cannot vanish, for otherwise α ceases to be a good local coordinate. We can thus always rescale y so that the linear coefficient is 1. If we plug the series expansion $\alpha(y)$ in eq. (3.34) and compare it with eq. (3.39), we can get a series of relations between $p_{\vec{k}}$ and c_i

$$\begin{aligned} 0 &= p_{(2)} - c_1^2 + c_2, \\ 0 &= p_{(1,1)} + 2c_1^3 + 2p_{(2)}c_1 - 4c_1c_2, \\ 0 &= p_{(0,2)} - 6c_1^4 + 4p_{(2)}c_1^2 + 16c_1^2c_2 + 4p_{(1,1)}c_1 - 6c_2^2, \\ 0 &= p_{(1,0,1)} - 3c_1^4 + 9c_1^2c_2 + 3p_{(1,1)}c_1 + 3p_{(2)}c_2 - 3c_2^2, \\ &\dots \dots \end{aligned} \quad (3.41)$$

By removing c_i from these relations we obtain a series of identities which involve $p_{\vec{k}}$ only. For instance, the very first identity reads

$$J_1 = 6p_{(2)}^2 - 4p_{(1,0,1)} + 3p_{(0,2)} = 0 . \quad (3.42)$$

Assuming the Ooguri–Vafa conjecture is correct and the Bergman kernel is the generating function of worldsheet annulus instantons, $p_{\vec{k}}$ can be read off from quantum knot invariants through eq. (3.37), and we can explicitly check these identities for the knots whose knot invariants are known. For instance, for the first two torus knots $\mathcal{K}_{2,3}$ and $\mathcal{K}_{2,5}$, the J_1 invariant turns out to be¹⁰

$$\begin{aligned} J_1(\mathcal{K}_{2,3}) &= 36(-1 + Q)^4(5 - 4Q + Q^2) , \\ J_1(\mathcal{K}_{2,5}) &= 60(-1 + Q)^4(98 - 168Q + 105Q^2 - 28Q^3 + 3Q^4) . \end{aligned} \quad (3.43)$$

which manifestly do not vanish. Therefore even if we assume the spectral curve is of genus zero, contradictions concerning the Bergman kernel are inevitable.

It seems that unless we give up the Ooguri–Vafa conjecture for nontrivial knots, identifying the generating function of worldsheet annulus instantons with the Bergman kernel of the spectral curve always leads to contradictions, regardless of the genus of the spectral curve. Since there are strong evidences for the verity of the Ooguri–Vafa conjecture (for instance the proof of the integrality structure of the quantum knot invariants mentioned in section 2.5.6), we are

⁹ For instance on S^2 the north coordinate chart only misses the south pole. Since the spectral curve is defined in $(\mathbb{C}^*)^2$ there are in fact punctures on the curve. Here we ignore these punctures for the moment, and compactify the spectral curve by filling up all the punctures.

¹⁰ We note here although the quantum knot invariants of the two torus knots are framing dependent, the invariant J_1 is framing *independent*, which may indicate some underlying symmetry.

forced to abandon the assumption that the Bergman kernel is the annulus instanton generating function.

This conclusion is bolstered by the following observation. By definition the Bergman kernel satisfies the normalization condition that its integral along an A cycle of the spectral curve vanishes, which is consistent with the filling fraction conditions in Hermitian matrix models discussed in section 2.5.1. One can convince oneself that this A cycle normalization condition is the reason that the Bergman kernel is a transcendental function of the parameter Q of the spectral curve. This is evident in the case of the Akemann kernel in eq. (3.32) for an elliptic spectral curve. The integral of the Akemann kernel along an A cycle would produce various elliptic integrals which would be cancelled by $E(k^2)$ and $K(k^2)$ in the formula for the integral to vanish.

The filling fraction conditions can be proved in Hermitian matrix models (see for instance ref. [142]), where the A cycles of the spectral curve play an important role. For instance we know that the integrals of the Seiberg–Witten differential along A cycles give the filling fractions of the matrix model. Besides we know thanks to the BKMP theorem that the usual topological recursion applies to the spectral curve of the mirror dual of a toric Calabi–Yau threefold, and therefore the filling fraction conditions are also satisfied. In this scenario the A cycles of the spectral curve likewise have physical meanings. The integrals of the Seiberg–Witten differential along A cycles are the flat coordinates on the closed topological string moduli space as in eq. (2.117), i.e. the moduli of the background Calabi–Yau threefold. In fact it was argued in ref. [29] that for many toric Calabi–Yau threefolds one may construct matrix models whose free energies coincide with those of type A closed topological string theory on these geometries and these matrix models are in some way similar to the usual Hermitian matrix models. This could be the underlying reason of the BKMP theorem, and as a corollary the filling fraction conditions. On the other hand, it is not known whether there are matrix model interpretations underlying the AV spectral curves for nontrivial knots, and even if they exist whether they are similar to the usual Hermitian matrix models. In fact the meaning of the A cycles of the AV spectral curves are rather mysterious. They certainly do not correspond to the moduli of the background geometry. The background resolved conifold has only one modulus, while the AV spectral curves have more and more A cycles due to increasing genera when the associated knots become more complicated. Therefore we can contemplate abandoning the filling fraction conditions.

On the other hand, even without the filling fraction conditions, we can still apply the formula eq. (2.272) of the topological recursion to compute meaningful quantities as long as we have a proper substitute for the Bergman kernel. These quantities, as we stressed at the end of section 2.5.1, are still solutions to the loop equations which are the consequence of some symmetries of the system.

Furthermore we know that any Riemann surface $\Sigma_{g,h}$ of genus g with h boundary components can be decomposed to tubes and pairs-of-pants, and it was argued in ref. [161] that the formula eq. (2.272) describes precisely the recursive procedure to decompose a Riemann surface. We can use eq. (2.272) recursively to write down for an arbitrary correlation differential $\omega_h^{(g)}$ a finite sum of products, each of which consists of the symmetric bidifferential $\omega_2^{(0)}$ and the recursion kernel K only. Each product corresponds to one way of decomposing the Riemann surface $\Sigma_{g,h}$, and can in fact be obtained from the decomposition scheme by substituting a tube with the symmetric bidifferential and a pair-of-pants with the recursion kernel. Let us illustrate this by some examples. By applying the topological recursion the genus one one-point correlation

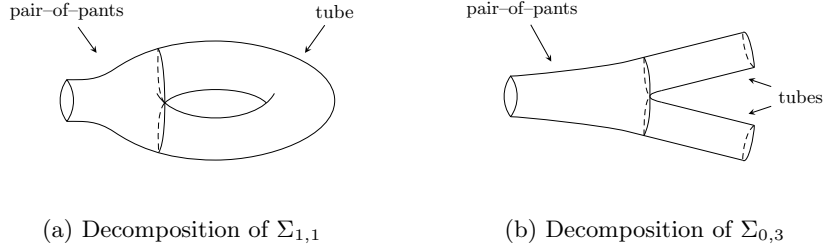


Figure 3.4: The decomposition of $\Sigma_{g=1,h=1}$ and $\Sigma_{0,3}$ into tubes and pairs-of-pants.

differential is computed by

$$\omega_1^{(1)}(p) = \sum_i \operatorname{Res}_{q \rightarrow a_i} K(p, q) \omega_2^{(0)}(q, \bar{q}) , \quad (3.44)$$

where a_i is a ramification point on the spectral curve. Accordingly there is only one way to decompose $\Sigma_{1,1}$ to tubes and pairs-of-pants, as seen in Fig. 3.4a. After replacing each component by the bidifferential or the recursion kernel, we get the integrand on the right hand side of eq. (3.44). Note that the gluing slice in Fig. 3.4a corresponds to in the recursion formula an internal point q in terms of which we will take the residue of the integrand at the ramification points. Besides the two ends of the tube glued from the right are assigned the coordinate q and its conjugate \bar{q} respectively. We can also compute the planar three-point correlation differential by the topological recursion, and it reads,

$$\omega_3^{(0)}(p_1, p_2, p_3) = 2 \operatorname{Res}_{q \rightarrow a} K(p_1, q) \omega_2^{(0)}(q, p_2) \omega_2^{(0)}(\bar{q}, p_3) . \quad (3.45)$$

Likewise there is only one way of decomposing $\Sigma_{0,3}$ to tubes and pairs-of-pants as see in Fig. 3.4a, and we can also obtain the correct integrand by doing the replacement. Note the factor of 2 in eq. (3.45) corresponds to two ways of gluing the pair-of-pants to the two different tubes.

Having established the similarity between the topological recursion formula and the cut-and-glue scheme of Riemann surfaces, it was further argued in ref. [161] that if $\omega_2^{(0)}(p_1, p_2)$ is the generating function of worldsheet annulus instantons, and $K(p, q)$ is the generating function of worldsheet pair-of-pants instantons, then $\omega_h^{(g)}(p_1, \dots, p_h)$ computed by the topological recursion would be the generating function of worldsheet instantons on the Riemann surface $\Sigma_{g,h}$. Besides it can be shown that the kernel $K(p, q)$ is related to $\omega_2^{(0)}$ and the disk generating function $\omega_1^{(0)}$ through eq. (2.269).

Naturally in the context of the AV spectral curves for the branes associated to knots, the idea is to look for the true generating function of the worldsheet annulus instantons, substitute it for the Bergman kernel, and check if the formula of the topological recursion can reproduce the correct higher worldsheet instanton generating functions.

3.2.2 Constructing the Annulus Kernel

Constructing the annulus generating function from scratch would be a daunting task. Instead we used a short-cut [170] by applying the same technique we exploited in section 3.1.2 to compute

AV spectral curves. Recall that the integral of the Bergman kernel of a BEM spectral curve for a torus knot when expanded in α_1, α_2 has terms proportional to $\alpha_1^{n_1/r} \alpha_2^{n_2/r}$, where n_1, n_2 are positive integers. Although the coefficients of the terms with either n_1 or n_2 not divisible by r (fractional power terms) do not have physical meanings, the coefficients of the terms with both n_1 and n_2 divisible by r (integral power terms) count the numbers of worldsheet annulus instantons. Similar to our computation of AV spectral curves in the beginning of section 3.1.2, we can therefore construct the pure annulus generating function for branes associated to a torus knot by removing the fractional power terms from the Bergman kernel $B_{r,s}^{\text{BEM}}(\beta_1, \beta_2)$ of the BEM spectral curve. To do this, we note again that because of the fractional power terms, α_1 and α_2 are not good local coordinates, and we need to express the BEM Bergman kernel in eq. (3.5) in terms of the local coordinate $\zeta = \alpha^{1/n}$

$$B_{r,s}^{\text{BEM}}(\beta_1, \beta_2) = B_{r,s}^{(k,\ell)}(\zeta_1, \zeta_2) = \frac{(r\rho^{(k)}(\zeta_1)^{r-1}\rho^{(k)\prime}(\zeta_1)) (r\rho^{(\ell)}(\zeta_2)^{r-1}\rho^{(\ell)\prime}(\zeta_2))}{(\rho^{(k)}(\zeta_1)^r - \rho^{(\ell)}(\zeta_2)^r)^2} d\zeta_1 d\zeta_2 . \quad (3.46)$$

Recall that the coordinate patch near $\alpha = 0$ splits to r different coordinate patches for ζ , and we need to specify in $B_{r,s}^{(k,\ell)}(\zeta_1, \zeta_2)$ for both ζ_1 and ζ_2 which coordinate patches they belong to by the superscripts (k) and (ℓ) on the functions $\rho(\zeta)$. To remove this uncertainty we need to sum over all the r^2 representations of this BEM Bergman kernel with k and ℓ running from 1 through r .

$$B_{r,s}(\alpha_1, \alpha_2) = \sum_{k,\ell=1}^r B_{r,s}^{(k,\ell)}(\zeta_1, \zeta_2) , \quad \alpha_\mu = (\zeta_\mu)^r , \quad \mu = 1, 2 . \quad (3.47)$$

Since the r different coordinate patches for ζ can be cyclically accessed through phase shifting $\zeta \rightarrow e^{2\pi i/r} \zeta$, similar to what happens in the construction of the pure disk instanton generating function $W_{r,s}$ in eq. (3.9), the summation in eq. (3.47) removes all the expansion terms $\zeta_1^{n_1} \zeta_2^{n_2} = \alpha_1^{n_1/r} \alpha_2^{n_2/r}$ where either n_1 or n_2 is indivisible by r . Therefore $B_{r,s}(\alpha_1, \alpha_2)$ is the pure generating function of worldsheet annulus instantons for branes associated to the torus knot $\mathcal{K}_{r,s}$, and we call it the *annulus kernel*. It is possible to express the annulus kernel in terms of α and β instead of ζ and $\rho^{(k)}, \rho^{(\ell)}$. To do this, we notice that the numerator and the denominator of the annulus kernel are symmetric functions in $\rho^{(k)}$. Therefore we can decompose them in terms of the elementary symmetric functions $S^{(j)}, j = 1, \dots, r$ of $\rho^{(k)}$ and use the relations eqs. (3.17) to remove $S^{(j)}$ in favor of α and β . ζ always appears in the annulus kernel as powers of ζ^r and thus it can be easily replaced in terms of α . The end result has the form

$$B_{r,s}(p_1, p_2) = \frac{N_{r,s}(\alpha(p_1), \beta(p_1), \alpha(p_2), \beta(p_2); Q)}{D_{r,s}(\alpha(p_1), \beta(p_1), \alpha(p_2), \beta(p_2); Q)} d\alpha(p_1) d\alpha(p_2) , \quad (3.48)$$

where both the numerator and the denominator are polynomials in $\alpha_1, \alpha_2, \beta_1, \beta_2$ and Q . The polynomials $N_{r,s}$ and $D_{r,s}$ computed this way can be horrendously lengthy. There may exist a simpler presentation of the annulus kernel $B_{r,s} = \tilde{N}_{r,s}/\tilde{D}_{r,s}$ with shorter polynomials $\tilde{N}_{r,s}, \tilde{D}_{r,s}$, which satisfy

$$\frac{r \cdot N_{r,s} + \sum_{\mu} p_{\mu} \cdot F_{r,s}(\alpha_{\mu}, \beta_{\mu}; Q)}{r \cdot D_{r,s} + \sum_{\mu} q_{\mu} \cdot F_{r,s}(\alpha_{\mu}, \beta_{\mu}; Q)} = \frac{\tilde{r} \cdot \tilde{N}_{r,s} + \sum_{\mu} \tilde{p}_{\mu} \cdot F_{r,s}(\alpha_{\mu}, \beta_{\mu}; Q)}{\tilde{r} \cdot \tilde{D}_{r,s} + \sum_{\mu} \tilde{q}_{\mu} \cdot F_{r,s}(\alpha_{\mu}, \beta_{\mu}; Q)} , \quad (3.49)$$

Here $p_\mu, q_\mu, \tilde{p}_\mu, \tilde{q}_\mu$ are some polynomials in $\alpha_1, \alpha_2, \beta_1, \beta_2$ and Q . Although it is in principle not necessary for the application of the topological recursion, it is computationally beneficial to find the simplest presentation of the annulus kernel, which is a difficult problem.

Before we proceed, we notice that near the diagonal loci $(\alpha_1, \beta_1) = (\alpha_2, \beta_2)$ each BEM Bergman kernel $B_{r,s}^{(k,\ell)}(\zeta_1, \zeta_2)$ with $\ell = k = 1, \dots, r$ has a double pole. This is the double pole of a usual Bergman kernel and therefore its principal part is

$$\frac{d\zeta_1 d\zeta_2}{(\zeta_1 - \zeta_2)^2} \sim \frac{d\alpha_1 d\alpha_2}{(\alpha_1 - \alpha_2)^2}, \quad (3.50)$$

where \sim means identical up to regular terms. As a consequence the principal part of the annulus kernel near the diagonal loci is

$$\frac{r d\alpha_1 d\alpha_2}{(\alpha_1 - \alpha_2)^2}. \quad (3.51)$$

Unfortunately this principal part is not r, s symmetric, and therefore the annulus kernel would be different for the torus knots $\mathcal{K}_{r,s}$ and $\mathcal{K}_{s,r}$. This problem can be cured by simply doing the subtraction

$$\widehat{B}_{r,s}(\alpha_1, \alpha_2) = B_{r,s}(\alpha_1, \alpha_2) - \frac{(r-1)d\alpha_1 d\alpha_2}{(\alpha_1 - \alpha_2)^2}, \quad (3.52)$$

and we call $\widehat{B}_{r,s}(\alpha_1, \alpha_2)$ the *calibrated annulus kernel*. We note that the calibration does not change the numbers of worldsheet annulus instantons, and therefore the calibrated annulus kernel is an equally good annulus generating function. Furthermore it can be shown that the calibrated annulus kernel as opposed to the uncalibrated annulus kernel is covariant under the framing transformation, i.e. it remains a correct annulus generating function after a framing transformation. In fact we will show in the next subsection that without calibration the annulus kernel will make the topological recursion ill-defined, and this problem is cured exactly by the calibration. In the later sections we will use the calibrated annulus kernel in place of the Bergman kernel to perform the topological recursion.

3.2.3 Calibration and Poles

Here we discuss the necessity of doing the calibration as in eq. (3.52), as well as the pole structure of the calibrated annulus kernel. This subsection is a bit technical, and we refer the readers not interested in technical details to the last paragraph of this subsection which summarizes the discussions.

We start by looking at the computation of the AV spectral curve through the ideal eq. (3.14) in the beginning of section 3.1.2 more closely. The BEM spectral curve in eq. (3.6) we started with has degree $r+s$ in the variable ρ , and it is therefore a $(r+s)$ -sheeted cover of the ζ complex plane. Among the $(r+s)$ sheets, r of them are continued to the points $(\zeta, \rho) = (0, e^{2\pi i k/r} Q^{-1/r})$ in the limit $\zeta \rightarrow 0$ and they correspond locally to the r coordinate patches we have discussed about. The other s sheets are continued in the limit $\zeta \rightarrow 0$ to the point $(\zeta, \rho) = (0, \infty)$. In the ideal eq. (3.14) that leads to the AV spectral curve, each variable $\rho^{(k)}$ is not restricted to any particular covering sheet. Therefore the r components $\rho^{(k)}$ of the variable β can take values in any of the $(r+s)$ covering sheets. It is only when we expand the annulus amplitude $W_{r,s}$ in eq. (3.9) about the point $(\alpha, \beta) = (0, Q^{-1})$ are the components $\rho^{(k)}$ forced to take values in the first r coordinate patches, for if any $\rho^{(k)}$ takes value in one of the rest s covering sheets, the value of β will explode at $\alpha = 0$.

To stress the random choice of the ρ components of β among the $r + s$ covering sheets, we rewrite eq. (3.10) for the variables α and β

$$\alpha = \zeta^r, \quad \beta = (-1)^{r+1} \rho^{(\ell_1)} \dots \rho^{(\ell_r)}, \quad (3.53)$$

where $1 \leq \ell_1 < \dots < \ell_r \leq r + s$. It immediately implies that the AV spectral curve has degree $\binom{r+s}{r}$ in β . The annulus kernel now has the form

$$\begin{aligned} B_{r,s}(\alpha_1, \alpha_2) &= \sum_{m,n=1}^r B_{r,s}^{(m,n)}(\zeta_1, \zeta_2) \\ &= \sum_{m,n=1}^r \frac{(r\rho^{(\ell_m)}(\zeta_1)^{r-1} \rho^{(\ell_m)' }(\zeta_1)) (r\rho^{(\ell_n)}(\zeta_2)^{r-1} \rho^{(\ell_n)' }(\zeta_2))}{(\rho^{(\ell_m)}(\zeta_1)^r - \rho^{(\ell_n)}(\zeta_2)^r)^2} d\zeta_1 d\zeta_2. \end{aligned} \quad (3.54)$$

This uncalibrated annulus kernel has double pole when $\rho^{(\ell_m)}(\zeta_1) = \rho^{(\ell_n)}(\zeta_2)^{11}$, and its principal part is simply given by the double pole of the BEM Bergman kernel

$$\frac{d\zeta_1 d\zeta_2}{(\zeta_1 - \zeta_2)^2}. \quad (3.55)$$

Although this implies $\zeta_1 = \zeta_2$ and consequently $\alpha_1 = \alpha_2$, it does not necessarily mean $\beta_1 = \beta_2$ and only requires that some ρ components of β_1 be identical with some ρ components of β_2 . Therefore there can be many more double poles than those at the diagonal loci. They can spell trouble for the topological recursion.

In the topological recursion the annulus kernel $B_{r,s}(q, \bar{q})$ with \bar{q} being the conjugate point of q near a ramification point a of the spectral curve appears frequently. However the annulus kernel is singular at (q, \bar{q}) . To see this, we notice that a pair of conjugate points q, \bar{q} is such that when q stays away from the ramification point a , we have

$$\alpha(q) = \alpha(\bar{q}), \quad \beta(q) \neq \beta(\bar{q}); \quad (3.56)$$

and when q approaches the ramification point a

$$\lim_{q \rightarrow a} (\alpha(q) - \alpha(\bar{q})) = 0, \quad \lim_{q \rightarrow a} (\beta(q) - \beta(\bar{q})) = 0. \quad (3.57)$$

From the perspective of the ρ components of β , this happens when $r - 1$ of the r component ρ 's of $\beta(q)$ are identical with $r - 1$ component ρ 's of $\beta(\bar{q})$, while the last component ρ of $\beta(q)$ is the conjugate point of the last component ρ of $\beta(\bar{q})$ near a ramification point, say \tilde{a} , on the BEM spectral curve in eq. (3.6). In other words, without loss of generality we have

$$\begin{aligned} \beta(q) &= (-1)^{r+1} \rho^{(\ell_1)} \rho^{(\ell_2)} \dots \rho^{(\ell_r)}, \\ \beta(\bar{q}) &= (-1)^{r+1} \rho^{(\ell_1)} \rho^{(\ell_2)} \dots \bar{\rho}^{(\ell_r)}. \end{aligned} \quad (3.58)$$

In fact this is the only possible way to get conjugate points on an AV spectral curve of a torus knot. Suppose there is a second conjugate pair $\rho^{(\ell_i)}$ and $\bar{\rho}^{(\ell_i)}$ with $i \neq r$ near a ramification

¹¹ We are being sloppy here. The double pole condition is $\rho^{(\ell_m)}(\zeta_1)^r = \rho^{(\ell_n)}(\zeta_2)^r$, and hence a possible phase factor of r -th root of unity can arise. Nevertheless we can always absorb this phase factor by appropriately shifting the phase of ζ as we discussed in footnote 1 on page 74. So we ignore the phase factor.

point \tilde{a}' on the BEM spectral curve such that $\rho^{(\ell_i)}$ is a component of $\beta(q)$ and $\bar{\rho}^{(\ell_i)}$ a component of $\beta(\bar{q})$. The condition eq. (3.57) demands that

$$\zeta(\tilde{a}) = \zeta(\tilde{a}') . \quad (3.59)$$

On the other hand by the construction through eq. (3.14) it is known that $\rho^{(\ell_i)} \neq \rho^{(\ell_r)}$ and therefore $\tilde{a} \neq \tilde{a}'$. It indicates two ramification points are stacked over one single branch point, which does not happen for the BEM spectral curve eq. (3.6).

Given the structure of a pair of conjugate points in eq. (3.58), we know that the uncalibrated annulus kernel $B_{r,s}(q, q')$ has double pole at $q' = \bar{q}$, and furthermore the principal part of the double pole is

$$\frac{(r-1)d\zeta_1 d\zeta_2}{(\zeta_1 - \zeta_2)^2} \sim \frac{(r-1)d\alpha_1 d\alpha_2}{(\alpha_1 - \alpha_2)^2} . \quad (3.60)$$

This double pole is removed precisely through the calibration in eq. (3.52). This is the reason the annulus kernel *must* be calibrated for it to be used in the topological recursion.

Using eq. (3.54) we can not only see the reason for calibration, but also find out all the double poles of the (calibrated) annulus kernel. Let us fix the first point (α_1, β_1) , and also the r distinct ρ components of β_1 : $\rho^{(\ell_k)}$ with $k = 1, \dots, r$. Let the values of ρ on the rest s covering sheets be $\rho^{(\ell_k)}$, $k = r+1, \dots, r+s$. The calibrated annulus kernel has a double pole when among the r component ρ 's of β_2 , i of them are identical with the ρ components of β_1 , where i is an arbitrary integer between 0 and r but $i \neq r-1$. (Because of the calibration, the kernel also has double pole when $i = 0$. See eq. (3.61). This lower bound of i will be improved shortly.) So we can classify the double poles of the calibrated kernel into different types labelled by index i , and the principal part of a double pole of type i is

$$\frac{i d\zeta_1 d\zeta_2}{(\zeta_1 - \zeta_2)^2} - \frac{(r-1)d\alpha_1 d\alpha_2}{(\alpha_1 - \alpha_2)^2} \sim \frac{(i+1-r)d\alpha_1 d\alpha_2}{(\alpha_1 - \alpha_2)^2} . \quad (3.61)$$

To find a double pole, we pick arbitrary i values of ρ among $\rho^{(\ell_k)}$, $k = 1, \dots, r$, drop the rest of them, and pick another $r-i$ values of ρ among $\rho^{(\ell_k)}$, $k = r+1, \dots, r+s$. The requirement $r-i \leq s$ corrects the lower bound of i from 0 to $\max(0, r-s)$. The r values of ρ now at hand can be used to construct a new β , which we choose to be β_2 . There are in total $\binom{r}{i} \binom{s}{r-i}$ such choices. Let us use index $j := r-i$ instead of i to label the type of double poles, and it runs over $0, 2, \dots, \min(r, s)$. Then we have just found out for a fixed β_1 , the number of double poles N_j of type j and their principal parts P_j of the calibrated annulus kernel are

$$N_j = \binom{r}{j} \binom{s}{j}, \quad P_j = \frac{(1-j)d\alpha_1 d\alpha_2}{(\alpha_1 - \alpha_2)^2} . \quad (3.62)$$

The case of $j = 0$ is simply the double pole at the diagonal loci. Besides, the total number of double poles is

$$\sum_{j=0, j \neq 1}^{\min(r,s)} N_j = \binom{r+s}{s} - r s . \quad (3.63)$$

Let us summarize this subsection. One of the crucial reasons for using the calibrated annulus kernel in favor of the uncalibrated annulus kernel $B_{r,s}(q, q')$ is that the latter is singular when $q' = \bar{q}$, which makes it unsuitable as $\omega_2^{(0)}$ in the topological recursion. After calibration this

singularity goes away. Furthermore we find out that when the first point in the calibrated annulus kernel is fixed, the kernel has $\min(r, s) - 1$ types of double poles. Labelled by $j = 0, 2, \dots, \min(r, s)$, the number of double poles N_j and the principal part P_j of the double pole of each type are given by eqs. (3.62), and the total number of double poles is given by eq. (3.63). Note that this pole structure is manifestly r, s symmetric.

3.2.4 Stretched Annulus Instantons

Recall that as discussed in section 3.1.2, the resolved conifold enjoys the involution symmetry described by eq. (3.30), and a stack of branes \mathcal{L} embedded in the resolved conifold is mapped to their images $\iota(\mathcal{L})$ under the involution. In this setup, other than worldsheet annulus instantons whose two boundary components only end on \mathcal{L} , there are also annulus instantons stretched between \mathcal{L} and $\iota(\mathcal{L})$. To count the numbers of these annulus instantons, we notice that the branes $\iota(\mathcal{L})$ are in the same moduli space of \mathcal{L} . But the limit of large disk instantons is mapped by ι from the point $(\alpha, \beta) = (0, Q^{-1})$ to $(\alpha, \beta) = (\infty, 1)$. Therefore we should do the change of variables on the second point in the calibrated annulus kernel

$$\alpha_2 = \frac{Q^{f-1}}{\tilde{\alpha}_2}, \quad \beta_2 = \frac{1}{Q\tilde{\beta}_2} \quad (3.64)$$

and expand the calibrated annulus kernel $\widehat{B}_{r,s}(p_1, p_2)$ in terms of α_1 and $\tilde{\alpha}_2$ about the point $\alpha_1 = \tilde{\alpha}_2 = 0$. In the case of the torus knot $\mathcal{K}_{2,3}$ in the framing $6 = 2 \cdot 3$, after rescaling $\alpha_1 \mapsto Q^5 \alpha_1, \tilde{\alpha}_2 \mapsto Q^5 \tilde{\alpha}_2$ we have

$$\begin{aligned} \widehat{B}_{2,3}(p_1, p_2) &= \widehat{B}_{2,3}(p_1, \iota(p_2)) = d\alpha_1 d\tilde{\alpha}_2 \left[-9Q + 16Q^2 - 9Q^3 + Q^4 \right. \\ &\quad + (-168Q + 504Q^2 - 576Q^3 + 300Q^4 - 60Q^5)(\alpha_1 + \tilde{\alpha}_2) \\ &\quad + (-3861Q + 16236Q^2 - 28215Q^3 + 25920Q^4 \\ &\quad \quad \quad - 13230Q^5 + 3528Q^6 - 378Q^7)(\alpha_1^2 + \tilde{\alpha}_2^2) \\ &\quad + (-3136Q + 13230Q^2 - 23040Q^3 + 21280Q^4 - 11088Q^5 \\ &\quad \quad \quad \left. + 3150Q^6 - 400Q^7 + 2Q^8)\alpha_1 \tilde{\alpha}_2 + \dots \right]. \quad (3.65) \end{aligned}$$

Similar to the usual expansion of the Bergman kernel illustrated in eq. (3.34), the coefficient polynomial of Q in front of the differential $\alpha_1^n \tilde{\alpha}_2^{n'} d\alpha_1 d\tilde{\alpha}_2$ should encode the numbers of annulus instantons with winding numbers $n + 1$ and $n' + 1$ on the two stacks of branes \mathcal{L} and $\iota(\mathcal{L})$ respectively. We follow the notation below eq. (2.293) and record the winding numbers on the two stacks of branes by two vectors $\vec{k} = (k_1, k_2, \dots)$ and $\vec{k}' = (k'_1, k'_2, \dots)$. The coefficient polynomials can then be denoted by $p_{\vec{k}, \vec{k}'}$, and they satisfy the involution symmetry $p_{\vec{k}, \vec{k}'} = p_{\vec{k}', \vec{k}}$. They are identified with the free energies of the worldsheet annulus instantons stretched between \mathcal{L} and $\tilde{\mathcal{L}}$ through

$$p_{\vec{k}, \vec{k}'} = \prod_j j^{k_j + k'_j} \mathcal{F}_{g=0, \vec{k}, \vec{k}'}(Q) \quad \text{for} \quad |\vec{k}| = |\vec{k}'| = 1. \quad (3.66)$$

Therefore from eq. (3.65) we can read off the free energies of the stretched annulus instantons between the pair of branes $\mathcal{L}_{2,3}$ and $\iota(\mathcal{L}_{2,3})$

$$p_{(1),(1)} = -9Q + 16Q^2 - 9Q^3 + Q^4,$$

$$\begin{aligned}
 p_{(0,1),(1)} &= -168Q + 504Q^2 - 576Q^3 + 300Q^4 - 60Q^5 , \\
 p_{(0,0,1),(1)} &= -3861Q + 16236Q^2 - 28215Q^3 + 25920Q^4 - 13230Q^5 + 3528Q^6 - 378Q^7 , \\
 p_{(0,1),(0,1)} &= -3136Q + 13230Q^2 - 23040Q^3 + 21280Q^4 - 11088Q^5 + 3150Q^6 - 400Q^7 \\
 &\quad + 2Q^8 .
 \end{aligned} \tag{3.67}$$

Note in each polynomial the leading order of Q is 1, meaning that a stretched annulus must wrap around the \mathbb{P}^1 in the background resolved conifold at least once. This is different from ordinary annulus instantons ending on one brane only.

In order to verify these results, we compute the free energies from two other avenues. The first is the adaptation of the equivariant localization techniques by Diaconescu, Shende, and Vafa [154], and this was discussed in [170]. The free energies computed in this way coincide with the results presented above. The second is by generalizing the formula eq. (2.293) of the Ooguri–Vafa conjecture. It was pointed out in ref. [186] that the most generic representations of the gauge group $U(N)$ are composite representations $(R; S)$ labelled by a pair of Young diagrams, and that the quantum knot invariants corresponding to the worldsheet instantons stretched between the pair of branes \mathcal{L} and $\iota(\mathcal{L})$ are those colored in composite representations. Concretely by going through the derivations similar to those in section 2.3.5 concerning the free energies of the deformed Chern–Simons theory, but with the usual quantum knot invariants in eq. (2.170) replaced by those colored in composite representations, we can derive connected vevs of Wilson loops $\mathcal{W}_{\vec{k}, \vec{k}'}^{(c)}$ with composite labelling. These connected vevs should be identified with the free energies of the stretched worldsheet instantons via

$$\frac{1}{\prod_j j^{k_j + \bar{k}_j}} \mathcal{W}_{\vec{k}, \vec{k}', g}^{(c)}(t) = \mathcal{F}_{g, \vec{k}, \vec{k}'}(t) , \tag{3.68}$$

analogous to eq. (2.293). Therefore once we know the quantum knot invariants in composite representations, we can also compute the free energies of the worldsheet instantons stretched between \mathcal{L} and $\iota(\mathcal{L})$. To compare with the results from expanding the calibrated annulus kernel, we combine eq. (3.66) and eq. (3.68) and find

$$p_{\vec{k}, \vec{k}'}(Q) = \mathcal{W}_{\vec{k}, \vec{k}'}^{(c)}(q = 1, Q), \quad \text{with} \quad |\vec{k}| = |\vec{k}'| = 1 . \tag{3.69}$$

The composite representations of $U(N)$ and the quantum knot invariants colored in them are discussed in Appendix A. For torus knots, the quantum knot invariants in composite representations can be written down by a simple adaptation of the Rosso–Jones formula (c.f. eq. (A.13)). Therefore we can also compute the connected vev of Wilson loops with ease. For the torus knot $\mathcal{K}_{2,3}$ in the limit $q \rightarrow 1$, the results are

$$\begin{aligned}
 \mathcal{W}_{(1),(1)}^{(c)}(Q) &\rightarrow Q(-9 + 16Q - 9Q^2 + Q^4) , \\
 \mathcal{W}_{(0,1),(1)}^{(c)}(Q) &\rightarrow 2Q(Q-1)(-24 + 18f + 78Q - 41fQ - 84Q^2 + 34fQ^2 + 24Q^3 \\
 &\quad - 9fQ^3 + 12Q^4 - 2fQ^4 - 6Q^5 + fQ^5) , \\
 \mathcal{W}_{(0,1),(0,1)}^{(c)}(Q) &\rightarrow 2Q(-128 + 855Q - 2376Q^2 + 3296Q^3 - 2088Q^4 - 9Q^5 + 808Q^6 \\
 &\quad - 432Q^7 + 72Q^8 + Q^9 - 24f(Q-1)^5(Q-2)(Q^2 + Q - 4) \\
 &\quad + 2f^2(Q-2)^2(Q-1)^2(Q^4 - 9Q^2 + 16Q - 9)) ,
 \end{aligned}$$

$$\begin{aligned}
 \mathcal{W}_{(0,0,1),(1)}^{(c)}(Q) &\rightarrow \frac{3}{2}Q(Q-1)(6(Q-1))^3(-27+88Q-52Q^2-16Q^3+13Q^4) \\
 &\quad - f(246-1242Q+2399Q^2-2209Q^3+859Q^4+59Q^5-145Q^6 \\
 &\quad + 31Q^7) + 3f^2(Q-1)(Q-2)^2(-9+16Q-9Q^2+Q^4) , \tag{3.70}
 \end{aligned}$$

where f is the framing of the knot. Plugging in the framing $6 = 2 \cdot 3$, they agree with results in eq. (3.67) through the identity eq. (3.69).

We point out that the confluence of the three results provides a nontrivial check on the calibrated annulus kernel, because in computing the free energies of the stretched annulus instantons through the expansion of $\widehat{B}_{r,s}(p_1, \iota(p_2))$ we probe different coordinate patches of the spectral curve, and consequently the global structure of the calibrated annulus kernel on the spectral curve.

3.3 Modified Topological Recursion

3.3.1 Normalization and Free Energies

With the calibrated annulus kernel $\widehat{B}_{r,s}(p_1, p_2)$ in hand, we can proceed to apply the topological recursion formula eq. (2.272) on the AV spectral curve for a torus knot $\mathcal{K}_{r,s}$, with the problematic Bergman kernel replaced by the calibrated annulus kernel. We call this procedure the modified topological recursion, and claim that the correlation differentials computed by the modified topological recursion provide us the free energies of the branes associated to the torus knot $\mathcal{K}_{r,s}$ as in the usual way through eq. (2.294). In fact we can do better. Since the branes associated to knots also probe the background geometry, i.e. the resolved conifold, it is conceivable that the moduli space of these branes also encodes the information of the background geometry described by the free energies of the closed topological string. We will demonstrate that the modified topological recursion is able to compute the closed string free energies from the AV spectral curves as well.

Let us first point out that the correlation differentials computed by the modified topological recursion applied on the AV spectral curve of a torus knot $\mathcal{K}_{r,s}$ also satisfy the variational formula in eq. (2.277), with a slight twist. To be precise, these correlation differentials satisfy [170]

$$\delta_\Omega \omega_n^{(g)}(p_1, \dots, p_n) = \frac{1}{N_{r,s}} \int_{p \in \partial\Omega} \omega_{n+1}^{(g)}(p, p_1, \dots, p_n) \Lambda(p) . \tag{3.71}$$

Here the extra normalization factor $N_{r,s}$ is

$$N_{r,s} = \binom{r+s-2}{r-1} , \tag{3.72}$$

which is actually half the number of ramification points with respect to the projection onto the α plane [170]. The integration path $\partial\Omega$ and the multiplier $\Lambda(p)$ in the eq. (3.71) are defined in line with their counterparts in the usual topological recursion in eq. (2.276), with the role of the Bergman kernel played by the calibrated annulus kernel

$$\Omega(q) = \int_{p \in \partial\Omega} \widehat{B}_{r,s}(p, q) \Lambda(p) . \tag{3.73}$$

In contrast to the case in the usual topological recursion, we shall rather treat this as a formal

definition, since given an arbitrary $\Omega(q)$ one may not be able to find an integration path and the multiplier so that the equation above is satisfied. Nevertheless we can always use this definition to eliminate the integration path and the multiplier on the right hand side of the variational formula eq. (3.71), if we stipulate that the formal integral in eq. (3.73) commutes with any conventional integral. The reason is that in the variational formula the correlation differential $\omega_{n+1}^{(g)}$ is convoluted with the multiplier $\Lambda(p)$ through the first argument p , while this first argument belongs to the calibrated annulus kernel inside the recursion kernel (c.f. eqs. (2.272),(2.269) with the Bergman kernel replaced by the calibrated annulus kernel). So when we compute the right hand side of eq. (3.71), by shifting the order of integrations we can first evaluate the formal integral with respect to the argument p before any conventional integration, eliminating the multiplier $\Lambda(p)$ and the integration path $\partial\Omega$ together with the calibrated annulus kernel containing p in favor of the deformation differential Ω .

The variational formula eq. (3.71) has two implications. The first is that the correlation differential computed by the modified recursion may actually be greater than what we expected by a factor of several powers of $N_{r,s}$. One can show that when one computes the stable correlation differential $\omega_n^{(g)}$ with the modified topological recursion, each time the recursion formula eq. (2.272) is applied, a factor of $N_{r,s}$ appears. Since each application of the recursion formula increases the Euler characteristic $\chi = 2 - 2g - n$ by one and one stops at $\omega_2^{(0)}$ with $\chi = 0$, the recursion formula has to be applied χ times, indicating a factor of $N_{r,s}^{2g-2+n}$. We therefore define the normalized stable correlation differential

$$\widehat{\omega}_n^{(g)}(p_1, \dots, p_n) = \frac{1}{N_{r,s}^{2g-2+n}} \omega_n^{(g)}(p_1, \dots, p_n) . \quad (3.74)$$

They satisfy the variational formula

$$\delta_\Omega \widehat{\omega}_n^{(g)}(p_1, \dots, p_n) = \int_{\partial\Omega} \widehat{\omega}_{n+1}^{(g)}(p, p_1, \dots, p_n) \Lambda(p) . \quad (3.75)$$

which looks exactly like the one in the usual topological recursion.

The second implication is that we can generalize the variational formula and use it to *define* the free energies in the modified topological recursion. In other words, we have

$$\delta_\Omega \mathcal{F}_g = \int_{\partial\Omega} \widehat{\omega}_1^{(g)}(p) \Lambda(p) , \quad g \geq 1 , \quad (3.76)$$

$$\delta_{\Omega_i} \delta_{\Omega_j} \delta_{\Omega_k} \mathcal{F}_0 = \int_{\partial\Omega_i} \Lambda_j(p_1) \int_{\partial\Omega_j} \Lambda_j(p_2) \int_{\partial\Omega_k} \Lambda_k(p_3) \widehat{\omega}_3^{(0)}(p_1, p_2, p_3) . \quad (3.77)$$

Since the free energies given by the topological recursion are supposed to be identified with the free energies of the closed topological string, the formulae above give us the means to compute the latter by the modified topological recursion.

By plugging in the recursion formula for computing $\omega_1^{(1)}$, the genus one free energy is found to be

$$\mathcal{F}_1 = \frac{1}{24N_{r,s}} \ln \left(\tau_B^{12} \prod_i \frac{\beta'(a_i)}{\beta(a_i)\alpha(a_i)} \right) . \quad (3.78)$$

The symbol τ_B stands for a function over the moduli space of the spectral curve \mathcal{C} ,¹² and it is

¹² Strictly speaking τ_B is a function on the moduli space of the branched covering $\alpha : \mathcal{C} \rightarrow \mathbb{P}^1$. We refer readers

characterized by its derivative with respect to branch points $\alpha(a_i)$

$$\frac{\partial \ln \tau_B}{\partial \alpha(a_i)} = \text{Res}_{q \rightarrow a_i} \frac{\widehat{B}_{r,s}(q, \bar{q})}{d\alpha}. \quad (3.79)$$

Besides the derivative $\beta'(a_i)$ in eq. (3.78) is with respect to the local coordinate z_i in the neighborhood of the i -th ramification point a_i defined by

$$\alpha = \alpha(a_i) + z_i^2. \quad (3.80)$$

We point out that the expression of the genus one free energy given by eq. (3.78) should also be valid in the usual topological recursion when it is applied to spectral curves in type B topological string (i.e. in the B-model remodelling as in refs. [113, 156]), with $N_{r,s} = 1$ and with the Bergman kernel replacing the calibrated annulus kernel in eq. (3.79).

By plugging in the recursion formula for $\omega_3^{(0)}$ the variational formula for the planar free energy in eq. (3.77) can be simplified

$$\delta_{\Omega_i} \delta_{\Omega_j} \delta_{\Omega_k} \mathcal{F}_0 = \frac{1}{N_{r,s}} \sum_{\ell} \frac{\Omega_i(a_{\ell}) \Omega_j(a_{\ell}) \Omega_k(a_{\ell}) \alpha(a_{\ell}) \beta(a_{\ell})}{d^2 \alpha(a_{\ell}) / d\beta^2}. \quad (3.81)$$

The triple derivative of the planar free energy is also called the Yukawa coupling. Remarkably the above formula shows the computation of the Yukawa coupling does not require the knowledge of the calibrated annulus kernel and we need only the differential Ω which encodes the deformation of the AV spectral curve. We will exploit this point in section 3.3.3 to compute extensively the Yukawa couplings up to the normalization factor $N_{\mathcal{K}}$ even from AV spectral curves of hyperbolic knots, for which we do not have the knowledge of the calibrated annulus kernels yet.

In the next two subsections we verify the modified topological recursion by computing the normalized correlation differentials and the free energies respectively for branes associated to (torus) knots.

3.3.2 Computing Correlation Differentials

In this subsection we take the example of the AV spectral curve eq. (3.16) for the trefoil torus knot with framing $r \cdot s = 6$ and compute the normalized correlation differentials, taking the results from [170]. Since the calibrated annulus kernel we used in the computation is very lengthy, we relegate it to Appendix B.

The planar three-point correlation differential is computed by eq. (3.45), with the Bergman kernel in the recursion kernel replaced by the calibrated annulus kernel. The formula can be simplified to

$$\widehat{\omega}_3^{(0)}(p_1, p_2, p_3) = \frac{1}{N_{2,3}} \sum_i \text{Res}_{q \rightarrow a_i} \frac{\widehat{B}_{r,s}(p_1, q) \widehat{B}_{r,s}(p_2, q) \widehat{B}_{r,s}(p_3, q) \alpha(q) \beta(q)}{d\alpha(q) d\beta(q)}, \quad (3.82)$$

where we have included the normalization factor $N_{2,3} = 3$. The result is a symmetric tridifferential. We expand it in terms of α_1, α_2 , and α_3 and record the coefficients with the same

to ref. [170] and reference therein.

notation as in eq. (3.34) after rescaling $\alpha_\mu \rightarrow Q^5 \alpha_\mu, \mu = 1, 2$

$$\begin{aligned}
 p_{(3)} &= -7200 + 24192Q - 31536Q^2 + 19980Q^3 - 6264Q^4 + 864Q^5 - 36Q^6, \\
 p_{(2,1)} &= -302400 + 1378944Q - 2624832Q^2 + 2699424Q^3 - 1620216Q^4 + 570960Q^5 \\
 &\quad - 112320Q^6 + 10800Q^7 - 360Q^8, \\
 p_{(1,2)} &= -12700800 + 73156608Q - 183145536Q^2 + 261128448Q^3 - 233372160Q^4 \\
 &\quad + 135520560Q^5 - 51246720Q^6 + 12283200Q^7 - 1749600Q^8 + 129600Q^9 \\
 &\quad - 3600Q^{10}.
 \end{aligned} \tag{3.83}$$

The coefficient function $p_{\vec{k}}$ encodes the numbers of worldsheet instantons with boundary data \vec{k} . Similar to the calibrated annulus kernel discussed in section 3.2.4, the tridifferential $\widehat{\omega}_3^{(0)}(p_1, p_2, p_3)$ also encodes the numbers of planar worldsheet instantons with three boundary components stretched between the branes $\mathcal{L}_{2,3}$ and their images $\iota(\mathcal{L}_{2,3})$ under the involution map of eq. (3.28). To access this data, we do the change of variables $\alpha_3 = Q^5/\tilde{\alpha}_3, \beta_3 = 1/(Q\tilde{\beta}_3)$ on the third insertion point in $\widehat{\omega}_3^{(0)}(p_1, p_2, p_3)$ and expand it in terms of α_1, α_2 , and $\tilde{\alpha}_3$. We record the coefficients with the notation in line with section 3.2.4, after rescaling $\alpha_\mu \rightarrow Q^5 \alpha_\mu, \mu = 1, 2$

$$\begin{aligned}
 p_{(2),(1)} &= 432Q - 1224Q^2 + 1296Q^3 - 612Q^4 + 108Q^5, \\
 p_{(1,1),(1)} &= 18144Q - 72576Q^2 + 118944Q^3 - 101952Q^4 + 47880Q^5 - 11520Q^6 + 1080Q^7, \\
 p_{(2),(0,1)} &= 8064Q - 33264Q^2 + 56160Q^3 - 49824Q^4 + 24624Q^5 - 6480Q^6 + 720Q^7.
 \end{aligned} \tag{3.84}$$

For instance $p_{(1,1),(1)}$ encodes the numbers of worldsheet instantons with winding numbers 1 and 2 on one stack of branes and winding number 1 on the other stack of branes.

We also compute the normalized genus one one-point correlation differential by eq. (3.44) with necessary adaptation. We expand the result in terms of α and record the coefficients after rescaling $\alpha_\mu \rightarrow Q^5 \alpha_\mu, \mu = 1, 2$ in the following

$$\begin{aligned}
 p_{(1)} &= \frac{1}{24}(22 - 21Q - Q^2), \\
 p_{(0,1)} &= \frac{1}{12}(1722 - 3752Q + 2625Q^2 - 620Q^3 + 25Q^4), \\
 p_{(0,0,1)} &= \frac{1}{24}(213213 - 719433Q + 940500Q^2 - 595980Q^3 + 185850Q^4 - 25074Q^5 \\
 &\quad + 924Q^6).
 \end{aligned} \tag{3.85}$$

These polynomials encode the numbers of worldsheet instantons of genus one and with one boundary component.

The polynomials $p_{\vec{k}}$ and $p_{\vec{k}, \vec{k}'}$ should be identical with the connected vevs $\mathcal{W}_{\vec{k}}^{(c)}$ and $\mathcal{W}_{\vec{k}, \vec{k}'}^{(c)}$ of the Wilson loop along the trefoil knot in the $U(N)$ Chern–Simons theory according to the Ooguri–Vafa conjecture. Since the quantum knot variants of the trefoil torus knot including those colored in composite representations of $U(N)$ are known, the connected vevs can be computed explicitly, and they do match the results presented above. This provides a nontrivial check for the validity of the modified topological recursion applied to branes associated to torus knots.

3.3.3 Computing Free Energies

With the AV spectral curve for the trefoil torus knot and the calibrated annulus kernel $\widehat{B}_{2,3}(p_1, p_2)$ we can also compute the free energies \mathcal{F}_g using the variational formulae in eqs. (3.76), (3.77). We vary the complex structure of the spectral curve by an infinitesimal deformation

$$t \rightarrow t + \delta t \quad (3.86)$$

and consequently $Q = e^{-t} \rightarrow Q - Q\delta t$. The variations of the free energies on the left hand side of eqs. (3.76), (3.77) are then simply derivatives with respect to the modulus t . We postulate that these free energies \mathcal{F}_g coincide with the free energies of the type A closed topological string (in the holomorphic limit) on the resolved conifold, and as such they should not depend on the framing of the probing Lagrangian branes associated to knots.

It turns out that with an arbitrary framing f retained throughout the computation, we get the following genus one free energy

$$\frac{\partial}{\partial t} \mathcal{F}_1 = 2\pi i \left(\frac{Q}{12(1-Q)} + \frac{f^3 - 4f^2 + 28f - 69}{72f(f-3)} \right). \quad (3.87)$$

The first term is framing independent and it does coincide with the derivative of the genus one free energy (in the holomorphic limit) of the type A closed topological string on the resolved conifold! The second term depends on the framing and is absent in the type A closed topological string theory. We interpret it as a classical ambiguity due to the noncompactness of the background geometry. Furthermore the planar free energy, or rather the Yukawa coupling, is computed to be

$$\frac{\partial^3}{\partial t^3} \mathcal{F}_0 = (2\pi i)^3 \left(\frac{Q}{1-Q} + \frac{f^3 + f^2 - 5f + 3}{3f(f-3)} \right). \quad (3.88)$$

Here again the first term is framing independent, and it coincides with the Yukawa coupling of the type A topological string on the resolved conifold. The second term as the classical ambiguity again depends on the framing.

Up to now we have been providing evidence for the validity of the modified topological recursion for branes associated to torus knots in both the open string and the closed string sectors. Here we take a leap of faith and conjecture that the modified topological recursion works for branes associated to hyperbolic knots as well. We are encouraged by the observation that the modified topological recursion can produce the correct Yukawa couplings from the AV spectral curves of hyperbolic knots. Indeed, although we do not know yet how to compute the calibrated annulus kernel for hyperbolic knots, we can still compute the Yukawa couplings from their AV spectral curves since the computation of the Yukawa coupling does not require the knowledge of the calibrated annulus kernel. We perform the computations for the four hyperbolic knots denoted in the knot theory by $\mathbf{4}_1$, $\mathbf{5}_2$, $\mathbf{6}_1$, and $\mathbf{6}_2$ with a generic framing¹³. The planar projection graphs of these knots are included in Fig. B.1. We list the Yukawa couplings computed from these hyperbolic knots in Tab. 3.1, including the unknown normalization factor $N_{\mathcal{K}}$ (ignore the last column of the table for the moment).

¹³ With a generic framing, the AV spectral curve of a knot has a fixed number of ramification points with respect to the projection onto the α plane. However there may exist several bad framings with which the AV spectral curve has a reduced number of ramification points as some of them are sent to the punctures at infinity. In these cases the topological recursion would fail to compute the correct free energies. This phenomenon was first observed in ref. [187] and then fully explained in ref. [170].

| knot | Yukawa coupling | normalization |
|-------|---|---------------|
| 4_1 | $(2\pi i)^3 \frac{3}{N_{4_1}} \frac{Q}{1-Q} + \text{classical terms}$ | 3 |
| 5_2 | $(2\pi i)^3 \frac{3}{N_{5_2}} \frac{Q}{1-Q} + \text{classical terms}$ | 3 |
| 6_1 | $(2\pi i)^3 \frac{3}{N_{6_1}} \frac{Q}{1-Q} + \text{classical terms}$ | 3 |
| 6_2 | $(2\pi i)^3 \frac{5}{N_{6_2}} \frac{Q}{1-Q} + \text{classical terms}$ | 5 |

Table 3.1: The Yukawa coupling (triple derivative of the planar free energy) computed from the AV spectral curves of four hyperbolic knots

Note that up to the ambiguous classical terms, all these Yukawa couplings are proportional to the Yukawa coupling of the type A topological string on the resolved conifold. This lends support to our conjecture that extends the validity of the modified topological recursion over hyperbolic knots. In other words, we would be able to compute all the other symplectic invariants for branes associated to hyperbolic knots, had we known the calibrated annulus kernels in addition to the AV spectral curves. These kernels are by definition the pure generating functions of the worldsheet annulus instantons, and they differ from the Bergman kernels on the AV spectral curves. Furthermore we propose that the normalization factors $N_{\mathcal{K}}$ should be such that the Yukawa couplings are exactly the same as the Yukawa coupling of the closed topological string. For the four hyperbolic knots, we record the conjectured normalization factors in the last column of Tab. 3.1. We notice that unlike the cases of torus knots, these normalization factors are not half of the numbers of the ramification points of the spectral curves with respect to the projection onto the α plane. For instance the normalization factor for the figure eight knot 4_1 is 3, while one can check there are 10 ramification points¹⁴ on the AV spectral curve of the figure eight knot with respect to the projection onto the α plane.

3.4 Implications for and from Knot Theory

In this subsection we discuss some implications of our work for and from the knot theory. To stress the connection with the knot theory, here we will always use the name (colored) HOMFLY invariants instead of quantum knot invariants.

We see from the construction of Aganagic and Vafa [173] in section 3.1.2 that we only need the knowledge of HOMFLY invariants of a knot colored in symmetric representations to derive the AV spectral curve. On the other hand, we can build the calibrated annulus kernel once we know the numbers of worldsheet annulus instantons, which can be extracted using the Ooguri–Vafa conjecture from colored HOMFLY invariants of the knot in question. It can be shown that for this purpose we only need the subset of HOMFLY invariants colored in representations whose associated Young diagrams have at most two rows [170]. Once we have the AV spectral curve and the calibrated annulus kernel, assuming our conjecture that the modified topological recursion works for the branes associated to an arbitrary knot (including hyperbolic knots) is

¹⁴ As mentioned in footnote 13 on page 95, with some bad framings the number of ramification points is reduced. For the figure eight knot, the bad framings are $-2, 0$, and 2 , with which the number of ramification points is reduced to 8.

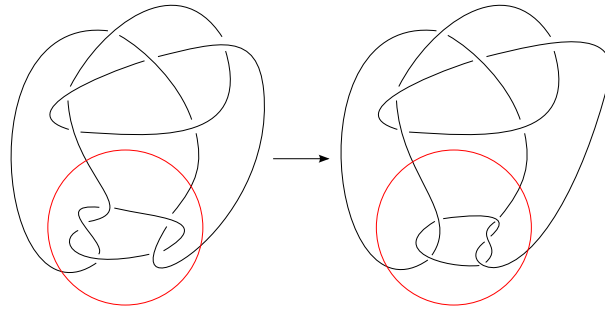
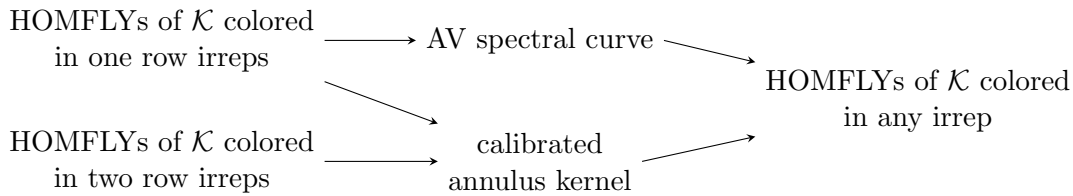


Figure 3.5: The mutant pair of the Kinoshita–Terasaka knot (left) and the Conway (right) knot. From wikipedia.

correct, we can compute all the correlation differentials, from which we can extract using the Ooguri–Vafa conjecture in the reverse direction all the colored HOMFLY invariants of the knot in question. In summary we have the following flows of information



Therefore, a natural corollary of our conjecture is that the information of the full set of HOMFLY invariants can be deduced from the subset containing only HOMFLY invariants colored in at most two row representations.

We have noted in section 2.3.2 that one of the goals in the knot theory is to design a knot invariant which is cable of distinguishing apart all knots. In other words, given an arbitrary pair of two topologically distinct knots, their associated knot invariants should be different. Such a knot invariant is called complete. A complete knot invariant is difficult to find. And even if a knot invariant can distinguish all the knot pairs people can think of, it is still far from proving that this knot invariant is in fact complete. A simple test for a complete knot invariant is to check whether it can distinguish mutant pairs.

The mutant partner of a knot is given as follows. We pick a tangle of the knot, which is a part of the knot contained in a disk in the planar projection graph connected to the rest of the knot by four strands (see for instance the part inside the red circle in either of the two diagrams in Fig. 3.5). There are two reflections of the disk, i.e. horizontally and vertically, which exchange pairs of neighbouring endpoints of the tangle. Then a mutant partner of the knot is obtained by performing either of the two reflections, or the composition of the two reflections, which amounts to a 180° rotation of the disk, and gluing the tangle back to the rest of the knot. For a simple knot, its mutant partner is itself. The simplest mutant pair of distinct knots have both 11 crossings, and the two knots are called the Conway knot and the Kinoshita–Terasaka knot respectively (see Fig. 3.5). Many knot invariants, including the HOMFLY invariant colored in the fundamental representation (the original HOMFLY invariant), the Jones polynomial, and the Alexander polynomial¹⁵ fail the test of distinguishing the Conway/Kinoshita–Terasaka

¹⁵ For an introduction to these knot invariants we refer to the interesting book [117]. In this thesis we are only

mutant pair. In fact it was proved by Morton and Cromwell [188] that a HOMFLY knot invariant colored in any symmetric representation cannot distinguish mutant pairs¹⁶. On the other hand it has been conjectured (see for instance [189]) that the full set of all colored HOMFLY invariants is a complete knot invariant. It means that there exists a HOMFLY invariant colored in some representation which can distinguish mutant pairs. Combined with the chart of information flows earlier in this subsection, our conjecture of the modified topological recursion would indicate that the HOMFLY invariant colored in some two row representation should be able to distinguish mutant pairs. Indeed the mutant pair of the Conway knot and the Kinoshita–Terasaka knot can be distinguished by the representation associated to the partition $(2, 1)$ [188]. Furthermore, given the different roles in distinguishing mutant pairs played by the HOMFLY invariants colored in symmetric and two row representations, one is naturally lead to the conclusion that at least for knots with mutant partners it is not possible to derive the calibrated annulus kernel from the AV spectral curve itself alone. The calibrated annulus kernel may well be truly an input of the modified topological recursion independent of the AV spectral curve.

interested in (colored) HOMFLY invariants.

¹⁶ A theorem in ref. [188] states that a HOMFLY invariant colored by a representation R is incapable of distinguishing mutant pairs if the decomposition of the tensor product $R \otimes R$ has no repeated summands. This is certainly the case for any symmetric representation.

Knot Invariants and RCFT

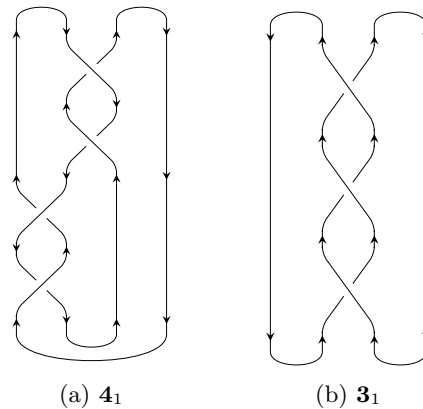
After verifying the validity of the modified topological recursion for torus knots, naturally the next step is to check our conjecture extending the validity of the modified topological recursion over hyperbolic knots. For this purpose, two inputs are required, the AV spectral curve and the calibrated annulus kernel. The former can be easily computed with Ng's algorithm for augmentation varieties, assuming the conjecture that AV spectral curves and augmentation varieties are identical is valid. The latter is much more difficult to obtain. There is no longer BEM Bergman kernel from which we can derive the annulus kernel. Instead one hopes to construct the annulus kernel as the generating function of worldsheet annulus instanton numbers, which in turn are extracted via the Ooguri–Vafa duality map from the HOMFLY knot invariants colored in one- or two-row representations (c.f. discussion in section 3.4)¹.

Computation of colored HOMFLY invariants of hyperbolic knots in one-row representations, i.e. totally symmetric representations, have been studied extensively [118, 124, 125, 166–169]. On the other hand, computation of colored HOMFLY invariants of hyperbolic knots in two-row or more general non-symmetric representations remains a difficult problem, and up to now it has only been approached in refs. [190, 191]. Here we provide methods and tools to compute these knot invariants for a large variety of hyperbolic knots. The key step in our method turns out to be the computation of crossing matrices, or fusion matrices, in $\widehat{su}(N)_k$ WZW models. For generic N , the crossing matrices have only been computed for simple representations. Recently the values of the crossing matrices which only involve symmetric representations have been conjectured in ref. [192]. The crossing matrices in fact are proportional to quantum $6j$ -symbols in $\mathcal{U}_q(sl_N)$ quantum group. Inspired by methods for computing Racah $6j$ -symbols in classical Lie algebra $su(N)$ [193, 194], we use the bootstrap strategy to compute values of quantum $6j$ -symbols involving relatively small but arbitrary representations. Equipped with the knowledge of these quantum $6j$ -symbols and consequently the corresponding crossing matrices, we are able to compute as the first step colored HOMFLY invariants of hyperbolic knots in the \boxplus representation.

Clearly the values of crossing matrices should be useful beyond the application here for computing colored HOMFLY invariants. They may find applications directly in the $\widehat{su}(N)_k$ WZW models. Furthermore, the classical limit of these crossing matrices can be used to compute group factors of scattering amplitudes [195, 196].

The outline of this chapter is as follows. We review the method to compute colored HOMFLY invariants for a large variety of knots in section 4.1. It enables us to write down the

¹ Recall that to verify the modified topological recursion is essentially is to verify the Ooguri–Vafa conjecture. However using the Ooguri–Vafa duality map to compute partially the inputs of the modified topological recursion does not make the whole process of verification tautological. In principle one can compute infinitely many correlation differentials to compare with HOMFLY invariants colored in beyond two-row representations.

Figure 4.1: A quasi-plat presentation of 4_1 and a plat presentation of 3_1 .

computational formulae whose only unknown components are the crossing matrices. The relation of the crossing matrices in $\widehat{su}(N)_k$ WZW models and quantum $6j$ -symbols in quantum group $\mathcal{U}_q(sl_N)$ are explained in section 4.2. We also discuss the rich symmetry properties of the quantum $6j$ -symbols. These symmetry properties become the pillars of the bootstrap strategy for computing the values of the quantum $6j$ -symbols, which is described in section 4.3. Section 4.4 lists the results and discusses some properties of the colored HOMFLY invariants we have computed.

4.1 Braiding Method

4.1.1 Basic Ideas

First we describe the type of (hyperbolic) knots for which we can compute colored HOMFLY invariants. As we mentioned in section 2.3.2, a knot may be represented by its planar projection graph. A particular type of planar projection graph is called the quasi-plat presentation. It consists of a braid with even number of strands in the middle (all the strands in a braid flow in one direction; no strand should turn back at any point in a braid), and all the strands of the braid close off pairwise at either end of the braid (see Fig. 4.1a for an example). If in addition on both ends the $(2i - 1)$ -th strand is joined with the $2i$ -th strand, $i = 1, 2, \dots$, the planar projection graph is called a plat presentation (see Fig. 4.1b for an example). A knot may have more than one quasi-plat presentation. If the minimal number of strands in quasi-plat presentations of a knot is $2m$, its *bridge index* is defined to be m . We will call a knot with bridge index m an m -bridged knot. The only 1-bridged knot is unknot. 2-bridged knots include $(2, s)$ torus knots and infinitely many hyperbolic knots. We will only be computing colored HOMFLY invariants for 2-bridged knots using their quasi-plat presentations with four strands².

We will be using the surgery technique for computing colored HOMFLY invariants/quantum knot invariants in $U(N)$ Chern-Simons theory introduced by Witten [20]. In section 2.3.3 we covered its general idea and its application for unknot and torus knots. The surgery technique was adapted by refs. [124, 166, 197] to compute colored HOMFLY invariants for 2-bridged

² The possible extension of the method described here to compute knots with bridge index three or more can be found in ref. [169].

knots colored mostly in symmetric/anti-symmetric representations. We refined their method in ref. [119] so that HOMFLY invariants colored in nonsymmetric representations can also be dealt with. Here we stress that the colored HOMFLY invariant is a function of q and λ , and the functional form of the knot invariant does not depend on the values of N and k . Therefore we can choose appropriate limits of k and N to facilitate the computation of the functional forms of the knot invariants. As noted in the footnote 30 on page 42, in the limit $k \rightarrow \infty$ that we will be working with, the highest weight integrable representations (these are the representations of the WZW primaries) of the affine Lie algebra $\widehat{su}(N)_k$ can be identified with the irreducible representations of the simple Lie algebra $su(N)$, and the fusion algebra in $\widehat{su}(N)_k$ WZW model behaves the same as the tensor products in $su(N)$. In the chapter we will not distinguish between representations of the two algebras, as well as between fusion algebra and tensor products.

Given a quasi-plat presentation of a 2-bridged knot \mathcal{K} , it is natural to cut the S^3 in a way such that the four strands of the quasi-plat presentation pass through the shared boundary Σ of the two three-manifolds M_1 and M_2 transversely (see Fig. 4.2). Let us call the partial knot inside M_1 or M_2 a tangle. The tangle can be made more complicated by a braiding operation (see Fig. 4.4), which winds two neighboring strands around each other once to produce a new crossing. On the other hand the braiding operations are effectively quantum operators acting on the Hilbert space $\mathcal{H}(\Sigma)$ on the boundary Σ . Let us call them simply braiding operators. An ideal basis of $\mathcal{H}(\Sigma)$ consists of eigenstates of the braiding operators. The idea to compute the colored HOMFLY invariants of \mathcal{K} is then as follows. We first cut the S^3 near the top of the quasi-plat presentation, so that the simple tangle in M_1 does not contain any crossing. The associated quantum state can be easily decomposed in terms of the ideal basis, as we will demonstrate in the next subsection. Apply successive braiding operations according to the quasi-plat presentation, until all the crossings have been accounted for. Effectively we are moving the boundary Σ downwards through all the crossings. Finally we take the inner product of the resulting quantum state associated to the now complicated tangle in M_1 with the quantum state associated to the simple tangle at the bottom of the quasi-plat presentation inside M_2 , which gives us the colored HOMFLY invariant. This computational procedure is illustrated in Fig. 4.2. In the computation the framing of the knot is given by minus the writhe w of the quasi-plat presentation, and the latter is defined by the number of overcrossings subtracted by the number of undercrossings

$$w = \#(\text{overcrossing}) - \#(\text{undercrossing}) . \quad (4.1)$$

One can use the framing transformation formula eq. (2.138) to convert the computed colored HOMFLY invariant to any framing that one desires.

For this braiding method to work, we need to find the ideal basis, clarify the action of the braiding operations on the states in the ideal basis, and understand how to decompose the quantum states associated to simple tangles in terms of the ideal basis. These are explained in the next subsection.

4.1.2 Eigenstates of Braiding Operators

We know from section 2.3.3 that the basis states in $\mathcal{H}(\Sigma)$ correspond one-to-one with conformal blocks in $\widehat{su}(N)_k$ WZW models. Since there are three different ways to write down conformal blocks corresponding to t -channel, s -channel, and u -channel respectively, there are

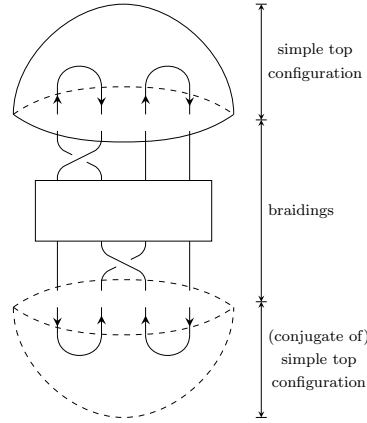


Figure 4.2: A quasi-plat presentation can be split into two simple tangles at the top and the bottom and the braidings in the middle.

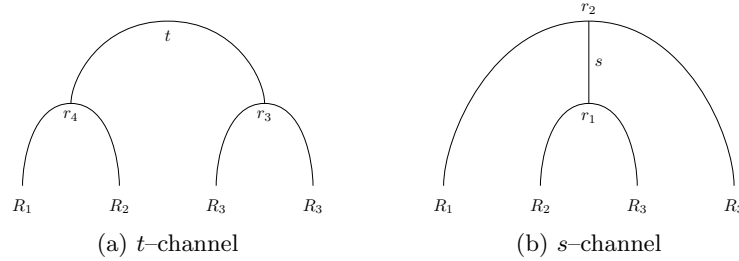
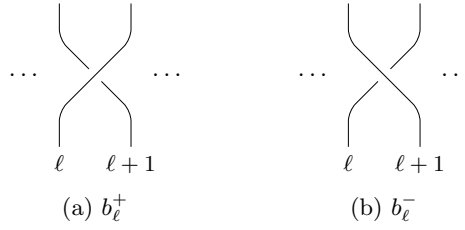
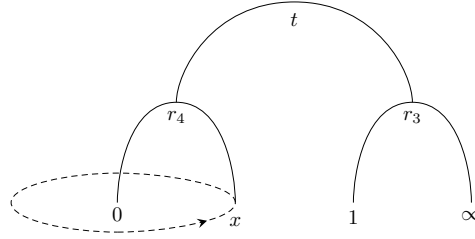


Figure 4.3: Four-point conformal blocks in t -channel and s -channel respectively.

correspondingly three different bases of $\mathcal{H}(\Sigma)$. We will see that the two bases corresponding to t - and s -channels as shown in Fig. 4.3 are the ideal bases, and we call them the t -basis and the s -basis respectively. The basis states in each basis are labelled by the intermediate WZW primary and the two multiplicity labels at the two vertices. We will represent a WZW primary by its associated representation of the affine Lie algebra $\widehat{su}(N)_k$. In the t -basis, a basis state is denoted by $|\phi_{t,r_3,r_4}^{(1)}(R_1, R_2, R_3, R_4)\rangle$, and the corresponding conformal block is given in Fig. 4.3a. Here the four WZW primaries at the four legs of the conformal block are colored in four arbitrary representations R_1, R_2, R_3, R_4 to keep the discussion generic. In the computation of colored HOMFLY invariants for knots, the representation at each leg can be either R that colors the knot, or the conjugate representation \bar{R} , depending on at the associated puncture on the boundary Σ whether the strand enters or exits the three-manifold M_1 . The intermediate state t should satisfy $t \in (R_1 \times R_3) \cap (\bar{R}_3 \times \bar{R}_4)$, belonging to both fusion decompositions. The multiplicity labels r_3 or r_4 take values in $0, 1, \dots, \mathcal{N}_{R_1 R_2}^t - 1$ and $0, 1, \dots, \mathcal{N}_{\bar{R}_3 \bar{R}_4}^t - 1$ respectively, where $\mathcal{N}_{R_1 R_2}^t$ or $\mathcal{N}_{\bar{R}_3 \bar{R}_4}^t$ are the corresponding fusion coefficients. Similarly, we denote a basis state in the s -basis corresponding to the s -channel conformal block in Fig. 4.3b by $|\phi_{s,r_1,r_2}^{(2)}(R_1, R_2, R_3, R_4)\rangle$, with the intermediate state $s \in (R_2 \times R_3) \cap (\bar{R}_1 \times \bar{R}_4)$, and multiplicity labels r_1, r_2 .

Braiding operations are classified by the strands they wind around each other and the directions of the winding. We use symbol b_ℓ^+ ($\ell = 1, 2, 3$) to denote the braiding operation that when viewed from top (from inside M_1 toward Σ) winds clockwise the ℓ -th and the $(\ell + 1)$ -th strands


 Figure 4.4: Two braiding operations b_ℓ^+ and b_ℓ^- with opposite directions.

 Figure 4.5: The monodromy of the 4-point conformal block in the t -channel.

together (Fig. 4.4a) as well as the associated quantum braiding operator, and b_ℓ^- the braiding operation that winds anticlockwise the two strands together (Fig. 4.4b) as well as the associated quantum braiding operator. Since the conformal blocks in the t -channel are invariant when two legs on one side (R_1 and R_2 or R_3 and R_4) are swapped, the basis states in the t -basis are eigenstates of b_1^\pm, b_3^\pm . On the other hand, the conformal blocks in the s -channel do not change when the two central legs are swapped. Accordingly the basis states in the s -basis are eigenstates of b_2^\pm . The eigenvalues of the braiding operations can also be easily determined. In the example of a conformal block in the t -channel, we can use conformal symmetry to send the first, third, and fourth legs to $0, 1, \infty$ respectively, and label the position of the second leg x . The conformal block then has the following form [120]

$$\mathcal{F}_{34}^{21}(x|t) = x^{h_t - h_{R_1} - h_{R_2}} \cdot P(x), \quad (4.2)$$

where h_t, h_{R_1}, h_{R_2} are conformal weights, and $P(x)$ is a polynomial of x . Clearly when we wind the point x around the point 0 and back to the original position (Fig. 4.5), the conformal block has the monodromy

$$\mathcal{F}_{34}^{21}(x|t) \mapsto q^{\pm(C_t - C_{R_1} - C_{R_2})} \mathcal{F}_{34}^{21}(x|t), \quad (4.3)$$

because

$$e^{2\pi i h_R} = e^{2\pi i \cdot C_R / (k+N)} = q^{C_R} \quad (4.4)$$

and the sign \pm depends on the direction of the winding. A b_1^\pm braiding operation amounts to moving x half way around 0 , so the eigenvalue of b_1^\pm should be the square root of the monodromy. In general, the eigenvalue of a braiding operator is

$$b_\ell^\pm : \lambda_{R_i, R_j; R_k, r}^\pm = \{R_i, R_j, \bar{R}_k, r\} q^{\pm(C_{R_i} + C_{R_j} - C_{R_k})/2}, \quad \ell = 1, 2, 3. \quad (4.5)$$

Here R_i, R_j are the representations of the WZW primaries at the two legs being wound together. R_k is the representation of the intermediate WZW primary the two R_i and R_j primaries are

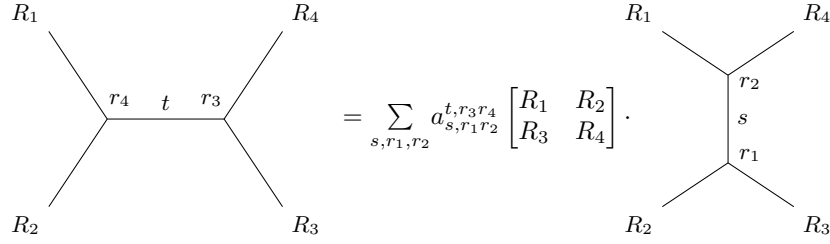


Figure 4.6: t - and s -channel conformal blocks are related by a crossing matrix.

fused into, and r is the associated multiplicity label. The phase factor $\{R_i, R_j, \bar{R}_k, r\}$ is the $3j$ -phase in $su(N)$, which is the phase that arises in front of the Clebsch–Gordan coefficient $\langle r R_k m_k | R_i m_i R_j m_j \rangle$ when the two representations R_i and R_j are exchanged,

$$\langle r R_k m_k | R_i m_i R_j m_j \rangle = \{R_i, R_j, \bar{R}_k, r\} \langle r R_k m_k | R_j m_j R_i m_i \rangle . \quad (4.6)$$

Here m_i refers to a state in the representation R_i . The $3j$ -phase can only take the value of ± 1 , and its value is not changed if all three representations are replaced by their conjugates.

$$\{R_i, R_j, \bar{R}_k, r\} = \{\bar{R}_i, \bar{R}_j, R_k, r\} . \quad (4.7)$$

Furthermore we have conjugated R_k in the notation of $3j$ -phase to emphasize that the three representations R_i, R_j, \bar{R}_k constitute a *triad*, meaning that the tensor product of them contains the singlet

$$R_i \otimes R_j \otimes \bar{R}_k \ni \mathbf{1} . \quad (4.8)$$

Then it is easy to see the $3j$ -phases satisfy the permutation symmetry

$$\{R_i, R_j, \bar{R}_k, r\} = \{\sigma(R_i), \sigma(R_j), \sigma(\bar{R}_k), r\}, \quad \sigma \in S_3 . \quad (4.9)$$

The values of $3j$ -phases are largely unfixed, except for when two of the three representations are identical. In this case, the value $\{R, R, \bar{R}_k, r\}$ is fixed by group theoretical considerations

$$\{R, R, \bar{R}_k, r\} = \begin{cases} +1, & R_k \in \text{Sym}^2 R \\ -1, & R_k \in \wedge^2 R \\ 0, & \text{otherwise} \end{cases} . \quad (4.10)$$

If no two representations are identical, we have the freedom to choose the sign of the $3j$ -phase. When $r = 0$ the multiplicity label is often omitted in the notation. Furthermore if one of the three representations is singlet, we use the shorthand notation

$$\{R, \bar{R}, \mathbf{1}\} = \{R\} \quad (4.11)$$

and call it a $2j$ -phase. A consistent convention for the signs of $3j$ -phases and $2j$ -phases will be given in section 4.3.1.

Coming back to the formula of the eigenvalues of the braiding operators in eq. (4.5). Combining it with the fact that the basis states in the t -basis of $\mathcal{H}(\Sigma)$ are eigenstates of b_1^\pm, b_3^\pm , and

the basis states in the s -basis of $\mathcal{H}(\Sigma)$ are eigenstates of b_2^\pm , we can write down concretely the eigenvalue equations

$$\begin{aligned} b_1^\pm |\phi_{t,r_3r_4}^{(1)}(R_1, R_2, R_3, R_4)\rangle &= \lambda_{R_1, R_2; \bar{t}, r_4}^\pm |\phi_{t,r_3r_4}^{(1)}(R_1, R_2, R_3, R_4)\rangle, \\ b_2^\pm |\phi_{s,r_1r_2}^{(2)}(R_1, R_2, R_3, R_4)\rangle &= \lambda_{R_2, R_3; s, r_1}^\pm |\phi_{s,r_1r_2}^{(2)}(R_1, R_2, R_3, R_4)\rangle, \\ b_3^\pm |\phi_{t,r_3r_4}^{(1)}(R_1, R_2, R_3, R_4)\rangle &= \lambda_{R_3, R_4; \bar{t}, r_3}^\pm |\phi_{t,r_3r_4}^{(1)}(R_1, R_2, R_3, R_4)\rangle. \end{aligned} \quad (4.12)$$

Since the braiding operators b_1^\pm , b_3^\pm and b_2^\pm have different eigenstates, when we apply successively braiding operations according to the quasi-plat presentation of a knot, we usually need to switch between the t -basis and the s -basis. The t -channel and the s -channel conformal blocks are related to each other by the crossing matrices (also called fusion matrices, see Fig. 4.6). Correspondingly in $\mathcal{H}(\Sigma)$ these crossing matrices serve as the transition matrices between the two bases

$$|\phi_{t,r_3r_4}^{(1)}(R_1, R_2, R_3, R_4)\rangle = \sum_{s, r_1, r_2} a_{s, r_1 r_2}^{t, r_3 r_4} \begin{bmatrix} R_1 & R_2 \\ R_3 & R_4 \end{bmatrix} |\phi_{s, r_1 r_2}^{(2)}(R_1, R_2, R_3, R_4)\rangle, \quad (4.13)$$

The crossing matrices satisfy the unitarity relation

$$\sum_{t, r_3, r_4} a_{s, r_1 r_2}^{t, r_3 r_4} \begin{bmatrix} R_1 & R_2 \\ R_3 & R_4 \end{bmatrix} a_{s', r_1' r_2'}^{t, r_3 r_4} \begin{bmatrix} R_1 & R_2 \\ R_3 & R_4 \end{bmatrix}^* = \delta_{s, s'} \delta_{r_1, r_1'} \delta_{r_2, r_2'}. \quad (4.14)$$

These crossing matrices are the only unknown ingredients in this program of computing colored HOMFLY knot invariants. In the simple case when one of the four representations is singlet, the value of the crossing matrix is known,

$$\begin{aligned} a_{s, r_1 r_2}^{0, 00} \begin{bmatrix} R_1 & \bar{R}_1 \\ R_2 & \bar{R}_2 \end{bmatrix} &= \{R_2\} \{R_1, \bar{R}_2, s, r_1\} \frac{\sqrt{\dim_q s}}{\sqrt{\dim_q R_1 \dim_q R_2}} \delta_{r_1, r_2}, \\ a_{0, 00}^{t, r_3 r_4} \begin{bmatrix} R_1 & R_2 \\ \bar{R}_2 & \bar{R}_1 \end{bmatrix} &= \{R_2\} \{R_1, R_2, \bar{t}, r_3\} \frac{\sqrt{\dim_q t}}{\sqrt{\dim_q R_1 \dim_q R_2}} \delta_{r_3, r_4}. \end{aligned} \quad (4.15)$$

Here we use 0 to represent a singlet representation. $\dim_q R$ is the quantum dimension of the representation R . We have touched upon the definition of quantum dimension in WZW models in section 2.3.3 and will also discuss its meaning in quantum group in the next section. The formulae for computing the quantum dimensions are given in eqs. (A.8),(A.9) in appendix A. In the generic case, a crossing matrix is difficult to compute. We discuss the computation of crossing matrices in the next section by exploiting their relations to quantum $6j$ -symbols in quantum groups.

Let us assume the crossing matrices are already known. We still need to decompose a quantum state in $\mathcal{H}(\Sigma)$ associated to a simple tangle in terms of basis states in either the t - or the s -bases. Let us take the simple tangle inside M_1 in Fig. 4.7 as an example. We notice that it is a trivial eigenstate of the braiding operators b_1^\pm, b_3^\pm . Therefore the associated quantum state $|\Phi_1^{(1)}\rangle$ is proportional to $|\phi_{0,00}^{(1)}(R_1, \bar{R}_1, R_2, \bar{R}_2)\rangle$. We fix the proportionality constant by requiring that the inner product of this state with its own conjugate yields the colored HOMFLY invariant of

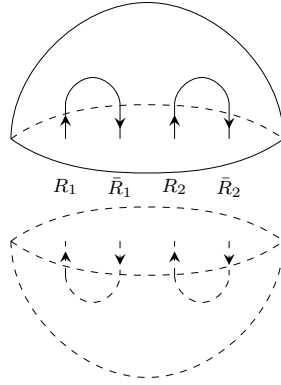


Figure 4.7: A simple tangle in M_1 . When glued with its conjugate in M_2 (mirror image with the orientation flipped) we have two disconnected unknots.

two disconnected unknots (Fig. 4.7)

$$\langle \Phi_1^{(1)} | \Phi_1^{(1)} \rangle = \mathcal{W}_{R_1}^{SU(N)}(\bigcirc) \mathcal{W}_{R_2}^{SU(N)}(\bigcirc) = \dim_q R_1 \dim_q R_2 . \quad (4.16)$$

Note the conjugate state is associated to the mirror image of the tangle in M_2 with the orientation of the strands reversed. Together with the normalization

$$\langle \phi_{0,00}^{(1)}(R_1, \bar{R}_1, R_2, \bar{R}_2) | \phi_{0,00}^{(1)}(R_1, \bar{R}_1, R_2, \bar{R}_2) \rangle = 1 , \quad (4.17)$$

we find

$$|\Phi_1^{(1)}\rangle = \sqrt{\dim_q R_1 \dim_q R_2} |\phi_{0,00}^{(1)}(R_1, \bar{R}_1, R_2, \bar{R}_2)\rangle . \quad (4.18)$$

Now by using appropriate crossing matrix to convert $|\phi_{0,00}^{(1)}(R_1, \bar{R}_1, R_2, \bar{R}_2)\rangle$ to the basis states in the s -basis, we can easily write down the decomposition of $|\Phi_1^{(1)}\rangle$ in terms of the latter. The crossing matrix involved in the basis transformation involves singlet, so its value is known. In the end, we have

$$|\Phi_1^{(1)}\rangle = \sum_{s, r_1, r_2} \{R_2\} \{R_1, \bar{R}_2, s, r_1\} \sqrt{\dim_q s} \delta_{r_1, r_2} |\phi_{s, r_1 r_2}^{(2)}(R_1, \bar{R}_1, R_2, \bar{R}_2)\rangle . \quad (4.19)$$

We can use similar analysis to write down the basis decomposition of the quantum states associated to all possible simple tangles in M_1 . The results are listed in Tab. 4.1 and Tab. 4.2. The relative signs between two quantum states are fixed by requiring the inner product of the two quantum states (one of them is conjugated) yields the correct colored HOMFLY invariant of the knot obtained by gluing the corresponding two simple tangles together. Sometimes a braiding operation needs to be inserted in between for the gluing to be possible if the orientations of the strands from the two tangles conflict. Two examples of the gluing process for normalization, with and without an extra braiding, are given in Figs. 4.8. The result of such a gluing process is always either a unknot or two disconnected unknots, whose colored HOMFLY invariants are already known.

| | |
|--|---|
| | $ \Phi_1^{(1)}\rangle = \sqrt{ R_1 R_2 } \phi_{0,00}^{(1)}(\dots)\rangle$ $= \{R_2\} \sum_{s,r_1,r_2} \{\bar{R}_1, R_2, \bar{s}, r_2\} \sqrt{ s } \delta_{r_1,r_2} \phi_{s,r_1r_2}^{(2)}(\dots)\rangle$ |
| | $ \Phi_2^{(1)}\rangle = \{R_2\} \sqrt{ R_1 R_2 } \phi_{0,00}^{(1)}(\dots)\rangle$ $= \sum_{s,r_1,r_2} \{\bar{R}_1, \bar{R}_2, \bar{s}, r_2\} \sqrt{ s } \delta_{r_1,r_2} \phi_{s,r_1r_2}^{(2)}(\dots)\rangle$ |
| | $ \Phi_3^{(1)}\rangle = \{R_1\} \sqrt{ R_1 R_2 } \phi_{0,00}^{(1)}(\dots)\rangle$ $= \{R_1\} \{R_2\} \sum_{s,r_1,r_2} \{R_1, R_2, \bar{s}, r_2\} \sqrt{ s } \delta_{r_1,r_2} \phi_{s,r_1r_2}^{(2)}(\dots)\rangle$ |
| | $ \Phi_4^{(1)}\rangle = \{R_1\} \{R_2\} \sqrt{ R_1 R_2 } \phi_{0,00}^{(1)}(\dots)\rangle$ $= \{R_1\} \sum_{s,r_1,r_2} \{R_1, \bar{R}_2, \bar{s}, r_2\} \sqrt{ s } \delta_{r_1,r_2} \phi_{s,r_1r_2}^{(2)}(\dots)\rangle$ |

Table 4.1: Depicted are the first four simple tangles in M_1 together with the associated quantum states. The conjugate quantum states are associated to the mirrored tangles in M_2 with the orientation of the strands reversed. We use $|R|$ as a shorthand for $\dim_q R$. The ellipses in the parentheses are to be filled in with appropriate WZW primaries.

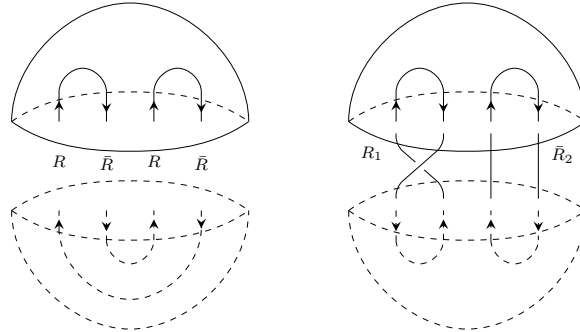


Figure 4.8: Two examples of gluing a pair of simple tangles together. In the right diagram, a braiding has to be inserted. This kind of diagrams is used to fix the relative phases between the quantum states associated to different simple tangles.

4.1.3 Summary

We have described all the ingredients needed in the surgery computation of colored HOMFLY invariants using the quasi-plat presentations of the knots. Let us summarize the procedure of the computation.

- Given an arbitrary knot \mathcal{K} with bridge index two, draw a quasi-plat presentation. Cut the three-sphere containing the knot to three parts: two hemispheres containing the simple tangles at the top and the bottom, and the cylinder containing the braid of the quasi-plat

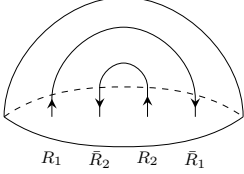
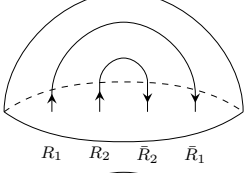
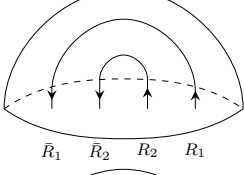
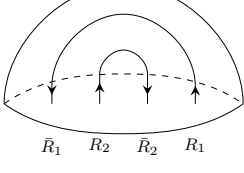
| | |
|---|---|
|  | $ \begin{aligned} \Phi_1^{(2)}\rangle &= \{R_1\}\{R_2\}\sqrt{ R_1 R_2 } \phi_{0,00}^{(2)}(\dots)\rangle \\ &= \{R_1\} \sum_{t,r_3,r_4} \{R_1, \bar{R}_2, \bar{t}, r_4\} \sqrt{ t } \delta_{r_3,r_4} \phi_{t,r_3r_4}^{(1)}(\dots)\rangle \end{aligned} $ |
|  | $ \begin{aligned} \Phi_2^{(2)}\rangle &= \{R_1\}\sqrt{ R_1 R_2 } \phi_{0,00}^{(2)}(\dots)\rangle \\ &= \{R_1\}\{R_2\} \sum_{t,r_3,r_4} \{R_1, R_2, \bar{t}, r_4\} \sqrt{ t } \delta_{r_3,r_4} \phi_{t,r_3r_4}^{(1)}(\dots)\rangle \end{aligned} $ |
|  | $ \begin{aligned} \Phi_3^{(2)}\rangle &= \{R_2\}\sqrt{ R_1 R_2 } \phi_{0,00}^{(2)}(\dots)\rangle \\ &= \sum_{t,r_3,r_4} \{\bar{R}_1, \bar{R}_2, \bar{t}, r_4\} \sqrt{ t } \delta_{r_3,r_4} \phi_{t,r_3r_4}^{(1)}(\dots)\rangle \end{aligned} $ |
|  | $ \begin{aligned} \Phi_4^{(2)}\rangle &= \sqrt{ R_1 R_2 } \phi_{0,00}^{(2)}(\dots)\rangle \\ &= \{R_2\} \sum_{t,r_3,r_4} \{\bar{R}_1, R_2, \bar{t}, r_4\} \sqrt{ t } \delta_{r_3,r_4} \phi_{t,r_3r_4}^{(1)}(\dots)\rangle \end{aligned} $ |

Table 4.2: The second four simple tangles in M_1 and the quantum states associated to them. The conjugate quantum states are associated to the mirrored tangles in M_2 with the orientation of the strands reversed. $|R|$ is short for $\dim_q R$. The ellipses in the parentheses are to be filled in with appropriate WZW primaries.

presentation (Fig. 4.2).

- Decompose the quantum state associated to the simple tangle at the top in terms of the t -basis or the s -basis, depending on whether the first braiding operation in the braid is b_1^\pm, b_3^\pm or b_2^\pm . This can be done by simply looking up in Tab. 4.1 and Tab. 4.2.
- Apply successive braiding operations on the quantum state according to the braid of the quasi-plat presentation. The eigenvalues of the braiding operations are given in eqs. (4.12). In this process, sometimes one needs to switch from the t -basis to the s -basis if a b_1^\pm, b_3^\pm braiding is followed by a b_2^\pm braiding, or switch from the s -basis to the t -basis if a b_2^\pm braiding is followed by a b_1^\pm, b_3^\pm braiding. The basis transition is given by eq. (4.13).
- When all the crossings in the braid have been accounted for, take the inner product of the resulting quantum state with the quantum state associated to the simple tangle at the bottom. The latter can also be decomposed in terms of the t - or the s -bases by looking up in Tab. 4.1 and Tab. 4.2.
- As discussed in section 2.3.3, this inner product is only the $SU(N)$ part of the quantum knot invariant. To obtain the colored HOMFLY invariant ($U(N)$ quantum knot invariant), one needs to multiply the $SU(N)$ invariant with the $U(1)$ invariant given by eq. (2.149). The latter only depends on the framing of the quasi-plat presentation, which is given by eq. (4.1).

- One can apply eq. (2.134) to convert the obtained colored HOMFLY invariant to a different framing. One can also normalize the colored HOMFLY invariant $H_R(\mathcal{K})$ as in eq. (2.142) to obtain the normalized HOMFLY polynomial $\overline{H}_R(\mathcal{K})$.

4.2 Quantum Group and Quantum 6j-Symbols

As discussed in section 4.1.2, to apply the surgery method described above to compute colored HOMFLY knot invariants, we need the knowledge of crossing matrices in the $\widehat{su}(N)_k$ WZW model. To compute these crossing matrices, it is beneficial to have some understanding of the $\mathcal{U}_q(sl_N)$ quantum group and its representation theory. In this section we mainly follow the excellent treatment on this subject in ref. [198].

Despite its name, the quantum group $\mathcal{U}_q(sl_N)$ is an algebra. It can be understood as the quantum deformation of the universal enveloping algebra $\mathcal{U}(sl_N)$ of sl_N , which is the complexification of the Lie algebra $su(N)$. Some explanations are in order. The universal enveloping algebra $\mathcal{U}(sl_N)$ is the unital associative algebra of (finite) formal power series generated by the generators of the simple Lie algebra sl_N , subject to the relations given by the commutators of these generators, which coincide with the corresponding Lie brackets of sl_N . In the simplest example, the Lie algebra sl_2 has three generators E, F, H and the Lie brackets

$$[H, E] = 2E, [H, F] = -2F, [E, F] = H . \quad (4.20)$$

The universal enveloping algebra $\mathcal{U}(sl_2)$ is an associate algebra with multiplicative unit 1 and three generators E, F, H . The three generators satisfy the following relations

$$HE - EH = 2E, HF - FH = -2F, EF - FE = H . \quad (4.21)$$

The quantum group $\mathcal{U}_q(sl_N)$ is obtained by a deformation of the relations of $\mathcal{U}(sl_N)$ measured by a formal parameter q such that in the ‘‘classical limit’’ $q \rightarrow 1$, the quantum group returns to the universal enveloping algebra. Continuing with the example of $\mathcal{U}(sl_2)$, the quantum group $\mathcal{U}_q(sl_2)$ has four generators E, F, K, K^{-1} subject to the relations

$$\begin{aligned} K \cdot K^{-1} &= K^{-1} \cdot K = 1 \\ KE &= qEK, KF = q^{-1}FK, EF - FE = \frac{K - K^{-1}}{q^{1/2} - q^{-1/2}} . \end{aligned} \quad (4.22)$$

The first relation is trivial. Let us denote $K = q^{H/2}$. Then it is easy to see the first two relations in the second row of eqs. (4.22) are implied by the first two relations of $\mathcal{U}(sl_2)$, while the right hand side of the last identity in eq. (4.22) is the q -deformed H defined by

$$[H] = \frac{q^{H/2} - q^{-H/2}}{q^{1/2} - q^{-1/2}} , \quad (4.23)$$

and it goes back to H in the classical limit $q \rightarrow 1$

$$\frac{K - K^{-1}}{q^{1/2} - q^{-1/2}} = [H] \xrightarrow{q \rightarrow 1} H . \quad (4.24)$$

We will content ourselves with this heuristic understanding of quantum groups and refrain from

giving the precise definition of $\mathcal{U}_q(sl_N)$, which can be found for example in ref. [198]. Next we proceed to its representation theory³.

Given the similarity between the quantum group $\mathcal{U}_q(sl_N)$ and the Lie algebra sl_N , a representation of $\mathcal{U}_q(sl_N)$ can be constructed via the same techniques as applied in sl_N . Namely one starts with an arbitrary dominant weight as the highest weight and then apply the lowering operators to find all possible weights in the representation. In fact for a generic value of q which is not a root of unity, the irreducible representations of $\mathcal{U}_q(sl_N)$ correspond one-to-one with the irreducible representations of sl_N . More interesting case is when q is a root of unity, and it will be seen shortly this is the case when the quantum group $\mathcal{U}_q(sl_N)$ is closely related to the $\widehat{su}(N)_k$ WZW model. In this case, the nature of the highest weight representation depends crucially on the highest weight λ . Suppose $q = \exp(\frac{2\pi i}{k+N})$, and θ is the greatest root of sl_N . If $(\lambda, \theta) \leq k$, the highest weight representation is a usual irreducible representation. If $(\lambda, \theta) = 0 \pmod{k+1}$, the highest weight representation is irreducible but non-unitarizable, because the states in the representation have zero norm. Finally for the highest weight representations with $(\lambda, \theta) > k$ and $(\lambda, \theta) \neq 0 \pmod{k+1}$, while some of them are also non-unitarizable irreducible representations, most of them combine with another representation with a different highest weight λ' to form a reducible yet indecomposable representation. The latter means there is an invariant subspace in the representation space, but the representation space cannot be decomposed to a direct sum of invariant subspaces. These peculiarly behaving representations of $\mathcal{U}_q(sl_N)$ with $(\lambda, \theta) > k$ are prevalent. They can arise in the decomposition of the tensor product

$$R_i \otimes R_j = \sum_k \mathcal{L}_{ij}^k R_k , \quad (4.25)$$

even if both R_i and R_j are unitarizable and irreducible. On the other hand, if either R_i or R_j is a peculiarly behaving representation, all the representations on the right hand side will be of this type.

It is easier to organize these representations by the quantum dimension. In quantum group, the quantum dimension of a representation R with the highest weight λ is defined as the q -deformation of the dimension of the representation space

$$\dim_q R = \sum_{\lambda' \in \Omega_R} \text{mult}_R(\lambda') q^{(\rho, \lambda')} , \quad (4.26)$$

where Ω_R is the space of weights in the representation R , and ρ is the Weyl vector. Clearly in the limit $q \rightarrow 1$, the quantum dimension reduces to the usual dimension of the representation R . One nice property of quantum dimension is that, given the tensor product decomposition of two representations in eq. (4.25), the quantum dimensions of the representations involved satisfy the natural identity

$$\dim_q R_i \cdot \dim_q R_j = \sum_k \mathcal{L}_{ij}^k \dim_q R_k . \quad (4.27)$$

On the other hand, if q is a root of unity, for instance $\exp(\frac{2\pi i}{k+N})$, the quantum dimension is only finite for the irreducible highest weight representations with $(\lambda, \theta) \leq k$, and it vanishes for all

³ As explained for example in ref. [198], a technical but important feature of the $\mathcal{U}_q(sl_N)$ quantum group is that it remains a so-called *Hopf algebra* so that tensor products of its representations are well-defined. This is not the case for a generic algebra.

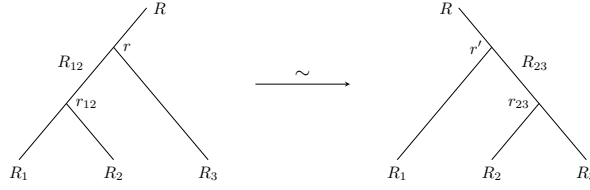


Figure 4.9: Diagrammatic illustration of the associativity isomorphism of the truncated tensor products.

the peculiarly behaving representations. Therefore, when both R_i and R_j are unitarizable and irreducible, we can remove the null contributions of peculiarly behaving representations from the right hand side of (4.27), and the equality still holds. In other words, we have

$$\dim_q R_i \cdot \dim_q R_j = \sum'_k \mathcal{L}_{ij}^k \dim_q R_k , \quad (4.28)$$

where \sum' means only representations with nonzero quantum dimensions are included. This encourages one to define the truncated tensor product

$$R_i \star R_j \equiv \sum'_k (\mathcal{L}_{ij}^k) R_k , \quad (4.29)$$

where R_i, R_j , and R_k are all unitarizable and irreducible representations. It can be shown the truncated tensor product is also associative.

We will be focusing on the finite (quantum) dimensional highest weight representations of $\mathcal{U}_q(sl_N)$. They can also be denoted by partitions or Young diagrams. In fact, we will use the composite labelling as explained in Appendix A, and use the *powers* of the representations (c.f. Appendix A) to partially order them. A bigger representation means higher power, and a smaller representation lower power.

Now we can state the link between the $\widehat{su}(N)_k$ WZW models and the $\mathcal{U}_q(sl_N)$ quantum groups. With the dictionary

$$q = \exp\left(\frac{2\pi i}{k+N}\right) , \quad (4.30)$$

the WZW primaries correspond one-to-one with the finite (quantum) dimensional representations of $\mathcal{U}_q(sl_N)$. Note that the WZW primaries are representations of the affine Lie algebra $\widehat{su}(N)_k$, and the highest weight integrable representations of the latter also satisfy $(\lambda, \theta) \leq k$. Furthermore, the fusion rules of the WZW model are isomorphic with the truncated tensor products of $\mathcal{U}_q(sl_N)$, and the crossing matrices of the WZW model are identified with the (quantum) recoupling coefficients in the quantum group.

The quantum recoupling coefficients characterize the associativity isomorphism

$$\alpha : (R_1 \star R_2) \star R_3 \xrightarrow{\sim} R_1 \star (R_2 \star R_3) . \quad (4.31)$$

The sequential decompositions of the truncated tensor products on the two sides of the isomorphism provide two different bases of the representation space, and the quantum recoupling coefficients are the linear transformation coefficients of this isomorphism. More concretely, the coupling of the three states $|R_1 m_1\rangle_q$, $|R_2 m_2\rangle_q$, and $|R_3 m_3\rangle_q$ in the three representations R_1, R_2, R_3 can be decomposed in two different ways. According to the left hand side of eq. (4.31)

we can first decompose the coupling between the first two states and then with the third state

$$\begin{aligned}
 & |R_1 m_1\rangle_q |R_2 m_2\rangle_q |R_3 m_3\rangle_q \\
 &= \sum_{r_{12} R_{12} m_{12}} |(R_1 R_2), r_{12} R_{12} m_{12}\rangle_q |R_3 m_3\rangle_q \cdot \langle r_{12} R_{12} m_{12} | R_1 m_1, R_2 m_2\rangle_q \\
 &= \sum_{\substack{r_{12} R_{12} m_{12} \\ r R m}} |(R_1 R_2) r_{12} R_{12}, R_3, r R m\rangle_q \cdot \langle r_{12} R_{12} m_{12} | R_1 m_1, R_2 m_2\rangle_q \\
 &\quad \times \langle r R m | R_{12} m_{12}, R_3 m_3\rangle_q .
 \end{aligned} \tag{4.32}$$

Here $\langle r_{12} R_{12} m_{12} | R_1 m_1, R_2 m_2\rangle_q$ and $\langle r R m | R_{12} m_{12}, R_3 m_3\rangle_q$ are the quantum Clebsch–Gordan coefficients with respect to the truncated tensor product decomposition. Note that multiple copies of the state $|R m\rangle$ can appear in the end, and these states are labelled by the intermediate representation R_{12} and the two multiplicity labels r_{12}, r from the two truncated tensor products $R_1 \star R_2$ and $R_{12} \star R_3$ respectively. They furnish an orthonormal basis of the subspace $V(R, m)$ of the left hand side of eq. (4.31) consisting of the states of the type $|R m\rangle$ only. This is the case illustrated by the left diagram in Fig. 4.9. On the other hand, we can also follow the right hand side of eq. (4.31) and decompose the coupling of the last two states $|R_2 m_2\rangle$ and $|R_3 m_3\rangle$ first

$$\begin{aligned}
 |R_1 m_1\rangle_q |R_2 m_2\rangle_q |R_3 m_3\rangle_q &= \sum_{\substack{R_{23} R_{23} m_{23} \\ r' R m}} |R_1 (R_2 R_3) r_{23} R_{23}, r' R m\rangle_q \cdot \langle r' R m | R_1 m_1, R_{23} m_{23}\rangle_q \\
 &\quad \times \langle r_{23} R_{23} m_{23} | R_2 m_2, R_3 m_3\rangle_q .
 \end{aligned} \tag{4.33}$$

Thus we find another orthonormal basis of $V(R, m)$ labelled by the intermediate state R_{23} and the multiplicity labels r_{23}, r' from the truncated tensor products $R_2 \star R_3$ and $R_1 \star R_{23}$ respectively. This is the case illustrated in the right diagram of Fig. 4.9. The quantum recoupling coefficients $\langle (R_1 R_2) r_{12} R_{12}, R_3; r R | R_1 (R_2 R_3) r_{23} R_{23}; r' R \rangle_q$ are the transition coefficients between the two bases of $V(R, m)$

$$\begin{aligned}
 |R_1 (R_2 R_3) r_{23} R_{23}, r' R m\rangle_q &= \sum_{r_{12} R_{12} r} |(R_1 R_2) r_{12} R_{12}, R_3, r R m\rangle_q \\
 &\quad \times \langle (R_1 R_2) r_{12} R_{12}, R_3; r R | R_1 (R_2 R_3) r_{23} R_{23}; r' R \rangle_q .
 \end{aligned} \tag{4.34}$$

It is customary to normalize a quantum recoupling coefficient

$$\begin{aligned}
 {}_q \left\{ \begin{array}{ccc} R_1 & R_2 & \bar{R}_{12} \\ R_3 & R & R_{23} \end{array} \right\}_{r', r_{23}, r, r_{12}} &= \frac{\{R_2\} \{R_1 R_2 \bar{R}_{12} r_{12}\} \{R_{12} R_3 \bar{R} r\}}{\sqrt{\dim_q R_{12} \dim_q R_{23}}} \\
 &\quad \times \langle (R_1 R_2) r_{12} R_{12}, R_3; r R | R_1 (R_2 R_3) r_{23} R_{23}; r' R \rangle_q .
 \end{aligned} \tag{4.35}$$

and call the left hand side a quantum $6j$ -symbol. They coincide with the Racah $6j$ -symbols in $su(N)$ in the classical limit $q \rightarrow 1$. Since the crossing matrices in $\widehat{su}(N)_k$ WZW model can be identified with the quantum recoupling coefficients

$$\langle (R_1 R_2) r_{12} R_{12}, R_3; r R | R_1 (R_2 R_3) r_{23} R_{23}; r' R \rangle_q = a_{R_{23}, r' r_{23}}^{R_{12}, r r_{12}} \begin{bmatrix} R_1 & R_2 \\ R_3 & R \end{bmatrix}, \tag{4.36}$$

and therefore with the quantum $6j$ -symbols up to the normalization, the problem of computing crossing matrices in WZW models is converted to computing quantum $6j$ -symbols in $\mathcal{U}_q(\mathfrak{sl}_N)$.

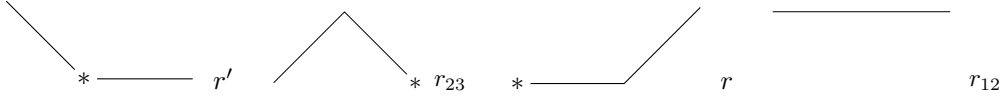
The quantum $6j$ -symbol

$${}_q \left\{ \begin{array}{ccc} R_1 & R_2 & \bar{R}_{12} \\ R_3 & R & R_{23} \end{array} \right\}_{r', r_{23}, r, r_{12}}$$

is rather an elegant and convenient notation, as it puts the six representations involved in the recoupling coefficient on an equal footing. Let us borrow from eq. (4.8) and introduce *triads* in $\mathcal{U}_q(\mathfrak{sl}_N)$, which now mean three finite (quantum) dimensional representations of $\mathcal{U}_q(\mathfrak{sl}_N)$ whose truncated tensor product contains the singlet. There are four triads involved in the associativity isomorphism eq. (4.31) (c.f. Fig. 4.9)

$$\begin{aligned} R_1 \star R_{23} \star \bar{R} \ni \mathbf{1}_{r'} , & \quad R_2 \star R_3 \star \bar{R}_{23} \ni \mathbf{1}_{r_{23}} , \\ R_{12} \star R_3 \star \bar{R} \ni \mathbf{1}_r , & \quad R_1 \star R_2 \star \bar{R}_{12} \ni \mathbf{1}_{r_{12}} , \end{aligned} \quad (4.37)$$

where we have recorded the multiplicity labels as the subscripts of the singlets. The following four diagrams,



when superimposed on the $6j$ -symbol, can help us track the four representations in each triad, together with the given multiplicity label. In these diagrams the symbol $*$ means one has to conjugate the corresponding representation.

Furthermore the symmetry properties of the recoupling coefficients can be cast in simple forms in terms of quantum $6j$ -symbols. From the definition of the recoupling coefficients eq. (4.34) and eqs. (4.32),(4.33), it is easy to see that the quantum recoupling coefficients and therefore the quantum $6j$ -symbols can be expressed in terms of quantum Clebsch–Gordan coefficients

$$\begin{aligned} & \langle (R_1 R_2) r_{12} R_{12}, R_3; r R | R_1 (R_2 R_3) r_{23} R_{23}; r' R \rangle_q \\ &= \frac{1}{\dim_q R} \sum_{\substack{m_1 m_2 m_3 \\ m, m_{12} m_{23}}} \langle r_{12} R_{12} m_{12} | R_1 m_1, R_2 m_2 \rangle_q \langle r R m | R_{12} m_{12}, R_3 m_3 \rangle_q \\ & \quad \times \langle r' R m | R_1 m_1, R_{23} m_{23} \rangle_q^* \langle r_{23} R_{23} m_{23} | R_2 m_2, R_3 m_3 \rangle_q^* . \end{aligned} \quad (4.38)$$

One can derive from this relation abundant symmetry properties of quantum $6j$ -symbols, which we list in the following [199]. From now on we will suppress the little q symbol in the notation of quantum $6j$ -symbols as well as quantum Clebsch–Gordan coefficients. In addition we will use the shorthand notation $|\cdot|$ for quantum dimension in the list below.

1. Tetrahedral symmetry

$$\begin{aligned} \left\{ \begin{array}{ccc} \lambda_1 & \lambda_2 & \lambda_3 \\ \mu_1 & \mu_2 & \mu_3 \end{array} \right\}_{r_1 r_2 r_3 r_4} &= \left\{ \begin{array}{ccc} \lambda_2 & \lambda_3 & \lambda_1 \\ \mu_2 & \mu_3 & \mu_1 \end{array} \right\}_{r_2 r_3 r_1 r_4} \\ &= \{ \mu_1 \} \{ \mu_2 \} \{ \mu_3 \} \{ \lambda_1 \bar{\mu}_2 \mu_3 r_1 \} \{ \mu_1 \lambda_2 \bar{\mu}_3 r_2 \} \\ & \quad \times \{ \bar{\mu}_1 \mu_2 \lambda_3 r_3 \} \{ \lambda_1 \lambda_2 \lambda_3 r_4 \} \left\{ \begin{array}{ccc} \lambda_2 & \lambda_1 & \lambda_3 \\ \bar{\mu}_2 & \bar{\mu}_1 & \bar{\mu}_3 \end{array} \right\}_{r_2 r_1 r_3 r_4} \end{aligned}$$

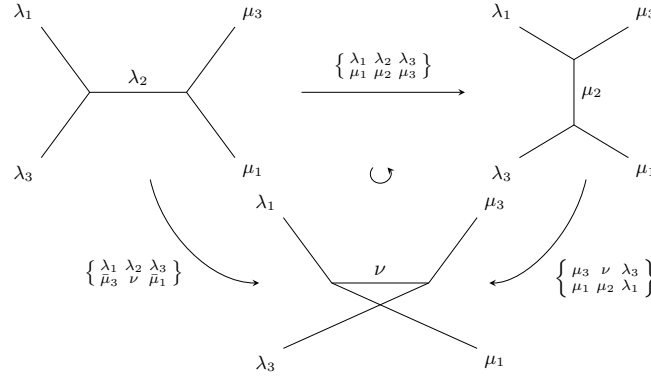


Figure 4.10: Diagrammatic illustration of the generalized Racah backcoupling rule. We suppress multiplicity labels here.

$$\begin{aligned}
 &= \begin{Bmatrix} \bar{\lambda}_1 & \mu_2 & \bar{\mu}_3 \\ \bar{\mu}_1 & \lambda_2 & \bar{\lambda}_3 \end{Bmatrix}_{r_4 r_3 r_2 r_1} = \begin{Bmatrix} \bar{\mu}_1 & \bar{\lambda}_2 & \mu_3 \\ \bar{\lambda}_1 & \bar{\mu}_2 & \lambda_3 \end{Bmatrix}_{r_3 r_4 r_1 r_2} \\
 &= \begin{Bmatrix} \mu_1 & \bar{\mu}_2 & \bar{\lambda}_3 \\ \lambda_1 & \bar{\lambda}_2 & \bar{\mu}_3 \end{Bmatrix}_{r_2 r_1 r_4 r_3} . \tag{4.39}
 \end{aligned}$$

We can freely permute the columns, or exchange the rows along two columns, and the value of the quantum $6j$ -symbol is not changed up to a sign.

2. Complex conjugation

$$\begin{Bmatrix} \lambda_1 & \lambda_2 & \lambda_3 \\ \mu_1 & \mu_2 & \mu_3 \end{Bmatrix}_{r_1 r_2 r_3 r_4}^* = \begin{Bmatrix} \bar{\lambda}_1 & \bar{\lambda}_2 & \bar{\lambda}_3 \\ \bar{\mu}_1 & \bar{\mu}_2 & \bar{\mu}_3 \end{Bmatrix}_{r_1 r_2 r_3 r_4} . \tag{4.40}$$

3. Unitarity

$$\sum_{\lambda_3 r_3 r_4} |\lambda_3| |\mu_3| \begin{Bmatrix} \lambda_1 & \lambda_2 & \lambda_3 \\ \mu_1 & \mu_2 & \mu_3 \end{Bmatrix}_{r_1 r_2 r_3 r_4} \begin{Bmatrix} \lambda_1 & \lambda_2 & \lambda_3 \\ \mu_1 & \mu_2 & \mu'_3 \end{Bmatrix}_{r'_1 r'_2 r_3 r_4}^* = \delta_{\mu_3 \mu'_3} \delta_{r_1 r'_1} \delta_{r_2 r'_2} . \tag{4.41}$$

4. The generalized Racah backcoupling rule

$$\begin{aligned}
 & q^{(C_{\lambda_1} + C_{\mu_1} + C_{\lambda_3} + C_{\mu_3})/2} \begin{Bmatrix} \lambda_1 & \lambda_2 & \lambda_3 \\ \mu_1 & \mu_2 & \mu_3 \end{Bmatrix}_{r_1 r_2 r_3 r_4} \\
 &= \sum_{\nu r s} q^{(C_\nu + C_{\lambda_2} + C_{\mu_2})/2} |\nu| \{ \lambda_3 \} \{ \lambda_1 \bar{\mu}_2 \mu_3 r_1 \} \{ \mu_1 \lambda_2 \bar{\mu}_3 r_2 \} \\
 & \quad \cdot \{ \bar{\lambda}_1 \mu_1 \nu r \} \begin{Bmatrix} \mu_3 & \nu & \lambda_3 \\ \mu_1 & \mu_2 & \lambda_1 \end{Bmatrix}_{r_1 r r_3 s} \begin{Bmatrix} \lambda_1 & \lambda_2 & \lambda_3 \\ \bar{\mu}_3 & \nu & \bar{\mu}_1 \end{Bmatrix}_{r r_2 s r_4} . \tag{4.42}
 \end{aligned}$$

From the WZW model point of view this symmetry means that the conformal blocks of t -, s - and u -channels are related to each other via the triangular commutative diagram as shown in Fig. 4.10.

5. The pentagon relation (Biedenharn–Elliott sum rule)

$$\begin{aligned}
 \left\{ \begin{matrix} \lambda_1 & \lambda_2 & \lambda_3 \\ \mu_1 & \mu_2 & \mu_3 \end{matrix} \right\}_{r_1 r_2 r_3 r_4} &= \sum_{\substack{\lambda \nu_3 \\ t_1 t_2 t_3 s_1 s_2}} |\lambda_3| |\nu_3| |\lambda| \{ \lambda_1 \} \{ \nu_1 \} \{ \lambda_1 \bar{\mu}_2 \mu_3 r_1 \} \\
 &\cdot \{ \mu_1 \lambda_2 \bar{\mu}_3 r_2 \} \{ \bar{\mu}_1 \mu_2 \lambda_3 r_3 \} \{ \lambda \bar{\mu}_1 \nu_1 t_1 \} \{ \lambda \bar{\mu}_2 \nu_2 t_2 \} \{ \lambda \bar{\mu}_3 \nu_3 t_3 \} \\
 &\cdot \left\{ \begin{matrix} \nu_2 & \bar{\mu}_2 & \lambda \\ \mu_3 & \nu_3 & \bar{\lambda}_1 \end{matrix} \right\}_{s_1 r_1 t_3 t_2} \left\{ \begin{matrix} \nu_3 & \bar{\mu}_3 & \lambda \\ \mu_1 & \nu_1 & \bar{\lambda}_2 \end{matrix} \right\}_{s_2 r_2 t_1 t_3} \\
 &\cdot \left\{ \begin{matrix} \nu_1 & \bar{\mu}_1 & \lambda \\ \mu_2 & \nu_2 & \bar{\lambda}_3 \end{matrix} \right\}_{s_3 r_3 t_2 t_1} \left\{ \begin{matrix} \lambda_1 & \lambda_2 & \lambda_3 \\ \nu_1 & \nu_2 & \nu_3 \end{matrix} \right\}_{s_1 s_2 s_3 r_4}. \tag{4.43}
 \end{aligned}$$

On the right hand side we have the freedom to choose the two representations ν_1 and ν_2 as long as all the triads in the quantum $6j$ -symbols involving ν_1 and ν_2 are valid so that the right hand side does not vanish identically. This symmetry can be diagrammatically represented by Fig. 4.11 which looks like a pentagon, hence the name pentagon relation.

6. q - q^{-1} symmetry. The parameter q only appears in the values of quantum $6j$ -symbols in q -deformed numbers, so a quantum $6j$ -symbol is not changed if q is replaced by q^{-1} .

Most of these symmetry properties degenerate to known symmetry properties of classical Racah $6j$ -symbols in the limit $q \rightarrow 1$. Note that the last q - q^{-1} symmetry is trivial in the classical limit, and it can be regarded as the property unique to quantum groups.

4.3 Computing $6j$ -Symbols

Since we want to compute colored HOMFLY knot invariants in the representation $R = \boxplus$, we need to know the values of the quantum $6j$ -symbols of the following two kinds

$$\begin{aligned}
 \left\{ \begin{matrix} R & \bar{R} & \rho_1 \\ R & R & \rho_2 \end{matrix} \right\}_{r_1 r_2 r_3 r_4} & \quad \left\{ \begin{matrix} \bar{R} & R & \rho_3 \\ R & R & \rho_4 \end{matrix} \right\}_{r'_1 r'_2 r'_3 r'_4} \tag{4.44} \\
 \text{first kind} & \quad \text{second kind}
 \end{aligned}$$

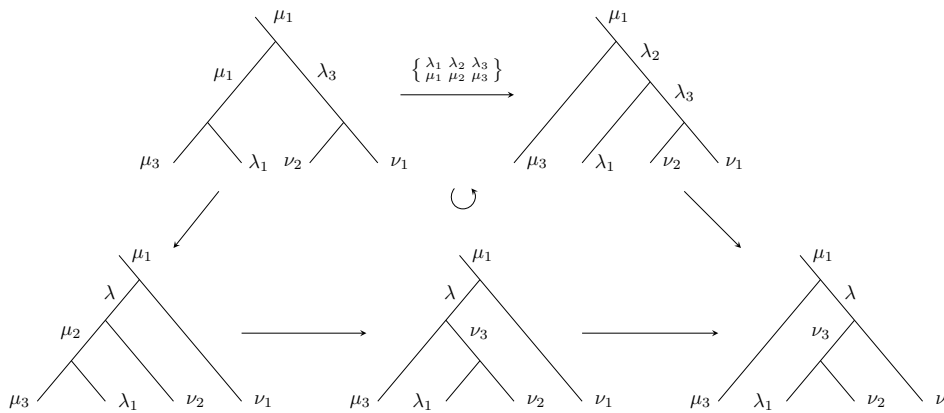


Figure 4.11: Diagrammatic illustration of the pentagon relation. Multiplicity labels are suppressed here.

In general the values of quantum $6j$ -symbols are only known for the trivial $6j$ -symbols which contain the singlet

$$\left\{ \begin{array}{ccc} \lambda_1 & \lambda_2 & \lambda_3 \\ \bar{\lambda}_2 & \lambda_1 & 0 \end{array} \right\}_{00rs} = \frac{\{\lambda_1 \lambda_2 \lambda_3 r\}}{\sqrt{\dim_q \lambda_1 \dim_q \lambda_2}} \delta_{rs} . \quad (4.45)$$

Note that since we will use composite labelling (like $(1; 1)$) or sometimes single partitions (like $(2, 1)$) to refer to representations of $\mathcal{U}_q(\mathfrak{sl}_N)$, the singlet is denoted by $(0; 0)$ or 0 . These values of trivial quantum $6j$ -symbols are consistent with the values of crossing matrices in eq. (4.15). On the other hand, it was pointed out in ref. [199] that the bootstrap method developed in refs. [193, 200, 201] for computing classical Racah $6j$ -symbols of $su(N)$ can be adapted to compute values of generic quantum $6j$ -symbols, and examples were given for $\mathcal{U}_q(\mathfrak{sl}_2)$. We generalized the method and computed quantum $6j$ -symbols for $\mathcal{U}_q(\mathfrak{sl}_N)$ in ref. [119]. The idea is to exploit the symmetry properties of quantum $6j$ -symbols in a systematic way to constrain the values of $6j$ -symbols or to relate them to the trivial $6j$ -symbols. Before embarking on the exposition of the bootstrap method in sections 4.3.3 and 4.3.4, we first clarify some technical points here, and later discuss in section. 4.3.2 an expedient way to reduce the numbers of quantum $6j$ -symbols that need to be bootstrapped.

First, as argued in the beginning of section 4.1.1, we can work in the convenient limit where k is large. In this case, there is no difference between representations of $\mathcal{U}_q(\mathfrak{sl}_N)$ and the representations of $su(N)$ with not too high powers, as well as between truncated tensor products in $\mathcal{U}_q(\mathfrak{sl}_N)$ and tensor products in $su(N)$.

Second, we will not be applying the original form of the generalized Racah backcoupling rule where the formal parameter q appears explicitly. Instead by using the q - q^{-1} symmetry of quantum $6j$ -symbols, we can cast the generalized Racah backcoupling rule in a form where q only appears in q -deformed numbers, and where the number of terms is reduced on the right hand side. To achieve this, we apply the generalized Racah backcoupling rule two times. In the first time, we write down the original formula and rescale it by $q^{-(C_{\nu_m} + C_{\lambda_2} + C_{\mu_2})/2}$, where ν_m is the ν with the greatest quadric Casimir. In the second time, we write down the Racah backcoupling rule with q replaced by q^{-1} , and rescale the formula by $q^{(C_{\nu_m} + C_{\lambda_2} + C_{\mu_2})/2}$. In the difference of the two formulae, the terms with the ν 's whose Casimirs equal C_{ν_m} are removed. These representations have higher powers than the other ν 's. Besides, all the q 's can be packed into q -deformed numbers. In the following when we speak of applying the generalized Racah backcoupling rule, we mean this modified form of the symmetry property unless otherwise specified.

Finally, there is in fact a freedom in fixing the values of quantum $6j$ -symbols, which stems from the freedom in the values of quantum Clebsch–Gordan coefficients. We can assign a common phase η with $|\eta| = 1$ to all the states $|\lambda m\rangle$ in the representation λ , and these new states $\eta|\lambda m\rangle$ still constitute an invariant representation space. The phase condition $|\eta| = 1$ is due to the normalization of the states. This implies the values of quantum (classical) Clebsch–Gordan coefficients $\langle \lambda_1 m_1, \lambda_2 m_2 | r \lambda m \rangle$ are only fixed up to a phase, a $U(1)$ freedom, which should not depend on the individual states m_1, m_2 , and m . Let us denote the phase by $U(\lambda_1 \lambda_2 \bar{\lambda})_{rr}$

$$\langle \lambda_1 m_1, \lambda_2 m_2 | r \lambda m \rangle_{\text{new}} = \langle \lambda_1 m_1, \lambda_2 m_2 | r \lambda m \rangle_{\text{old}} U(\lambda_1 \lambda_2 \bar{\lambda})_{rr} \quad (4.46)$$

In the case when $\lambda_1 \star \lambda_2$ has n copies of λ with $n > 1$ and the multiplicity label r can be nontrivial, we can even mix up uniformly states in the n copies of the representation λ , and the

free phase $U(\lambda_1\lambda_2\lambda)_{rr}$ is promoted to a matrix $U(\lambda_1\lambda_2\bar{\lambda})_{r'r}$ with $r', r = 0, \dots, n-1$

$$\langle \lambda_1 m_1, \lambda_2 m_2 | r \lambda m \rangle_{\text{new}} = \sum_{r'=0}^{n-1} \langle \lambda_1 m_1, \lambda_2 m_2 | r' \lambda m \rangle_{\text{old}} U(\lambda_1 \lambda_2 \bar{\lambda})_{r'r} . \quad (4.47)$$

The orthonormality condition of quantum Clebsch–Gordan coefficients demands that $U(\lambda_1\lambda_2\bar{\lambda})_{r'r}$ is a $U(n)$ matrix. This freedom translates into quantum $6j$ -symbols via the relation eq. (4.38).

A generic quantum $6j$ -symbol

$$\left\{ \begin{array}{ccc} \lambda_1 & \lambda_2 & \lambda_3 \\ \mu_1 & \mu_2 & \mu_3 \end{array} \right\}_{r_1 r_2 r_3 r_4} \quad (4.48)$$

has a $U(n_i)$ freedom or uncertainty for each multiplicity label $r_i, i = 1, \dots, 4$, the rank n_i being the total multiplicity of the corresponding triad. For instance if $\lambda_1 \star \lambda_2 \ni n_4 \cdot \bar{\lambda}_3$, we have the following $U(n_4)$ freedom

$$\left\{ \begin{array}{ccc} \lambda_1 & \lambda_2 & \lambda_3 \\ \mu_1 & \mu_2 & \mu_3 \end{array} \right\}_{r_1 r_2 r_3 r_4, \text{new}} = \sum_{r'_4=0}^{n_4-1} U(\lambda_1 \lambda_2 \lambda_3)_{r_4 r'_4} \left\{ \begin{array}{ccc} \lambda_1 & \lambda_2 & \lambda_3 \\ \mu_1 & \mu_2 & \mu_3 \end{array} \right\}_{r_1 r_2 r_3 r'_4, \text{old}} . \quad (4.49)$$

Therefore any tabulation of values of quantum $6j$ -symbols depends on a particular scheme to fix these $U(n_i)$ uncertainties.

In the multiplicity-free case (no multiplicity label can be greater than 0), the quantum $6j$ -symbols only suffer from $U(1)$ uncertainties. As seen from the symmetry properties of quantum $6j$ -symbols at the end of section 4.2, these $U(1)$ uncertainties are intertwined with the sign freedom of $3j$ - and $2j$ -phases. When the $U(1)$ uncertainties of quantum $6j$ -symbols are completely fixed, the signs of $3j$ -phases are partially constrained by the symmetry properties, and vice versa. We will discuss in the next subsection a consistent convention for the $3j$ - and $2j$ -phases so that the freedom one has to fix by hand is minimized. The extra $SU(n_i)$ freedom of quantum $6j$ -symbols due to nontrivial multiplicity labels is fixed by *multiplicity separation schemes*, which will be discussed in section 4.3.4.

4.3.1 Phase Convention

Since in the large k limit we will be working with, truncated tensor products of $\mathcal{U}_q(\mathfrak{sl}_N)$ are not different from tensor products of $\mathfrak{su}(N)$, we will simply adopt the convention of $3j$ - and $2j$ -phases in $\mathfrak{su}(N)$ [193, 200].

2j-phases

It is easy to see that $\{\lambda\} = \{\bar{\lambda}\}$. Besides $SU(N)$ is a so-called *quasi-ambivalent group*, which means that consistent choices of $2j$ -phases can be made such that

$$\{\lambda_1\}\{\lambda_2\}\{\lambda_3\} = 1 \quad (4.50)$$

whenever $\lambda_1, \lambda_2, \lambda_3$ constitute a valid triad. Using this rule repeatedly one can reduce any $2j$ -phase to either 1 or $\{(1; 0)\} = \{(0; 1)\}$.

3j-phases

A consistent choice of $3j$ -phases can be made such that they satisfy

$$\{\mu_1\}\{\mu_2\}\{\mu_3\}\{\lambda_1\bar{\mu}_2\mu_3r_1\}\{\mu_1\lambda_2\bar{\mu}_3r_2\}\{\bar{\mu}_1\mu_2\lambda_3r_3\}\{\lambda_1\lambda_2\lambda_3r_4\} = (-1)^{r_1+r_2+r_3+r_4}. \quad (4.51)$$

With this choice of $3j$ -phases, the second equality in the tetrahedral symmetry involving transposition of two columns in the quantum $6j$ -symbol (c.f. eq. (4.39)) can be simplified

$$\left\{ \begin{array}{ccc} \lambda_1 & \lambda_2 & \lambda_3 \\ \mu_1 & \mu_2 & \mu_3 \end{array} \right\}_{r_1r_2r_3r_4} = (-1)^{r_1+r_2+r_3+r_4} \left\{ \begin{array}{ccc} \lambda_2 & \lambda_1 & \lambda_3 \\ \bar{\mu}_2 & \bar{\mu}_1 & \bar{\mu}_3 \end{array} \right\}_{r_2r_1r_3r_4}. \quad (4.52)$$

Furthermore, we also choose

$$\{\lambda_1\lambda_2\lambda_3r\} = (-1)^r\{\lambda_1\lambda_2\lambda_30\} \equiv (-1)^r\{\lambda_1\lambda_2\lambda_3\}. \quad (4.53)$$

With these rules together with the symmetry properties of $3j$ -phases, one can reduce any $3j$ -phase to products of $\{\epsilon\lambda'\lambda\}$, where ϵ is either fundamental or anti-fundamental, and $p(\lambda) = p(\lambda') + 1$. Besides, all the $\{\epsilon\lambda'\lambda\}$'s with the same λ and different λ' are related to each other, and one only has to fix by hand one of them. The reduction of the first few $3j$ -phases can be found in the appendix of ref. [200].

We point out an example of mutual constraining between the choice of $3j$ -phases and fixing the $U(1)$ freedom of quantum $6j$ -symbols. Eq. (4.52) as a result of our convention of $3j$ -phases constrains that at least some quantum $6j$ -symbols with an even sum of multiplicity labels have to be real, while some quantum $6j$ -symbols with an odd sum of multiplicity labels have to be imaginary. For instance eq. (4.52) implies

$$\left\{ \begin{array}{ccc} 1;0 & 0;1 & 1;1 \\ 21;0 & 21;0 & 2;0 \end{array} \right\}_{00r_30} = (-1)^{r_3} \left\{ \begin{array}{ccc} 0;1 & 1;0 & 1;1 \\ 0;21 & 0;21 & 0;2 \end{array} \right\}_{00r_30}. \quad (4.54)$$

Here $21;0$ is short for the composite labelling $(\mu;\nu)$ with $\mu = (2,1)$ and $\nu = (0)$. In fact we can consistently choose all the quantum $6j$ -symbols with even sum of multiplicity labels to be real, and all the quantum $6j$ -symbols with odd sum of multiplicity labels to be imaginary [200]. This is the convention we will use.

4.3.2 Eigenvector Method

Not all the quantum $6j$ -symbols of the two kinds (c.f. eq. (4.44)) need to be computed through the bootstrap strategy. Indeed by using the generalized Racah backcoupling rule and the column permutation symmetry, we find

$$\left\{ \begin{array}{ccc} \bar{R} & R & \rho_3 \\ R & R & \rho_4 \end{array} \right\}_{r'_1r'_2r'_3r'_4} = \sum_{\nu,r,r'} (-1)^{r+r'+r'_3+r'_4} \{R\}\{R, R, \bar{\rho}_4, r'_2\}\{R, \bar{R}, \rho_3, r'_3\}\{R, \bar{R}, \nu, r\} \\ q^{-2C_R+(C_{\rho_3}+C_{\rho_4}+C_\nu)/2} \dim_q \nu \left\{ \begin{array}{ccc} R & \bar{R} & \rho_3 \\ R & R & \bar{\nu} \end{array} \right\}_{rr'r'_3r'_4} \left\{ \begin{array}{ccc} \bar{R} & R & \nu \\ R & R & \rho_4 \end{array} \right\}_{r'_1r'_2rr'}.$$

Let us define

$$T_{\nu,rr'}^{\rho_3,r'_3r'_4} = (-1)^{r+r'+r'_3+r'_4} \{R\}\{R, \bar{R}, \rho_3, r'_3\}\{R, \bar{R}, \nu, r\} q^{-2C_R+(C_{\rho_3}+C_{\rho_4}+C_\nu)/2}$$

$$\sqrt{\dim_q \rho_3 \dim_q \nu} \begin{Bmatrix} R & \bar{R} & \rho_3 \\ R & R & \bar{\nu} \end{Bmatrix}_{rr'r'_3r'_4}, \quad (4.55)$$

$$U_{\rho_4, r'_1 r'_2}^{\nu, rr'} = \sqrt{\dim_q \nu \dim_q \rho_4} \begin{Bmatrix} \bar{R} & R & \nu \\ R & R & \rho_4 \end{Bmatrix}_{r'_1 r'_2 rr'}, \quad (4.56)$$

then the above identity becomes a matrix eigenvalue equation

$$T_{\nu, rr'}^{\rho_3, r'_3 r'_4} U_{\rho_4, r'_1 r'_2}^{\nu, rr'} = \{R, R, \bar{\rho}_4, r'_2\} U_{\rho_4, r'_1 r'_2}^{\rho_3, r'_3 r'_4}. \quad (4.57)$$

As discussed before, the $3j$ -phase $\{R, R, \bar{\rho}_4, r'_2\}$ here is not a free choice. It is $+1$ if ρ_4 belongs to $\text{Sym}^2 R$, and it is -1 if ρ_4 belongs to $\wedge^2 R$.

If we have already computed all the quantum $6j$ -symbols of the first kind and thus the matrix T is known, we can try to simply construct the matrix U whose columns are eigenvectors of T . On the other hand, since the eigenvalues of T are highly degenerate, the eigenvectors of T associated to the same eigenvalue can be mixed. We still need to compute some entries in each column of U in order to fix the column vectors. Nevertheless the eigenvalue equation eq. (4.57) can greatly reduce the number of quantum $6j$ -symbols that need to be computed.

4.3.3 Bootstrap: Reduction to Cores

Nontrivial quantum $6j$ -symbols can be classified into those with fundamental or anti-fundamental representations and those without. We call them primitive $6j$ -symbols and non-primitive $6j$ -symbols respectively. The first step of the bootstrap strategy is to reduce non-primitive $6j$ -symbols to primitive $6j$ -symbols [193]. Given an arbitrary non-primitive $6j$ -symbol

$$\begin{Bmatrix} \lambda_1 & \lambda_2 & \lambda_3 \\ \mu_1 & \mu_2 & \mu_3 \end{Bmatrix}_{r_1 r_2 r_3 r_4}$$

we can always use the tetrahedral symmetry to make sure that λ_3 is the smallest representation among the six (lowest power, or fewest boxes in the Young diagram). Then we apply the pentagon relation, where we choose that ν_1 is either fundamental or anti-fundamental, and ν_2 has one power less than λ_3 such that $\bar{\nu}_1, \nu_2, \lambda_3$ constitute a valid triad. The pentagon relation becomes

$$\begin{Bmatrix} \lambda_1 & \lambda_2 & \lambda_3 \\ \mu_1 & \mu_2 & \mu_3 \end{Bmatrix}_{r_1 r_2 r_3 r_4} = \sum_{\substack{\lambda \nu_3 \\ r'_2 r'_3 r'_1}} c \begin{Bmatrix} \lambda_1 & \nu_3 & \bar{\nu}_2 \\ \lambda & \mu_2 & \mu_3 \end{Bmatrix}_{r_1 r'_3 r'_2 r'_1}.$$

In each summand on the right hand side, c is the product of some primitive $6j$ -symbols, while in the last $6j$ -symbol the smallest representation is either ν_2 or even smaller than ν_2 . In either case the smallest representation in the last $6j$ -symbol must have lower power than λ_3 . If this last $6j$ -symbol is not primitive, we repeat the process until we have primitive $6j$ -symbols only.

Next it was shown in [201] that every primitive $6j$ -symbol can be further reduced to combinations of quantum $6j$ -symbols of the following two types:

- Type II (Core $6j$ -symbols)

$$\begin{Bmatrix} \lambda_1 & \lambda_2 & \lambda_3 \\ \mu_1 & \epsilon & \mu_3 \end{Bmatrix}_{0 r_2 0 r_4}. \quad (4.58)$$

Here ϵ is either fundamental or anti-fundamental. The remaining representations satisfy

$p(\lambda_1) \geq p(\lambda_2) \geq p(\lambda_3)$ as well as $p(\lambda_3) > p(\mu_1)$ or $p(\lambda_1) > p(\mu_3)$.

- Type IV

$$\left\{ \begin{array}{ccc} \lambda_1 & \lambda_2 & \epsilon_1 \\ \mu_1 & \mu_2 & \epsilon_2 \end{array} \right\}_{0000}, \quad (4.59)$$

where ϵ_1 and ϵ_2 are either fundamental or anti-fundamental.

To explain this second reduction process, we need to introduce some concepts. A triad which contains either a fundamental or anti-fundamental representation is called a primitive triad. A triad $(\lambda_1\lambda_2\lambda_3r_4)$ is partially ordered if $p(\lambda_1) \geq p(\lambda_2) \geq p(\lambda_3)$. Furthermore, two partially ordered triads can be compared. $(\lambda_1\lambda_2\lambda_3) > (\mu_1\mu_2\mu_3)$ if

- $p(\lambda_3) > p(\mu_3)$; or
- $p(\lambda_3) = p(\mu_3), p(\lambda_2) > p(\mu_2)$; or
- $p(\lambda_3) = p(\mu_3), p(\lambda_2) = p(\mu_2), p(\lambda_1) > p(\mu_1)$.

The algorithm to further reduce a primitive $6j$ -symbol is as follows. A primitive $6j$ -symbol has either two or four primitive triads. If the latter is the case, it must be a type IV $6j$ -symbol and the reduction stops. If the former is the case, we can use the tetrahedral symmetry to make sure that the triad $(\lambda_1\lambda_2\lambda_3r_4)$ in the first row of

$$\left\{ \begin{array}{ccc} \lambda_1 & \lambda_2 & \lambda_3 \\ \mu_1 & \mu_2 & \mu_3 \end{array} \right\}_{r_1r_2r_3r_4}$$

is partially order and the greatest among the four triads. Then the fundamental or anti-fundamental representation must be in the second row. Let us denote it by ϵ . Three things can happen.

1. If μ_1 is ϵ and $p(\lambda_1) > p(\lambda_2)$ (type I), we permute the three columns of the $6j$ -symbol by the cycle (132) and apply the generalized Racah backcoupling rule. For each of the resulting $6j$ -symbols we reduce it to a primitive $6j$ -symbol (if it is non-primitive) and rerun this further reduction algorithm from the beginning, unless it is already a trivial, type II, or type IV $6j$ -symbol.
2. If μ_3 is ϵ and $p(\lambda_2) > p(\lambda_3)$ (type III), we apply the pentagon relation with ν_2 being a fundamental or anti-fundamental. For each of the resulting $6j$ -symbols we reduce it to a primitive $6j$ -symbol (if it is non-primitive) and then rerun this reduction algorithm from the beginning, unless it is already a trivial, type II, or type IV $6j$ -symbol.
3. Otherwise the $6j$ -symbol is either already a type II, or we can simple transpose two neighboring columns to make it so (μ_1 is ϵ and $p(\lambda_1) = p(\lambda_2)$, or μ_3 is ϵ and $p(\lambda_2) = p(\lambda_3)$). The reduction stops.

It can be shown [201] that this algorithm terminates and a primitive $6j$ -symbol is completely reduced to combinations of type II (core), type IV, and trivial $6j$ -symbols.

4.3.4 Bootstrap: Crushing the Cores

A type IV $6j$ -symbol can be solved easily. Let us assume that ϵ_1 and ϵ_2 in eq. (4.58) are conjugate to each other (if this is not the case, we can transpose the two columns to their left to make it so). If λ_1 and μ_1 are identical, we apply the the generalized Racah backcoupling rule and get

$$q^{C_{\lambda_1}+C_{\epsilon_1}} \left\{ \begin{array}{ccc} \lambda_1 & \lambda_2 & \epsilon_1 \\ \lambda_1 & \mu_2 & \epsilon_2 \end{array} \right\}_{0000} = \sum_{\nu,r} q^{(C_\nu+C_{\lambda_2}+C_{\nu_2})/2} \dim_q \nu \{ \dots \} \left\{ \begin{array}{ccc} \epsilon_2 & \nu & \epsilon_1 \\ \lambda_1 & \mu_2 & \lambda_1 \end{array} \right\}_{0r00} \left\{ \begin{array}{ccc} \lambda_1 & \lambda_2 & \epsilon_1 \\ \bar{\epsilon}_2 & \nu & \bar{\lambda}_1 \end{array} \right\}_{r000},$$

where the phase factors consisting of $3j$ - and $2j$ -phases are represented by $\{ \dots \}$ and not explicitly spelled out. The representation ν that is summed over can be either the singlet $(0;0)$ or the adjoint $(1;1)$. By using the technique in the beginning of section 4.3 (the discussion of the modified form of backcoupling rule before section 4.3.1), we can remove the adjoint representation. Thus the type IV $6j$ -symbol is related to trivial $6j$ -symbols only, and its value can be computed without ambiguity. If λ_1 is different from μ_1 , we can ask what possible representations can replace ν with all the other five representations kept fixed for the type IV $6j$ -symbol still to be valid (i.e. all four triads in the $6j$ -symbol are valid), since the $6j$ -symbols which differ only by the representation at position $(2,1)$ (second row first column) are related to each other by the unitarity condition. It is not difficult to convince oneself that only two things can happen. Either μ_1 cannot be replaced by any other representation, so that the absolute value of the $6j$ -symbol is completely constrained by the unitarity condition

$$\dim_q \lambda_1 \dim_q \mu_1 \left| \left\{ \begin{array}{ccc} \lambda_1 & \lambda_2 & \epsilon_1 \\ \mu_1 & \mu_2 & \epsilon_2 \end{array} \right\} \right|^2 = 1;$$

or it can only be replaced by λ_1 , and the absolute value of the $6j$ -symbol can still be determined as we already know how to solve the new $6j$ -symbol after replacement

$$\dim_q \lambda_1 \dim_q \mu_1 \left| \left\{ \begin{array}{ccc} \lambda_1 & \lambda_2 & \epsilon_1 \\ \mu_1 & \mu_2 & \epsilon_2 \end{array} \right\} \right|^2 + (\dim_q \lambda_1)^2 \left| \left\{ \begin{array}{ccc} \lambda_1 & \lambda_2 & \epsilon_1 \\ \lambda_1 & \mu_2 & \epsilon_2 \end{array} \right\} \right|^2 = 1.$$

Besides, in either case, we have the freedom to choose a sign for the type IV $6j$ symbol.

Core (type II) $6j$ -symbols, on the contrary, cannot be solved by a mechanized routine, and must be dealt with case by case. Here we discuss various techniques we use to solve core $6j$ -symbols. Suppose $p(\lambda_3) > p(\mu_1)$. One relatively simple variety of core $6j$ -symbols are those when the other five representations are fixed, the representation λ_3 can only be replaced by representations with lower powers for the $6j$ -symbol to be valid. We call these $6j$ -symbols λ_3 -*descendable* and say that they can “descend” to $6j$ -symbols with smaller representations at position $(1,3)$ (row one column three) of the $6j$ -symbol through the unitarity relation (When $p(\lambda_1) > p(\mu_3)$ there are also λ_1 -descendable $6j$ -symbols, and the discussion is similar). A simple example is

$$\left\{ \begin{array}{ccc} \lambda_1 & \bar{\lambda}_1 & 1;1 \\ 1;0 & 1;0 & \mu_3 \end{array} \right\}_{000r_4},$$

where the adjoint representation $(1;1)$ at position $(1,3)$ can only be replaced by the singlet

(0;0). Using the unitary relation the absolute values of these $6j$ -symbols can be related to the values of the relatively simpler $6j$ -symbols that they descend to, and therefore can be recursively solved. On the other hand, unlike those type IV $6j$ -symbols with $\lambda_1 \neq \mu_1$, we do not have the freedom to choose signs for all the λ_3 -descendable core $6j$ -symbols. For instance, the λ_3 -descendable $6j$ -symbols which differ only by μ_3 are also related through the unitarity condition

$$\sum_{\lambda_3 r_4} \dim_q \lambda_3 \dim_q \mu_3 \left\{ \begin{matrix} \lambda_1 & \lambda_2 & \lambda_3 \\ \mu_1 & \epsilon & \mu_3 \end{matrix} \right\}_{0r_2 0r_4} \left\{ \begin{matrix} \lambda_1 & \lambda_2 & \lambda_3 \\ \mu_1 & \epsilon & \mu'_3 \end{matrix} \right\}_{0r_2 0r_4}^* = 0, \quad \mu_3 \neq \mu'_3, \quad (4.60)$$

and we only have the freedom to choose the sign for one of them (usually the one with the smallest μ_3). Here we assume the $6j$ -symbols that these λ_3 -descendables can descend to have already been solved.

Strictly speaking the absolute value of a λ_3 -descendable can only be fixed if r_4 cannot be greater than 0. The unitarity relation (c.f. eq. (4.41)) sums over not only λ_3 but also r_4 (r_3 is always 0 for a core $6j$ -symbol). In the case when r_4 can be greater than 0 the λ_3 -descendables that differ by r_4 cannot be separated. More concretely, suppose $\lambda_1 \star \lambda_2 \ni n \cdot \bar{\lambda}_3$ so that r_4 can take value in $0, 1, \dots, n-1$. By relating to simpler $6j$ -symbols that can be descended to, we are only allowed to compute

$$\sum_{r_4=0}^{n-1} \left| \left\{ \begin{matrix} \lambda_1 & \lambda_2 & \lambda_3 \\ \mu_1 & \epsilon & \mu_3 \end{matrix} \right\}_{0r_2 0r_4} \right|^2 \quad (4.61)$$

and

$$\sum_{r_4=0}^{n-1} \left\{ \begin{matrix} \lambda_1 & \lambda_2 & \lambda_3 \\ \mu_1 & \epsilon & \mu_3 \end{matrix} \right\}_{0r_2 0r_4} \left\{ \begin{matrix} \lambda_1 & \lambda_2 & \lambda_3 \\ \mu_1 & \epsilon & \mu'_3 \end{matrix} \right\}_{0r_2 0r_4}^*, \quad \mu_3 \neq \mu'_3 \quad (4.62)$$

for various possible μ_3 s (μ'_3 s). Let us call eq. (4.61) and eq. (4.62) a unitarity sum and an orthogonality sum respectively. These quantities are not enough to fix the values of individual $6j$ -symbols, and nor shall we expect them to, because these $6j$ -symbols should suffer from $U(n)$ uncertainty with respect to r_4 as we discussed in the beginning of section. 4.3. And both the unitarity sum and the orthogonality sum are indeed invariant under a $U(n)$ transformation acting on r_4 as in eq. (4.49). Therefore to fix the values of these $6j$ -symbols we have to implement a *multiplicity separation scheme* by hand to fix the $U(n)$ uncertainty.

Our choice of the multiplicity separation scheme is as follows. Suppose μ_3 can be $\mu_3^{(1)}, \mu_3^{(2)}, \dots$. First consider the $6j$ -symbols with $\mu_3 = \mu_3^{(1)}$. We set the $6j$ -symbols with $r_4 = 1, \dots, n-1$ to 0. Then the absolute value of the $6j$ -symbol with $r_4 = 0$ is fixed by the unitarity sum, and we assign an arbitrary sign to this $6j$ -symbol. Next consider the $6j$ -symbols with $\mu_3 = \mu_3^{(2)}$. The value of the first $6j$ -symbol ($r_4 = 0$) is now fixed by the orthogonality sum with the help of the values of the $6j$ -symbols with $\mu_3 = \mu_3^{(1)}$. We set the $6j$ -symbols with $r_4 = 2, \dots, n-1$ to 0, and the absolute value of the $6j$ -symbol with $r_4 = 1$ is then fixed by the unitarity sum. We again assign an arbitrary sign to this $6j$ -symbol. Repeat this process through the list of possible μ_3 s and the values of all these $6j$ -symbols can be fixed. The whole procedure can be summarized in the following table:

| | | | | | |
|------------------------|---------------|---------------|---------------|---------|---|
| $r_4 \backslash \mu_3$ | $\mu_3^{(1)}$ | $\mu_3^{(2)}$ | $\mu_3^{(3)}$ | \dots | |
| 0 | * | - | - | | |
| 1 | 0 | * | - | | |
| 2 | 0 | 0 | * | | * absolute value fixed by unitarity sums - value (w/ sign) fixed by orthogonality sums |
| 3 | 0 | 0 | 0 | | |
| \vdots | \vdots | \vdots | \vdots | | |
| $n - 1$ | 0 | 0 | 0 | | |

Note that the values of the 6j-symbols computed in this way depend on the order in the list of possible μ_3 s: $\mu_3^{(1)}, \mu_3^{(2)}, \dots$. A different ordering of the μ_3 's amounts to a different multiplicity separation scheme. Besides, in this separation scheme, we have fixed $2(n - 1) + 1$ degrees of freedom for $\mu_3^{(1)}$, $2(n - 2) + 1$ degrees of freedom for $\mu_3^{(2)}$, so on and so forth. In the end we at most fix $n^2 - 1$ degrees of freedom, which are the degrees of freedom in the group of uncertainty $SU(n) \subset U(n)$.

To solve core 6j-symbols which are not descendable, we need to look for other features. For instance, for some 6j-symbols, the representation at one position is unique, and the absolute values of these 6j-symbols are determined through the unitarity condition, just like the first case of the type IV 6j-symbols with $\lambda_1 \neq \mu_1$ discussed in the beginning of this subsection. For some other 6j-symbols, the representation at a position can only have two possibilities, and the corresponding two 6j-symbols are linearly related (through symmetries other than the unitarity condition). Typical examples are 6j-symbols of the following form

$$\left\{ \begin{matrix} \lambda_1 & \lambda_2 & 2; 0 \\ 1; 0 & 0; 1 & \nu \end{matrix} \right\}_{0000} \quad \text{or} \quad \left\{ \begin{matrix} \lambda_1 & \lambda_2 & 1^2; 0 \\ 1; 0 & 0; 1 & \nu \end{matrix} \right\}_{0000}, \tag{4.63}$$

where $1^2; 0$ is short for $(\mu; \nu)$ with $\mu = (1, 1)$ and $\nu = (0)$. Fixing the other five representations, ν is either unique or it has two distinct possibilities, denoted by $\nu^{(1)}$ and $\nu^{(2)}$ respectively. In the latter case, the generalized Racah backcoupling rule provides a linear relation between the two 6j-symbols with ν being $\nu^{(1)}$ and $\nu^{(2)}$. Together with the unitarity condition, the values of both 6j-symbols can be solved (we need to fix the sign of one 6j-symbol by hand). Finally, in the case of $p(\lambda_2) = p(\lambda_3)$, the following two types of core 6j-symbols,

$$\left\{ \begin{matrix} \lambda_1 & \lambda_2 & \lambda_3 \\ \mu_1 & \epsilon & \mu_3 \end{matrix} \right\}_{0r_2 0r_4} \quad \text{and} \quad \left\{ \begin{matrix} \lambda_1 & \lambda_3 & \lambda_2 \\ \mu'_1 & \epsilon' & \mu'_3 \end{matrix} \right\}_{0r'_2 0r'_4},$$

can be related to each other by first transposing the last two columns of either 6j-symbol and then applying the pentagon relation with ν_2 being fundamental or anti-fundamental. So we only have to solve one type of 6j-symbols.

With these tricks we have discussed, we were able to compute all the type IV and type II (core) 6j-symbols that were reduced from the quantum 6j-symbols of the two kinds in eq. (4.44) that one needed to compute. The results are given in the following section.

4.4 Results

4.4.1 Quantum $6j$ -Symbols of the Two Kinds

Let us first take a look at the quantum $6j$ -symbols of the first kind. Due to the tetrahedral symmetry and the complex conjugation relation, many quantum $6j$ -symbols of the first kind are identical. we group the quantum $6j$ -symbols of the first kind into a matrix

$$\hat{T}_{\rho_j, r_1 r_2}^{\rho_i, r_3 r_4} = \left\{ \begin{array}{ccc} R & \bar{R} & \rho_i \\ R & R & \rho_j \end{array} \right\}_{r_1 r_2 r_3 r_4},$$

with row index ρ_j, r_1, r_2 and column index ρ_i, r_3, r_4 . The symmetries of quantum $6j$ -symbols are translated into symmetries of the matrix \hat{T}

$$\hat{T}_{\rho_j, r_1 r_2}^{\rho_i, r_3 r_4} = \hat{T}_{\rho_j, r_2 r_1}^{\rho_i, r_4 r_3} = \hat{T}_{\rho_j, r_2 r_1}^{\bar{\rho}_i, r_3 r_4} = \left(\hat{T}_{\bar{\rho}_i, r_3 r_4}^{\rho_j, r_1 r_2} \right)^*, \quad (4.64)$$

which greatly reduce the number of its independent entries. In the case of $R = \boxplus$, we have

$$\begin{aligned} \rho_i, \rho_j &\in (21; 0) \otimes (0; 21) \\ &= (0; 0) \oplus 2(1; 1) \oplus (2; 2) \oplus (2; 1^2) \oplus (1^2; 2) \oplus (1^2; 1^2) \oplus (21; 21). \end{aligned}$$

which implies that \hat{T} is a 10×10 matrix. The number of independent entries of the matrix T , however, is reduced by symmetries from 100 to 37. All these independent entries will be covered below.

Besides, the values of the quantum $6j$ -symbols with non-trivial multiplicity labels depend on the multiplicity separation scheme we choose. However, physical quantities such as the colored HOMFLY invariants do *not* depend on the choice of multiplicity separation scheme. Therefore we can choose the most convenient multiplicity separation scheme such that the quantum $6j$ -symbols are as simple as possible.

Divided into five blocks, we tabulate the values of the quantum $6j$ -symbols of the first kind with $R = \boxplus$:

Trivial quantum $6j$ -symbols:

| | | | | | |
|---|-----------------------------|------------------------------|------------------------------|------------------------------|-----------------------------|
| $(\rho_j)_{r_1 r_2} \setminus (\rho_i)_{r_3 r_4}$ | $(1; 1)_{00}$ | $(1; 1)_{01}$ | $(1; 1)_{10}$ | $(1; 1)_{11}$ | $(0; 0)$ |
| $(0; 0)$ | $\frac{[3]}{[N-1][N][N+1]}$ | 0 | 0 | $-\frac{[3]}{[N-1][N][N+1]}$ | $\frac{[3]}{[N-1][N][N+1]}$ |
| $(\rho_j)_{r_1 r_2} \setminus (\rho_i)_{r_3 r_4}$ | $(2; 2)$ | $(2; 1^2)$ | $(1^2; 2)$ | $(1^2; 1^2)$ | $(21; 21)$ |
| $(0; 0)$ | $\frac{[3]}{[N-1][N][N+1]}$ | $-\frac{[3]}{[N-1][N][N+1]}$ | $-\frac{[3]}{[N-1][N][N+1]}$ | $\frac{[3]}{[N-1][N][N+1]}$ | $\frac{[3]}{[N-1][N][N+1]}$ |

In the table above, the multiplicity labels are omitted when they are trivial. A gray cell means the quantum $6j$ -symbol contained inside can be related to other $6j$ -symbols via the tetrahedral symmetry or complex conjugation, so that it is not an independent entry. The trivial quantum $6j$ -symbols with $\rho_i = (0; 0)$ can also be read off from this table through the last equality in eq. (4.64).

$\rho_i = \rho_j = (1; 1)$:

| $(\rho_j)_{r_1 r_2} \setminus (\rho_i)_{r_3 r_4}$ | $(1; 1)_{00}$ | $(1; 1)_{01}$ | $(1; 1)_{10}$ | $(1; 1)_{11}$ |
|---|---|--|--|---------------------------------|
| $(1; 1)_{00}$ | long expression | $\frac{i[2N]}{[N-1][N]^2[N+1]\sqrt{[N-2][N+2]}}$ | $\frac{i[2N]}{[N-1][N]^2[N+1]\sqrt{[N-2][N+2]}}$ | $-\frac{[4]}{[2][N-1][N][N+1]}$ |
| $(1; 1)_{01}$ | $-\frac{i[2N]}{[N-1][N]^2[N+1]\sqrt{[N-2][N+2]}}$ | $-\frac{1}{[N-1][N][N+1]}$ | $-\frac{1}{[N-1][N][N+1]}$ | 0 |
| $(1; 1)_{10}$ | $\frac{i[2N]}{[N-1][N]^2[N+1]\sqrt{[N-2][N+2]}}$ | $-\frac{1}{[N-1][N][N+1]}$ | $-\frac{1}{[N-1][N][N+1]}$ | 0 |
| $(1; 1)_{11}$ | $-\frac{[4]}{[2][N-1][N][N+1]}$ | 0 | 0 | $-\frac{1}{[N-1][N][N+1]}$ |

The quantum $6j$ -symbol labelled by ‘long expression’ reads

$$\begin{aligned}
& \left\{ \begin{array}{ccc} 21; 0 & 0; 21 & 1; 1 \\ 21; 0 & 21; 0 & 1; 1 \end{array} \right\}_{0000} \\
&= \frac{[3]^2([N-3][N+2] + [N-2][N+3])}{[N-2][N-1][N][N+1][N+2]([N-2][N+1] + [N-1][N+2])} \\
&+ \frac{[2][3]^2[2N]^2}{[N-2][N-1]^3[N]^3[N+1]^3[N+2]([N-2][N+1] + [N-1][N+2])} \\
&+ \frac{[2][N-2][N+2]([N-2][N+1]^2 + [N-1]^2[N+2]) - 2[3]([N-1]^3 + [N+1]^3)}{[2][N-1]^3[N]^2[N+1]^3}.
\end{aligned}$$

The appearance of many zeros in the table is due to a proper choice of multiplicity separation scheme. Let us view this table as a 4×4 submatrix M of T . Changing the multiplicity separation scheme amounts to a unitary transformation,

$$M \mapsto U M U^\dagger, \quad U \in U(4).$$

As a consequence the four $U(4)$ Casimirs of M should be invariant after a change of the multiplicity separation scheme, which we have checked indeed to be the case.

$\rho_i = (2; 2), (2; 1^2), (1^2; 2), (1^2; 1^2)$ and $\rho_j = (1; 1)$:

| $(\rho_j)_{r_1 r_2} \setminus (\rho_i)_{r_3 r_4}$ | $(2; 2)$ | $(2; 1^2)$ | $(1^2; 2)$ | $(1^2; 1^2)$ |
|---|--|--|--|---|
| $(1; 1)_{00}$ | long expression | long expression | long expression | long expression |
| $(1; 1)_{01}$ | $\frac{i\sqrt{[N-2]}}{[N-1][N]^2\sqrt{[N+2]}}$ | $-\frac{i}{[N][N+1]\sqrt{[N-2][N+2]}}$ | $\frac{i}{[N-1][N]\sqrt{[N-2][N+2]}}$ | $-\frac{i\sqrt{[N+2]}}{[N]^2[N+1]\sqrt{[N-2]}}$ |
| $(1; 1)_{10}$ | $\frac{i\sqrt{[N-2]}}{[N-1][N]^2\sqrt{[N+2]}}$ | $\frac{i}{[N-1][N]\sqrt{[N-2][N+2]}}$ | $-\frac{i}{[N][N+1]\sqrt{[N-2][N+2]}}$ | $-\frac{i\sqrt{[N+2]}}{[N]^2[N+1]\sqrt{[N-2]}}$ |
| $(1; 1)_{11}$ | $-\frac{[N-2]}{[N-1][N]^2[N+1]}$ | $-\frac{1}{[N-1][N][N+1]}$ | $-\frac{1}{[N-1][N][N+1]}$ | $-\frac{[N+2]}{[N-1][N]^2[N+1]}$ |

The values of the quantum $6j$ -symbols in the first row are as follows.

$$\begin{aligned}
& \left\{ \begin{array}{ccc} 21; 0 & 0; 21 & 2; 2 \\ 21; 0 & 21; 0 & 1; 1 \end{array} \right\}_{0000} \\
&= -(-[2][N-2]^3[N+1][N+2]^2 + 2[3][N-2][N+2]([3][N-1]^2 + [N+1]^2) \\
&+ [2]^2[3]^2 - [3]^2[N-1][N]([N-3][N+2] + [N-2][N+3])) \\
&/ ([2][N-2][N-1]^3[N]^2[N+1]^2[N+2]),
\end{aligned}$$

$$\begin{aligned}
 & \left\{ \begin{array}{cccc} 21; 0 & 0; 21 & 2; 1^2 \\ 21; 0 & 21; 0 & 1; 1 \end{array} \right\}_{0000} = \left\{ \begin{array}{cccc} 21; 0 & 0; 21 & 1^2; 2 \\ 21; 0 & 21; 0 & 1; 1 \end{array} \right\}_{0000} \\
 & = - ([3]^2[N]([N-3][N+2] + [N-2][N+3]) - [3][N-2][N+2]([N-3] + [N+3]) \\
 & \quad - [2][3]^2[N-2][N][N+2] + [2][N-2]^2[N][N+2]^2) \\
 & \quad / ([2][N-2][N-1]^2[N]^2[N+1]^2[N+2]) ,
 \end{aligned}$$

$$\begin{aligned}
 & \left\{ \begin{array}{cccc} 21; 0 & 0; 21 & 1^2; 1^2 \\ 21; 0 & 21; 0 & 1; 1 \end{array} \right\}_{0000} \\
 & = - (-[2][N-2]^2[N-1][N+2]^3 + 2[3][N-2][N+2]([N-1]^2 + [3][N+1]^2) \\
 & \quad + [2]^2[3]^2 - [3]^2[N][N+1]([N-3][N+2] + [N-2][N+3])) \\
 & \quad / ([2][N-2][N-1]^2[N]^2[N+1]^3[N+2])
 \end{aligned}$$

The $6j$ -symbols with $\rho_i = (1; 1)$ and $\rho_j = (2; 2), (2; 1^2), (1^2; 2), (1^2; 1^2)$ can also be read off from the table above using the last equality in eq. (4.64).

$\rho_i, \rho_j = (2; 2), (2; 1^2), (1^2; 2), (1^2; 1^2)$:

| $(\rho_j)_{r_1 r_2} \setminus (\rho_i)_{r_3 r_4}$ | (2; 2) | (2; 1 ²) | (1 ² ; 2) | (1 ² ; 1 ²) |
|---|--|---------------------------------------|---------------------------------------|--|
| (2; 2) | $\frac{[N-1][2]^2 + [N+1][2]^2 - [N-4][N][N+3]}{[N-2][N-1][N]^3[N+1][N+2][N+3]}$ | $\frac{[3]}{[N-1][N]^2[N+1][N+2]}$ | $\frac{[3]}{[N-1][N]^2[N+1][N+2]}$ | $-\frac{[3]^2}{[N-2][N-1][N][N+1][N+2]}$ |
| (2; 1 ²) | $\frac{[3]}{[N-1][N]^2[N+1][N+2]}$ | $\frac{[3]}{[N-2][N-1][N][N+1][N+2]}$ | $\frac{[3]}{[N-2][N-1][N][N+1][N+2]}$ | $\frac{[3]}{[N-2][N-1][N]^2[N+1]}$ |
| (1 ² ; 2) | $\frac{[3]}{[N-1][N]^2[N+1][N+2]}$ | $\frac{[3]}{[N-2][N-1][N][N+1][N+2]}$ | $\frac{[3]}{[N-2][N-1][N][N+1][N+2]}$ | $\frac{[3]}{[N-2][N-1][N]^2[N+1]}$ |
| (1 ² ; 1 ²) | $-\frac{[3]^2}{[N-2][N-1][N][N+1][N+2]}$ | $\frac{[3]}{[N-2][N-1][N]^2[N+1]}$ | $\frac{[3]}{[N-2][N-1][N]^2[N+1]}$ | $\frac{[N-1][2]^2 + [N+1][2]^2 - [N-3][N][N+4]}{[N-3][N-2][N-1][N]^3[N+1][N+2]}$ |

$\rho_j = (21; 21)$:

| $(\rho_j)_{r_1 r_2} \setminus (\rho_i)_{r_3 r_4}$ | (1; 1) ₀₀ | (1; 1) ₀₁ | (1; 1) ₁₀ | (1; 1) ₁₁ |
|---|--|----------------------|----------------------|----------------------|
| (21; 21) | $-\frac{[3]^2}{[N-2][N-1][N][N+1][N+2]}$ | 0 | 0 | 0 |

| $(\rho_j)_{r_1 r_2} \setminus (\rho_i)_{r_3 r_4}$ | (2; 2) | (2; 1 ²) | (1 ² ; 2) | (1 ² ; 1 ²) | (21; 21) |
|---|---|----------------------|----------------------|---|--|
| (21; 21) | $\frac{[2][3]^2}{[N-2][N-1][N]^2[N+1][N+2][N+3]}$ | 0 | 0 | $\frac{[2][3]^2}{[N-3][N-2][N-1][N]^2[N+1][N+2]}$ | $-\frac{[3]^3}{[N-3][N-2][N-1]^2[N][N+1]^2[N+2][N+3]}$ |

Again the quantum $6j$ -symbols with $\rho_i = (21; 21)$ can be read off from the table above using the symmetry properties in eq. (4.64).

The quantum $6j$ -symbols of the second kind enjoy less symmetry. We group these $6j$ -symbols into the following matrix

$$\hat{U}_{\rho_j, r_1 r_2}^{\rho_i, r_3 r_4} = \left\{ \begin{array}{cc} \bar{R} & R \\ R & R \end{array} \right\}_{r_1 r_2 r_3 r_4}^{\rho_i \rho_j} ,$$

and it satisfies the following symmetry properties

$$\hat{U}_{\rho_j, r_1 r_2}^{\rho_i, r_3 r_4} = \hat{U}_{\rho_j, r_2 r_1}^{\bar{\rho}_i, r_3 r_4} = \left(\hat{U}_{\rho_j, r_2 r_1}^{\rho_i, r_4 r_3} \right)^* . \quad (4.65)$$

For $R = \boxplus$ the relevant representations ρ^i and ρ^j are

$$\begin{aligned}\rho^i &\in (21; 0) \otimes (0; 21) \\ &= (0; 0) \oplus 2(1; 1) \oplus (2; 2) \oplus (2; 1^2) \oplus (1^2; 2) \oplus (1^2; 1^2) \oplus (21; 21), \\ \rho^j &\in (21; 0) \otimes (21; 0) \\ &= (42; 0) \oplus (2^3; 0) \oplus (31^3; 0) \oplus 2(321; 0) \oplus (41^2; 0) \oplus (3^2; 0) \oplus (2^2 1^1; 0),\end{aligned}$$

therefore \hat{U} is also a 10×10 matrix. Its symmetry only reduces the number of independent entries to 66.

For the quantum $6j$ -symbols with $\rho_j = (321; 0)$ and $(r_1, r_2) = (1, 0)$ or $(0, 1)$, the symmetry eq. (4.65) together with our convention that $6j$ -symbols with $\sum_i r_i$ being odd are imaginary constrain almost all of them to be zero except for

$$\begin{aligned}&\left\{ \begin{matrix} 0; 21 & 21; 0 & 1; 1 \\ 21; 0 & 21; 0 & 321; 0 \end{matrix} \right\}_{1001} = \left\{ \begin{matrix} 0; 21 & 21; 0 & 1; 1 \\ 21; 0 & 21; 0 & 321; 0 \end{matrix} \right\}_{1010} \\ &= \left\{ \begin{matrix} 0; 21 & 21; 0 & 1; 1 \\ 21; 0 & 21; 0 & 321; 0 \end{matrix} \right\}_{0101} = \left\{ \begin{matrix} 0; 21 & 21; 0 & 1; 1 \\ 21; 0 & 21; 0 & 321; 0 \end{matrix} \right\}_{0110} \\ &= \frac{[3]\sqrt{[5]}}{2[N-1][N][N+1]\sqrt{[N-2][N+2]}},\end{aligned}\tag{4.66}$$

$$\begin{aligned}&\left\{ \begin{matrix} 0; 21 & 21; 0 & 2; 1^2 \\ 21; 0 & 21; 0 & 321; 0 \end{matrix} \right\}_{1000} = - \left\{ \begin{matrix} 0; 21 & 21; 0 & 1^2; 2 \\ 21; 0 & 21; 0 & 321; 0 \end{matrix} \right\}_{1000} \\ &= - \left\{ \begin{matrix} 0; 21 & 21; 0 & 2; 1^2 \\ 21; 0 & 21; 0 & 321; 0 \end{matrix} \right\}_{0100} = \left\{ \begin{matrix} 0; 21 & 21; 0 & 1^2; 2 \\ 21; 0 & 21; 0 & 321; 0 \end{matrix} \right\}_{0100} \\ &= - \frac{i[2][3]\sqrt{[5]}}{2[N-2][N-1][N][N+1][N+2]}.\end{aligned}\tag{4.67}$$

We list the remaining $6j$ -symbols of the second kind with $R = \boxplus$ in the following. This time, we divide them into four blocks.

Trivial $6j$ -symbols:

| $(\rho_j)_{r_1 r_2} \setminus (\rho_i)_{r_3 r_4}$ | (0; 0) | | (0; 0) |
|---|-----------------------------|-------------------------------------|------------------------------|
| (42; 0) | $\frac{[3]}{[N-1][N][N+1]}$ | (41 ² ; 0) | $-\frac{[3]}{[N-1][N][N+1]}$ |
| (2 ³ ; 0) | $\frac{[3]}{[N-1][N][N+1]}$ | (3 ² ; 0) | $-\frac{[3]}{[N-1][N][N+1]}$ |
| (31 ³ ; 0) | $\frac{[3]}{[N-1][N][N+1]}$ | (2 ² 1 ² ; 0) | $-\frac{[3]}{[N-1][N][N+1]}$ |
| (321; 0) ₀₀ | $\frac{[3]}{[N-1][N][N+1]}$ | (321; 0) ₁₁ | $-\frac{[3]}{[N-1][N][N+1]}$ |

$\rho_i = (1; 1)$ and $\rho_j \neq (321; 0)$:

| $(\rho_j)_{r_1 r_2} \setminus (\rho_i)_{r_3 r_4}$ | $(1; 1)_{00}$ | $(1; 1)_{01}$ | $(1; 1)_{10}$ | $(1; 1)_{11}$ |
|---|---|---|---------------|----------------------------------|
| $(42; 0)$ | $\frac{[2][3][N-1]+[4][N+1]}{[2][N-1][N]^2[N+1][N+2]}$ | $-\frac{i\sqrt{[N-2]}}{[N-1][N]^2[N+1]\sqrt{[N+2]}}$ | | $\frac{[2]}{[N-1][N]^2[N+1]}$ |
| $(2^3; 0)$ | $-\frac{[3]}{[N-2][N]^2[N+1]}$ | $\frac{i[3]\sqrt{[N+2]}}{[N-1][N]^2[N+1]\sqrt{[N-2]}}$ | | $\frac{[2][3]}{[N-1][N]^2[N+1]}$ |
| $(31^3; 0)$ | $\frac{[2][3][N-2][N-1]-[6][N-1][N+2]-[3][4][N+1][N+2]}{[4][N-2][N-1][N]^2[N+1][N+2]}$ | $-\frac{i[3]}{[N-1][N][N+1]\sqrt{[N-2][N+2]}}$ | | 0 |
| $(41^2; 0)$ | $-\frac{[3][4][N-2][N-1]+[6][N-2][N+1]-[2][3][N+1][N+2]}{[4][N-2][N-1][N]^2[N+1][N+2]}$ | $\frac{i[3]}{[N-1][N][N+1]\sqrt{[N-2][N+2]}}$ | | 0 |
| $(3^2; 0)$ | $-\frac{[3]}{[N-1][N]^2[N+2]}$ | $-\frac{i[3]\sqrt{[N-2]}}{[N-1][N]^2[N+1]\sqrt{[N+2]}}$ | | $\frac{[2][3]}{[N-1][N]^2[N+1]}$ |
| $(2^2 1^2; 0)$ | $\frac{[4][N-1]+[2][3][N+1]}{[2][N-2][N-1][N]^2[N+1]}$ | $\frac{i\sqrt{[N+2]}}{[N-1][N]^2[N+1]\sqrt{[N-2]}}$ | | $\frac{[2]}{[N-1][N]^2[N+1]}$ |

Duo to space constraint, the quantum $6j$ -symbols in the gray cells are omitted. They are equal to the opposite of the $6j$ -symbols immediately to their left because of the symmetry in eq. (4.65).

$\rho_i = (2; 2), (2; 1^2), \dots$ and $\rho_j \neq (321; 0)$:

| $(\rho_j)_{r_1 r_2} \setminus (\rho_i)_{r_3 r_4}$ | $(2; 2)$ | $(2; 1^2)$ | $(1^2; 2)$ | $(1^2; 1^2)$ | $(21; 21)$ |
|---|---|---------------------------------------|------------|--|---|
| $(42; 0)$ | $\frac{[2][3][N-1]+[4][N+1]}{[2][N-1][N]^2[N+1][N+2]}$ | $\frac{[3]}{[N-1][N]^2[N+1]}$ | | $\frac{[3]^2}{[N-1][N]^2[N+1][N+2]}$ | $\frac{[3]^2}{[N-1][N]^2[N+1][N+2]}$ |
| $(2^3; 0)$ | $-\frac{[3]^2}{[N-2][N-1][N]^2[N+1]}$ | $-\frac{[3]^2}{[N-2][N-1][N]^2[N+1]}$ | | $-\frac{[3]}{[N-2][N-1][N]^2[N+1]}$ | $\frac{[3]^2}{[N-2][N-1][N]^2[N+1]}$ |
| $(31^3; 0)$ | $-\frac{[3]^2}{[N-2][N-1][N]^2[N+1]}$ | $-\frac{[3]}{[N-2][N-1][N]^2[N+1]}$ | | $-\frac{[2][3][N-2][N-1]-[6][N+2][N-1]-[3][4][N+1][N+2]}{[4][N-3][N-2][N-1][N]^2[N+1][N+2]}$ | $\frac{[3]^2}{[N-3][N-2][N-1][N]^2[N+1]}$ |
| $(41^2; 0)$ | $-\frac{[3][4][N-2][N-1]+[6][N-2][N+1]-[2][3][N+1][N+2]}{[4][N-2][N-1][N]^2[N+1][N+2]}$ | $\frac{[3]}{[N-2][N-1][N]^2[N+1]}$ | | $\frac{[3]^2}{[N-2][N-1][N]^2[N+1]}$ | $\frac{[3]^2}{[N-2][N-1][N]^2[N+1]}$ |
| $(3^2; 0)$ | $\frac{[3]}{[N-1][N]^2[N+1]}$ | $\frac{[3]^2}{[N-1][N]^2[N+1]}$ | | $-\frac{[3]^2}{[N-1][N]^2[N+1]}$ | $\frac{[3]^2}{[N-1][N]^2[N+1]}$ |
| $(2^2 1^2; 0)$ | $-\frac{[3]^2}{[N-2][N-1][N]^2[N+1]}$ | $-\frac{[3]}{[N-2][N-1][N]^2[N+1]}$ | | $-\frac{[4][N-1]+[2][3][N+1]}{[2][N-3][N-2][N-1][N]^2[N+1]}$ | $\frac{[3]^2}{[N-3][N-2][N-1][N]^2[N+1]}$ |

The quantum $6j$ -symbols in the gray cells (omitted) equal the $6j$ -symbols immediately to their left.

$\rho_j = (321; 0)$:

| $(\rho_j)_{r_1 r_2} \setminus (\rho_i)_{r_3 r_4}$ | $(1; 1)_{00}$ | $(1; 1)_{01}$ | $(1; 1)_{10}$ | $(1; 1)_{11}$ |
|---|--|--|---------------|--------------------------------|
| $(321; 0)_{00}$ | $-\frac{[3][(2N)+1]}{[N-2][N-1][N]^2[N+1][N+2]}$ | $\frac{i([3][N-2]+[6][N]-[3][N+2])}{2[2][N-1][N]^2[N+1]\sqrt{[N-2][N+2]}}$ | | $-\frac{[3]}{[N-1][N]^2[N+1]}$ |
| $(321; 0)_{11}$ | $\frac{[3][(2N)-1]}{[N-2][N-1][N]^2[N+1][N+2]}$ | $\frac{i([3][N-2]-[6][N]-[3][N+2])}{2[2][N-1][N]^2[N+1]\sqrt{[N-2][N+2]}}$ | | $-\frac{[3]}{[N-1][N]^2[N+1]}$ |

| $(\rho_j)_{r_1 r_2} \setminus (\rho_i)_{r_3 r_4}$ | $(2; 2)$ | $(2; 1^2)$ | $(1^2; 2)$ | $(1^2; 1^2)$ | $(21; 21)$ |
|---|---|--|------------|---|---|
| $(321; 0)_{00}$ | $-\frac{[3]([N-2]-[N+1])}{[N-2][N-1][N]^2[N+1][N+2]}$ | $-\frac{[3]([3][N-2]-[4][N]-[3][N+2])}{2[2][N-2][N-1][N]^2[N+1][N+2]}$ | | $-\frac{[3]([N-1]+[N+2])}{[N-2][N-1][N]^2[N+1][N+2]}$ | $\frac{[3]^2}{[N-2][N-1][N]^2[N+1][N+2]}$ |
| $(321; 0)_{11}$ | $\frac{[3]([N-2]+[N+1])}{[N-2][N-1][N]^2[N+1][N+2]}$ | $-\frac{[3]([3][N-2]+[4][N]-[3][N+2])}{2[2][N-2][N-1][N]^2[N+1][N+2]}$ | | $-\frac{[3]([N-1]-[N+2])}{[N-2][N-1][N]^2[N+1][N+2]}$ | $\frac{[3]^2}{[N-2][N-1][N]^2[N+1][N+2]}$ |

The quantum $6j$ -symbols in the gray cells (omitted) in the first table equal minus the $6j$ -symbols immediately to their left, while those in the gray cells (omitted) in the second table are identical with the $6j$ -symbols immediately to their left.

4.4.2 HOMFLY Invariants Colored in (2,1) Representation

With the quantum $6j$ -symbols listed in the previous subsection, we are able to compute colored HOMFLY invariants of hyperbolic knots with bridge index two colored in the (2,1) representa-

tion. The quasi-plat presentations of hyperbolic knots with up to seven crossings are given in Figs. B.1. The *normalized* HOMFLY invariants of these knots colored in the (2,1) representation with framing 0 are listed below⁴

$$\begin{aligned}
\bar{H}_{\square}(4_1) &= \frac{1}{\lambda^3 q^5} (q^5 \lambda^6 + (-q^8 - q^6 + q^5 - q^4 - q^2) \lambda^5 \\
&\quad + (q^{10} - q^9 + 3q^8 - 3q^7 + 5q^6 - 4q^5 + 5q^4 - 3q^3 + 3q^2 - q + 1) \lambda^4 \\
&\quad + (-2q^{10} + 2q^9 - 5q^8 + 6q^7 - 8q^6 + 7q^5 - 8q^4 + 6q^3 - 5q^2 + 2q - 2) \lambda^3 \\
&\quad + (q^{10} - q^9 + 3q^8 - 3q^7 + 5q^6 - 4q^5 + 5q^4 - 3q^3 + 3q^2 - q + 1) \lambda^2 \\
&\quad + (-q^8 - q^6 + q^5 - q^4 - q^2) \lambda + q^5)
\end{aligned} \tag{4.68}$$

$$\begin{aligned}
\bar{H}_{\square}(5_2) &= \frac{1}{\lambda^9 q^7} ((q^{12} - 2q^{11} + 3q^{10} - 4q^9 + 5q^8 - 5q^7 + 5q^6 - 4q^5 + 3q^4 - 2q^3 + q^2) \lambda^6 \\
&\quad + (q^{13} - 2q^{12} + 5q^{11} - 7q^{10} + 9q^9 - 11q^8 + 13q^7 - 11q^6 + 9q^5 - 7q^4 + 5q^3 - 2q^2 + q) \lambda^5 \\
&\quad + (q^{14} - 2q^{13} + 4q^{12} - 6q^{11} + 9q^{10} - 12q^9 + 13q^8 - 14q^7 + 13q^6 - 12q^5 + 9q^4 - 6q^3 \\
&\quad + 4q^2 - 2q + 1) \lambda^4 + (-q^{14} + q^{13} - 3q^{12} + 3q^{11} - 5q^{10} + 7q^9 - 8q^8 + 7q^7 - 8q^6 + 7q^5 \\
&\quad - 5q^4 + 3q^3 - 3q^2 + q - 1) \lambda^3 + (q^{10} - 2q^7 + q^4) \lambda^2 + (q^{10} + q^8 - q^7 + q^6 + q^4) \lambda - q^7)
\end{aligned} \tag{4.69}$$

$$\begin{aligned}
\bar{H}_{\square}(6_1) &= \frac{1}{\lambda^6 q^7} (q^7 \lambda^9 + (-q^{10} + 2q^7 - q^4) \lambda^8 + (q^{12} - 2q^{11} + q^{10} - 4q^9 + 4q^8 - 3q^7 \\
&\quad + 4q^6 - 4q^5 + q^4 - 2q^3 + q^2) \lambda^7 + (q^{13} - 2q^{12} + 4q^{11} - 6q^{10} + 8q^9 - 9q^8 + 11q^7 - 9q^6 \\
&\quad + 8q^5 - 6q^4 + 4q^3 - 2q^2 + q) \lambda^6 + (q^{14} - 2q^{13} + 4q^{12} - 7q^{11} + 11q^{10} - 12q^9 + 15q^8 \\
&\quad - 17q^7 + 15q^6 - 12q^5 + 11q^4 - 7q^3 + 4q^2 - 2q + 1) \lambda^5 + (-2q^{14} + 3q^{13} - 7q^{12} + 9q^{11} \\
&\quad - 13q^{10} + 17q^9 - 19q^8 + 18q^7 - 19q^6 + 17q^5 - 13q^4 + 9q^3 - 7q^2 + 3q - 2) \lambda^4 \\
&\quad + (q^{14} - 2q^{13} + 4q^{12} - 5q^{11} + 8q^{10} - 10q^9 + 11q^8 - 12q^7 + 11q^6 - 10q^5 + 8q^4 - 5q^3 \\
&\quad + 4q^2 - 2q + 1) \lambda^3 + (q^{11} - q^{10} + q^9 - q^8 + 3q^7 - q^6 + q^5 - q^4 + q^3) \lambda^2 \\
&\quad + (-q^{10} - q^8 + q^7 - q^6 - q^4) \lambda + q^7)
\end{aligned} \tag{4.70}$$

$$\begin{aligned}
\bar{H}_{\square}(6_2) &= \frac{1}{\lambda^6 q^{10}} ((q^{15} + 2q^{13} - q^{12} + 2q^{11} + 2q^9 - q^8 + 2q^7 + q^5) \lambda^6 + (-q^{18} - 3q^{16} \\
&\quad + 2q^{15} - 5q^{14} + 3q^{13} - 8q^{12} + 4q^{11} - 8q^{10} + 4q^9 - 8q^8 + 3q^7 - 5q^6 + 2q^5 - 3q^4 - q^2) \lambda^5 \\
&\quad + (q^{20} - q^{19} + 5q^{18} - 7q^{17} + 13q^{16} - 14q^{15} + 24q^{14} - 22q^{13} + 29q^{12} - 26q^{11} + 32q^{10} \\
&\quad - 26q^9 + 29q^8 - 22q^7 + 24q^6 - 14q^5 + 13q^4 - 7q^3 + 5q^2 - q + 1) \lambda^4 + (-2q^{20} + 3q^{19} \\
&\quad - 8q^{18} + 12q^{17} - 22q^{16} + 24q^{15} - 33q^{14} + 35q^{13} - 42q^{12} + 39q^{11} - 44q^{10} + 39q^9 - 42q^8 \\
&\quad + 35q^7 - 33q^6 + 24q^5 - 22q^4 + 12q^3 - 8q^2 + 3q - 2) \lambda^3 + (q^{20} - 2q^{19} + 5q^{18} - 6q^{17}
\end{aligned}$$

⁴ Colored HOMFLY invariants of 2-bridged knots with eight crossings can also be found in our paper[119].

$$\begin{aligned}
 &+ 12q^{16} - 14q^{15} + 17q^{14} - 16q^{13} + 21q^{12} - 18q^{11} + 18q^{10} - 18q^9 + 21q^8 - 16q^7 + 17q^6 \\
 &- 14q^5 + 12q^4 - 6q^3 + 5q^2 - 2q + 1)\lambda^2 + (-q^{18} + q^{17} - q^{16} - q^{14} - 2q^{13} + 5q^{12} - 6q^{11} \\
 &+ 4q^{10} - 6q^9 + 5q^8 - 2q^7 - q^6 - q^4 + q^3 - q^2)\lambda + q^{15} - 2q^{14} + 3q^{13} - 4q^{12} + 5q^{11} \\
 &- 5q^{10} + 5q^9 - 4q^8 + 3q^7 - 2q^6 + q^5) \tag{4.71}
 \end{aligned}$$

$$\begin{aligned}
 \bar{H}_{\square}(\mathbf{6}_3) = & \frac{1}{\lambda^3 q^{10}} ((-q^{15} + 2q^{14} - 3q^{13} + 4q^{12} - 5q^{11} + 5q^{10} - 5q^9 + 4q^8 - 3q^7 + 2q^6 \\
 &- q^5)\lambda^6 + (q^{18} - q^{17} + 2q^{16} - 2q^{15} + 4q^{14} - 4q^{13} + 6q^{12} - 5q^{11} + 7q^{10} - 5q^9 + 6q^8 \\
 &- 4q^7 + 4q^6 - 2q^5 + 2q^4 - q^3 + q^2)\lambda^5 + (-q^{20} + 2q^{19} - 6q^{18} + 9q^{17} - 17q^{16} + 23q^{15} \\
 &- 36q^{14} + 41q^{13} - 55q^{12} + 56q^{11} - 62q^{10} + 56q^9 - 55q^8 + 41q^7 - 36q^6 + 23q^5 - 17q^4 \\
 &+ 9q^3 - 6q^2 + 2q - 1)\lambda^4 + (2q^{20} - 4q^{19} + 10q^{18} - 16q^{17} + 31q^{16} - 40q^{15} + 60q^{14} \\
 &- 71q^{13} + 90q^{12} - 92q^{11} + 105q^{10} - 92q^9 + 90q^8 - 71q^7 + 60q^6 - 40q^5 + 31q^4 - 16q^3 \\
 &+ 10q^2 - 4q + 2)\lambda^3 + (-q^{20} + 2q^{19} - 6q^{18} + 9q^{17} - 17q^{16} + 23q^{15} - 36q^{14} + 41q^{13} \\
 &- 55q^{12} + 56q^{11} - 62q^{10} + 56q^9 - 55q^8 + 41q^7 - 36q^6 + 23q^5 - 17q^4 + 9q^3 - 6q^2 \\
 &+ 2q - 1)\lambda^2 + (q^{18} - q^{17} + 2q^{16} - 2q^{15} + 4q^{14} - 4q^{13} + 6q^{12} - 5q^{11} + 7q^{10} - 5q^9 + 6q^8 \\
 &- 4q^7 + 4q^6 - 2q^5 + 2q^4 - q^3 + q^2)\lambda - q^{15} + 2q^{14} - 3q^{13} + 4q^{12} - 5q^{11} + 5q^{10} - 5q^9 \\
 &+ 4q^8 - 3q^7 + 2q^6 - q^5) \tag{4.72}
 \end{aligned}$$

$$\begin{aligned}
 \bar{H}_{\square}(\mathbf{7}_2) = & \frac{1}{\lambda^{12} q^9} ((q^{14} - 2q^{13} + 3q^{12} - 4q^{11} + 5q^{10} - 5q^9 + 5q^8 - 4q^7 + 3q^6 - 2q^5 \\
 &+ q^4)\lambda^9 + (q^{15} - 2q^{14} + 3q^{13} - 5q^{12} + 7q^{11} - 8q^{10} + 8q^9 - 8q^8 + 7q^7 - 5q^6 + 3q^5 \\
 &- 2q^4 + q^3)\lambda^8 + (q^{16} - 2q^{15} + 3q^{14} - 4q^{13} + 7q^{12} - 8q^{11} + 9q^{10} - 9q^9 + 9q^8 - 8q^7 \\
 &+ 7q^6 - 4q^5 + 3q^4 - 2q^3 + q^2)\lambda^7 + (q^{17} - 2q^{16} + 3q^{15} - 6q^{14} + 9q^{13} - 12q^{12} + 14q^{11} \\
 &- 17q^{10} + 17q^9 - 17q^8 + 14q^7 - 12q^6 + 9q^5 - 6q^4 + 3q^3 - 2q^2 + q)\lambda^6 + (q^{18} - 2q^{17} \\
 &+ 4q^{16} - 7q^{15} + 11q^{14} - 14q^{13} + 19q^{12} - 22q^{11} + 24q^{10} - 25q^9 + 24q^8 - 22q^7 + 19q^6 \\
 &- 14q^5 + 11q^4 - 7q^3 + 4q^2 - 2q + 1)\lambda^5 + (-q^{18} + q^{17} - 3q^{16} + 4q^{15} - 7q^{14} + 9q^{13} \\
 &- 12q^{12} + 14q^{11} - 16q^{10} + 16q^9 - 16q^8 + 14q^7 - 12q^6 + 9q^5 - 7q^4 + 4q^3 - 3q^2 \\
 &+ q - 1)\lambda^4 + (q^{15} + q^{12} + q^{10} - 2q^9 + q^8 + q^6 + q^3)\lambda^3 + (-q^{13} + q^{12} - q^{11} + q^{10} \\
 &- 3q^9 + q^8 - q^7 + q^6 - q^5)\lambda^2 + (q^{12} + q^{10} - q^9 + q^8 + q^6)\lambda - q^9) \tag{4.73}
 \end{aligned}$$

$$\begin{aligned}
 \bar{H}_{\square}(\mathbf{7}_3) = & -\frac{\lambda^6}{q^{12}} ((q^{17} + 2q^{15} - q^{14} + 2q^{13} + 2q^{11} - q^{10} + 2q^9 + q^7)\lambda^6 + (-q^{20} - 3q^{18} \\
 &+ 2q^{17} - 5q^{16} + 3q^{15} - 8q^{14} + 4q^{13} - 8q^{12} + 4q^{11} - 8q^{10} + 3q^9 - 5q^8 + 2q^7 \\
 &- 3q^6 - q^4)\lambda^5 + (-q^{19} + 2q^{18} - 3q^{17} + 8q^{16} - 9q^{15} + 13q^{14} - 13q^{13} + 18q^{12} - 13q^{11} \\
 &+ 13q^{10} - 9q^9 + 8q^8 - 3q^7 + 2q^6 - q^5)\lambda^4 + (q^{24} - q^{23} + 4q^{22} - 5q^{21} + 9q^{20} - 10q^{19}
 \end{aligned}$$

$$\begin{aligned}
& + 14q^{18} - 13q^{17} + 14q^{16} - 11q^{15} + 10q^{14} - 7q^{13} + 6q^{12} - 7q^{11} + 10q^{10} - 11q^9 + 14q^8 \\
& - 13q^7 + 14q^6 - 10q^5 + 9q^4 - 5q^3 + 4q^2 - q + 1)\lambda^3 + (-q^{24} + 2q^{23} - 5q^{22} + 9q^{21} \\
& - 16q^{20} + 22q^{19} - 28q^{18} + 33q^{17} - 40q^{16} + 41q^{15} - 39q^{14} + 41q^{13} - 44q^{12} + 41q^{11} \\
& - 39q^{10} + 41q^9 - 40q^8 + 33q^7 - 28q^6 + 22q^5 - 16q^4 + 9q^3 - 5q^2 + 2q - 1)\lambda^2 \\
& + (-q^{23} + 2q^{22} - 6q^{21} + 11q^{20} - 17q^{19} + 23q^{18} - 31q^{17} + 35q^{16} - 38q^{15} + 41q^{14} \\
& - 42q^{13} + 40q^{12} - 42q^{11} + 41q^{10} - 38q^9 + 35q^8 - 31q^7 + 23q^6 - 17q^5 + 11q^4 - 6q^3 \\
& + 2q^2 - q)\lambda - q^{22} + 2q^{21} - 3q^{20} + 6q^{19} - 10q^{18} + 11q^{17} - 12q^{16} + 15q^{15} - 16q^{14} \\
& + 15q^{13} - 15q^{12} + 15q^{11} - 16q^{10} + 15q^9 - 12q^8 + 11q^7 - 10q^6 + 6q^5 - 3q^4 + 2q^3 - q^2)
\end{aligned} \tag{4.74}$$

$$\begin{aligned}
\bar{H}_{\square}(7_4) = & -\frac{\lambda^3}{q^9} (q^9\lambda^9 + (-q^{12} + q^{11} - q^{10} + 2q^9 - q^8 + q^7 - q^6)\lambda^8 + (-q^{14} - 3q^{12} + q^{11} \\
& - 2q^{10} + 4q^9 - 2q^8 + q^7 - 3q^6 - q^4)\lambda^7 + (q^{16} + q^{14} - q^{13} - 2q^{12} - q^{11} + 4q^9 - q^7 - 2q^6 \\
& - q^5 + q^4 + q^2)\lambda^6 + (q^{18} - 2q^{17} + 4q^{16} - 6q^{15} + 13q^{14} - 16q^{13} + 21q^{12} - 28q^{11} + 33q^{10} \\
& - 28q^9 + 33q^8 - 28q^7 + 21q^6 - 16q^5 + 13q^4 - 6q^3 + 4q^2 - 2q + 1)\lambda^5 + (-q^{18} + 4q^{17} \\
& - 8q^{16} + 14q^{15} - 24q^{14} + 37q^{13} - 48q^{12} + 57q^{11} - 66q^{10} + 70q^9 - 66q^8 + 57q^7 - 48q^6 \\
& + 37q^5 - 24q^4 + 14q^3 - 8q^2 + 4q - 1)\lambda^4 + (-2q^{17} + 6q^{16} - 14q^{15} + 21q^{14} - 36q^{13} \\
& + 51q^{12} - 61q^{11} + 70q^{10} - 78q^9 + 70q^8 - 61q^7 + 51q^6 - 36q^5 + 21q^4 - 14q^3 \\
& + 6q^2 - 2q)\lambda^3 + (-3q^{16} + 8q^{15} - 15q^{14} + 22q^{13} - 32q^{12} + 47q^{11} - 51q^{10} + 48q^9 - 51q^8 \\
& + 47q^7 - 32q^6 + 22q^5 - 15q^4 + 8q^3 - 3q^2)\lambda^2 + (-2q^{15} + 6q^{14} - 10q^{13} + 16q^{12} - 22q^{11} \\
& + 26q^{10} - 28q^9 + 26q^8 - 22q^7 + 16q^6 - 10q^5 + 6q^4 - 2q^3)\lambda - q^{14} + 4q^{13} - 6q^{12} + 6q^{11} \\
& - 9q^{10} + 12q^9 - 9q^8 + 6q^7 - 6q^6 + 4q^5 - q^4)
\end{aligned} \tag{4.75}$$

$$\begin{aligned}
\bar{H}_{\square}(7_5) = & \frac{1}{\lambda^{12}q^{12}} ((q^{22} - 2q^{21} + 5q^{20} - 9q^{19} + 15q^{18} - 20q^{17} + 27q^{16} - 32q^{15} + 38q^{14} \\
& - 40q^{13} + 42q^{12} - 40q^{11} + 38q^{10} - 32q^9 + 27q^8 - 20q^7 + 15q^6 - 9q^5 + 5q^4 - 2q^3 \\
& + q^2)\lambda^6 + (q^{23} - 3q^{22} + 9q^{21} - 19q^{20} + 33q^{19} - 49q^{18} + 69q^{17} - 90q^{16} + 107q^{15} \\
& - 121q^{14} + 130q^{13} - 134q^{12} + 130q^{11} - 121q^{10} + 107q^9 - 90q^8 + 69q^7 - 49q^6 + 33q^5 \\
& - 19q^4 + 9q^3 - 3q^2 + q)\lambda^5 + (q^{24} - 3q^{23} + 8q^{22} - 18q^{21} + 30q^{20} - 48q^{19} + 69q^{18} \\
& - 92q^{17} + 111q^{16} - 133q^{15} + 146q^{14} - 156q^{13} + 158q^{12} - 156q^{11} + 146q^{10} - 133q^9 \\
& + 111q^8 - 92q^7 + 69q^6 - 48q^5 + 30q^4 - 18q^3 + 8q^2 - 3q + 1)\lambda^4 + (-q^{24} + 2q^{23} \\
& - 6q^{22} + 10q^{21} - 17q^{20} + 24q^{19} - 32q^{18} + 41q^{17} - 47q^{16} + 51q^{15} - 55q^{14} + 58q^{13} \\
& - 56q^{12} + 58q^{11} - 55q^{10} + 51q^9 - 47q^8 + 41q^7 - 32q^6 + 24q^5 - 17q^4 + 10q^3 - 6q^2 \\
& + 2q - 1)\lambda^3 + (q^{21} + 2q^{19} - 4q^{18} + 9q^{17} - 12q^{16} + 17q^{15} - 24q^{14} + 27q^{13} - 26q^{12} \\
& + 27q^{11} - 24q^{10} + 17q^9 - 12q^8 + 9q^7 - 4q^6 + 2q^5 + q^3)\lambda^2 + (q^{20} - 2q^{19} + 3q^{18} - 6q^{17} \\
& + 9q^{16} - 11q^{15} + 12q^{14} - 14q^{13} + 16q^{12} - 14q^{11} + 12q^{10} - 11q^9 + 9q^8 - 6q^7 + 3q^6
\end{aligned}$$

$$-2q^5 + q^4)\lambda - q^{17} + 2q^{16} - 3q^{15} + 4q^{14} - 5q^{13} + 5q^{12} - 5q^{11} + 4q^{10} - 3q^9 + 2q^8 - q^7) \quad (4.76)$$

$$\begin{aligned} \bar{H}_{\boxplus}(\mathbf{7_6}) = & \frac{1}{\lambda^9 q^{10}} ((q^{15} - 2q^{14} + 3q^{13} - 4q^{12} + 5q^{11} - 5q^{10} + 5q^9 - 4q^8 + 3q^7 \\ & - 2q^6 + q^5)\lambda^9 + (-q^{18} + 2q^{17} - 4q^{16} + 7q^{15} - 11q^{14} + 14q^{13} - 18q^{12} + 20q^{11} - 21q^{10} \\ & + 20q^9 - 18q^8 + 14q^7 - 11q^6 + 7q^5 - 4q^4 + 2q^3 - q^2)\lambda^8 + (q^{20} - 3q^{19} + 9q^{18} - 19q^{17} \\ & + 34q^{16} - 51q^{15} + 74q^{14} - 95q^{13} + 113q^{12} - 124q^{11} + 131q^{10} - 124q^9 + 113q^8 - 95q^7 \\ & + 74q^6 - 51q^5 + 34q^4 - 19q^3 + 9q^2 - 3q + 1)\lambda^7 + (-3q^{20} + 9q^{19} - 22q^{18} + 41q^{17} \\ & - 71q^{16} + 105q^{15} - 142q^{14} + 177q^{13} - 213q^{12} + 229q^{11} - 236q^{10} + 229q^9 - 213q^8 \\ & + 177q^7 - 142q^6 + 105q^5 - 71q^4 + 41q^3 - 22q^2 + 9q - 3)\lambda^6 + (3q^{20} - 8q^{19} + 19q^{18} \\ & - 34q^{17} + 58q^{16} - 83q^{15} + 117q^{14} - 143q^{13} + 169q^{12} - 183q^{11} + 194q^{10} - 183q^9 \\ & + 169q^8 - 143q^7 + 117q^6 - 83q^5 + 58q^4 - 34q^3 + 19q^2 - 8q + 3)\lambda^5 + (-q^{20} + 2q^{19} \\ & - 7q^{18} + 11q^{17} - 20q^{16} + 26q^{15} - 39q^{14} + 44q^{13} - 52q^{12} + 53q^{11} - 61q^{10} + 53q^9 \\ & - 52q^8 + 44q^7 - 39q^6 + 26q^5 - 20q^4 + 11q^3 - 7q^2 + 2q - 1)\lambda^4 + (2q^{18} - q^{17} + 3q^{16} \\ & - 2q^{15} + 2q^{14} + 5q^{13} + 6q^{11} - 7q^{10} + 6q^9 + 5q^7 + 2q^6 - 2q^5 + 3q^4 - q^3 + 2q^2)\lambda^3 \\ & + (-q^{16} - 3q^{15} + q^{14} - 2q^{13} + 4q^{12} - 7q^{11} + q^{10} - 7q^9 + 4q^8 - 2q^7 + q^6 - 3q^5 - q^4)\lambda^2 \\ & + (2q^{13} + q^{12} + q^{11} - 2q^{10} + q^9 + q^8 + 2q^7)\lambda - q^{10}) \end{aligned} \quad (4.77)$$

$$\begin{aligned} \bar{H}_{\boxplus}(\mathbf{7_7}) = & \frac{1}{\lambda^3 q^{10}} (q^{10}\lambda^9 + (-2q^{13} - 2q^{11} + 2q^{10} - 2q^9 - 2q^7)\lambda^8 + (q^{16} + 2q^{15} + 4q^{13} \\ & - 4q^{12} + 8q^{11} - 4q^{10} + 8q^9 - 4q^8 + 4q^7 + 2q^5 + q^4)\lambda^7 + (-2q^{18} + 2q^{17} - 8q^{16} + 8q^{15} \\ & - 15q^{14} + 16q^{13} - 24q^{12} + 21q^{11} - 28q^{10} + 21q^9 - 24q^8 + 16q^7 - 15q^6 + 8q^5 - 8q^4 \\ & + 2q^3 - 2q^2)\lambda^6 + (q^{20} - 2q^{19} + 10q^{18} - 18q^{17} + 36q^{16} - 58q^{15} + 88q^{14} - 110q^{13} \\ & + 145q^{12} - 156q^{11} + 164q^{10} - 156q^9 + 145q^8 - 110q^7 + 88q^6 - 58q^5 + 36q^4 - 18q^3 \\ & + 10q^2 - 2q + 1)\lambda^5 + (-3q^{20} + 8q^{19} - 22q^{18} + 46q^{17} - 82q^{16} + 124q^{15} - 186q^{14} \\ & + 240q^{13} - 286q^{12} + 319q^{11} - 340q^{10} + 319q^9 - 286q^8 + 240q^7 - 186q^6 + 124q^5 \\ & - 82q^4 + 46q^3 - 22q^2 + 8q - 3)\lambda^4 + (3q^{20} - 10q^{19} + 23q^{18} - 45q^{17} + 83q^{16} \\ & - 127q^{15} + 178q^{14} - 234q^{13} + 284q^{12} - 314q^{11} + 326q^{10} - 314q^9 + 284q^8 - 234q^7 \\ & + 178q^6 - 127q^5 + 83q^4 - 45q^3 + 23q^2 - 10q + 3)\lambda^3 + (-q^{20} + 4q^{19} - 10q^{18} + 18q^{17} \\ & - 32q^{16} + 54q^{15} - 75q^{14} + 95q^{13} - 122q^{12} + 136q^{11} - 134q^{10} + 136q^9 - 122q^8 + 95q^7 \\ & - 75q^6 + 54q^5 - 32q^4 + 18q^3 - 10q^2 + 4q - 1)\lambda^2 + (q^{18} - 3q^{17} + 3q^{16} - 2q^{15} + 6q^{14} \\ & - 8q^{13} + q^{12} - 3q^{11} + 10q^{10} - 3q^9 + q^8 - 8q^7 + 6q^6 - 2q^5 + 3q^4 - 3q^3 + q^2)\lambda \\ & - q^{15} + 4q^{14} - 6q^{13} + 6q^{12} - 9q^{11} + 12q^{10} - 9q^9 + 6q^8 - 6q^7 + 4q^6 - q^5) \end{aligned} \quad (4.78)$$

These normalized HOMFLY invariants enjoy the symmetry properties discussed in section 2.3.4. The knots $\mathbf{4_1}$ and $\mathbf{6_3}$ are amphicheiral knots, and indeed their HOMFLY invariants

satisfy the symmetry given by eq. (2.160), while the HOMFLY invariants of the other knots do not. Furthermore, all the computed HOMFLY invariants satisfy the symmetry given by eq. (2.162) because the \boxplus representation is transpose-symmetric.

Some of these invariants, namely those of the knots **4₁**, **5₂**, **6₂**, **6₃**, **7₃**, **7₅**, have already been computed using a different method in refs. [190, 191]. Their results are in perfect agreement with ours, which serves as a non-trivial check on both approaches.

Conclusions and Prospect

In topological string theories, statements of dualities like mirror symmetry, large N duality, and etc, can be made very precise, and in conjunction with the powerful computational methods in topological string theories, these dualities can be verified very explicitly. The Ooguri–Vafa conjecture [25] claims that for an arbitrary knot in S^3 there is a unique stack of branes (the number of branes in this stack is not fixed) in type A topological string on the resolved conifold, such that the vevs of the Wilson loop along the knot in $U(N)$ Chern–Simons theory on S^3 evaluated in various representations, also known as quantum knot invariants or colored HOMFLY invariants, can be related to the free energies on the branes in the type A topological open string theory. These free energies in turn can be identified with the free energies on the mirror branes in the type B topological open string theory on the mirror geometry of the resolved conifold. Our goal is to directly verify the Ooguri–Vafa conjecture for non-trivial knots by comparing the quantum knot invariants and the free energies on the associated branes in the topological string theories.

On the topological string side, the BKMP theorem [52, 113, 156] claims that the topological recursion [22, 23] developed by Eynard and Orantin to solve matrix models can be applied on the spectral curves in type B topological string theory to compute the free energies on the toric special Lagrangian branes in the mirror type A topological string theory, or equivalently the free energies on the mirror special holomorphic branes in the type B topological string theory. When the type A topological string is compactified on the resolved conifold, these toric special Lagrangian branes are the branes associated to a unknot in S^3 according to the Ooguri–Vafa conjecture. We find out that to apply the topological recursion on the Aganagic–Vafa spectral curve of the branes associated to a non-trivial knot, the recursion has to be modified by substituting the Bergman kernel with the genuine generating function of worldsheet annulus instantons on the branes, and we call the latter the calibrated annulus kernel [170]. We compute the calibrated annulus kernel for branes associated to the simplest torus knot, which enable us to apply the modified topological recursion on these branes. We verify that the modified recursion can reproduce the correct free energies on the branes, in the sense that they are consistent with the quantum knot invariants à la the Ooguri–Vafa conjecture. In addition our method of the modified topological recursion can reproduce the free energies of the topological closed string theory, which encode the information of the background geometry. This is in line with the observation that these branes also probe the background geometry.

Although the validity of our method of the modified topological recursion has only been confirmed for the branes associated to torus knots, we conjecture that when it is applied to the branes associated to hyperbolic knots, it should also reproduce the correct free energies on the branes, and they should be consistent with the quantum knot invariants in the sense of the Ooguri–Vafa conjecture. We are encouraged by the observation that the modified topological

recursion can reproduce the correct planar free energies of the topological closed string when it is applied to the Aganagic–Vafa spectral curves of hyperbolic knots. Our conjecture has a natural corollary in the knot theory, namely, any pair of mutant knots can be distinguished by colored HOMFLY invariants in some two row presentations of $U(N)$. On the other hand, to verify our conjecture concerning hyperbolic knots, we need to compute the calibrated annulus kernels for the branes associated to these knots. This proves to be a daunting task. We argue that this kernel can be extracted from the colored HOMFLY invariants in symmetric and two row representations of $U(N)$. There are existing methods to compute the colored HOMFLY invariants in symmetric representations. We develop techniques in $U(N)$ Chern–Simons theory to compute the colored HOMFLY invariants for hyperbolic knots in nonsymmetric representations [119], based on the works in refs. [124, 166, 197], which in turn heavily draw on Witten’s insights that relates the 3d $SU(N)$ Chern–Simons theory to the $\widehat{su}(N)_k$ WZW models. Our techniques require the knowledge of nontrivial crossing matrices in the WZW models. These crossing matrices are proportional to the quantum $6j$ -symbols in the quantum group $\mathcal{U}_q(\mathfrak{sl}_N)$. Using symmetries of the quantum $6j$ -symbols, we compute the values of many nontrivial quantum $6j$ -symbols through the bootstrap strategy. Once this is done, we can compute the HOMFLY invariants for many hyperbolic knots colored in the $\{2, 1\}$ representation [119].

Admittedly these colored HOMFLY invariants are not enough for the derivation of the calibrated annulus kernels for the branes associated to these hyperbolic knots. Therefore a natural direction of future research is to compute colored HOMFLY invariants for hyperbolic knots in more two row representations. On the other hand it might be interesting to look for a probably exotic matrix model underlying the modified topological recursion, which may shed light on a more convenient way to compute the calibrated annulus kernels. Furthermore recently a refined version of the topological recursion has been proposed by Eynard and Orantin based on the β -ensemble [202], but it has not been applied successfully in the refined topological string theory. It would be interesting to find out how the refined recursion should be modified to be applicable in refined topological string, and even for the branes associated to knots.

Concerning the computation of quantum knot invariants, it is natural to generalize them to other gauge groups like $SO(N)$, $Sp(N)$, or even exceptional groups, and to consider different ambient three-manifolds for knots like Lens spaces. A more interesting direction is toward the refined Chern–Simons theory, where the vevs of Wilson loops along torus knots in the fundamental representation are known [203] to coincide with the superpolynomials in the HOMFLY knot homology [204], which is the categorification of the HOMFLY knot invariants. It would be interesting to find out whether it is possible to generalize our techniques to compute the vevs of Wilson loops in generic representations in the refined Chern–Simons theory and explore further connections of the refined Chern–Simons theory to the HOMFLY knot homology.

Composite Representations of $U(N)$

Here we discuss composite representations of $U(N)$ and quantum knot invariants colored in composite representations. We will also introduce composite labelling of representations of $SU(N)$. In this section we always refer to a representation by its associated partition.

A generic irreducible representation of $U(N)$ is a composite representation labelled by two partitions $(\mu; \nu)$. Let μ_i, ν_j be the i -th and j -th components of the partitions μ, ν respectively. The two partitions satisfy the usual conditions $\mu_1 \geq \mu_2 \geq \dots \geq \mu_p > 0$ and $\nu_1 \geq \nu_2 \geq \dots \geq \nu_q > 0$, and in addition the sum of the lengths (number of components) of μ and ν cannot exceed N . In terms of Young diagrams the representation $(\mu; \nu)$ is usually depicted as in Fig. A.1a, where the Young diagram of ν is rotated by 180° and is drawn to the left of the Young diagram of μ , and the total height of the diagram is N .

To have an intuitive understanding of the representation $(\mu; \nu)$, we notice that $U(N) = U(1) \times SU(N)$, and therefore a representation of $U(N)$ always gives a representation of $U(1)$ and a representation of $SU(N)$. Let us write the pair of partitions $(\mu; \nu)$ as

$$(\mu; \nu) = \underbrace{(\mu_1, \dots, \mu_p, 0, \dots, 0, -\nu_q, \dots, -\nu_1)}_N =: (f) . \quad (\text{A.1})$$

Then the corresponding $U(1)$ representation has charge $\ell(f) = \sum_{i=1}^N f_i$, and the irreducible $SU(N)$ representation is given by the partition

$$(\lambda) = (\lambda_1, \dots, \lambda_N) = (\mu_1 + \nu_1, \dots, \mu_p + \nu_1, \nu_1, \dots, \nu_1, \nu_1 - \nu_q, \dots, 0) . \quad (\text{A.2})$$

In other words we make a universal shift in the components of the partition (f) by ν_1 and every component of the partition becomes nonnegative. The Young diagram corresponding to (λ) is the juxtaposition of the vertical complement of the rotated Young diagram of ν with the Young diagram of μ , as illustrated in Fig. A.1b.

Clearly a $U(N)$ composite representation corresponds to a unique $SU(N)$ irreducible representation, but the opposite is not true. Given a composite representation $(\mu; \nu) = (f)$, we can get infinitely many composite representations through a universal shift of the components of (f) by an arbitrary integer n

$$(f) \rightarrow (f') = (f_1 + n, \dots, f_N + n) = (\mu'; \nu') \quad (\text{A.3})$$

and all these composite representations correspond to the same $SU(N)$ representation. On the other hand, the $U(1)$ charges of these composite representations differ from each other by multiples of N . In the limit $N \rightarrow \infty$, given an irreducible representation (λ) of $SU(N)$, there is only one corresponding composite representation $(\mu; \nu)$ whose $U(1)$ charge is finite. We call

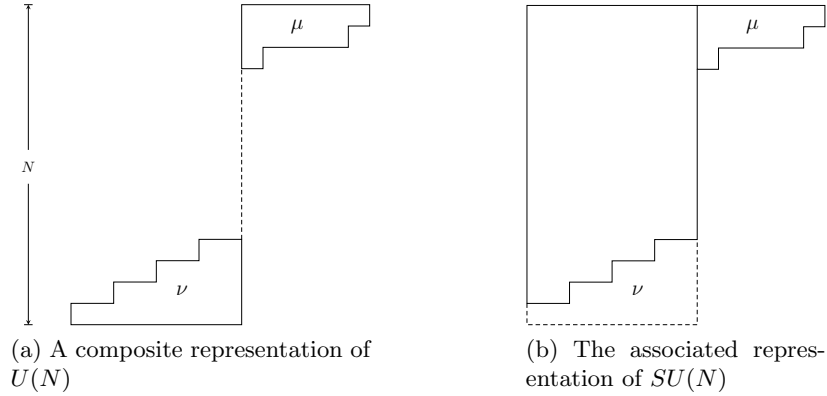


Figure A.1: The Young diagram of a composite representation $(\mu; \nu)$ of $U(N)$, and that of the associated representation of $SU(N)$.

it the canonical composite representation associated to (λ) , or simply the composite labelling of (λ) . For instance the composite labellings of the fundamental and antifundamental representations of $SU(N)$ are $(1; 0)$ and $(0; 1)$ respectively, and the composite labelling of the adjoint representation is $(1; 1)$. In addition given an arbitrary irreducible representation (λ) of $SU(N)$ we can always find it in the decomposition of the tensor product of a string of fundamental and antifundamental representations, and we define the power $p(\lambda)$ of the representation to be the minimum number of fundamental and antifundamental representations needed in this construction. It is easy to convince oneself the power $p(\lambda)$ is simply the total number of boxes in its composite labelling; in other words

$$p(\lambda) = \ell(\mu) + \ell(\nu) . \tag{A.4}$$

Let us come back to the composite representations of the group $U(N)$. They can in fact be rigorously defined by [205]

$$(\mu; \nu) = \sum_{\zeta, \rho, \sigma} (-1)^{\ell(\zeta)} N_{\zeta\rho}^{\mu} V_{\zeta^T\sigma}^{\nu} (\rho \otimes \bar{\sigma}) , \tag{A.5}$$

where $\bar{\sigma}$ is the conjugate of σ and $N_{\zeta\rho}^{\mu}$ the Littlewood–Richard coefficient. The tensor product of two composite representations can be decomposed via [206]

$$(\mu; \nu) \otimes (\rho; \sigma) = \sum_{\zeta, \eta} ((\mu/\zeta) \otimes (\rho/\eta); (\nu/\eta) \otimes (\sigma/\zeta)) . \tag{A.6}$$

Here the division of two partitions is defined with the help of the Littlewood–Richardson coefficients

$$\mu/\zeta = \sum_{\rho} N_{\zeta\rho}^{\mu} \rho . \tag{A.7}$$

It’s precisely the opposite operation of tensor product decomposition.

Since the quantum knot invariants are formulated in $U(N)$ Chern–Simons theory, the most generic quantum knot invariants are colored in composite representations. The quantum knot invariants of unknot are still given by the quantum dimensions of the coloring representations.

The quantum dimension of the composite representation $(\mu; \nu)$ is [170]

$$\begin{aligned} \dim_q(\mu; \nu) &= Q^{-\frac{1}{2}(|\mu|+|\nu|)} s_\mu(q^{-\rho}) s_\nu(q^{-\rho}) \frac{\prod_{i=1}^{c_\mu^t} \prod_{j=1}^{c_\nu^t} (1 - Q q^{i+j-\mu_i^t-\nu_j^t-1})}{\prod_{i=1}^{c_\mu^t} \prod_{j=1}^{c_\nu^t} (1 - Q q^{i+j-1})} \\ &\times \left(\prod_{i=1}^{c_\mu^t} \prod_{j=c_{\nu^t}-\mu_i^t+1}^{c_\nu^t} (1 - Q q^{i+j-1}) \right) \left(\prod_{i=1}^{c_\nu^t} \prod_{j=c_{\mu^t}-\nu_i^t+1}^{c_\mu^t} (1 - Q q^{i+j-1}) \right), \end{aligned} \quad (\text{A.8})$$

where $Q = q^N$, $s_\mu(\cdot)$ is a Schur polynomial, and c_μ is the height of the Young diagram of μ . The quantum dimension can also be written as

$$\dim_q(\mu; \nu) = \frac{N_n(\mu; \nu)}{H(\mu)H(\nu)} \quad (\text{A.9})$$

where $H(\mu)$ and $H(\nu)$ are the q -deformed hook length products of the respective Young diagrams with each factor x in the hook length product replaced by the corresponding q -deformed number

$$[x] = \frac{q^{x/2} - q^{-x/2}}{q^{1/2} - q^{-1/2}}. \quad (\text{A.10})$$

$[x]$ usually differs from x but returns to x in the limit $q \rightarrow 1$. Besides the numerator $N_n(\mu; \nu)$ is given by

$$N_n(\mu; \nu) = \prod_{i,j,k,\ell} [N - i - j + \mu_i + \nu_j + 1][N + k + \ell - (\mu^T)_k - (\nu^T)_\ell - 1]. \quad (\text{A.11})$$

In the formula above, $(\mu^T)_k$ and $(\nu^T)_\ell$ are the k -th and ℓ -th components of the transposed partitions, and the right hand side of the formula is multiplied over all the cells with row and column indices (i, j) in the Young diagram of μ as well as all the cells with row and column indices (k, ℓ) in the Young diagram of ν . Whenever j exceeds c_ν or k exceeds c_{μ^T} , the corresponding ν_j or $(\mu^T)_k$ vanishes.

Finally the quantum knot invariants of torus knots colored in composite representations can also be computed using the Rosso–Jones formula. We observe that the quadratic Casimir eigenvalue satisfies [207]

$$C_{(\mu;\nu)} = C_\mu + C_\nu. \quad (\text{A.12})$$

Since the conformal weight h_V in the Rosso–Jones formula eq. (2.158) is proportional to the quadratic Casimir eigenvalue of V , we can immediately write down

$$\mathcal{W}_{(\mu;\nu)}(\mathcal{K}_{r,s}) = \sum_{\substack{\ell(\rho)=r \cdot \ell(\mu) \\ \ell(\sigma)=r \cdot \ell(\nu)}} c_{(\mu;\nu),r}^{(\rho;\sigma)} e^{(h_\rho+h_\sigma) \cdot 2\pi i s/r} \dim_q(\rho; \sigma). \quad (\text{A.13})$$

Here the coefficients of the Adams' operation $c_{(\mu;\nu),r}^{(\rho;\sigma)}$ involving composite representations can be computed using formulae in [205], and some results are given explicitly in [170]. Note the formula above also computes invariants for a torus knot $\mathcal{K}_{r,s}$ in the framing $r \cdot s$.

Calibrated Annulus Kernel

Here we lay out explicitly the calibrated annulus kernel of the trefoil torus knot. It is

$$\widehat{B}_{2,3}(p_1, p_2) = B_{2,3}(p_1, p_2) - \frac{d\alpha_1 d\alpha_2}{(\alpha_1 - \alpha_2)^2}, \quad (\text{B.1})$$

where the uncalibrated annulus kernel has the form

$$B_{2,3}(p_1, p_2) = \frac{U_{2,3}(\alpha_1, \beta_1, \alpha_2, \beta_2; Q) + U_{2,3}(\alpha_2, \beta_2, \alpha_1, \beta_1; Q)}{V_{2,3}(\alpha_1, \beta_1, \alpha_2, \beta_2; Q) + V_{2,3}(\alpha_2, \beta_2, \alpha_1, \beta_1; Q)} d\alpha_1 d\alpha_2, \quad (\text{B.2})$$

with the convention $\alpha_\mu = \alpha(p_\mu), \beta_\mu = \beta(p_\mu), \mu = 1, 2$. The polynomials $U_{2,3}$ and $V_{2,3}$ are respectively

$$\begin{aligned} U_{2,3}(\alpha_1, \beta_1, \alpha_2, \beta_2; Q) = & (1 - Q)\beta_2^3 \\ \times [& Q^2\alpha_2(24Q\alpha_1\beta_2^8 + (11 - 24Q)\alpha_1\beta_2^7 - 6Q^4\beta_2^6 - 2(Q - 4)Q^3\beta_2^5 + 4Q^2(6Q - 5)\beta_2^4 + 2Q(4Q^2 - 9Q + 5)\beta_2^3 \\ & + 4(1 - 3Q)Q\beta_2^2 - 6(Q - 1)Q\beta_2 + 4Q)\beta_1^{10} + \alpha_2(-6Q^4\alpha_1\beta_2^{10} + 6(Q - 1)Q^3\alpha_1\beta_2^9 + 2Q^2(4Q - 19)\alpha_1\beta_2^8 \\ & + Q(-2Q^2 + 61Q - 65)\alpha_1\beta_2^7 - 2(16Q^2 - 41Q + 25)\alpha_1\beta_2^6 + 9Q^4\beta_2^5 + 3Q^2(7Q^2 - 18Q + 5)\beta_2^4 \\ & + 6(Q - 1)^2Q^2\beta_2^3 + 9Q^2\beta_2 - 6(Q - 1)Q^2)\beta_1^9 + \alpha_2(-2(Q - 4)Q^3\alpha_1\beta_2^{10} + Q^2(2Q^2 - 10Q + 17)\alpha_1\beta_2^9 \\ & - 75(Q - 1)Q\alpha_1\beta_2^8 + (24Q^5 + (2Q^3 + 57Q^2 - 240Q + 275)\alpha_1)\beta_2^7 + (2(7Q - 19)Q^4 + (-3Q^2 + 95Q - 140)\alpha_1)\beta_2^6 \\ & + (2(Q^2 - 41Q + 40)Q^3 + (2Q^2 + 29Q - 74)\alpha_1)\beta_2^5 - 4Q^2(12Q^2 - 15Q + 5)\beta_2^4 + 2Q(-4Q^3 + 37Q^2 - 38Q + 5)\beta_2^3 \\ & + 4(1 - 3Q)^2Q\beta_2^2 + 6(Q - 1)^2Q\beta_2 + 4(1 - 3Q)Q)\beta_1^8 + (\alpha_2(4Q^2(6Q - 5)\alpha_1\beta_2^{10} - 4Q(6Q^2 - 11Q + 5)\alpha_1\beta_2^9 \\ & - 8Q(3Q - 2)\alpha_1\beta_2^8 - 26Q^4\beta_2^7 + ((59Q - 71)Q^3 + (46Q - 48)\alpha_1)\beta_2^6 + (Q^2(11Q^2 - 97Q + 132) - 6(3Q - 4)\alpha_1)\beta_2^5 \\ & - 8Q(14Q^2 - 29Q + 15)\beta_2^4 + (-80Q^3 + 197Q^2 - 132Q + 25)\beta_2^3 + (-8Q^3 + 74Q^2 - 76Q + 10)\beta_2^2 \\ & + 3(7Q^2 - 18Q + 5)\beta_2 + 2(4Q^2 - 9Q + 5)) - 13Q^6\beta_2^4)\beta_1^7 - \alpha_2(-2Q(4Q^2 - 9Q + 5)\alpha_1\beta_2^{10} \\ & + (8Q^3 - 47Q^2 + 82Q - 25)\alpha_1\beta_2^9 + 3(2Q^4 + (7Q^2 - 43Q + 40)\alpha_1)\beta_2^8 + (2(19Q - 22)Q^3 + (8Q^2 + 67Q - 97)\alpha_1)\beta_2^7 \\ & + 4(Q - 1)(3(Q - 4)Q^2 - 4\alpha_1)\beta_2^6 - 2(2Q(27Q^2 - 52Q + 25) + (20 - 3Q)\alpha_1)\beta_2^5 - 4(2 - 3Q)^2Q\beta_2^4 \\ & + (8(14Q^2 - 29Q + 15) + 13\alpha_1)\beta_2^3 + 4(12Q^2 - 15Q + 5)\beta_2^2 - 24Q + 20)\beta_1^6 + (Q^2(9Q^4\beta_2^4 + 2(20 - 3Q)Q^2\beta_2^2 \\ & - 6Q(3Q - 4)\beta_2 + 2Q^2 + 29Q - 74)\beta_2^2 + \alpha_2(4(1 - 3Q)Q\alpha_1\beta_2^{10} + (9Q^4 + 2(9Q^2 - 14Q + 5)\alpha_1)\beta_2^9 \\ & + ((-6Q^2 + 42Q - 20)\alpha_1 - 9(Q - 1)Q^3)\beta_2^8 + ((187 - 105Q)Q^2 + (38 - 14Q)\alpha_1)\beta_2^7 - (3Q(16Q^2 - 57Q + 55) \\ & + 4(Q + 7)\alpha_1)\beta_2^6 + (329Q^2 - 690Q + 275)\beta_2^5 + 4(27Q^2 - 52Q + 25)\beta_2^4 + (11Q^2 - 97Q + 132)\beta_2^3 \\ & + 2(Q^2 - 41Q + 40)\beta_2^2 + 9\beta_2 - 2Q + 8))\beta_1^5 + (\beta_2(4Q^6\beta_2^6 - 4Q^4(Q + 7)\beta_2^4 + 16(Q - 1)Q^3\beta_2^3 + 2Q^2(23Q - 24)\beta_2^2 \\ & + Q(-3Q^2 + 95Q - 140)\beta_2 - 32Q^2 + 82Q - 50) + \alpha_2(2Q(2Q^3 - 3(Q - 1)\alpha_1)\beta_2^{10} + (3(2Q^2 - 4Q + 5)\alpha_1 \\ & - 4(Q - 1)Q^3)\beta_2^9 + 2Q^2(3Q - 19)\beta_2^8 + 2(5Q(Q^2 + 3Q - 4) + 3(Q - 4)\alpha_1)\beta_2^7 + 4(Q^3 - 19Q^2 + 41Q - 25)\beta_2^6 \\ & - 3(16Q^2 - 57Q - 3\alpha_1 + 55)\beta_2^5 - 12(Q^2 - 5Q + 4)\beta_2^4 + (59Q - 71)\beta_2^3 + 2(7Q - 19)\beta_2^2 - 6)\beta_1^4 \\ & + (2Q(3Q^2 + 2\alpha_1)\alpha_2\beta_2^{10} - 2(9Q^2 + 5(Q - 1)\alpha_1)\alpha_2\beta_2^9 + (Q(-6Q^2 + 43Q - 25) + (6Q - 20)\alpha_1)\alpha_2\beta_2^8 \\ & + (6Q^5 + (49Q^2 - 290Q + 6\alpha_1 + 275)\alpha_2)\beta_2^7 + 2(3(Q - 4)Q^4 + (5(Q^2 + 3Q - 4) + 2\alpha_1)\alpha_2)\beta_2^6 \\ & + (2(19 - 7Q)Q^3 + (187 - 105Q)\alpha_2)\beta_2^5 + ((-8Q^2 - 67Q + 97)Q^2 + (44 - 38Q)\alpha_2)\beta_2^4 - 26\alpha_2\beta_2^3 \\ & + (2Q^3 + 57Q^2 - 240Q + 24\alpha_2 + 275)\beta_2^2 + (-2Q^2 + 61Q - 65)\beta_2 - 24Q + 11)\beta_1^3 + (2Q^2(3Q - 10)\alpha_2\beta_2^{10} \\ & - 2Q(3Q^2 - 13Q + 10)\alpha_2\beta_2^9 + 16Q\alpha_2\beta_2^8 + (2(3Q - 10)Q^4 + (-6Q^2 + 43Q - 25)\alpha_2)\beta_2^7 + 2(3Q - 19)\alpha_2\beta_2^6 \end{aligned}$$

$$\begin{aligned}
& + (-2(3Q^2 - 21Q + 10)Q^2 - 9(Q-1)\alpha_2)\beta_2^5 - 3(Q(7Q^2 - 43Q + 40) + 2\alpha_2)\beta_2^4 - 8Q(3Q-2)\beta_2^3 - 75(Q-1)\beta_2^2 \\
& + (8Q-38)\beta_2 + 24)\beta_1^2 + \beta_2(-10(Q-1)Q\alpha_2\beta_2^9 + (16Q^2 - 32Q + 25)\alpha_2\beta_2^8 - 2(3Q^2 - 13Q + 10)\alpha_2\beta_2^7 \\
& - 2(5(Q-1)Q^3 + 9\alpha_2)\beta_2^6 + (3Q^2(2Q^2 - 4Q + 5) - 4(Q-1)\alpha_2)\beta_2^5 + (2Q(9Q^2 - 14Q + 5) + 9\alpha_2)\beta_2^4 \\
& + (-8Q^3 + 47Q^2 - 82Q + 25)\beta_2^3 - 4(6Q^2 - 11Q + 5)\beta_2^2 + (2Q^2 - 10Q + 17)\beta_2 + 6(Q-1)\beta_1 \\
& + 2\beta_2(2Q\alpha_2\beta_2^9 - 5(Q-1)\alpha_2\beta_2^8 + (3Q-10)\alpha_2\beta_2^7 + (2Q^3 + 3\alpha_2)\beta_2^6 + (2\alpha_2 - 3(Q-1)Q^2)\beta_2^5 \\
& + 2(1-3Q)Q\beta_2^4 + (4Q^2 - 9Q + 5)\beta_2^3 + 2(6Q-5)\beta_2^2 - (Q-4)\beta_2 - 3) \Big],
\end{aligned}$$

$$V_{2,3}(\alpha_1, \beta_1, \alpha_2, \beta_2; Q) =$$

$$\begin{aligned}
& 24(Q-4)\alpha_1^2\alpha_2^3\beta_2^9\beta_1^9 - 6Q(4Q^2 - 23Q + 25)\alpha_1\alpha_2^3\beta_2^9\beta_1^9 - 2(61Q^3 - 447Q^2 + 975Q - 625)\alpha_1^2\alpha_2^2\beta_2^9\beta_1^9 \\
& + 36Q^5\alpha_1\alpha_2^2\beta_2^9\beta_1^9 + 18(Q-1)Q^4\alpha_1\alpha_2^2\beta_2^8\beta_1^9 - 90(Q-1)Q\alpha_1\alpha_2^3\beta_2^7\beta_1^9 + 36Q^3(Q^2 - 6Q + 5)\alpha_1\alpha_2^3\beta_2^7\beta_1^9 \\
& - 6Q^2(16Q^2 - 35Q + 25)\alpha_1\alpha_2^2\beta_2^8\beta_1^9 - 18Q^2(Q^2 + 4Q - 5)\alpha_1\alpha_2^2\beta_2^5\beta_1^9 + 9Q(3Q^2 - 28Q + 25)\alpha_1\alpha_2^3\beta_2^4\beta_1^9 \\
& + 18(5-3Q)Q^2\alpha_1\alpha_2^2\beta_2^3\beta_1^9 + (132-24Q)\alpha_1^2\alpha_2^3\beta_2^9\beta_1^8 + 6Q(4Q^2 - 21Q + 35)\alpha_1\alpha_2^3\beta_2^9\beta_1^8 + (82Q^3 - 1185Q^2 \\
& + 3120Q - 2125)\alpha_1^2\alpha_2^2\beta_2^9\beta_1^8 + 12Q^4(14Q-23)\alpha_1\alpha_2^2\beta_2^9\beta_1^8 + 4(10Q^3 + 3Q^2 - 63Q + 50)\alpha_1^2\alpha_2^2\beta_2^8\beta_1^8 \\
& - 6Q^3(37Q^2 - 92Q + 55)\alpha_1\alpha_2^2\beta_2^8\beta_1^8 + 54(Q-1)Q\alpha_1\alpha_2^3\beta_2^7\beta_1^8 - 6Q^2(6Q^3 - 14Q^2 - 17Q + 25)\alpha_1\alpha_2^3\beta_2^7\beta_1^8 \\
& + 6Q(16Q^3 - 98Q^2 + 225Q - 125)\alpha_1\alpha_2^2\beta_2^6\beta_1^8 + 6Q(9Q^3 - 32Q^2 + 73Q - 50)\alpha_1\alpha_2^2\beta_2^5\beta_1^8 - 9Q(17Q^2 - 52Q \\
& + 35)\alpha_1\alpha_2^2\beta_2^4\beta_1^8 - 6Q(Q^2 - 33Q + 50)\alpha_1\alpha_2^2\beta_2^3\beta_1^8 - 36\alpha_1^2\alpha_2^3\beta_2^9\beta_1^7 + 20(Q^2 - 5Q - 5)\alpha_1\alpha_2^3\beta_2^9\beta_1^7 \\
& - 3(8Q^3 - 163Q^2 + 518Q - 375)\alpha_1^2\alpha_2^3\beta_2^9\beta_1^7 + 2Q^3(47Q^2 - 487Q + 530)\alpha_1\alpha_2^3\beta_2^9\beta_1^7 + 6(4Q^3 - 43Q^2 + 104Q \\
& - 65)\alpha_1^2\alpha_2^2\beta_2^8\beta_1^7 + Q^2(-94Q^3 + 1167Q^2 - 2448Q + 1375)\alpha_1\alpha_2^2\beta_2^8\beta_1^7 + 12(Q^2 + 4Q - 5)\alpha_1\alpha_2^3\beta_2^7\beta_1^7 \\
& + 12(4Q^2 - 5Q + 1)\alpha_1^2\alpha_2^3\beta_2^7\beta_1^7 + Q(-373Q^3 + 2013Q^2 - 3015Q + 1375)\alpha_1\alpha_2^3\beta_2^7\beta_1^7 + 2(72Q^3 + 163Q^2 \\
& - 950Q + 625)\alpha_1\alpha_2^2\beta_2^6\beta_1^7 - 2(6Q^4 + 10Q^3 + 9Q^2 + 225Q - 250)\alpha_1\alpha_2^2\beta_2^5\beta_1^7 + 6(7Q^3 + 23Q^2 - 55Q \\
& + 25)\alpha_1\alpha_2^2\beta_2^4\beta_1^7 + 20(Q^3 + 8Q^2 - 25Q + 25)\alpha_1\alpha_2^2\beta_2^3\beta_1^7 - 12Q^3(2Q^2 - 7Q + 5)\alpha_2^3\beta_2^9\beta_1^6 + 4(6Q^3 - 26Q^2 \\
& - 8Q + 55)\alpha_1\alpha_2^3\beta_2^9\beta_1^6 + 24(5Q^2 - 18Q + 10)\alpha_1^2\alpha_2^3\beta_2^9\beta_1^6 + 2Q^2(-61Q^3 + 256Q^2 - 338Q + 125)\alpha_1\alpha_2^2\beta_2^9\beta_1^6 \\
& + 36Q^7\alpha_1\alpha_2\beta_2^9\beta_1^6 + 54(Q-1)Q^6\alpha_2^3\beta_2^8\beta_1^6 - 12(10Q^2 - 57Q + 38)\alpha_1^2\alpha_2^3\beta_2^8\beta_1^6 + Q(-40Q^4 + 438Q^3 - 2451Q^2 \\
& + 5320Q - 3375)\alpha_1\alpha_2^2\beta_2^8\beta_1^6 + 12Q^6(14Q-23)\alpha_1\alpha_2\beta_2^8\beta_1^6 - 36(Q-1)Q^3\alpha_2^3\beta_2^7\beta_1^6 - 36(3Q-2)\alpha_1^2\alpha_2^2\beta_2^7\beta_1^6 \\
& + 18Q^5(2Q^2 - 7Q + 5)\alpha_2^2\beta_2^7\beta_1^6 - (24Q^5 - 204Q^4 + 329Q^3 + 915Q^2 - 1725Q + 625)\alpha_1\alpha_2^2\beta_2^7\beta_1^6 \\
& + 2Q^5(47Q^2 - 433Q + 476)\alpha_1\alpha_2\beta_2^7\beta_1^6 - 72(Q-1)\alpha_1^2\alpha_2^3\beta_2^6\beta_1^6 - 12Q^4(17Q^2 - 37Q + 20)\alpha_2^3\beta_2^6\beta_1^6 \\
& + 2(68Q^4 + 67Q^3 - 1261Q^2 + 2055Q - 875)\alpha_1\alpha_2^2\beta_2^6\beta_1^6 - 2Q^4(245Q^2 - 745Q + 554)\alpha_1\alpha_2\beta_2^6\beta_1^6 \\
& - 36Q^4(2Q^2 - 3Q + 1)\alpha_2^2\beta_2^5\beta_1^6 + 2(24Q^4 - 50Q^3 - 90Q^2 + 441Q - 325)\alpha_1\alpha_2^2\beta_2^5\beta_1^6 + 18Q^3(3Q^2 - 8Q \\
& + 5)\alpha_2^3\beta_2^4\beta_1^6 - 24(Q-1)^2(2Q-5)\alpha_1\alpha_2^2\beta_2^4\beta_1^6 + 36(Q-1)Q^4\alpha_2^3\beta_2^3\beta_1^6 - 4(6Q^3 + 19Q^2 - 98Q + 100)\alpha_1\alpha_2^2\beta_2^3\beta_1^6 \\
& - 90(Q-1)Q^5\alpha_2\beta_2^3\beta_1^6 + 36(Q-1)Q^4\alpha_2\beta_2^6\beta_1^6 - 18Q^4(2Q^2 - 7Q + 5)\alpha_2\beta_2\beta_1^6 + 12(Q^2 + 10Q - 11)\alpha_1\alpha_2^3\beta_2^9\beta_1^5 \\
& + 12(4Q^2 - 17Q + 13)\alpha_1^2\alpha_2^2\beta_2^9\beta_1^5 + Q(-323Q^3 + 1593Q^2 - 2145Q + 875)\alpha_1\alpha_2^2\beta_2^9\beta_1^5 - 24(2Q^2 - 13Q \\
& + 11)\alpha_1^2\alpha_2^2\beta_2^8\beta_1^5 + (206Q^4 - 2094Q^3 + 6888Q^2 - 8750Q + 3750)\alpha_1\alpha_2^3\beta_2^8\beta_1^5 - 36(Q-1)\alpha_1\alpha_2^3\beta_2^7\beta_1^5 \\
& - 108(Q-1)\alpha_1^2\alpha_2^3\beta_2^7\beta_1^5 - 12(2Q^4 - 58Q^3 + 241Q^2 - 310Q + 125)\alpha_1\alpha_2^2\beta_2^7\beta_1^5 + 243Q^4(Q^2 - 4Q + 3)\alpha_1\alpha_2\beta_2^7\beta_1^5 \\
& + 288(Q-1)Q\alpha_1\alpha_2^2\beta_2^6\beta_1^5 - Q^3(188Q^3 - 891Q^2 + 588Q + 115)\alpha_1\alpha_2\beta_2^6\beta_1^5 + 8(13Q^3 - 9Q^2 + 6Q - 10)\alpha_1\alpha_2^2\beta_2^5\beta_1^5 \\
& - 2Q^2(319Q^3 - 1755Q^2 + 2661Q - 1225)\alpha_1\alpha_2\beta_2^5\beta_1^5 - 18(7Q^2 - 16Q + 9)\alpha_1\alpha_2^2\beta_2^4\beta_1^5 - 24(4Q^2 + Q - 5)\alpha_1\alpha_2^2\beta_2^3\beta_1^5 \\
& + 4Q(14Q^3 - 21Q^2 - 18Q + 25)\alpha_2^3\beta_2^9\beta_1^4 - 12(4Q^2 - 17Q + 13)\alpha_1\alpha_2^3\beta_2^9\beta_1^4 - 108(Q-1)Q^5\alpha_2^2\beta_2^9\beta_1^4 \\
& - 72(Q-1)\alpha_1^2\alpha_2^2\beta_2^9\beta_1^4 + 2(130Q^4 - 749Q^3 + 1944Q^2 - 2575Q + 1250)\alpha_1\alpha_2^2\beta_2^9\beta_1^4 - 126(Q-1)Q^5\alpha_1\alpha_2\beta_2^9\beta_1^4 \\
& + 72(Q-1)\alpha_1^2\alpha_2^2\beta_2^8\beta_1^4 - 18Q^4(5Q^2 - 16Q + 11)\alpha_2^3\beta_2^8\beta_1^4 + (64Q^4 - 349Q^3 + 315Q^2 + 845Q - 875)\alpha_1\alpha_2^3\beta_2^8\beta_1^4 \\
& - 6Q^4(41Q^2 - 127Q + 86)\alpha_1\alpha_2\beta_2^8\beta_1^4 + 12Q(Q^2 + 4Q - 5)\alpha_2^3\beta_2^7\beta_1^4 - 6Q^3(10Q^3 - 87Q^2 + 132Q - 55)\alpha_2^2\beta_2^7\beta_1^4 \\
& + 6(8Q^4 - 73Q^3 + 259Q^2 - 319Q + 125)\alpha_1\alpha_2^2\beta_2^7\beta_1^4 - 2Q^3(100Q^3 - 861Q^2 + 1566Q - 805)\alpha_1\alpha_2\beta_2^7\beta_1^4 \\
& + 4Q^2(77Q^3 - 147Q^2 + 45Q + 25)\alpha_2^2\beta_2^6\beta_1^4 + (-208Q^3 + 708Q^2 - 540Q + 40)\alpha_1\alpha_2^2\beta_2^6\beta_1^4 + 6Q^2(145Q^3 - 439Q^2 \\
& + 419Q - 125)\alpha_1\alpha_2\beta_2^6\beta_1^4 + 12Q^2(10Q^3 - 31Q^2 + 26Q - 5)\alpha_2^2\beta_2^5\beta_1^4 - 6(16Q^3 - 87Q^2 + 132Q - 61)\alpha_1\alpha_2^2\beta_2^5\beta_1^4 \\
& + Q(400Q^4 - 2773Q^3 + 6543Q^2 - 6295Q + 2125)\alpha_1\alpha_2\beta_2^5\beta_1^4 - 6Q(15Q^3 - 17Q^2 - 23Q + 25)\alpha_2^3\beta_2^4\beta_1^4 \\
& + 48(Q^2 - 5Q + 4)\alpha_1\alpha_2^2\beta_2^4\beta_1^4 + 72(Q-1)Q^5\alpha_2\beta_2^4\beta_1^4 - 2(Q-1)^2(53Q^2 + 350Q - 625)\alpha_1\alpha_2\beta_2^4\beta_1^4 \\
& - 60(Q-1)^2Q^2\alpha_2^2\beta_2^3\beta_1^4 + 12(4Q^2 - 17Q + 13)\alpha_1\alpha_2^2\beta_2^3\beta_1^4 + 108(Q-1)Q^4\alpha_2\beta_2^3\beta_1^4 + 30Q^3(5Q^2 - 16Q + 11)\alpha_2\beta_2^2\beta_1^4 \\
& - 60(Q-1)^2Q^2\alpha_2\beta_1^4 + 30(Q-1)^2Q^2(2Q-5)\alpha_2\beta_2\beta_1^4 + 6Q(14Q^2 - 43Q + 35)\alpha_2^3\beta_2^9\beta_1^3 - 24(4Q-7)\alpha_1\alpha_2^3\beta_2^9\beta_1^3
\end{aligned}$$

$$\begin{aligned}
& -36Q^4\alpha_2^2\beta_2^9\beta_1^3 - 24(Q-4)\alpha_1^2\alpha_2^2\beta_2^9\beta_1^3 + (700Q^3 - 4164Q^2 + 7320Q - 4000)\alpha_1\alpha_2^2\beta_2^9\beta_1^3 - 36Q^4(3Q-2)\alpha_1\alpha_2\beta_2^9\beta_1^3 \\
& + 12(2Q-11)\alpha_1^2\alpha_2^2\beta_2^8\beta_1^3 - 27Q^3(7Q^2 - 22Q + 15)\alpha_2^2\beta_2^8\beta_1^3 + (8Q^3 + 819Q^2 - 2244Q + 1525)\alpha_1\alpha_2^2\beta_2^8\beta_1^3 \\
& - 6Q^3(93Q^2 - 266Q + 155)\alpha_1\alpha_2\beta_2^8\beta_1^3 + 54(Q-1)Q\alpha_2^3\beta_2^7\beta_1^3 + 36\alpha_1^2\alpha_2^2\beta_2^7\beta_1^3 - 9Q^2(14Q^3 - 51Q^2 + 62Q - 25)\alpha_2^2\beta_2^7\beta_1^3 \\
& + (116Q^3 - 597Q^2 + 1260Q - 815)\alpha_1\alpha_2^2\beta_2^7\beta_1^3 + 2Q^2(-348Q^3 + 2122Q^2 - 3239Q + 1375)\alpha_1\alpha_2\beta_2^7\beta_1^3 \\
& + 6Q(117Q^3 - 386Q^2 + 400Q - 125)\alpha_2^2\beta_2^6\beta_1^3 - 12(31Q^2 - 60Q + 23)\alpha_1\alpha_2^2\beta_2^6\beta_1^3 - 36Q^6\alpha_2\beta_2^6\beta_1^3 \\
& + 2Q(47Q^4 + 758Q^3 - 4147Q^2 + 5985Q - 2625)\alpha_1\alpha_2\beta_2^6\beta_1^3 + 12Q(25Q^3 - 69Q^2 + 69Q - 25)\alpha_2^2\beta_2^5\beta_1^3 \\
& - 12(23Q^2 - 49Q + 26)\alpha_1\alpha_2^2\beta_2^5\beta_1^3 + 72(Q-1)Q^5\alpha_2\beta_2^5\beta_1^3 + (1859Q^4 - 10557Q^3 + 19323Q^2 - 14375Q \\
& + 3750)\alpha_1\alpha_2\beta_2^5\beta_1^3 - 9Q(9Q^2 - 44Q + 35)\alpha_2^2\beta_2^4\beta_1^3 + 72(Q-1)\alpha_1\alpha_2^2\beta_2^4\beta_1^3 + 126(Q-1)Q^4\alpha_2\beta_2^4\beta_1^3 \\
& - 2(100Q^4 - 592Q^3 + 1827Q^2 - 2710Q + 1375)\alpha_1\alpha_2\beta_2^4\beta_1^3 - 6Q(29Q^2 - 73Q + 50)\alpha_2^2\beta_2^3\beta_1^3 + 24(7Q-10)\alpha_1\alpha_2^2\beta_2^3\beta_1^3 \\
& + 12Q^3(4Q^2 - 11Q + 10)\alpha_2\beta_2^3\beta_1^3 - 4(200Q^3 - 1041Q^2 + 1623Q - 800)\alpha_1\alpha_2\beta_2^3\beta_1^3 + 9Q^2(17Q^2 - 42Q + 25)\alpha_2\beta_2^2\beta_1^3 \\
& - 6Q(29Q^2 - 73Q + 50)\alpha_2\beta_1^3 + 6Q(29Q^3 - 129Q^2 + 225Q - 125)\alpha_2\beta_2\beta_1^3 - 2(20Q^3 + 24Q^2 - 165Q + 175)\alpha_2^3\beta_2^9\beta_1^2 \\
& + 12(2Q-11)\alpha_1\alpha_2^3\beta_2^9\beta_1^2 + 6Q^3(33Q^2 - 100Q + 85)\alpha_2^2\beta_2^9\beta_1^2 - 3(46Q^3 - 385Q^2 + 928Q - 625)\alpha_1\alpha_2^2\beta_2^9\beta_1^2 \\
& + 18Q^3(3Q^2 - 13Q + 10)\alpha_1\alpha_2\beta_2^9\beta_1^2 + 12Q^3(2Q^2 - 13Q + 11)\alpha_2^2\beta_2^8\beta_1^2 - 12(Q-1)^2(2Q-5)\alpha_1\alpha_2^2\beta_2^8\beta_1^2 \\
& + 6Q^2(15Q^3 - 37Q^2 + 47Q - 25)\alpha_1\alpha_2\beta_2^8\beta_1^2 - 90(Q-1)\alpha_2^3\beta_2^7\beta_1^2 + 2Q(20Q^4 - 2Q^3 - 423Q^2 + 655Q - 250)\alpha_2^2\beta_2^7\beta_1^2 \\
& - 12(2Q^3 - 17Q^2 + 52Q - 37)\alpha_1\alpha_2^2\beta_2^7\beta_1^2 - 162(Q-1)Q^6\alpha_2\beta_2^7\beta_1^2 + Q(114Q^4 - 1015Q^3 + 2541Q^2 - 3015Q \\
& + 1375)\alpha_1\alpha_2\beta_2^7\beta_1^2 - 2(28Q^4 + 124Q^3 - 798Q^2 + 1325Q - 625)\alpha_2^2\beta_2^6\beta_1^2 + 12(6Q^2 - 37Q + 22)\alpha_1\alpha_2^2\beta_2^6\beta_1^2 \\
& - 6Q^5(7Q-25)\alpha_2\beta_2^6\beta_1^2 + (-222Q^4 + 1015Q^3 - 2535Q^2 + 2475Q - 625)\alpha_1\alpha_2\beta_2^6\beta_1^2 - 10(Q-1)^2(8Q^2 + 15Q \\
& - 50)\alpha_2^2\beta_2^5\beta_1^2 + 24(2Q^2 - 13Q + 11)\alpha_1\alpha_2^2\beta_2^5\beta_1^2 + 324(Q-1)^2Q^4\alpha_2\beta_2^5\beta_1^2 - 2(114Q^4 - 946Q^3 + 2817Q^2 - 3360Q \\
& + 1375)\alpha_1\alpha_2\beta_2^5\beta_1^2 + (-48Q^3 + 423Q^2 - 900Q + 525)\alpha_2^2\beta_2^4\beta_1^2 + 18Q^3(26Q^2 - 71Q + 45)\alpha_2\beta_2^4\beta_1^2 - 12(10Q^3 \\
& - 97Q^2 + 212Q - 125)\alpha_1\alpha_2\beta_2^4\beta_1^2 + 2(20Q^3 + 9Q^2 - 225Q + 250)\alpha_2^2\beta_2^3\beta_1^2 + (132 - 24Q)\alpha_1\alpha_2^2\beta_2^3\beta_1^2 - 6Q^2(27Q^3 \\
& - 117Q^2 + 233Q - 125)\alpha_2\beta_2^3\beta_1^2 + 3(38Q^3 - 313Q^2 + 694Q - 455)\alpha_1\alpha_2\beta_2^3\beta_1^2 - 2Q(41Q^3 + 114Q^2 - 405Q \\
& + 250)\alpha_2\beta_2^2\beta_1^2 + 12(2Q^2 - 13Q + 11)\alpha_1\alpha_2\beta_2^2\beta_1^2 + 2(20Q^3 + 9Q^2 - 225Q + 250)\alpha_2\beta_1^2 + (-40Q^4 - 161Q^3 \\
& + 1476Q^2 - 2525Q + 1250)\alpha_2\beta_2\beta_1^2 + (-80Q^2 + 40Q + 220)\alpha_2^3\beta_2^9\beta_1 + 36\alpha_1\alpha_2^3\beta_2^9\beta_1 + 2Q^2(88Q^2 - 53Q \\
& - 125)\alpha_2^2\beta_2^9\beta_1 - 3(61Q^2 - 194Q + 145)\alpha_1\alpha_2^2\beta_2^9\beta_1 + 45Q^2(3Q^2 - 8Q + 5)\alpha_1\alpha_2\beta_2^9\beta_1 + Q(184Q^3 - 1629Q^2 \\
& + 3570Q - 2125)\alpha_2^2\beta_2^8\beta_1 - 12(5Q^2 - 28Q + 23)\alpha_1\alpha_2^2\beta_2^8\beta_1 + 3Q(47Q^3 - 272Q^2 + 475Q - 250)\alpha_1\alpha_2\beta_2^8\beta_1 \\
& + 5(12Q^4 - 43Q^3 - 39Q^2 + 195Q - 125)\alpha_2^2\beta_2^7\beta_1 - 36(Q-1)^2\alpha_1\alpha_2^2\beta_2^7\beta_1 + (151Q^4 - 1007Q^3 + 2631Q^2 - 3025Q \\
& + 1250)\alpha_1\alpha_2\beta_2^7\beta_1 - 10(22Q^3 + 71Q^2 - 286Q + 175)\alpha_2^2\beta_2^6\beta_1 + 36(3Q-2)\alpha_1\alpha_2^2\beta_2^6\beta_1 - 2Q^4(47Q^2 - 325Q \\
& + 368)\alpha_2\beta_2^6\beta_1 + (24Q^4 - 437Q^3 + 1467Q^2 - 1215Q + 125)\alpha_1\alpha_2\beta_2^6\beta_1 + (-76Q^3 + 24Q^2 + 702Q - 650)\alpha_2^2\beta_2^5\beta_1 \\
& + 72(Q-1)\alpha_1\alpha_2^2\beta_2^5\beta_1 - 15Q^3(29Q^2 - 100Q + 71)\alpha_2\beta_2^5\beta_1 - 6(41Q^3 - 219Q^2 + 303Q - 125)\alpha_1\alpha_2\beta_2^5\beta_1 \\
& - 24(Q^2 + 4Q - 5)\alpha_2^2\beta_2^4\beta_1 + 2Q^2(100Q^3 - 717Q^2 + 1242Q - 625)\alpha_2\beta_2^4\beta_1 - 24(2Q^3 - 11Q^2 + 19Q - 10)\alpha_1\alpha_2\beta_2^4\beta_1 \\
& + 4(2Q^2 + 53Q - 100)\alpha_2^2\beta_2^3\beta_1 - 36\alpha_1\alpha_2^2\beta_2^3\beta_1 + 2Q(436Q^3 - 2581Q^2 + 4235Q - 2000)\alpha_2\beta_2^3\beta_1 + 3(Q^2 - 32Q \\
& + 43)\alpha_1\alpha_2\beta_2^3\beta_1 + 162(Q-1)Q^5\beta_2^3\beta_1 + (-114Q^4 + 829Q^3 - 1815Q^2 + 1725Q - 625)\alpha_2\beta_2^2\beta_1 + 24(Q^2 - 5Q \\
& + 4)\alpha_1\alpha_2\beta_2^2\beta_1 + 4(2Q^2 + 53Q - 100)\alpha_2\beta_1 - 72(Q-1)Q^4\beta_2\beta_1 + (-179Q^3 + 519Q^2 - 465Q + 125)\alpha_2\beta_2\beta_1 \\
& + 36(Q-1)\alpha_1\alpha_2\beta_2\beta_1 - 4(4Q^2 - 50Q + 73)\alpha_2^3\beta_2^9 + 2Q(46Q^3 - 493Q^2 + 965Q - 500)\alpha_2^2\beta_2^9 - 24(Q-4)\alpha_1\alpha_2^2\beta_2^9 \\
& - 36Q^6\alpha_2\beta_2^9 + 18(5-3Q)Q^2\alpha_1\alpha_2\beta_2^9 + 2(8Q^4 - 168Q^3 + 1464Q^2 - 3125Q + 1875)\alpha_2^2\beta_2^8 + 12(2Q-11)\alpha_1\alpha_2^2\beta_2^8 \\
& + 12(14-5Q)Q^5\alpha_2\beta_2^8 - 6Q(Q^2 - 33Q + 50)\alpha_1\alpha_2\beta_2^8 + (16Q^4 - 228Q^3 + 981Q^2 - 1180Q + 375)\alpha_2^2\beta_2^7 \\
& + 36\alpha_1\alpha_2^2\beta_2^7 - 2Q^4(38Q^2 - 361Q + 413)\alpha_2\beta_2^7 + 20(Q^3 + 8Q^2 - 25Q + 25)\alpha_1\alpha_2\beta_2^7 + (-48Q^3 + 548Q^2 \\
& - 1108Q + 500)\alpha_2^2\beta_2^6 + 2Q^3(145Q^2 - 692Q + 655)\alpha_2\beta_2^6 - 4(6Q^3 + 19Q^2 - 98Q + 100)\alpha_1\alpha_2\beta_2^6 + (-32Q^3 \\
& + 348Q^2 - 1086Q + 770)\alpha_2^2\beta_2^5 + Q^2(152Q^3 - 873Q^2 + 696Q + 25)\alpha_2\beta_2^5 - 24(4Q^2 + Q - 5)\alpha_1\alpha_2\beta_2^5 - 76Q^4 \\
& + 72(Q-1)\alpha_2^2\beta_2^4 + 2Q(-92Q^3 + 327Q^2 - 360Q + 125)\alpha_2\beta_2^4 + 12(4Q^2 - 17Q + 13)\alpha_1\alpha_2\beta_2^4 + 518Q^3 + 36Q^5\beta_2^3 \\
& + 4(4Q^2 - 32Q + 55)\alpha_2^2\beta_2^3 + (-76Q^4 - 298Q^3 + 4088Q^2 - 7500Q + 3750)\alpha_2\beta_2^3 + 24(7Q-10)\alpha_1\alpha_2\beta_2^3 - 550Q^2 \\
& - 6Q^4(17Q+1)\beta_2^2 + (98Q^3 - 651Q^2 + 1320Q - 875)\alpha_2\beta_2^2 + (132-24Q)\alpha_1\alpha_2\beta_2^2 + 4(4Q^2 - 32Q + 55)\alpha_2 \\
& + 2Q^3(38Q^2 - 253Q + 305)\beta_2 + (-16Q^3 + 315Q^2 - 888Q + 625)\alpha_2\beta_2 - 36\alpha_1\alpha_2\beta_2.
\end{aligned}$$

The numerator of the kernel $B_{2,3}(p_1, p_2)$ is of degree one in α_μ and degree 13 in β_μ for $\mu = 1, 2$, while its denominator is of degree 3 in α_μ and degree 9 in β_μ for $\mu = 1, 2$.

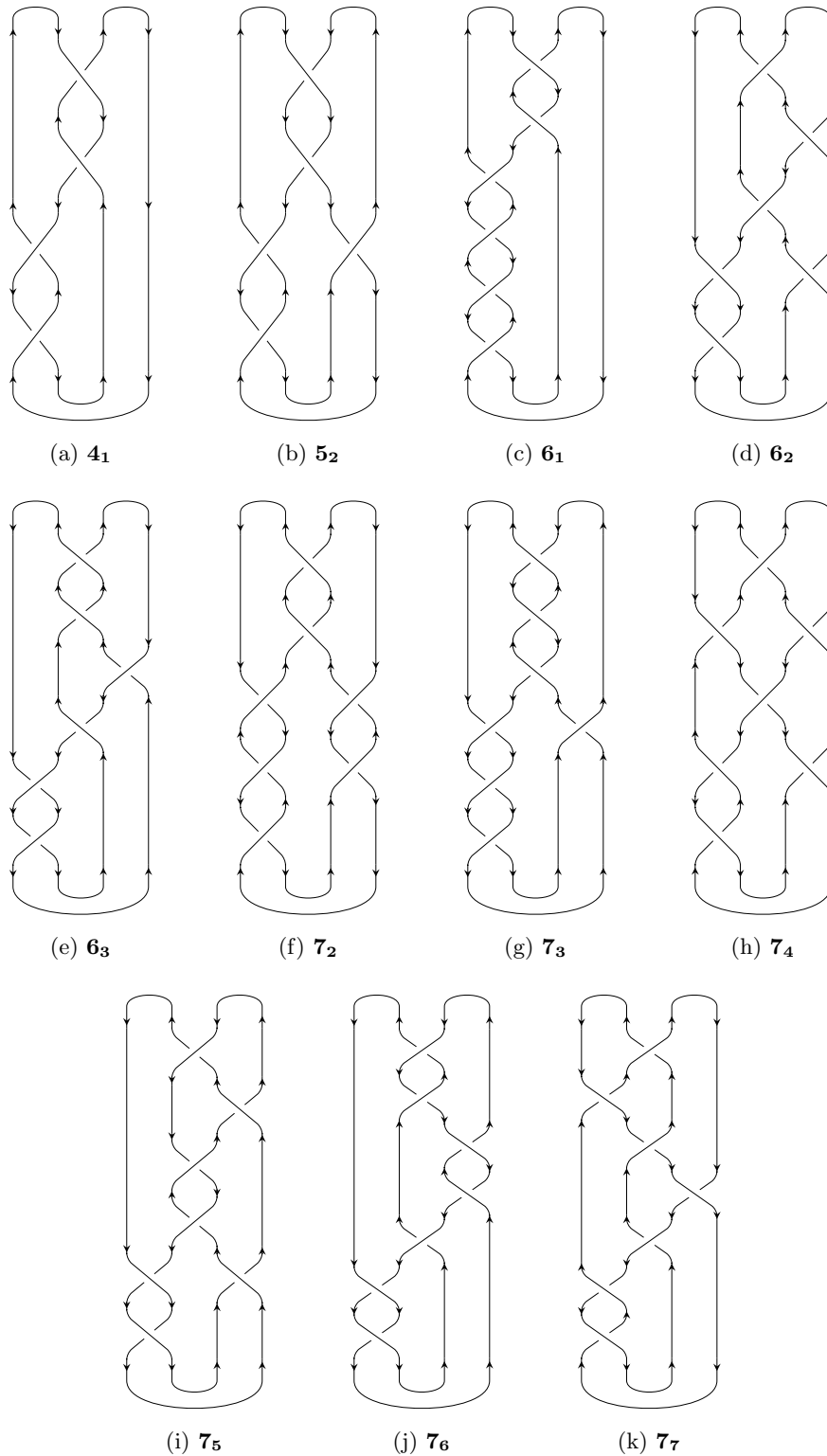


Figure B.1: Quasi-plat presentations of hyperbolic knots with up to seven crossings.

Bibliography

- [1] S. R. Coleman and J. Mandula, *All Possible Symmetries of the S Matrix*, Phys.Rev. **159** (1967) 1251–1256 (cit. on p. 1).
- [2] R. Haag, J. T. Lopuszanski and M. Sohnius, *All Possible Generators of Supersymmetries of the s Matrix*, Nucl.Phys. **B88** (1975) 257 (cit. on p. 1).
- [3] J. Wess and J. Bagger, *Supersymmetry and Supergravity*, Princeton University Press, 1992 (cit. on p. 2).
- [4] J. Polchinski, *String Theory. Vol. 1: An Introduction to the Bosonic String*, Cambridge University Press, 1998 (cit. on p. 2).
- [5] J. Polchinski, *String Theory. Vol. 2: Superstring Theory and Beyond*, Cambridge University Press, 1998 (cit. on p. 2).
- [6] M. B. Green, J. Schwarz and E. Witten, *Superstring Theory. Vol. 2: Loop Amplitudes, Anomalies and Phenomenology*, Cambridge University Press, 1987 (cit. on p. 2).
- [7] M. B. Green, J. Schwarz and E. Witten, *Superstring Theory. Vol. 1: Introduction*, Cambridge University Press, 1987 (cit. on p. 2).
- [8] R. Blumenhagen, D. Lüüst and S. Theisen, *Basic Concepts of String Theory*, Springer, 2013 (cit. on p. 2).
- [9] K. Becker, M. Becker and J. Schwarz, *String Theory and M-Theory: A Modern Introduction*, Cambridge University Press, 2007 (cit. on p. 2).
- [10] F. Gliozzi, J. Scherk and D. I. Olive, *Supersymmetry, Supergravity Theories and the Dual Spinor Model*, Nucl.Phys. **B122** (1977) 253–290 (cit. on p. 2).
- [11] F. Gmeiner et al., *One in a billion: MSSM-like D-brane statistics*, JHEP **0601** (2006) 004, arXiv: hep-th/0510170 [hep-th] (cit. on p. 2).
- [12] M. J. Dolan, S. Krippendorff and F. Quevedo, *Towards a Systematic Construction of Realistic D-brane Models on a del Pezzo Singularity*, JHEP **1110** (2011) 024, arXiv: 1106.6039 [hep-th] (cit. on p. 2).
- [13] H. P. Nilles et al., *The Orbifolder: A Tool to study the Low Energy Effective Theory of Heterotic Orbifolds*, Comput.Phys.Commun. **183** (2012) 1363–1380, arXiv: 1110.5229 [hep-th] (cit. on p. 2).
- [14] V. Braun, Y.-H. He and B. A. Ovrut, *Supersymmetric Hidden Sectors for Heterotic Standard Models*, JHEP **1309** (2013) 008, arXiv: 1301.6767 [hep-th] (cit. on p. 2).

- [15] S. Groot Nibbelink and O. Loukas, *MSSM-like models on $Z(8)$ toroidal orbifolds*, JHEP **1312** (2013) 044, arXiv: 1308.5145 [hep-th] (cit. on p. 2).
- [16] E. Palti, “Review of model building in string theory”, Talk presented at the String Phenomenology 2014, ICTP, Trieste, Italy, July 2014, URL: <http://stringpheno2014.ictp.it/lecturenotes/Palti.pdf> (cit. on p. 2).
- [17] J. M. Maldacena, *The Large N limit of superconformal field theories and supergravity*, Int.J.Theor.Phys. **38** (1999) 1113–1133, arXiv: hep-th/9711200 [hep-th] (cit. on pp. 3, 56).
- [18] G. 't Hooft, *Dimensional reduction in quantum gravity* (1993) 0284–296, arXiv: gr-qc/9310026 [gr-qc] (cit. on p. 3).
- [19] I. Antoniadis et al., *Topological amplitudes in string theory*, Nucl.Phys. **B413** (1994) 162–184, arXiv: hep-th/9307158 [hep-th] (cit. on p. 4).
- [20] E. Witten, *Quantum field theory and the Jones polynomial*, Commun.Math.Phys. **121** (1989) 351–399 (cit. on pp. 5, 37, 39–42, 100).
- [21] R. Gopakumar and C. Vafa, *On the gauge theory / geometry correspondence*, Adv.Theor.Math.Phys. **3** (1999) 1415–1443, arXiv: hep-th/9811131 [hep-th] (cit. on pp. 5, 57).
- [22] B. Eynard and N. Orantin, *Invariants of algebraic curves and topological expansion*, Commun.Num.Theor.Phys. **1** (2007) 347–452, arXiv: math-ph/0702045 [math-ph] (cit. on pp. 5, 61, 63–65, 135).
- [23] B. Eynard and N. Orantin, *Algebraic methods in random matrices and enumerative geometry* (2008), arXiv: 0811.3531 [math-ph] (cit. on pp. 5, 61, 63–65, 135).
- [24] B. Eynard, *A short overview of the “Topological recursion”* (2014), arXiv: 1412.3286 [math-ph] (cit. on pp. 5, 61).
- [25] H. Ooguri and C. Vafa, *Knot invariants and topological strings*, Nucl.Phys. **B577** (2000) 419–438, arXiv: hep-th/9912123 [hep-th] (cit. on pp. 5, 29, 45, 66, 70, 135).
- [26] P. Freyd et al., *A new polynomial invariant of knots and links*, Bull. Amer. Math. Soc. (N.S.) **12.2** (1985) 239–246, ISSN: 0273-0979 (cit. on pp. 5, 39).
- [27] Y. Hatsuda et al., *Non-perturbative effects and the refined topological string*, JHEP **1409** (2014) 168, arXiv: 1306.1734 [hep-th] (cit. on p. 6).
- [28] A. Grassi, Y. Hatsuda and M. Marino, *Topological strings from quantum mechanics* (2014), arXiv: 1410.3382 [hep-th] (cit. on p. 6).
- [29] M. Marino and S. Zakany, *Matrix models from operators and topological strings* (2015), arXiv: 1502.02958 [hep-th] (cit. on pp. 6, 68, 83).
- [30] J. Gu et al., *work in progress* (201x) (cit. on p. 6).
- [31] K. Hori et al., *Mirror Symmetry*, American Mathematical Society, 2003 (cit. on pp. 7–9, 11, 13, 22, 23, 34).
- [32] E. Witten, *Mirror manifolds and topological field theory* (1991), arXiv: hep-th/9112056 [hep-th] (cit. on pp. 10, 11, 13, 14, 17).

-
- [33] E. Witten, *Topological sigma models*, Commun.Math.Phys. **118** (1988) 411 (cit. on p. 11).
- [34] C. Vafa, *Topological Landau-Ginzburg models*, Mod.Phys.Lett. **A6** (1991) 337–346 (cit. on p. 11).
- [35] J. Labastida and P. Llatas, *Topological matter in two-dimensions*, Nucl.Phys. **B379** (1992) 220–258, arXiv: hep-th/9112051 [hep-th] (cit. on pp. 11, 13).
- [36] M. Marino, *Chern-Simons Theory, Matrix Models, and Topological Strings*, vol. 131, Oxford Science Publications, 2005 1–197 (cit. on pp. 12, 13, 22, 28, 30, 37, 44, 48, 49, 53).
- [37] P. Candelas and X. de la Ossa, *Moduli space of Calabi-Yau manifolds*, Nucl.Phys. **B355** (1991) 455–481 (cit. on p. 18).
- [38] A. Strominger, *Special geometry*, Commun.Math.Phys. **133** (1990) 163–180 (cit. on p. 18).
- [39] R. L. Bryant and P. A. Griffiths, “Some observations on the infinitesimal period relations for regular threefolds with trivial canonical bundle”, *Arithmetic and geometry, Vol. II*, vol. 36, Progr. Math. Birkhäuser Boston, Boston, MA, 1983 77–102 (cit. on p. 19).
- [40] G. Tian, “Smoothness of the universal deformation space of compact Calabi-Yau manifolds and its Petersson-Weil metric”, *Mathematical aspects of string theory (San Diego, Calif., 1986)*, vol. 1, Adv. Ser. Math. Phys. World Sci. Publishing, Singapore, 1987 629–646 (cit. on p. 19).
- [41] A. N. Todorov, *The Weil-Petersson geometry of the moduli space of $SU(n \geq 3)$ (Calabi-Yau) manifolds. I*, Comm. Math. Phys. **126.2** (1989) 325–346, ISSN: 0010-3616 (cit. on p. 19).
- [42] V. I. Arnold, S. M. Gusein-Zade and A. N. Varchenko, *Singularities of differentiable maps. Volume 1*, Modern Birkhäuser Classics, Classification of critical points, caustics and wave fronts, Translated from the Russian by Ian Porteous based on a previous translation by Mark Reynolds, Reprint of the 1985 edition, Birkhäuser/Springer, New York, 2012 xii+382, ISBN: 978-0-8176-8339-9 (cit. on p. 20).
- [43] V. I. Arnold, S. M. Gusein-Zade and A. N. Varchenko, *Singularities of differentiable maps. Volume 2*, Modern Birkhäuser Classics, Monodromy and asymptotics of integrals, Translated from the Russian by Hugh Porteous and revised by the authors and James Montaldi, Reprint of the 1988 translation, Birkhäuser/Springer, New York, 2012 x+492, ISBN: 978-0-8176-8342-9 (cit. on p. 20).
- [44] M. Bershadsky et al., *Extended $N=2$ superconformal structure of gravity and W gravity coupled to matter*, Nucl.Phys. **B401** (1993) 304–347, arXiv: hep-th/9211040 [hep-th] (cit. on p. 21).
- [45] R. Dijkgraaf, H. L. Verlinde and E. P. Verlinde, *Notes on topological string theory and 2-D quantum gravity* (1990) (cit. on p. 21).

- [46] B. Gato-Rivera and A. Semikhatov, $d \leq 1$ $ud \Rightarrow 25$ and W constraints from BRST invariance in the c does not = 3 topological algebra, Phys.Lett. **B293** (1992) 72–80, arXiv: hep-th/9207004 [hep-th] (cit. on p. 21).
- [47] M. Bershadsky et al.,
Kodaira-Spencer theory of gravity and exact results for quantum string amplitudes, Commun.Math.Phys. **165** (1994) 311–428, arXiv: hep-th/9309140 [hep-th] (cit. on pp. 21, 22, 31, 34).
- [48] P. Deligne and D. Mumford, *The irreducibility of the space of curves of given genus*, Inst. Hautes Études Sci. Publ. Math. **36** (1969) 75–109, ISSN: 0073-8301 (cit. on p. 22).
- [49] P. S. Aspinwall, *Compactification, geometry and duality: $N=2$* (2000) 723–805, arXiv: hep-th/0001001 [hep-th] (cit. on p. 22).
- [50] M. Aganagic and C. Vafa, *Mirror symmetry, D-branes and counting holomorphic discs* (2000), arXiv: hep-th/0012041 [hep-th] (cit. on pp. 22, 28, 35).
- [51] M. Aganagic, V. Bouchard and A. Klemm,
Topological strings and (almost) modular forms, Commun.Math.Phys. **277** (2008) 771–819, arXiv: hep-th/0607100 [hep-th] (cit. on pp. 22, 32, 68).
- [52] B. Eynard and N. Orantin, *Computation of open Gromov-Witten invariants for toric Calabi-Yau 3-folds by topological recursion, a proof of the BKMP conjecture* (2012), arXiv: 1205.1103 [math-ph] (cit. on pp. 22, 29, 69, 135).
- [53] E. Witten, *Two-dimensional gravity and intersection theory on moduli space*, Surveys Diff.Geom. **1** (1991) 243–310 (cit. on p. 23).
- [54] M. Kontsevich,
Intersection theory on the moduli space of curves and the matrix Airy function, Comm. Math. Phys. **147.1** (1992) 1–23, ISSN: 0010-3616 (cit. on p. 23).
- [55] M. Kontsevich, “Enumeration of rational curves via torus actions”,
The moduli space of curves (Texel Island, 1994), vol. 129, Progr. Math. Birkhäuser Boston, Boston, MA, 1995 335–368 (cit. on p. 23).
- [56] D. Cox and S. Katz, *Mirror Symmetry and Algebraic Geometry*, American Mathematical Society, 2000 (cit. on pp. 23, 34).
- [57] C. Faber and R. Pandharipande, *Hodge integrals and Gromov-Witten theory*, Invent. Math. **139.1** (2000) 173–199, ISSN: 0020-9910, arXiv: math/9810173 [math] (cit. on p. 23).
- [58] T. Chiang et al., *Local mirror symmetry: Calculations and interpretations*, Adv.Theor.Math.Phys. **3** (1999) 495–565, arXiv: hep-th/9903053 [hep-th] (cit. on p. 23).
- [59] A. Klemm and E. Zaslow, *Local mirror symmetry at higher genus* (1999), arXiv: hep-th/9906046 [hep-th] (cit. on p. 23).
- [60] W. Fulton, *Introduction to Toric Varieties*, vol. 131, Annals of Mathematics Studies, The William H. Roever Lectures in Geometry, Princeton University Press, Princeton, NJ, 1993 xii+157, ISBN: 0-691-00049-2 (cit. on p. 23).

-
- [61] P. S. Aspinwall, B. R. Greene and D. R. Morrison, *Calabi-Yau moduli space, mirror manifolds and space-time topology change in string theory*, Nucl.Phys. **B416** (1994) 414–480, arXiv: hep-th/9309097 [hep-th] (cit. on p. 23).
- [62] V. Bouchard, *Lectures on complex geometry, Calabi-Yau manifolds and toric geometry* (2007), arXiv: hep-th/0702063 [hep-th] (cit. on p. 23).
- [63] D.-E. Diaconescu and B. Florea, *Localization and gluing of topological amplitudes*, Commun.Math.Phys. **257** (2005) 119–149, arXiv: hep-th/0309143 [hep-th] (cit. on p. 25).
- [64] J. Li et al., *A mathematical theory of the topological vertex*, Geom. Topol. **13.1** (2009) 527–621, ISSN: 1465-3060 (cit. on p. 25).
- [65] R. Gopakumar and C. Vafa, *M theory and topological strings. 2.* (1998), arXiv: hep-th/9812127 [hep-th] (cit. on p. 26).
- [66] P. Candelas et al., *A pair of Calabi-Yau manifolds as an exactly soluble superconformal theory*, Nucl.Phys. **B359** (1991) 21–74 (cit. on pp. 26, 33).
- [67] P. S. Aspinwall and D. R. Morrison, *Topological field theory and rational curves*, Commun.Math.Phys. **151** (1993) 245–262, arXiv: hep-th/9110048 [hep-th] (cit. on p. 26).
- [68] E. Witten, *Chern-Simons gauge theory as a string theory*, Prog.Math. **133** (1995) 637–678, arXiv: hep-th/9207094 [hep-th] (cit. on pp. 26, 33, 46, 47).
- [69] H. Ooguri, Y. Oz and Z. Yin, *D-branes on Calabi-Yau spaces and their mirrors*, Nucl.Phys. **B477** (1996) 407–430, arXiv: hep-th/9606112 [hep-th] (cit. on p. 26).
- [70] K. Hori, A. Iqbal and C. Vafa, *D-branes and mirror symmetry* (2000), arXiv: hep-th/0005247 [hep-th] (cit. on p. 26).
- [71] P. Mayr, *Summing up open string instantons and $N=1$ string amplitudes* (2002), arXiv: hep-th/0203237 [hep-th] (cit. on p. 28).
- [72] T. Graber and E. Zaslow, “Open-string Gromov-Witten invariants: calculations and a mirror “theorem””, *Orbifolds in mathematics and physics (Madison, WI, 2001)*, vol. 310, Contemp. Math. Amer. Math. Soc., Providence, RI, 2002 107–121 (cit. on p. 28).
- [73] J. Li and Y. S. Song, *Open string instantons and relative stable morphisms*, Adv. Theor. Math. Phys. **5.1** (2001) 67–91, ISSN: 1095-0761 (cit. on p. 28).
- [74] S. Katz and C.-C. M. Liu, *Enumerative geometry of stable maps with Lagrangian boundary conditions and multiple covers of the disc*, Adv. Theor. Math. Phys. **5.1** (2001) 1–49, ISSN: 1095-0761 (cit. on p. 28).
- [75] R. Harvey and H. B. Lawson Jr., *Calibrated geometries*, Acta Math. **148** (1982) 47–157, ISSN: 0001-5962 (cit. on p. 28).
- [76] J. Labastida, M. Marino and C. Vafa, *Knots, links and branes at large N* , JHEP **0011** (2000) 007, arXiv: hep-th/0010102 [hep-th] (cit. on pp. 29, 30, 66, 70).
- [77] M. Marino and C. Vafa, *Framed knots at large N* , Contemp.Math. **310** (2002) 185–204, arXiv: hep-th/0108064 [hep-th] (cit. on pp. 30, 77).

- [78] K. Kodaira, L. Nirenberg and D. C. Spencer,
On the existence of deformations of complex analytic structures,
Ann. of Math. (2) **68** (1958) 450–459, ISSN: 0003-486X (cit. on p. 31).
- [79] K. Kodaira and D. C. Spencer, *On deformations of complex analytic structures. I, II*,
Ann. of Math. (2) **67** (1958) 328–466, ISSN: 0003-486X (cit. on p. 31).
- [80] K. Kodaira and D. C. Spencer,
A theorem of completeness for complex analytic fibre spaces,
Acta Math. **100** (1958) 281–294, ISSN: 0001-5962 (cit. on p. 31).
- [81] K. Kodaira and D. C. Spencer, *On deformations of complex analytic structures. III. Stability theorems for complex structures*, Ann. of Math. (2) **71** (1960) 43–76,
ISSN: 0003-486X (cit. on p. 31).
- [82] M. Bershadsky et al., *Holomorphic anomalies in topological field theories*,
Nucl.Phys. **B405** (1993) 279–304, arXiv: hep-th/9302103 [hep-th] (cit. on p. 31).
- [83] B. Eynard and M. Marino, *A holomorphic and background independent partition function for matrix models and topological strings*, J.Geom.Phys. **61** (2011) 1181–1202,
arXiv: 0810.4273 [hep-th] (cit. on p. 32).
- [84] M.-x. Huang, A. Klemm and S. Quackenbush,
Topological string theory on compact Calabi-Yau: Modularity and boundary conditions,
Lect.Notes Phys. **757** (2009) 45–102, arXiv: hep-th/0612125 [hep-th] (cit. on p. 32).
- [85] B. Haghighat, A. Klemm and M. Rauch,
Integrability of the holomorphic anomaly equations, JHEP **0810** (2008) 097,
arXiv: 0809.1674 [hep-th] (cit. on p. 32).
- [86] M.-X. Huang, A. Klemm and M. Poretschkin,
Refined stable pair invariants for E -, M - and $[p, q]$ -strings, JHEP **1311** (2013) 112,
arXiv: 1308.0619 [hep-th] (cit. on p. 32).
- [87] A. Klemm et al., *Direct integration for mirror curves of genus two and an almost meromorphic siegel modular form* (2015), arXiv: 1502.00557 [hep-th] (cit. on p. 32).
- [88] S. Yamaguchi and S.-T. Yau, *Topological string partition functions as polynomials*,
JHEP **0407** (2004) 047, arXiv: hep-th/0406078 [hep-th] (cit. on p. 32).
- [89] M. Alim and J. D. Lange,
Polynomial structure of the (open) topological string partition function,
JHEP **0710** (2007) 045, arXiv: 0708.2886 [hep-th] (cit. on p. 32).
- [90] T. W. Grimm et al., *Direct Integration of the Topological String*,
JHEP **0708** (2007) 058, arXiv: hep-th/0702187 [HEP-TH] (cit. on p. 32).
- [91] P. S. Aspinwall, *D-branes on Calabi-Yau manifolds* (2004) 1–152,
arXiv: hep-th/0403166 [hep-th] (cit. on p. 33).
- [92] L. J. Dixon,
Some world sheet properties of superstring compactifications, on orbifolds and otherwise
(1987) (cit. on p. 33).
- [93] W. Lerche, C. Vafa and N. P. Warner, *Chiral rings in $N=2$ superconformal theories*,
Nucl.Phys. **B324** (1989) 427 (cit. on p. 33).

-
- [94] B. R. Greene and M. Plesser, *Duality in Calabi-Yau Moduli Space*, Nucl.Phys. **B338** (1990) 15–37 (cit. on p. 33).
- [95] P. Candelas et al., *An exactly soluble superconformal theory from a mirror pair of Calabi-Yau manifolds*, Phys.Lett. **B258** (1991) 118–126 (cit. on p. 33).
- [96] D. R. Morrison, *Picard-Fuchs equations and mirror maps for hypersurfaces* (1991), arXiv: hep-th/9111025 [hep-th] (cit. on p. 33).
- [97] A. Font, *Periods and duality symmetries in Calabi-Yau compactifications*, Nucl.Phys. **B391** (1993) 358–388, arXiv: hep-th/9203084 [hep-th] (cit. on p. 33).
- [98] A. Klemm and S. Theisen, *Considerations of one modulus Calabi-Yau compactifications: Picard-Fuchs equations, Kahler potentials and mirror maps*, Nucl.Phys. **B389** (1993) 153–180, arXiv: hep-th/9205041 [hep-th] (cit. on p. 33).
- [99] A. Libgober and J. Teitelbaum, *Lines on Calabi-Yau complete intersections, mirror symmetry, and Picard-Fuchs equations* (1993), arXiv: alg-geom/9301001 [alg-geom] (cit. on p. 33).
- [100] P. Candelas et al., *Mirror symmetry for two parameter models. 1.*, Nucl.Phys. **B416** (1994) 481–538, arXiv: hep-th/9308083 [hep-th] (cit. on p. 33).
- [101] V. V. Batyrev and D. van Straten, *Generalized hypergeometric functions and rational curves on Calabi-Yau complete intersections in toric varieties*, Commun.Math.Phys. **168** (1995) 493–534, arXiv: alg-geom/9307010 [alg-geom] (cit. on p. 33).
- [102] S. Hosono et al., *Mirror symmetry, mirror map and applications to Calabi-Yau hypersurfaces*, Commun.Math.Phys. **167** (1995) 301–350, arXiv: hep-th/9308122 [hep-th] (cit. on p. 33).
- [103] S. Hosono et al., *Mirror symmetry, mirror map and applications to complete intersection Calabi-Yau spaces*, Nucl.Phys. **B433** (1995) 501–554, arXiv: hep-th/9406055 [hep-th] (cit. on p. 33).
- [104] A. Strominger, S.-T. Yau and E. Zaslow, *Mirror symmetry is T duality*, Nucl.Phys. **B479** (1996) 243–259, arXiv: hep-th/9606040 [hep-th] (cit. on p. 33).
- [105] V. V. Batyrev, *Dual polyhedra and mirror symmetry for Calabi-Yau hypersurfaces in toric varieties*, J.Alg.Geom. **3** (1994) 493–545, arXiv: alg-geom/9310003 [alg-geom] (cit. on p. 33).
- [106] A. Givental, *Equivariant Gromov-Witten invariants*, Internat. Math. Res. Notices **13** (1996) 613–663, ISSN: 1073-7928 (cit. on p. 33).
- [107] B. H. Lian, K. Liu and S.-T. Yau, *Mirror principle. I*, Asian J. Math. **1.4** (1997) 729–763, ISSN: 1093-6106 (cit. on p. 33).
- [108] A. Givental, “A mirror theorem for toric complete intersections”, *Topological field theory, primitive forms and related topics (Kyoto, 1996)*, vol. 160, Progr. Math. Birkhäuser Boston, Boston, MA, 1998 141–175 (cit. on p. 33).
- [109] K. Hori and C. Vafa, *Mirror symmetry* (2000), arXiv: hep-th/0002222 [hep-th] (cit. on p. 34).

- [110] S. Hosono, A. Klemm and S. Theisen, *Lectures on mirror symmetry*, Lect.Notes Phys. **436** (1994) 235, arXiv: hep-th/9403096 [hep-th] (cit. on p. 34).
- [111] B. R. Greene, *String theory on Calabi-Yau manifolds* (1996) 543–726, arXiv: hep-th/9702155 [hep-th] (cit. on p. 34).
- [112] M. Aganagic, A. Klemm and C. Vafa, *Disk instantons, mirror symmetry and the duality web*, Z.Naturforsch. **A57** (2002) 1–28, arXiv: hep-th/0105045 [hep-th] (cit. on pp. 35, 36).
- [113] V. Bouchard et al., *Remodeling the B-model*, Commun.Math.Phys. **287** (2009) 117–178, arXiv: 0709.1453 [hep-th] (cit. on pp. 36, 68, 93, 135).
- [114] M. Aganagic et al., *Matrix model as a mirror of Chern-Simons theory*, JHEP **0402** (2004) 010, arXiv: hep-th/0211098 [hep-th] (cit. on pp. 37, 56, 68).
- [115] M. Aganagic and C. Vafa, *$G(2)$ manifolds, mirror symmetry and geometric engineering* (2001), arXiv: hep-th/0110171 [hep-th] (cit. on pp. 37, 68).
- [116] W. B. R. Lickorish, *An Introduction to Knot Theory*, vol. 175, Graduate Texts in Mathematics, Springer-Verlag, New York, 1997 x+201, ISBN: 0-387-98254-X (cit. on p. 39).
- [117] C. C. Adams, *The Knot Book*, An elementary introduction to the mathematical theory of knots, W. H. Freeman and Company, New York, 1994 xiv+306, ISBN: 0-7167-2393-X (cit. on pp. 39, 97).
- [118] K. Kawagoe, *On the formulae for the colored HOMFLY polynomials* (2012), arXiv: 1210.7574 [math.GT] (cit. on pp. 40, 70, 99).
- [119] J. Gu and H. Jockers, *A note on colored HOMFLY polynomials for hyperbolic knots from WZW models* (2014), arXiv: 1407.5643 [hep-th] (cit. on pp. 41, 70, 101, 116, 129, 136).
- [120] P. Di Francesco, P. Mathieu and D. Senechal, *Conformal Field Theory*, Springer, 1997 (cit. on pp. 42, 103).
- [121] M. Rosso and V. Jones, *On the invariants of torus knots derived from quantum groups*, J.Knot Theor.Ramifications **2** (1993) 97 (cit. on pp. 43, 70).
- [122] S. Stevan, *Chern-Simons invariants of torus links*, Annales Henri Poincare **11** (2010) 1201–1224, arXiv: 1003.2861 [hep-th] (cit. on p. 43).
- [123] H. Jockers, A. Klemm and M. Soroush, *Torus knots and the topological vertex*, Lett.Math.Phys. **104** (2014) 953–989, arXiv: 1212.0321 [hep-th] (cit. on pp. 44, 73, 74).
- [124] Zodinmawia and P. Ramadevi, *$SU(N)$ quantum Racah coefficients & non-torus links*, Nucl.Phys. **B870** (2013) 205–242, arXiv: 1107.3918 [hep-th] (cit. on pp. 44, 70, 99, 100, 136).
- [125] H. Itoyama et al., *HOMFLY and superpolynomials for figure eight knot in all symmetric and antisymmetric representations*, JHEP **1207** (2012) 131, arXiv: 1203.5978 [hep-th] (cit. on pp. 44, 70, 99).

-
- [126] G. 't Hooft, *A planar diagram theory for strong interactions*, Nucl.Phys. **B72** (1974) 461 (cit. on pp. 45, 56).
- [127] P. Di Francesco, P. H. Ginsparg and J. Zinn-Justin, *2-D gravity and random matrices*, Phys.Rept. **254** (1995) 1–133, arXiv: hep-th/9306153 [hep-th] (cit. on pp. 48, 59).
- [128] P. Di Francesco, *Matrix model combinatorics: Applications to folding and coloring* (1999), arXiv: math-ph/9911002 [math-ph] (cit. on p. 48).
- [129] P. Di Francesco, *2D quantum gravity, matrix models and graph combinatorics* (2004) 33–88, arXiv: math-ph/0406013 [math-ph] (cit. on p. 48).
- [130] E. Brezin et al., *Planar Diagrams*, Commun.Math.Phys. **59** (1978) 35 (cit. on p. 50).
- [131] L. Chekhov et al., *Complex geometry of matrix models*, Proc.Steklov Inst.Math. **251** (2005) 254–292, arXiv: hep-th/0506075 [hep-th] (cit. on pp. 53, 60).
- [132] L. Chekhov and B. Eynard, *Hermitean matrix model free energy: Feynman graph technique for all genera*, JHEP **0603** (2006) 014, arXiv: hep-th/0504116 [hep-th] (cit. on pp. 53, 60).
- [133] M. Marino, *Chern-Simons theory, matrix integrals, and perturbative three manifold invariants*, Commun.Math.Phys. **253** (2004) 25–49, arXiv: hep-th/0207096 [hep-th] (cit. on p. 53).
- [134] P. J. Forrester, *Properties of an exact crystalline many-body ground state*, Journal of statistical physics **76** (1994) 331–346 (cit. on p. 54).
- [135] M. Tierz, *Soft matrix models and Chern-Simons partition functions*, Mod.Phys.Lett. **A19** (2004) 1365–1378, arXiv: hep-th/0212128 [hep-th] (cit. on p. 54).
- [136] R. Dijkgraaf and C. Vafa, *Matrix models, topological strings, and supersymmetric gauge theories*, Nucl.Phys. **B644** (2002) 3–20, arXiv: hep-th/0206255 [hep-th] (cit. on pp. 55, 57).
- [137] M. Mariño, *Lectures on non-perturbative effects in large N gauge theories, matrix models and strings*, Fortsch.Phys. **62** (2014) 455–540, arXiv: 1206.6272 [hep-th] (cit. on p. 56).
- [138] S. R. Wadia, *On the Dyson-Schwinger equations approach to the large N limit: model systems and string representation of Yang-Mills theory*, Phys.Rev. **D24** (1981) 970 (cit. on p. 59).
- [139] A. A. Migdal, *Loop equations and $1/N$ expansion*, Phys.Rept. **102** (1983) 199–290 (cit. on p. 59).
- [140] F. David, *Loop equations and nonperturbative effects in two-dimensional quantum gravity*, Mod.Phys.Lett. **A5** (1990) 1019–1030 (cit. on p. 59).
- [141] Y. Makeenko, *Loop equations in matrix models and in 2-D quantum gravity*, Mod.Phys.Lett. **A6** (1991) 1901–1913 (cit. on p. 59).

- [142] B. Eynard, *Topological expansion for the 1-Hermitian matrix model correlation functions*, JHEP **0411** (2004) 031, arXiv: hep-th/0407261 [hep-th] (cit. on pp. 59, 60, 69, 83).
- [143] V. Bouchard et al., *A generalized topological recursion for arbitrary ramification*, Annales Henri Poincare **15** (2014) 143–169, arXiv: 1208.6035 [math-ph] (cit. on p. 61).
- [144] V. Bouchard and B. Eynard, *Think globally, compute locally*, JHEP **1302** (2013) 143, arXiv: 1211.2302 [math-ph] (cit. on p. 61).
- [145] A. P. Ferrer, *New recursive residue formulas for the topological expansion of the Cauchy Matrix Model*, JHEP **1010** (2010) 090, arXiv: 0912.2984 [math-ph] (cit. on p. 61).
- [146] A. Bilal, *Duality in $N=2$ SUSY $SU(2)$ Yang-Mills theory: A Pedagogical introduction to the work of Seiberg and Witten* (1995) 21–43, arXiv: hep-th/9601007 [hep-th] (cit. on p. 61).
- [147] W. Lerche, *Introduction to Seiberg-Witten theory and its stringy origin*, Nucl.Phys.Proc.Suppl. **55B** (1997) 83–117, arXiv: hep-th/9611190 [hep-th] (cit. on p. 61).
- [148] N. Seiberg and E. Witten, *Monopoles, duality and chiral symmetry breaking in $N=2$ supersymmetric QCD*, Nucl.Phys. **B431** (1994) 484–550, arXiv: hep-th/9408099 [hep-th] (cit. on p. 61).
- [149] N. Seiberg and E. Witten, *Electric - magnetic duality, monopole condensation, and confinement in $N=2$ supersymmetric Yang-Mills theory*, Nucl.Phys. **B426** (1994) 19–52, arXiv: hep-th/9407087 [hep-th] (cit. on p. 61).
- [150] B. Eynard and N. Orantin, *About the x - y symmetry of the F_g algebraic invariants* (2013), arXiv: 1311.4993 [math-ph] (cit. on p. 63).
- [151] B. Eynard and N. Orantin, *Topological expansion of mixed correlations in the hermitian 2 Matrix Model and x - y symmetry of the $F(g)$ invariants* (2007), arXiv: 0705.0958 [math-ph] (cit. on p. 63).
- [152] B. Eynard, M. Marino and N. Orantin, *Holomorphic anomaly and matrix models*, JHEP **0706** (2007) 058, arXiv: hep-th/0702110 [HEP-TH] (cit. on p. 66).
- [153] C. H. Taubes, *Lagrangians for the Gopakumar-Vafa conjecture*, Adv.Theor.Math.Phys. **5** (2001) 139–163, arXiv: math/0201219 [math-dg] (cit. on pp. 66, 70).
- [154] D. Diaconescu, V. Shende and C. Vafa, *Large N duality, lagrangian cycles, and algebraic knots*, Commun.Math.Phys. **319** (2013) 813–863, arXiv: 1111.6533 [hep-th] (cit. on pp. 66, 70, 77, 90).
- [155] D.-E. Diaconescu, B. Florea and A. Grassi, *Geometric transitions, del Pezzo surfaces and open string instantons*, Adv.Theor.Math.Phys. **6** (2003) 643–702, arXiv: hep-th/0206163 [hep-th] (cit. on p. 68).

-
- [156] M. Marino, *Open string amplitudes and large order behavior in topological string theory*, JHEP **0803** (2008) 060, arXiv: hep-th/0612127 [hep-th] (cit. on pp. 68, 93, 135).
- [157] G. Bertoldi, *Double scaling limits and twisted non-critical superstrings*, JHEP **0607** (2006) 006, arXiv: hep-th/0603075 [hep-th] (cit. on p. 69).
- [158] G. Akemann, *Higher genus correlators for the Hermitian matrix model with multiple cuts*, Nucl.Phys. **B482** (1996) 403–430, arXiv: hep-th/9606004 [hep-th] (cit. on pp. 69, 80).
- [159] L. Chen, *Bouchard-Klemm-Marino-Pasquetti conjecture for C^{**3}* (2009), arXiv: 0910.3739 [math.AG] (cit. on p. 69).
- [160] J. Zhou, *Local mirror symmetry for one-legged topological vertex* (2009), arXiv: 0910.4320 [math.AG] (cit. on p. 69).
- [161] B. Eynard and N. Orantin, *Geometrical interpretation of the topological recursion, and integrable string theories* (2009), arXiv: 0911.5096 [math-ph] (cit. on pp. 69, 83, 84).
- [162] B. Eynard, *Invariants of spectral curves and intersection theory of moduli spaces of complex curves*, Commun.Num.TheorPhys. **08** (2014) 541–588, arXiv: 1110.2949 [math-ph] (cit. on p. 69).
- [163] K. Liu and P. Peng, *Proof of the Labastida-Marino-Ooguri-Vafa conjecture* (2007), arXiv: 0704.1526 [math.QA] (cit. on p. 70).
- [164] K. Liu and P. Peng, *On a proof of the Labastida-Marino-Ooguri-Vafa conjecture*, Math.Res.Lett. **17** (2010) 493–506, arXiv: 1012.2635 [math.GT] (cit. on p. 70).
- [165] K. Liu and P. Peng, *New Structure of Knot Invariants* (2010), arXiv: 1012.2636 [math.GT] (cit. on p. 70).
- [166] P. Rama Devi, T. Govindarajan and R. Kaul, *Three-dimensional Chern-Simons theory as a theory of knots and links. 3. Compact semisimple group*, Nucl.Phys. **B402** (1993) 548–566, arXiv: hep-th/9212110 [hep-th] (cit. on pp. 70, 99, 100, 136).
- [167] S. Nawata et al., *Super- A -polynomials for Twist Knots*, JHEP **1211** (2012) 157, arXiv: 1209.1409 [hep-th] (cit. on pp. 70, 99).
- [168] H. Itoyama et al., *Eigenvalue hypothesis for Racah matrices and HOMFLY polynomials for 3-strand knots in any symmetric and antisymmetric representations*, Int.J.Mod.Phys. **A28** (2013) 1340009, arXiv: 1209.6304 [math-ph] (cit. on pp. 70, 99).
- [169] S. Nawata, P. Ramadevi and Zodinmawia, *Colored HOMFLY polynomials from Chern-Simons theory*, J.Knot Theor. **22** (2013) 1350078, arXiv: 1302.5144 [hep-th] (cit. on pp. 70, 99, 100).
- [170] J. Gu et al., *Knot invariants from topological recursion on augmentation varieties* (2014), arXiv: 1401.5095 [hep-th] (cit. on pp. 70, 84, 90, 91, 93, 95, 96, 135, 139).

- [171] S. Garoufalidis and M. Marino, *On Chern-Simons matrix models* (2006), arXiv: math/0601390 [math-gt] (cit. on p. 71).
- [172] A. Brini, B. Eynard and M. Marino, *Torus knots and mirror symmetry*, Annales Henri Poincaré **13** (2012) 1873–1910, arXiv: 1105.2012 [hep-th] (cit. on pp. 71, 73).
- [173] M. Aganagic and C. Vafa, *Large N Duality, Mirror Symmetry, and a Q-deformed A-polynomial for Knots* (2012), arXiv: 1204.4709 [hep-th] (cit. on pp. 71, 75, 96).
- [174] G. Borot, B. Eynard and N. Orantin, *Abstract loop equations, topological recursion, and applications* (2013), arXiv: 1303.5808 [math-ph] (cit. on p. 73).
- [175] B. Buchberger, *An algorithm for finding the basis elements of the residue class ring of a zero dimensional polynomial ideal*, J. Symbolic Comput. **41.3-4** (2006) 475–511, Translated from the 1965 German original by Michael P. Abramson, ISSN: 0747-7171 (cit. on p. 74).
- [176] D. Cox, J. Little and D. O’Shea, *Ideals, varieties, and algorithms*, Third, Undergraduate Texts in Mathematics, An introduction to computational algebraic geometry and commutative algebra, Springer, New York, 2007 xvi+551, ISBN: 978-0-387-35650-1; 0-387-35650-9 (cit. on p. 74).
- [177] M. Aganagic et al., *Topological strings and integrable hierarchies*, Commun.Math.Phys. **261** (2006) 451–516, arXiv: hep-th/0312085 [hep-th] (cit. on p. 76).
- [178] L. Ng, *Knot and braid invariants from contact homology. I*, Geom. Topol. **9** (2005) 247–297 (electronic), ISSN: 1465-3060 (cit. on p. 77).
- [179] L. Ng, *Knot and braid invariants from contact homology. II*, Geom. Topol. **9** (2005) 1603–1637 (electronic), With an appendix by the author and Siddhartha Gadgil, ISSN: 1465-3060 (cit. on p. 77).
- [180] L. Ng, *Framed knot contact homology*, Duke Math. J. **141.2** (2008) 365–406, ISSN: 0012-7094 (cit. on p. 77).
- [181] L. Ng, *Combinatorial knot contact homology and transverse knots*, Adv. Math. **227.6** (2011) 2189–2219, ISSN: 0001-8708 (cit. on p. 77).
- [182] L. Ng, *A topological introduction to knot contact homology* (2012), arXiv: 1210.4803 [math.GT] (cit. on pp. 77, 78).
- [183] T. Ekholm et al., *Knot contact homology*, Geom. Topol. **17.2** (2013) 975–1112, ISSN: 1465-3060 (cit. on p. 77).
- [184] M. Aganagic et al., *Topological strings, D-model, and knot contact homology*, Adv.Theor.Math.Phys. **18** (2014) 827–956, arXiv: 1304.5778 [hep-th] (cit. on p. 78).
- [185] H. M. Farkas and I. Kra, *Riemann surfaces*, Second, vol. 71, Graduate Texts in Mathematics, Springer-Verlag, New York, 1992 xvi+363, ISBN: 0-387-97703-1 (cit. on p. 82).

-
- [186] M. Marino, *String theory and the Kauffman polynomial*, Commun.Math.Phys. **298** (2010) 613–643, arXiv: 0904.1088 [hep-th] (cit. on p. 90).
- [187] V. Bouchard and P. Sulkowski, *Topological recursion and mirror curves*, Adv.Theor.Math.Phys. **16** (2012) 1443–1483, arXiv: 1105.2052 [hep-th] (cit. on p. 95).
- [188] H. R. Morton and P. R. Cromwell, *Distinguishing mutants by knot polynomials*, J. Knot Theory Ramifications **5.2** (1996) 225–238, ISSN: 0218-2165 (cit. on p. 98).
- [189] T. Ohtsuki, *Quantum Invariants*, vol. 29, Series on Knots and Everything, A study of knots, 3-manifolds, and their sets, World Scientific Publishing Co., Inc., River Edge, NJ, 2002 xiv+489, ISBN: 981-02-4675-7 (cit. on p. 98).
- [190] A. Anokhina et al., *Knot polynomials in the first non-symmetric representation*, Nucl.Phys. **B882** (2014) 171–194, arXiv: 1211.6375 [hep-th] (cit. on pp. 99, 133).
- [191] A. Anokhina and A. Morozov, *Cabling procedure for the colored HOMFLY polynomials*, Teor.Mat.Fiz. **178** (2014) 3–68, arXiv: 1307.2216 [hep-th] (cit. on pp. 99, 133).
- [192] S. Nawata, P. Ramadevi and Zodinmawia, *Multiplicity-free quantum 6j-symbols for $U_q(\mathfrak{sl}_N)$* , Lett.Math.Phys. **103** (2013) 1389–1398, arXiv: 1302.5143 [hep-th] (cit. on p. 99).
- [193] P. Butler, *Point Group Symmetry Applications: Methods and Tables*, Plenum Press, 1981 (cit. on pp. 99, 116, 117, 119).
- [194] R. W. Haase and R. Dirl, *The symmetric group: algebraic formulas for some S_f 6j symbols and $S_f \supset S_{f_1} \times S_{f_2}$ 3jm symbols*, J. Math. Phys. **27.4** (1986) 900–913, ISSN: 0022-2488 (cit. on p. 99).
- [195] P. Cvitanović, *Group theory*, Princeton University Press, Princeton, NJ, 2008 xiv+273, ISBN: 978-0-691-11836-9 (cit. on p. 99).
- [196] H. Elvang, P. Cvitanović and A. D. Kennedy, “Diagrammatic young projection operators for $U(n)$ ”, 2003 (cit. on p. 99).
- [197] P. Ramadevi and T. Sarkar, *On link invariants and topological string amplitudes*, Nucl.Phys. **B600** (2001) 487–511, arXiv: hep-th/0009188 [hep-th] (cit. on pp. 100, 136).
- [198] J. Fuchs, *Affine Lie Algebras and Quantum Groups: An Introduction, with Applications in Conformal Field Theory*, Cambridge University Press, 1992 (cit. on pp. 109, 110).
- [199] C. R. Lienert and P. H. Butler, *Racah-Wigner algebra for q-deformed algebras*, Journal of Physics A: Mathematical and General **25.5** (1992) 1223 (cit. on pp. 113, 116).
- [200] R. W. Haase, *The symmetric group and the unitary group: An application of group-subgroup transformation theory*, PhD thesis: University of Canterbury. Physics, 1983 (cit. on pp. 116–118).
- [201] B. Searle, *Calculation of 6j symbols*, PhD thesis: University of Canterbury. Physics, 1988 (cit. on pp. 116, 119, 120).

- [202] L. Chekhov and B. Eynard, *Matrix eigenvalue model: Feynman graph technique for all genera*, JHEP **0612** (2006) 026, arXiv: math-ph/0604014 [math-ph] (cit. on p. 136).
- [203] M. Aganagic and S. Shakhmurov, *Knot homology from refined Chern-Simons theory* (2011), arXiv: 1105.5117 [hep-th] (cit. on p. 136).
- [204] N. M. Dunfield, S. Gukov and J. Rasmussen, *The superpolynomial for knot homologies*, Experiment. Math. **15.2** (2006) 129–159, ISSN: 1058-6458 (cit. on p. 136).
- [205] K. Koike, *On the decomposition of tensor products of the representations of the classical groups: by means of the universal characters*, Adv. Math. **74.1** (1989) 57–86, ISSN: 0001-8708 (cit. on pp. 138, 139).
- [206] P. H. Butler and R. C. King, *Symmetrized Kronecker products of group representations*, Canad. J. Math. **26** (1974) 328–339, ISSN: 0008-414X (cit. on p. 138).
- [207] D. J. Gross and W. Taylor, *Two-dimensional QCD is a string theory*, Nucl.Phys. **B400** (1993) 181–208, arXiv: hep-th/9301068 [hep-th] (cit. on p. 139).

List of Figures

| | | |
|------|--|----|
| 2.1 | All possible stable degenerations of a genus two Riemann surface. Here we represent a double point by two marked points connected through a line. | 21 |
| 2.2 | Toric diagram of $\mathcal{O}(-1) \oplus \mathcal{O}(-1) \rightarrow \mathbb{P}^1$. The base \mathbb{P}^1 as indicated by the dashed lines is an S^1 fibration over the bounded edge in the center. | 24 |
| 2.3 | An invariant stable holomorphic map from a worldsheet on degenerate Σ_3 to the resolved conifold (represented by its toric digram), and the diagram $G \in \mathcal{G}_{3,0}$ that represents it. Here in G we suppress the ϵ_e symbols on the edges (see text). | 26 |
| 2.4 | Two toric special Lagrangian branes $\mathcal{L}_1, \mathcal{L}_2$ in the resolved conifold X . In the toric diagram Υ_X they are represented by two rays touching the edges of Υ_X | 28 |
| 2.5 | An invariant stable holomorphic map from a worldsheet on degenerate $\Sigma_{3,2}$ to the resolved conifold (represented by its toric digram) ending on the Lagrangian brane \mathcal{L} , as well as the diagram $G \in \mathcal{G}_{3,2}$ that represents it. Here in G we suppress the $\epsilon_e(\epsilon_c)$ symbols on the edges (half edges) (see text). | 29 |
| 2.6 | Diagrammatic illustration of the expansion of $F_2(t, \bar{t})$ in eq. (2.113). Here each connecting line with endpoints (I, J) is a factor of Δ^{IJ} , and each Riemann surface of genus g with h marked points I_1, \dots, I_h is $\partial_{I_1} \dots \partial_{I_h} \mathcal{F}_g$ | 32 |
| 2.7 | Spectral curve \mathcal{C} of the mirror of $\mathcal{O}(-1) \oplus \mathcal{O}(-1) \rightarrow \mathbb{P}^1$, the A and B cycles on \mathcal{C} , and its projection to \mathbb{C}^* | 34 |
| 2.8 | A toric special Lagrangian brane \mathcal{L} in the resolved conifold, and a disk instanton on \mathcal{L} | 35 |
| 2.9 | Overcrossing, undercrossing, and no crossing. | 40 |
| 2.10 | The torus knot $\mathcal{K}_{2,3} = \mathcal{K}_{3,2}$, also called the trefoil knot, and how to place it on the surface of a solid torus. | 43 |
| 2.11 | The conifold transition underlying the Gopakumar–Vafa conjecture. The three diagrams from left to right represent T^*S^3 , conifold singularity, and $\mathcal{O}(-1) \oplus \mathcal{O}(-1) \rightarrow \mathbb{P}^1$ respectively. In the first diagram, N stands for a stack of N branes wrapping S^3 | 57 |
| 2.12 | Mirror symmetry and large N duality form a circle of dualities. Here X is the conifold singularity and Y is the singular Calabi–Yau given by eq. (2.241). | 58 |
| 2.13 | Diagrammatic illustration of the expansion of $F_2^\Delta(\tau, \bar{\tau})$ in eq. (2.291). Here each connecting line with endpoints (i, j) is a factor of Δ_{ij} , and each Riemann surface of genus g with h marked points i_1, \dots, i_h is $\partial_{i_1} \dots \partial_{i_h} \mathcal{F}_g$ | 66 |
| 2.14 | The same circle of dualities as in Fig.2.12, but with the insertion of the branes associated to unknot in the topological string theories. | 67 |
| 2.15 | The BKMP conjecture. The topological recursion is applied on the spectral curve of the type B topological string. | 69 |

| | | |
|------|--|-----|
| 3.1 | The Lagrangian branes in the transition of geometries underlying the Ooguri–Vafa conjecture. | 78 |
| 3.2 | The toric diagram of the resolved conifold, and the spectral curve of its mirror. The former is invariant under the involution of eq. (3.30), and the latter is invariant under the involution of eq. (3.29). | 79 |
| 3.3 | The figure eight knot, also denoted by $\mathbf{4}_1$ in the knot theory. | 80 |
| 3.4 | The decomposition of $\Sigma_{g=1,h=1}$ and $\Sigma_{0,3}$ into tubes and pairs-of-pants. | 84 |
| 3.5 | The mutant pair of the Kinoshita–Terasaka knot (left) and the Conway (right) knot. From wikipedia. | 97 |
| 4.1 | A quasi-plat presentation of $\mathbf{4}_1$ and a plat presentation of $\mathbf{3}_1$ | 100 |
| 4.2 | A quasi-plat presentation can be split into two simple tangles at the top and the bottom and the braidings in the middle. | 102 |
| 4.3 | Four-point conformal blocks in t -channel and s -channel respectively. | 102 |
| 4.4 | Two braiding operations b_i^+ and b_i^- with opposite directions. | 103 |
| 4.5 | The monodromy of the 4-point conformal block in the t -channel. | 103 |
| 4.6 | t - and s -channel conformal blocks are related by a crossing matrix. | 104 |
| 4.7 | A simple tangle in M_1 . When glued with its conjugate in M_2 (mirror image with the orientation flipped) we have two disconnected unknots. | 106 |
| 4.8 | Two examples of gluing a pair of simple tangles together. In the right diagram, a braiding has to be inserted. This kind of diagrams is used to fix the relative phases between the quantum states associated to different simple tangles. | 107 |
| 4.9 | Diagrammatic illustration of the associativity isomorphism of the truncated tensor products. | 111 |
| 4.10 | Diagrammatic illustration of the generalized Racah backcoupling rule. We suppress multiplicity labels here. | 114 |
| 4.11 | Diagrammatic illustration of the pentagon relation. Multiplicity labels are suppressed here. | 115 |
| A.1 | The Young diagram of a composite representation $(\mu; \nu)$ of $U(N)$, and that of the associated representation of $SU(N)$ | 138 |
| B.1 | Quasi-plat presentations of hyperbolic knots with up to seven crossings. | 144 |

List of Tables

| | | |
|-----|--|-----|
| 2.1 | $U(1)$ R-charges as well as the chiralities (twice of spin) of the supercharges before and after the topological twistings. | 11 |
| 2.2 | $U(1)$ R-charges and the chiralities (twice of spin) of the chiral fields before and after the topological twistings. | 12 |
| 3.1 | The Yukawa coupling (triple derivative of the planar free energy) computed from the AV spectral curves of four hyperbolic knots | 96 |
| 4.1 | Depicted are the first four simple tangles in M_1 together with the associated quantum states. The conjugate quantum states are associated to the mirrored tangles in M_2 with the orientation of the strands reversed. We use $ R $ as a shorthand for $\dim_q R$. The ellipses in the parentheses are to be filled in with appropriate WZW primaries. | 107 |
| 4.2 | The second four simple tangles in M_1 and the quantum states associated to them. The conjugate quantum states are associated to the mirrored tangles in M_2 with the orientation of the strands reversed. $ R $ is short for $\dim_q R$. The ellipses in the parentheses are to be filled in with appropriate WZW primaries. | 108 |